The University of Nottingham

UNITED KINGDOM • CHINA • MALAYSIA

Application of microneedles for the treatment of nodular basal cell carcinoma

Akmal Hidayat Bin Sabri (MPharm)

Submitted to the University of Nottingham for the degree of Doctor of Philosophy

December 2020

General Abstract

Basal cell carcinoma (BCC) is one the most common skin cancer in humans. One of the most efficacious drugs used in treating BCC is imiquimod, which is available as a topical cream, Aldara™. Nevertheless, the drug has limited cutaneous permeation limiting its use only for the management of superficial BCC. The work presented in this thesis explored the utility of microneedles as a drug delivery platform for the intradermal delivery of imiquimod for the treatment of nodular BCC. This was achieved by first comparing the insertion profiles of two commercial microneedle systems, the Dermastamp™ and Dermapen®. It was discovered that the oscillating microneedle system, the Dermapen® required less force than the Dermastamp™ to puncture the skin while resulting in deeper insertion in *ex vivo* skin tissue to a depth needed to treat nodular BCC. Moving forward, the effectiveness of the Dermapen® to improve the delivery of imiquimod into the skin was investigated. It was discovered that post-treatment of the skin with the Dermapen® after Aldara™ application, known as "patch-and-poke", enhanced the intradermal delivery of imiquimod generating a depot that that persisted for up to 24 hours. However, such enhancement was not achieved when a "poke-and-patch" strategy was adopted, where skin was pre-treated with the Dermapen® prior to cream application.

Despite the effectiveness of the "patch-and-poke" strategy in delivering imiquimod intradermally, this approach may not be acceptable by patients owing to the two-step nature of the treatment. In order to overcome this limitation a one-step drug delivery strategy utilising dissolving polymeric microneedles was explored. This was achieved by fabricating a dissolving microneedle system out of the commercial PVPVA polymer, Kollidon® VA 64. The dissolving microneedle system demonstrated the capability of delivering similar quantities of imiquimod but into the deeper layers of the skin, despite a 6-fold lower drug loading, relative to the current clinical dose of Aldara™ cream used in BCC treatment. Furthering this, a series of polymeric microneedles of different designs and polymer chemistries were manufacture from pAMPS, pNAM and pHEAM that were synthesised via free radical polymerisation reactions. Drug release studies into *ex vivo* porcine skin tissues and *ex vivo* patient BCC

tumours demonstrated that the pNAM obelisk microneedle patches were capable of achieving higher intradermal delivery of imiquimod relative to the commercial cream, Aldara™. In addition, an *in vivo* tumour efficacy study using a mouse model for skin tumours highlighted that the microneedle patches were capable of slowing down tumour growth.

Lastly, this thesis demonstrated the analytical capability offered by time-of-flight secondary ion mass spectrometry (ToF-SIMS) in evaluating the effectiveness of microneedle-based drug delivery systems. This is exemplified by the ability of the instrument to track the dermal distribution of active (imiquimod) and excipients (polymers and surfactant) from different formulations within biological tissues in a label free fashion. Such unprecedented analysis enabled us to demonstrate active-excipient colocalisation thus expanding our mechanistic insight on how such delivery systems behave upon administration into the skin. Overall, this thesis expanded our knowledge on how some microneedle systems are capable of achieving enhanced intradermal delivery while highlighting the viability of this drug delivery platform for the treatment of nodular BCC in a minimally invasive fashion.

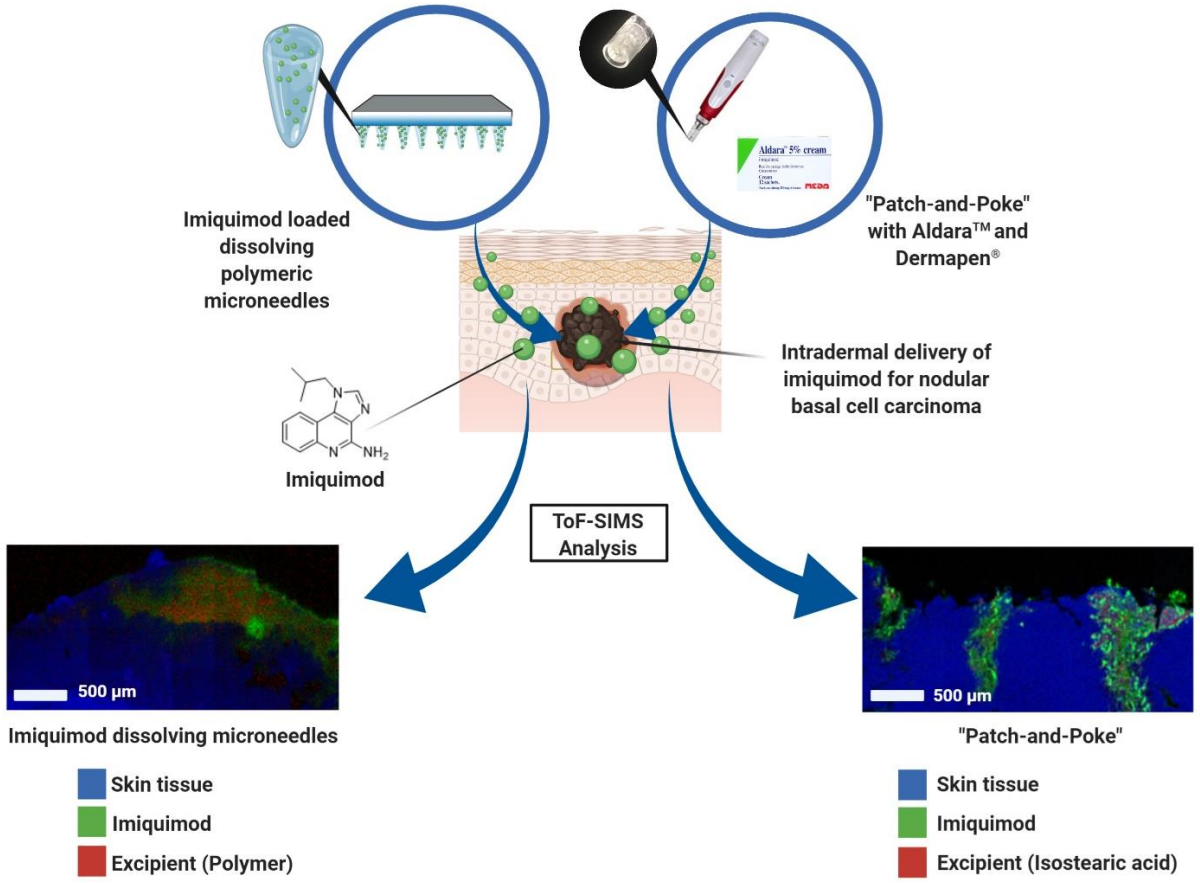

Declaration

Unless otherwise acknowledged, the work presented in this thesis is my own. No part has been submitted for any other degree at The University of Nottingham or any other institution. This work was supported by the following funding: The University of Nottingham Centre for Doctoral Training in Advanced Therapeutics and Nanomedicine, Walgreens Boots Alliance and the EPSRC [grant number: EP/L01646X/1]. This doctoral dissertation was conducted under the supervision of:

Dr. Maria Marlow, Associate Professor in Formulation Science and Pharmaceutical Materials at School of Pharmacy at the University of Nottingham, UK and

Dr. David Scurr, Senior Research Fellow in Surface Analysis at School of Pharmacy at the University of Nottingham, UK

Dr. Joel Segal, Associate Professor in Manufacturing Engineering, Faculty of Engineering at the University of Nottingham, UK

Dr. Jane Ogilvie, Medical Affairs Scientist, Medical Affairs Walgreens Boots Alliance – Global Brands

Dr. John McKenna, Consultant Dermatologist, Leicester Royal Infirmary University Hospitals Leicester Dermatology Department, Infirmary Square, Leicester, UK

Akmal Hidayat Bin Sabri

December 2020

Acknowledgements

This PhD study has indeed been long and arduous yet fulfilling and humbling. It was challenging from the very start when I had to see my mother's tears as she and my father sent me off at Kuala Lumpur International Airport knowing it would be many years before they could see their eldest son again. This PhD on its own is already challenging but doing without seeing your family for many years is a pain which is on a whole different level. The final year of this work was unprecedented and very challenging and with the Covid-19 pandemic that affected everyone globally- my prayers to everyone who has been affected by the pandemic.

Firstly, I would express my deepest gratitude to my primary supervisor and mentor Dr Maria Marlow for her endless support, guidance and encouragement throughout my research journey. You always reminded me to find balance in life- family, friends and research. I would also like to thank my co-supervisor's Dr David Scurr and Dr Joel Segal for their advice throughout my research. Thank you to my clinical supervisor Dr John McKenna and Dr Jane Ogilvie who also supported and guided me on the project. My gratitude to my examiners Prof David Barrett and Prof Abina Crean for their insightful question and discussion in my PhD viva. To the most wonderful technical staffs that I've met and become good friends with, your support was pivotal to this journey. Thank you, Paul Cooling, Esme Ireson, Douglas Crackett, Denise Mclean and Ian Ward, for being the most people I've ever met. To my wonderful friends who I've met along this journey, Dr Jatin Mistry, Dr Melissa Kirkby, Zachary Cater, Rebecca Olubi, Thathayaone Monkgogi, Jayne Hill, Dr Gustavo Trindade, Helen Sampaio, Mohammed Khan, Dr Khuriah Hamid Dr Pratik Gurnani and Dr Steffanie Kern and Fiona Smith. You were not only there for me during my scientific struggles but were my pillars of support during my personal struggles.To my parent's Dr Norsiah Kadir and Dr Sabri Nayan, my siblings Luqman Sabri and Kak Mariah-thank you for your prayers, love and unwavering support. Though you are far away, you are always close by my heart. Sorry for my absence mum. In memories of my loving grandad Kadir Mat, your poems will forever echo in my heart. I'm sorry I was not there to say one last good bye.

Publications related to this thesis

1. **A.H. Sabri**, Z. Cater, P. Gurnani, J. Ogilvie, J. McKenna, J. Segal, D. Scurr, M. Marlow, 2020. Int J. Pharmaceutics https://doi.org/10.1016/j.ijpharm.2020.119808
2. **A.H. Sabri**, J. Ogilvie, J. McKenna, J. Segal, D. Scurr, M. Marlow, 2020. Molecular Pharmaceutics https://doi.org/10.1021/acs.molpharmaceut.0c00347
3. **A.H. Sabri**, Z. Cater, J. Ogilvie, D. Scurr, M. Marlow, J. Segal, 2020. Journal of Drug Delivery Science and Technology https://doi.org/10.1016/j.jddst.2020.101766
4. **A.H. Sabri**, Y. Kim, M. Marlow, D. Scurr, J. Segal, A.K. Banga, L. Kagan, J.B. Lee, 2019. Advanced Drug Delivery Reviews https://doi.org/10.1016/j.addr.2019.10.004
5. **A.H. Sabri**, J. Ogilvie, K. Abdulhamid, V. Shpadaruk, J. McKenna, J. Segal, D.J. Scurr, M. Marlow, 2019. European Journal of Pharmaceutics and Biopharmaceutics https://doi.org/10.1016/j.ejpb.2019.05.001
6. M.H. Al-Mayahy, **A. H. Sabri**, C. Rutland, A. Holmes, J. McKenna, M. Marlow, D. Scurr, 2019. European Journal of Pharmaceutics and Biopharmaceutics https://doi.org/10.1016/j.ejpb.2019.02.006

Credit authorship contribution statement

Review articles:

Only sections written by A.H. Sabri in these reviews are used in the Chapter 1: Introduction

A.H. Sabri, J. Ogilvie, K. Abdulhamid, V. Shpadaruk, J. McKenna, J. Segal, D.J. Scurr, M. Marlow, 2019. Expanding the applications of microneedles in dermatology, European Journal of Pharmaceutics and Biopharmaceutics doi: https://doi.org/10.1016/j.ejpb.2019.05.001

- A.H. Sabri: Planned the review, structured the review, curated the literature and written the original draft.
- K. Abdulhamid and V. Shpadaruk: Critically reviewed the manuscript and editing.
- J. Ogilvie, J. McKenna, J. Segal, D.J. Scurr, M. Marlow: Supervisors to A.H. Sabri and supervised him during the writing of the review. Critically reviewed the manuscript and editing.

A.H. Sabri, Y. Kim, M. Marlow, D. Scurr, J. Segal, A.K. Banga, L. Kagan, J.B. Lee, 2019. Intradermal and transdermal drug delivery using microneedles – fabrication, performance evaluation and application to lymphatic delivery, Advanced Drug Delivery Reviews doi: https://doi.org/10.1016/j.addr.2019.10.004

- A.H. Sabri: Planned, structured, curated the literature and written Section 1 (Introduction), Section3 (Characterization and evaluation of microneedles) and Section 5 (Perspective).
- Y. Kim: Planned, structured, curated the literature and written Section 2 (Fabrication of different types of microneedles).
- J.B. Lee: Planned, structured, curated the literature and written Section 4 (Targeting the lymphatic system with microneedles).
- J. Segal, D.J. Scurr, M. Marlow: Supervisors to A.H. Sabri and supervised him during the writing of the review. Critically reviewed the manuscript and editing.
- A.K. Banga and L. Kagan: Critically reviewed the manuscript and editing.

Research Articles:

M.H. Al-Mayahy, **A. H. Sabri**, C. Rutland, A. Holmes, J. McKenna, M. Marlow, D. Scurr, 2019. Insight into imiquimod skin permeation and increased delivery using microneedle pre-treatment, European Journal of Pharmaceutics and Biopharmaceutics doi: https://doi.org/10.1016/j.ejpb.2019.02.006

(The data from article was not used in any of the experimental chapters of A.H. Sabri thesis)

- M.H. Al-Mayahy: Data curation, Formal analysis, Investigation, Methodology, Validation, Visualization.

- A.H. Sabri: Reanalysis of ToF-SIMS data and writing of the original draft of the manuscript.
- C. Rutland and A. Holmes: Critically reviewed the manuscript and editing.
- J. McKenna, D.J. Scurr, M. Marlow: Supervisors to A.H. Sabri and supervised him during the writing of the manuscript. Critically reviewed the manuscript and editing.

A.H. Sabri, Z. Cater, J. Ogilvie, D. Scurr, M. Marlow, J. Segal, 2020. Characterisation of mechanical insertion of commercial microneedles, Journal of Drug Delivery Science and Technology doi: https://doi.org/10.1016/j.jddst.2020.101766

(The article is written for Chapter 2)

- A.H. Sabri: Data curation, Formal analysis, Investigation, Methodology, Validation, Visualization, writing of the original draft of the manuscript. A.H. Sabri was involved the conceptualisation of the idea on the influence of skin stretching (strain) on microneedle insertion, designing of insertion studies, and commercial microneedle characterisation.
- Z. Cater: An undergraduate Mech Eng. student supervised by A.H. Sabri and J. Segal. Developed the biaxial stretch rig. Assisted A.H. Sabri in conducting the insertion studies.
- J. Ogilvie, D. Scurr, M. Marlow, J. Segal: Supervisors to A.H. Sabri and supervised him during the writing of the article. Critically reviewed the manuscript and editing.

A.H. Sabri, J. Ogilvie, J. McKenna, J. Segal, D. Scurr, M. Marlow, 2020. Intradermal Delivery of an Immunomodulator for Basal Cell Carcinoma; Expanding the Mechanistic Insight into Solid Microneedle-Enhanced Delivery of Hydrophobic Molecules, Molecular Pharmaceutics https://doi.org/10.1021/acs.molpharmaceut.0c00347

(The article is written for Chapter 3)

- A.H. Sabri: Data curation, Formal analysis, Investigation, Methodology, Validation, Visualization, writing of the original draft of the manuscript.

- J. Ogilvie, J. McKenna, J. Segal, D. Scurr, M. Marlow: Supervisors to A.H. Sabri and supervised him during the writing of the article. Critically reviewed the manuscript and editing.

A.H. Sabri, Z. Cater, P. Gurnani, J. Ogilvie, J. Segal, D. Scurr, M. Marlow, 2020. Intradermal delivery of imiquimod using polymeric microneedles for basal cell carcinoma, Int J. Pharmaceutics https://doi.org/10.1016/j.ijpharm.2020.119808

(The article is written for Chapter 4)

- A.H. Sabri: Data curation, Formal analysis, Investigation, Methodology, Validation, Visualization, writing of the original draft of the manuscript. A.H. Sabri was involved in designing the original dimension of the microneedles, PDMS mould production, formulation development, optimisation, characterisation and evaluation.
- Z. Cater: An undergraduate Mech Eng. student supervised by A.H. Sabri and J. Segal. Assisted A.H. Sabri with the computer aided design (CAD) for the microneedle master structures along with its subsequent production at the University of Nottingham Institute for Advanced Manufacturing. Critically reviewed the manuscript and editing.
- P. Gurnani: Assisted A.H. Sabri in polymer characterisation. Critically reviewed the manuscript and editing.
- J. Ogilvie, J. Segal, D. Scurr, M. Marlow: Supervisors to A.H. Sabri and supervised him during the writing of the article. Critically reviewed the manuscript and editing.

Thesis Chapter

(This forms Chapter 5 of the thesis and is yet to be published as the data is under patent pending)

Development and characterisation of a series of dissolving polymeric microneedles for targeted drug delivery for basal cell carcinoma, **A.H. Sabri**, Z. Cater, P. Gurnani, V. Brentville, L. Durrant, J. McKenna, J. Ogilvie, J. Segal, D. Scurr, M. Marlow.

- A.H. Sabri: Data curation, Formal analysis, Investigation, Methodology, Validation, Visualization, writing of the original draft of the manuscript. A.H. Sabri was involved in designing the original dimension of the microneedles, PDMS mould production, formulation development, optimisation, characterisation and evaluation. Clinical study planning, patient recruitment and ethics application.
- Z. Cater: An undergraduate Mech Eng. student supervised by A.H. Sabri and J. Segal. Assisted A.H. Sabri with the computer aided design (CAD) for the microneedle master structures along with its subsequent production at the University of Nottingham Institute for Advanced Manufacturing.
- P. Gurnani: Assisted and supervised A.H. Sabri in polymer synthesis and characterisation.
- V. Brentville and L. Durrant: *In vivo* study co-ordination and planning. V. Brentville was involved in conducting the *in vivo* study.
- J. McKenna: Patient recruitment and performed Mohs surgery and shipped patient samples to A.H. Sabri
- J. Ogilvie, J. Segal, D. Scurr, M. Marlow: Supervisors to A.H. Sabri and supervised him during the writing of the article. Critically reviewed the chapter and editing.

Contents

List of Figures

List of Tables

List of Abbreviations

µg	**Micrograms**
µm	Micrometres
$[M+H]^+$	Molecular ion in positive ionisation mode
$[M-H]^-$	Molecular ion in negative ionisation mode
5-FU	5-Fluorouracil
ACVA	4,4'-azobis(4-cyanovalericacid)
ALA	5-aminolevulinic acid
ANOVA	One-way analysis of variance
BCC	Basal cell carcinoma
CAD	Computer aided design
CLSM	Confocal laser scanning microscopy
CMC	Carboxymethyl cellulose
CO_2	Carbon dioxide
CSF	Colony stimulating factor
Đ	Dispersity
DMF	Dimethylformamide
DMSO	Dimethyl sulfoxide
DNA	Deoxyribose nucleic acid
DSC	Differential scanning calorimetry
ESEM	Environmental scanning electron microscope
FDA	USA Food and Drug Administration
FdUMP	Fluorodeoxyuridine monophosphate
FITC	Fluorescein isothiocyanate
GCIB	Gas cluster ion beam

GPC	Gel permeation chromatography
HMG-CoA	β-Hydroxy β-methylglutaryl-CoA
HPLC	High performance liquid chromatography
HU	Hyaluronate
Hz	Hertz
IL	Interleukin
INF-α	Interferon-alpha
IUPAC	International Union of Pure and Applied Chemistry
LC-MS	Liquid chromatography–mass spectrometry
Log P	Logarithm of partition coefficient (octanol: water)
m/z	Mass to charge ratio
MAL	Methyl aminolevulinate
MM	Malignant melanoma
MMS	Mohs micrographic surgery
MN	Microneedle
Mw	Molecular weight
MWCO	Molecular weight cut-off
NHS HRA	National Health Service Health Research Authority
NICE	National Institute for Health and Care Excellence
NMSC	Nonmelanoma skin cancer
OCT	Optical coherence tomography
OCT media	Optimum cutting temperature media
p.p.m.	parts per million
pAMPS	poly (2-acrylamido-2-methyl-1-propanesulfonic acid)
PD1	Programmed cell death protein 1

PDMS	Polydimethylsiloxane
PDT	Photodynamic therapy
PEG	Polyethylene glycol
pHEAM	Poly (N-hydroxyethyl acrylamide)
PIX	Protoporphyrin IX
pK_a	Acid dissociation constant
pNAM	Poly (N-acryloylmorpholine)
PVA	Poly (vinylalcohol)
PVP	Poly (vinylpyrrolidone)
PVPVA	Poly (vinylpyrrolidone-co-vinyl acetate)
RNA	Ribonucleic acid
RPM	Revolutions per minute
SC	Stratum corneum
SCC	Squamous cell carcinoma
SD	Standard deviation
SEC	size exclusion chromatography
SEM	Standard error of mean
SIMS	Secondary ion mass spectrometry
siRNA	Small interfering RNA
STAT3	Signal transducer and activator of transcription 3
TA	Texture analyser
T_g	Glass transition temperature
THF	Tetrahydrofuran
TLR	toll-like receptor
TMP	Meso-tetra (N-methyl-4-pyridyl) porphinetetratosylate

TNF- α	Tumour necrosis factor-alpha
ToF-SIMS	Time of flight secondary ion mass spectrometry
UV	Ultraviolet
v/v	volume by volume
VA-044	2,2'-azobis[2-(2-imidazolin-2-yl) propane] dihydrochloride
w/v	Weight by volume
w/w	Weight by weight
λ_{max}	Maximum wavelength of absorption

Chapter 1 General Introduction

Parts of this introduction have been published in the following review articles:

A.H. Sabri, J. Ogilvie, K. Abdulhamid, V. Shpadaruk, J. McKenna, J. Segal, D.J. Scurr, M. Marlow, *Expanding the applications of microneedles in dermatology*. European Journal of Pharmaceutics and Biopharmaceutics, 2019. **140:** p. 121-140 doi: https://doi.org/10.1016/j.ejpb.2019.05.001

- The section that has been published in this review articles are Sections 1.4.1, 1.4.2 and 1.4.4

A.H. Sabri, Y. Kim, M. Marlow, D. Scurr, J. Segal, A.K. Banga, L. Kagan, J.B. Lee, Intradermal and transdermal drug delivery using microneedles – Fabrication, performance evaluation and application to lymphatic delivery. Advanced Drug Delivery Reviews (2020). **153:** p. 195-215 doi: https://doi.org/10.1016/j.addr.2019.10.004

- The section that has been published in this review articles is ***Section 1.4.3***

This chapter will briefly review the anatomy and function of the skin followed by routes of drug administration into and through the skin. Indeed, there is now a considerable body of evidence on how skin diseases can result in psychological problems and a poor quality of life. One of the most common skin diseases is skin cancer, with basal cell carcinoma (BCC) being the most common out of all the skin malignancies combined. Given the widespread prevalence of BCC and its impact on the healthcare system, this chapter will also review the limitation of current treatments for BCC and how microneedles can be a viable drug delivery strategy in managing the disease. The history, types and application of microneedles in skin cancer will also be covered in this introduction followed by a review on time-of-flight secondary ion mass spectrometry (ToF-SIMS) as an emerging method in microneedle research.

1.1 Skin structure and function

The skin is the largest organ in the human body. Besides acting as a barrier between the human body and the external environment, the skin also forms a part of social communication in society. This organ accounts for 16% of the person's body weight and covers approximately 1.8 m^2 of the total body surface area of an average adult. The human skin is a complex organ that is metabolically active and plays an essential role in thermoregulation, production of vitamin D as well as the detection of various sensations ranging from heat, cold, pressure, touch and pain. In addition, the human skin also plays an important role in conferring protection against insults from the external environment ranging from ultraviolet (UV), microorganism, chemicals and allergens [1]. The skin is a multi-layered organ that comprises of three main histological layers: epidermis, dermis and hypodermis (subcutis). Besides that, the skin also consists appendages such as hair follicle, sebaceous glands and sweat gland as illustrated in Figure 1-1.

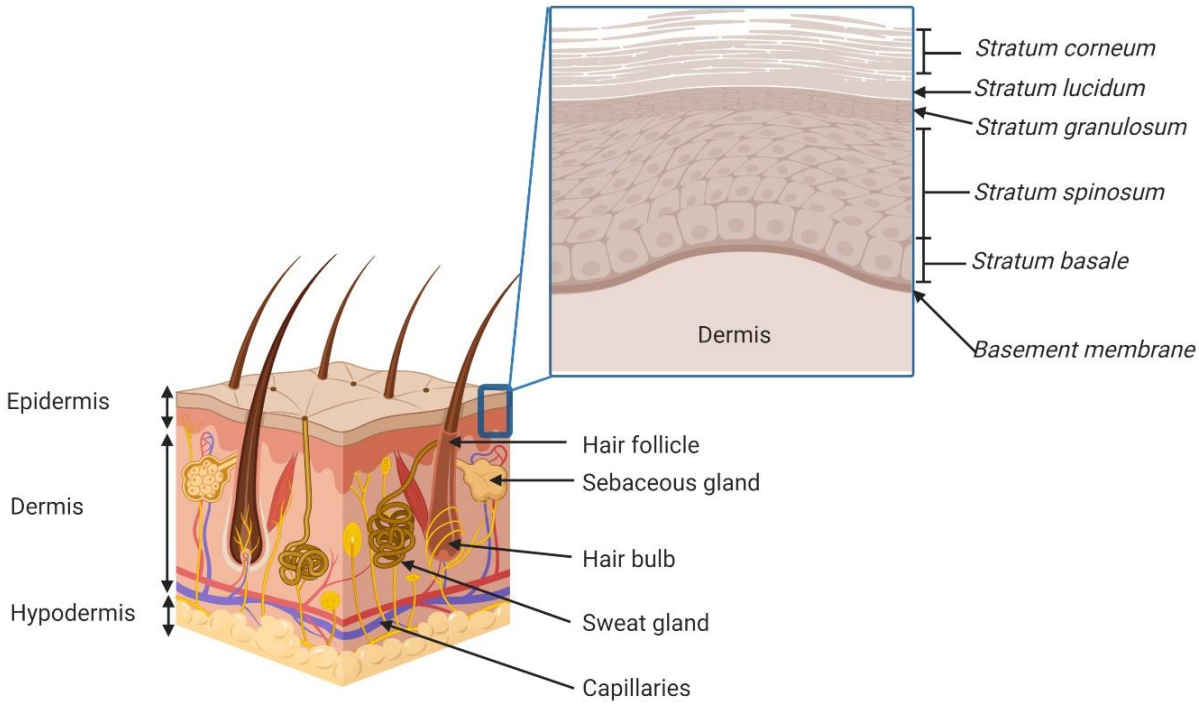

Figure 1-1 Schematic illustrating the structure of the human skin. Inset highlights the details of the different layers present within the epidermis.

1.1.1 Epidermis

The epidermis is a multilayer compartment of the skin that comprises of the *stratum corneum, stratum lucidum, stratum granulosum, stratum spinosum, stratum basale* and basement membrane as shown in Figure 1-1. This layer of the skin, the epidermis, is approximately 0.05-1 mm thick with thickness varying anatomically. As this layer of the skin is frequently exposed to both chemical and physical insults, the epidermis is in a constant regenerative state with an approximate renewal time of two months through the process of desquamation.

The *stratum basale* consist of basal cells which serve as the stem cells within the skin. These cells are responsible for the regeneration and replacement of new keratinocytes which are constantly being shed from the skin as a result of desquamation [1]. As the keratinocytes differentiate, these cells migrate into the *stratum spinosum*. Within this layer the cells establish a network of desmosomes that intercellularly link neighbouring keratinocytes. Upon migrating into the *stratum granulosum*, the cells begin to synthesise two types of granules which are the basophilic keratohyalin and lamellar granules. The basophilic keratohyalin are essentially prekeratin structures whereas the lamellar granules are secreted by the into extracellular space to form a lipid matrix. It is also at the *stratum granulosum* that keratinocytes begin to undergo anucleation. Within *stratum lucidum*, keratinocyte undergoes further keratinisation and becomes flattened followed by the disintegration of organelles [1].

The outermost layer of the skin is the *stratum corneum* which is the main barrier to drug penetration into the skin. This layer is typically 10-15 µm in thickness and consist of corneocytes embedded in a lipid matrix. This lipid matrix of the *stratum corneum* consist of ceramides, cholesterol sulphates and sterols that are arranged in a lamellar structure [2,3]. However, this lipid matrix is devoid of phospholipid due to hydrolysis of phospholipid into free fatty acids at the *stratum granulosum-stratum corneum* interface [4–6].

1.1.2 Dermis

Also known as the corium, this layer of the skin falls below the dermo-epidermal junction and is much thicker that the overlying epidermis which it supports. This layer of the skin is rich with collagen and elastin that is woven into a fibrous network that is then embedded in a matrix of proteoglycan. Due to this composition, the dermis confers elasticity and tensile strength to the skin. Sebaceous and sweat glands along with hair follicles also originates from this region [7]. The dermis receives a rich blood supply that is derived from the hypodermis. Therefore, it is postulated that any drug that reaches this layer of the skin after traversing the tortuous epidermal layers, are rapidly absorbed into systemic circulation [4]. Besides that, this layer also houses the lymphatic vessels and nerve endings. In humans, the dermis can be further categorised into two layers-the papillary dermis located near the epidermis and a deep thicker area known as the reticular dermis [6].

1.1.3 Hypodermis

The hypodermis also referred to as the subcutaneous layer is comprised primarily of adipocytes responsible for providing the body with buoyancy, insulation as well as acting as an energy reservoir. This subcutaneous layer consists of a network of fibrous septae that formed from collagen and large blood vessels. This septae anchors the adipocyte in place while providing support and structure to the hypodermis. The network of blood vessels that runs through these septae plays a pivotal role in delivering oxygen and nutrients to the hypodermis.

1.1.4 Skin Appendages

The skin appendages consist of sebaceous glands, eccrine glands, apocrine glands and hair follicles. The sebaceous glands secrete sebum which consist of a mixture of triglycerides, squalene, free fatty acid and wax ester [8]. The secreted sebum which is in involved in moisturising the skin while providing homeostatic control over the skin pH which is of around pH 5.0.

The eccrine glands, which are sometimes referred to merocine gland, are thermoresponsive to body temperature. The secretory coil of the eccrine gland resides in the dermis. Upon sensing a rise in body

temperature, these glands secrete a dilute saline solution (sweat) that evaporates thus providing thermoregulation to the body. The eccrine glands are distributed throughout the body but consist of higher density at the soles of the hand and feet. The apocrine glands which are also involved in sweat production reside in the hypodermis [9].

The hair follicles consist of hair bulb and hair shaft. The hair bulb can extend as deep as 3 mm into the hypodermis and consist of matrix cells involved in the production of hair shaft. The hair shafts are produced in a regular cycle which consist of three phases- anagen, catagen and telogen [10]. The density of skin appendages varies anatomically but accounts for approximately 0.1 % of the surface area of the human body [11].

1.2 Drug delivery to and through the skin and routes of permeation

Drug administration to the skin can be divided into topical, intradermal and transdermal delivery. A drug delivery system is considered as topical when the intended site of action of the dosed drug is on the superficial layers of the skin. On the other hand, drug delivery systems fall under the transdermal group when the drug is delivered through the skin and into the systemic circulation. A delivery system is considered intradermal when the intended target site is within the deeper layers of the skin such as the dermis [12]. Transdermal and intradermal drug delivery systems have increasingly been used in the past 20 years. These systems offer various advantages over oral delivery, including avoidance of hepatic first-pass metabolism, localised treatment of skin pathologies, controlled drug delivery, and improved patient compliance [13,14].

Advancement in the mechanistic understanding of skin permeation started to emerge in in 1943 with a notable review by Rothman -*The Principles of Percutaneous Absorption* [15]. Years of research in the area of skin permeation culminated with the regulatory approval of first transdermal patch for the delivery of the antiemetic drug, scopolamine in 1979 [16]. Since then, along with the progress in biophysical techniques, our understanding of skin permeation has evolved substantially.

The success of transdermal and intradermal drug delivery systems is dependent on the ability of the drug to permeate into the skin in sufficient quantities at an acceptable concentration to achieve the desired therapeutic effect. However, due to the efficient barrier function of the *stratum corneum*, the range of therapeutics that are available for transdermal and intradermal delivery are limited [17]. For a compound to conventionally traverse safely through the intact *stratum corneum*, a drug molecule should ideally possess the following attributes: Mw<600 Da, Log P: 1.0 - 3.0, low melting point, hydrogen bonding group ≤ 2, non-irritating and non-sensitizing [18–20]. The modes of drug transport to and through the skin along with the permeation pathway across the *stratum corneum* is illustrated in Figure 1-2

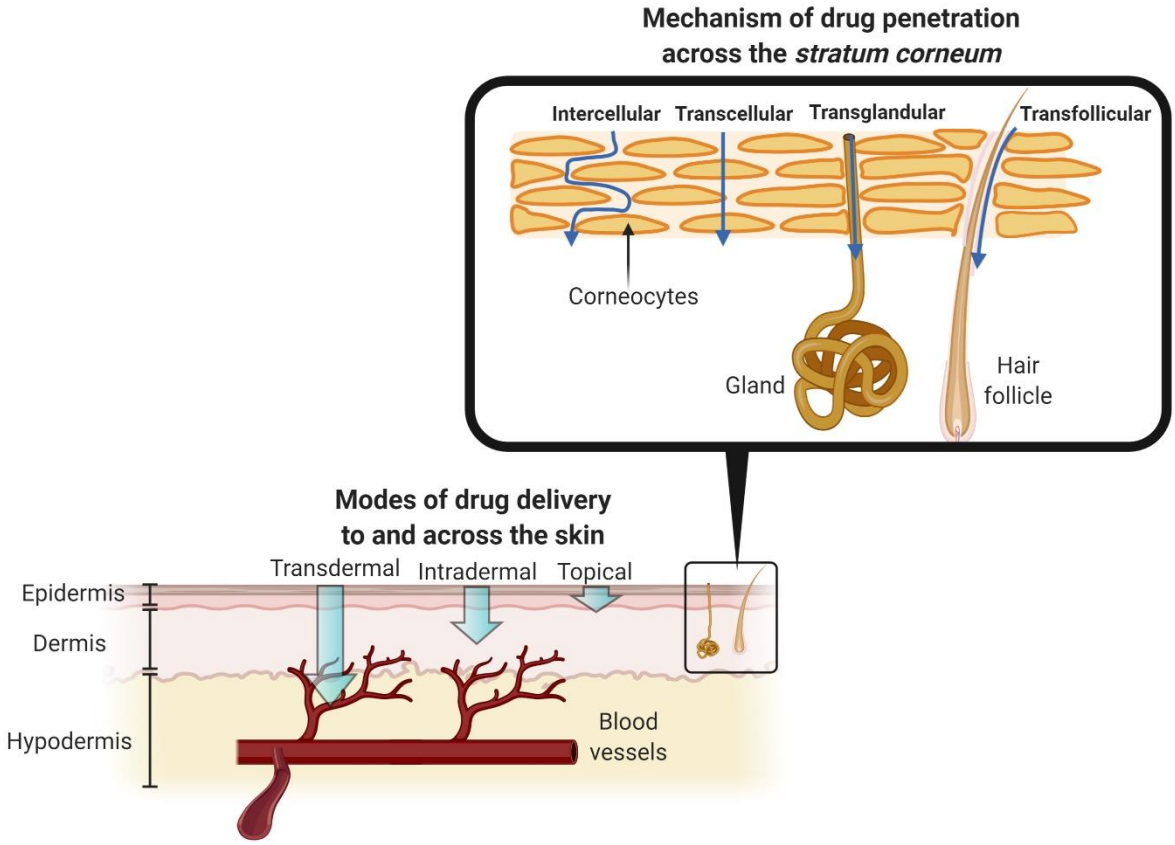

Figure 1-2 Schematic highlighting the modes of drug delivery to and through the skin. The inset highlights the schematic of drug penetration pathways across the stratum corneum.

Drug molecules may permeate across the *stratum corneum* via four main routes which are the intercellular, transcellular, transglandular and transfollicular routes. The intercellular and transcellular

routes are collectively known as the transepidermal route while the transglandular and transfollicular routes are frequently called the transappendageal route.

The transcellular is deemed the shortest route of permeation and involves the traversal of the permeants across alternating layers of corneocyte and the extracellular matrix. The interior of the corneocytes is considered hydrophilic while the extracellular matrix is lipophilic due to its' lipid constituents. On the other hand, the intercellular path involves the movement of permeant via diffusion through the tortuous extracellular lipid matrix without traversing the corneocytes. The diffusional pathlength for intercellular permeation route is estimated to be approximately 300-900 μm, which is much longer than the thickness of the *stratum corneum*. The majority of skin scientists view the intercellular route as the main route of permeation despite the longer permeation pathway. This is because this pathway circumvents the alternating partitioning steps between hydrophilic corneocytes and lipophilic extracellular matrix [21].

The transappendageal route comprises the transport of drug molecules through the skin via sweat glands (transglandular) or via the hair follicles (transfollicular), therefore obviating the need to permeate through the *stratum corneum*. However, as the skin appendages only account for approximately 0.1 % of the total skin surface area for an adult human, the overall contribution of these routes to drug permeation is considered negligible [22]. Nevertheless, transappendageal route is considered to play some role during the early phase of skin permeation before steady-state diffusion is established [23]. In addition, these permeation pathways, particularly the transfollicular route, have been considered to play some role in the permeation of high molecular weight drug delivery systems such as nanoparticles that display low diffusion coefficients across the *stratum corneum* [24].

Being the largest organ in the human body, the skin is one of the easiest organs to access in term of drug administration. The mode of drug delivery strategies highlighted above can be utilised not only for administering drug transdermally but also topically and intradermally where the intended target site is the skin itself. This may be of great clinical utility in managing diseased skin such as skin cancer

where the number of people affected by the disease is escalating globally to an increase in UV exposure [25].

1.3 Basal cell carcinoma

In general, skin cancer can be categorised into two main groups which are non-melanoma skin cancer (NMSC) and malignant melanoma (MM). NMSC can be further subdivided into basal cell carcinoma (BCC) and squamous cell carcinoma (SCC) [26]. BCC is the most prevalent type of skin cancer, with the number of individuals affected by the disease escalating worldwide. For instance, a large US sex-stratified cohort study by Wu *et al.* highlighted that the incidence rates of BCC in both men and women have doubled over the past 20 years [27]. In addition, similar trends have been reported in Canada, Asia, Australia and Europe [28]. Furthermore, it is anticipated that the incident rate will continue to escalate due to the rise in an aging population coupled with historical ultraviolet (UV) exposure [29].

Given that UV exposure is a risk factor in developing BCC, it therefore quite common that BCC typically manifests on sun exposed regions of the body such as the face, arms and necks [30]. The two most common BCC subtypes are superficial and nodular [31]. Superficial BCC generally manifests as flat red patches on the skin on the skin surface and proliferates parallel to the epidermis [32,33]. On the other hand, nodular BCC manifests as a translucent pearly nodule that resides within dermis at approximately 400 μm below the skin surface [34,35]. In addition, it has been reported that at least one-third of nodular BCC coexists with superficial BCC [36]. Despite displaying a low metastasis rate of 0.0028 %, this form of skin cancer can lead to considerable local tissue destruction (nose, ears and eyelids) leading to poor cosmetic outcomes and disfigurements at the disease sites [37,38]. The high incidence rate of the disease also forms a considerable proportion of a dermatologist's workload [39].

1.3.1 Current treatment strategies

The main aim of BCC treatment is complete tumour removal with acceptable cosmetic outcome to surrounding tissue. BCC tumours are treated either through surgery or non-surgical interventions. There are several surgical techniques that are used in the treatment of BCC such as curettage,

cryosurgery, carbon dioxide (CO_2) laser surgery and Mohs micrographic surgery (MMS). Out of these surgical techniques listed, MMS is the most effective surgical procedure in managing BCC which boast an overall 5-year cure rate of 99% [40]. MMS was first introduced in 1941 by Dr Federic E. Mohs in 1941 [41]. This surgical procedure also known as margin-controlled excision involves sequential removal of the cancer tissue coupled with careful microscopic examination. This meticulous surgical procedure ensures complete tumour removal has been achieved with maximal sparing of the surrounding healthy skin tissue. MMS is used in the management of approximately 30 % of all BCC cases in the United States. Although the use of MMS in much lower in Europe, there has been a rapid rise in the use of this surgical procedure in the management of BCC across the UK. This is attributed to the National Institute for Health and Clinical Excellence (NICE) skin cancer guidelines which recommend one MMS specialist per skin-cancer network across the UK [42].

Non-surgical modalities include radiotherapy, photodynamic therapy (PDT), and topical drug therapy [43,44]. PDT involves the eradication of cutaneous malignancy through the interaction of light of specific wavelength with a photosensitizing agent. Examples of photosensitising agents that are used in this treatment are 5-aminolevulinic acid Figure 1-3 **(a)** and Photofrin® Figure 1-3 **(b)**. Upon topical administration, these compounds will accumulate in rapidly dividing cells. This is then followed up with irradiating the patient at the targeted dermal region with light of a specific wavelength that will elicit the generation of reactive oxygen species from the photosensitizers. The interaction of reactive oxygen species with the cellular components at the target site will culminate in tumour death [45–47].

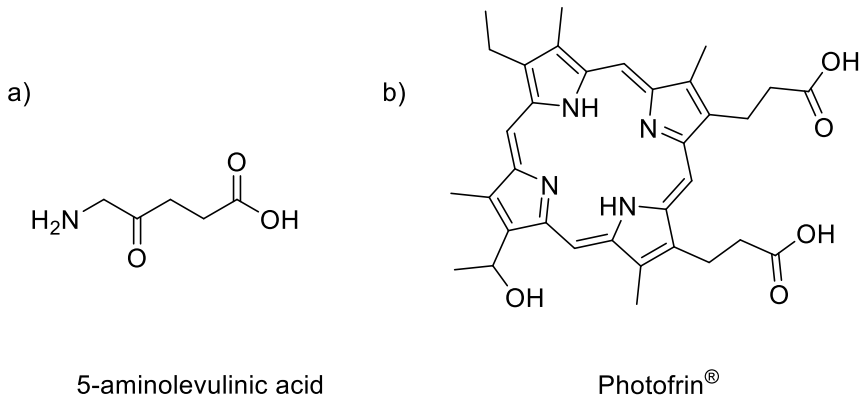

Figure 1-3 Chemical structure of drugs used in photodynamic therapy for NMSC a) 5-aminolevulinic acid and b) Photofrin®

One of the drugs that is used in the topical treatment of BCC is 5-fluorouracil (Efudix®). 5-fluorouracil (5-FU) Figure 1-4 on the other hand is an antimetabolite which is converted intracellularly to fluorodeoxyuridine monophosphate (FdUMP). This metabolite binds to the nucleoside binding site of thymidylate synthase and inhibits the enzyme causing a decrease in the synthesis of thymidine; a nucleoside essential in the DNA replication. Additionally, 5-FU may also be metabolised to other metabolites which are later incorporated into DNA of cancer cells leading to DNA damage and ultimately cell death [48].

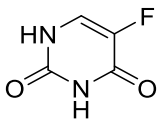

5 Fluorouracil

Figure 1-4: Chemical structure of 5-fluorouracil (5-FU) used in the management of non-melanoma skin cancer such as basal cell carcinoma

1.3.2 Imiquimod

Another drug that is used as a topical treatment for BCC is imiquimod, Figure 1-5. The drug is marketed Aldara™ cream (5% w/w imiquimod) by 3M Pharmaceuticals and was initially approved by the FDA for the managemental external genital and perianal warts in 1997. However, in 2004 Aldara™ was

approved for the management of actinic keratosis and superficial BCC. Imiquimod belongs to a class of drugs known as imidazoquinoline. The IUPAC name for imiquimod is *1-(2-methylpropyl)-1H-imidazo [4, 5- c] quinolin-4-amine* ($C_{14}H_{16}N_4$). This compound has a molecular weight 240.3 Daltons and display a relatively high melting point of 297-299 °C. The drug displays excellent chemical and physical stability [49]. In addition, imiquimod is a hydrophobic drug that is crystalline at room temperature causing it to have poor aqueous solubility at neutral and basic pH and is sparingly soluble in organic solvents. The drug has a log *P* of 2.7 and a pK_a of 7.3 [50]. However, with a primary amine (pK_a 7.3), the solubility and ionisation of imiquimod will ultimately be pH-dependent. In order to gauge the effect of pH on the ionisation of imiquimod, a log D profile of the drug as function of pH as shown in Figure 1-5 highlights that the drug ionises and thus becomes more water soluble in acidic pH. Thus, it can be postulated that topical application of the drug directly on the skin will cause a significant portion of the drug to become ionised at the *stratum corneum* as this layer of the skin is relatively acidic (pH 4.5) relative to the viable epidermis and dermis which has a near-neutral pH (7–8) [51]. The ionisation of the drug on the skin surface will hinder the permeation of the drug across the hydrophobic lipid rich matrix of the *stratum corneum*.

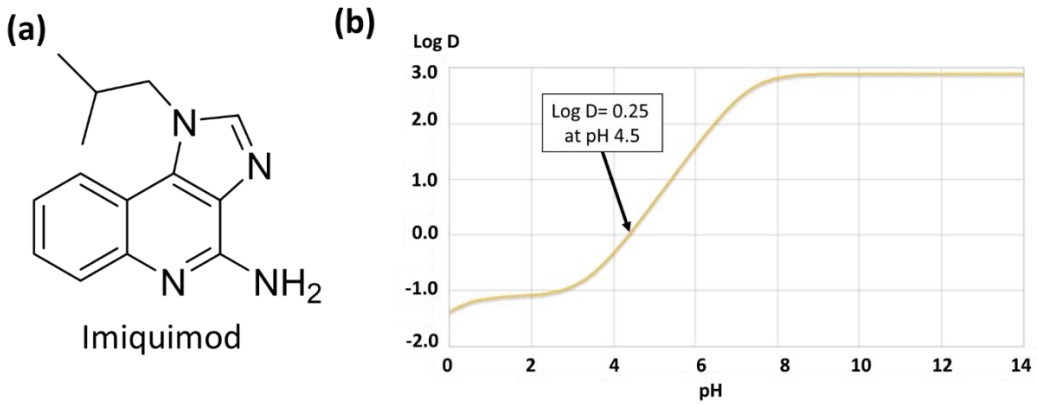

Figure 1-5 (a) Chemical structure of imiquimod used in the management of non-melanoma skin cancer such as basal cell carcinoma (b) Log D profile of imiquimod as a function of pH predicted using ACD/I-Lab software

Based on this Log D profile it is apparent that imiquimod displayed the highest solubility in acidic solution. In has been shown that the saturation solubility of imiquimod in acetate buffer pH 4.0 to be

as high as 1360.2 (μg/mL) [52]. Based on this information, many permeation study utilised acetate buffer with pH ranging from 3.7-4.0 in the receptor compartment order to maintain sink conditions [53–55].

Although this drug was initially developed to be use as a nucleoside analogue, it was later discovered that imiquimod does not have any nucleoside like activity. Instead, imiquimod is an immunomodulator which stimulates toll-like receptors-7 (TLR-7) on dendritic cells, macrophages and monocytes when applied topically. This stimulates downstream processes via the MyD88-dependent signalling pathway which causes an up regulation immunomodulatory gene leading to enhanced production of range of pro-inflammatory cytokines such as interferon-alpha (INF-α), tumour necrosis factor-alpha (TNF- α), interleukin (IL)-1 α, IL-1 β, IL-6, IL-8, IL-12, granulocyte-macrophage colony stimulating factor (CSF), granulocyte CSF, and macrophage inflammatory protein-1 α. This cytokine release results in an increase in the infiltration of cytotoxic T-cells and natural killer cells within the site of application which then elicit an antitumoral response again the BCC tumour. These proinflammatory mediators are also involved in inducing a Th1- dominant cellular antitumoral response again BCC. In addition, it has also been shown that imiquimod exerts direct pro-apoptotic effects on BCC tumour through direct induction of Fas receptors on the cancer cells [56].

Aldara™ cream was licensed by the FDA for the treatment small superficial BCC. Several clinical studies have highlighted the efficacy of imiquimod in the management of superficial BCC [57,58]. In addition, a randomized controlled multi-centre trial that enrolled 601 patients showed that 5 years post-treatment, the probability of tumour-free survival was 80.5% in patients receiving imiquimod cream while patients receiving methyl aminolevulinate photodynamic therapy the rate was 62.7% and those receiving 5-fluorouracil cream was 70.0%. This study highlighted that 5% w/w of imiquimod cream is superior to both methyl aminolevulinate photodynamic therapy and 5-fluorouracil cream in terms of efficacy for superficial BCC [59]. This trial highlighted that, out of three most common drug pharmacotherapy available for the management of superficial BCC, imiquimod displayed superior

efficacy and is considered as the first choice for non-invasive management in most primary superficial BCC.

1.3.3 Limitation of current treatment strategies

It has been highlighted that surgical interventions, particularly with MMS, is the most effective treatment for the management of BCC which has a cure rate of 99% [40]. Despite the effectiveness of surgical interventions, accurate detection of tumour margins prior and during surgery is pivotal in ensuring complete tumour resection. Such prerequisites are both time-consuming and technical, which are major limitations of surgical intervention [43,60–62]. Furthermore, the high incidence rate of BCC imposes a considerable burden to the workload of dermatologists particularly in managing the disease [39]. Therefore, it would be of great benefit if BCC can be managed via an effective non-surgical intervention that patients can safely self-administer at home. This would help lessen workload of dermatologists to enable them to manage much more severe skin conditions such as malignant melanoma. In addition, not all BCC patients are suitable for surgical intervention and some may opt for non-surgical treatment due to lower overall cost and better cosmetic outcomes [63,64].

Non-surgical intervention such as PDT with 5-aminolevulinic acid and Photofrin® may serve as a solution for patients that are not suited for surgical interventions. However, as the photosensitisers display poor skin permeation, these drugs are frequently administered intravenously. Such delivery route frequently results in side effects such prolonged cutaneous photosensitivity in patients post-treatment [45–47]. Furthermore, upon intravenous administration, the photosensitising agents can take between 24-72 hours to accumulate in the tumour before the intended treatment site can be irradiated [65]. Such pre-requisite may necessitate multiple visits to the dermatologist which could increase the workload of the clinician as well as having an impact on patients' daily activities while receiving PDT.

Due to the complications associated with PDT, topical treatment with 5-FU (Efudix®) cream may be a more preferred option as the patient can easily self-administered the treatment at home. However,

5-FU is limited to the management of superficial BCC as the drugs have poor permeation profile into the deeper layers of the skin for the treatment of nodular BCC which reside in the dermis. Although delivery of 5-FU across the stratum corneum is facilitated by its low molecular weight (130.08 Da), its skin permeation is limited due to its hydrophilicity (Log P −0.89) thus limiting its application for the management of superficial BCC [66].

Despite possessing superior potency than 5-FU and methyl aminolevulinate photodynamic therapy, imiquimod also suffers poor dermal permeation thus reducing its therapeutic value to superficial BCC [67]. William *et al*. highlighted that in the management of nodular BCC, it has been found that topical therapy with imiquimod has a much lower cure rate than surgical intervention [34]. Such a finding is attributed to the efficient barrier function of the *stratum corneum* which limits the permeation of imiquimod into the skin [68]. The location of nodular BCC that resides deep within the aqueous dermis presents another barrier for imiquimod delivery. The poor permeation properties of imiquimod deeper into the skin is attributed to the various physiochemical properties of the drug. It is suggested some of the ideal characteristics for a drug to permeate deeper into the skin include a Mw < 600 Da, a Log P 1.0 to 3.0, a low melting point, and ≤2 hydrogen bonding groups [18–20]. Although imiquimod meets some of these criteria, the drug has a total of 4 hydrogen bonding groups. The presence of such hydrogen bonding groups, especially the primary amine that may interact with the anionic components of the *stratum corneum*, contributing to the poor permeation profile of imiquimod deeper into the skin [68]. Furthermore, the drug has poor aqueous solubility which precludes the drug from permeating deeper into the aqueous and water rich dermal layers [50] . The combination of these factors presents a challenge in delivering imiquimod in a concentrated and localised fashion into the dermis for the treatment of nodular BCC.

In addition, it has been reported by patients that topical treatment such as creams are often unfavourable as this drug delivery vehicle typically has poor cosmetic feel upon administration as well as exuding an unpleasant scent once applied. In addition, the restriction in daily activities post-

application (e.g. not being able to shower and bathe after application) may result in poor compliance [69]. Also, the likelihood of the cream spreading onto clothes and healthy skin also raises the issue of unwanted side effects.

Given the limitations of current treatments for BCC specifically for the nodular variants which is the most common, there is an impetus to improve the delivery of therapeutic such as imiquimod into deeper BCC lesions. One of the early works investigating this strategy was conducted by Lee *et al*. The group evaluated the ability of fractional photothermolysis (using erbium: yttrim-aluminum-garnet laser) to enhance and control the delivery of imiquimod into porcine and murine skin under *in vitro* conditions [70]. This study highlighted that the creation of micron sized pores enhances dermal delivery of imiquimod whilst having a dose-sparing property. The clinical translation of such a strategy may be limited however, as the use of laser-assisted delivery is both expensive and requires the technical expertise of healthcare professionals. However, another strategy that could be adopted to create micron sized pores to enhance intradermal drug delivery, in a more cost-effective manner, is via the use of microneedle technology.

However, factors such as toxicity and safety ought to be considered should imiquimod be delivered via the use of microneedles. This is because the application of microneedle to the skin transiently disrupts the protective layer of the skin, the *stratum corneum* and this could lead to the breakthrough of the drug from the site of administration into the bloodstream. Such unwanted systemic exposure of imiquimod could lead to side effects such as influenza-like symptoms, transient shifts in leucocyte levels, myalgias and in some extreme cases, febrile seizure and chronic neuropathic pain [71]. These systemic side effects would not only affect the treatment outcomes for BCC but will ultimately jeopardise the overall quality of life for the patients. In order to circumvent these issues, imiquimod ought to be delivered in a suitable vehicle that is capable of forming an intradermal depot thus retaining the drug within the BCC tumour while minimising systemic exposure. This can be achieved via the use of polymers that forms a drug-polymer matrix upon microneedle administration to the

skin. The embedded matrix is hypothesised to generate localised regions of enhanced viscosity that mitigate the permeation of the drug across the skin thus reducing unwanted systemic exposure [72,73]. In order to achieve this delivery strategy, the polymer and excipient chosen as the drug delivery vehicle ought to be biocompatible and safe for clinical applications. This can be achieve by the use of FDA approved polymers that has been utilised for transdermal and topical applications such polylactic-co-glycolic acid (PLGA), polyvinylpyrrolidone (PVP) and polyvinyl alcohol (PVA) [74]. Besides that, the polymer and additive chosen must be compatible with the payload delivered, which in this case would be imiquimod.

Concerns may also arise from the risk of microbial invasion into the body following the permeabilization of the *stratum corneum* through microneedle application. Nevertheless, it has been shown by Donnelly *et al* microneedle puncture resulted in lower microbial penetration into the viable epidermis in comparison to hypodermic needle puncture [75]. Indeed, this landmark study highlighted that microneedle puncture was safer than conventional hypodermic injection with respect microbial penetration. Furthermore, it may be argued that the propensity for infection to arise via microbial penetration through microneedle-induced pores is further reduced due to the antimicrobial properties of the skin. The skin is known to produce antimicrobial peptides such as cathelicidins [76] and β-defensins [77,78] that function as an antimicrobial shield within the skin. In addition, the risk of infection could be further mitigated by aseptic fabrication and application of microneedles [79]. The aseptic production and sterilisation of microneedle would be an important factor to consider during the commercialisation and translation of microneedle technology into clinical practice. However, the choice of sterilisation during microneedle production must be carefully selected to damaging and altering the release profile of the microneedle formulation fabricated.

1.4 Microneedles

1.4.1 History and development of microneedle technology

Described as a hybrid between hypodermic needles and transdermal patches [80], microneedles are biomedical microdevices consisting of rows of fine needles [81]. Mark Prausnitz, one of the researchers who pioneered the research in the field, classified microneedles as a third-generation transdermal drug delivery system [16]. Such devices result in micron sized pores when applied to the skin and it is this creation of pores through the *stratum corneum* that can be exploited for drug delivery. Typically, microneedles have a shaft length between 250-1000 µm while possessing tips sharper than those of hypodermic needles [82]. Upon insertion, microneedles can breach the *stratum corneum* and improve the bioavailability of various therapeutics and large molecular weight compounds, a significant advantage relative to conventional transdermal delivery.

The first microneedle patent was filed in 1976 by Gerstel and Place from Alza Corporation, and at the time it was proposed that such micron-scale needles could be utilised for transdermal drug delivery in a painless manner [83]. However, it was not until the emergence of microfabrication tools from the microelectronics industry in the 1990s that research on utilising microneedles for drug delivery started to gain much pace. With the help of microfabrication tools, microneedles of varying dimensions, sizes and material were generated to meet specific drug delivery requirements. During this period, three main groups from Becton Dickinson, Alza Corporation and Georgia Institute of Technology pioneered microneedle research for drug delivery [84].

The first ever published paper on microneedle arrays was by Hashimi *et al*. in 1995 who developed a hollow microneedle array that injected bacterial plasmid for genetic transformation of nematodes [85]. However, it was not until 1998 that the first publication by Sebastien Henry on the use of microneedles for transdermal application emerged [86]. In 2004, significant progress in the area of microneedle emerged when Mark Prausnitz proposed that microneedle arrays may be utilised to enhance the

delivery of not only small molecular weight molecules but macromolecules such as peptides, proteins, oligonucleotides and even supramolecular complexes [87].

Since then, there has been an exponential rise in publications regarding microneedles for pharmaceutical application. It has been nearly five decades since the first patent for microneedle was filed. Currently, most microneedles that are available on the market are indicated for cosmetic purposes. More recently, microneedle devices for intradermal delivery of vaccines have been approved by regulatory authorities for seasonal influenza vaccination [88–93]. Despite these advances, microneedle-based drug delivery systems are yet to make a significant impact in a clinical setting as most devices are still in preclinical and clinical studies. However, based on the current progress in microneedle research as well as the rise in the number of commercialised cosmetic microneedle products, it is not unreasonable to predict the emergence of therapeutic microneedle products indicated for the management of either acute or chronic diseases in the near future.

1.4.2 Types of microneedles

In general microneedles can be characterised into five main groups based on their drug delivery strategies: solid microneedles, coated microneedles, dissolving microneedles, hollow microneedles and hydrogel-forming as shown in Figure 1-6.

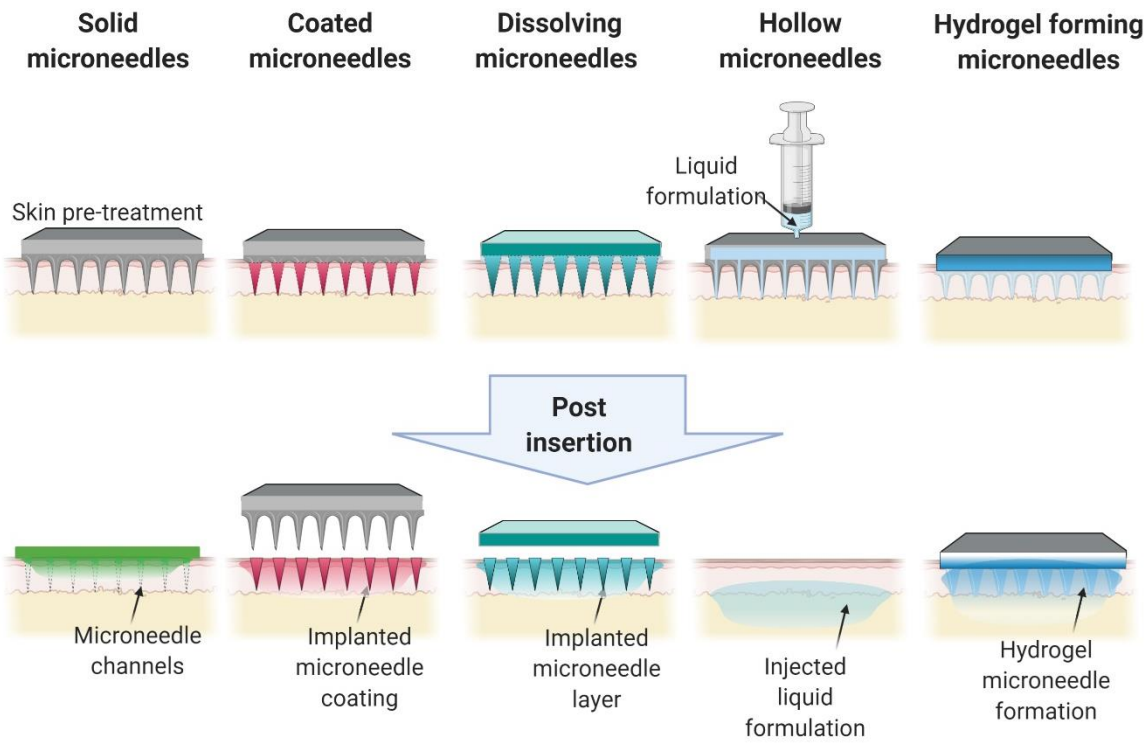

Figure 1-6 Schematic showing the different types of microneedles available for delivering drugs into and across the skin. The different types of microneedles are classified based on their drug delivery mechanisms. Solid microneedles are use as skin pre-treatment to create transient micropores, followed by topical application of the formulation at the application site. Coated microneedles are essentially solid microneedle that are coated with drug for instant delivery of therapeutic upon application into the skin. Dissolving microneedles implant the needle layer in the skin upon application which dissolve in the skin's interstitial fluid over time. Hollow microneedles mimic the hypodermic syringe needle, after insertion into the skin, liquid formulation can be infused through the needle bores. Hydrogel-forming MNs imbibe skin interstitial fluid upon skin application leading to the formation of swollen hydrogel network. This induces drug diffusion through the aqueous hydrogel network. Drugs are often stored above the microneedle layer in a lyophilised wafer prior to interstitial fluid uptake

1.4.2.1 Solid microneedles

Solid microneedles consist of fine arrays of micron lengths needles fabricated from either silicon, stainless steel and even biocompatible polymers. These types of microneedles are typically used as a skin pre-treatment to generate microneedle channels which is then followed by the application of a topical formulation. With solid microneedles-based drug delivery approach, the physiochemical

properties of the delivered therapeutic along with the needle design play a pivotal role on the permeation of therapeutic into and across the skin. One of the seminal works in the field by Banks *et al.* highlighted that solid microneedle skin pre-treatment, via the "poke-and-patch" strategy, leads to significant enhancement in the delivery of charged hydrophilic molecules across the aqueous microneedle channels. In contrast, the formation of such microneedle channels did not lead enhance the permeation of uncharged lipophilic compounds [94].

In the case of solid microneedles, the duration that microneedle channels remain open is a limiting factor for this drug delivery approach. Such limitation is attributed to the regenerative and elastic nature of the skin. The duration that microneedle channels remain viable using the 'poke and patch' approach has been reported to be as short as 15 minutes [95] and up to several hours [96,97]. This may reduce the amount of drug that could be delivered with this approach. However, strategies have been developed to prolong pore viability for drug delivery. These include the use of non-specific cyclooxygenase inhibitor such as diclofenac [98], HMG-CoA reductase such as fluvastatin [99] and even through simple occlusion [100].

1.4.2.2 Coated microneedles

These are a modified version of solid microneedle that contains an additional drug-polymer coating. Upon insertion into the skin, the microneedles are left in place over a set period to allow the coating to dissolve leading to drug release. This strategy is suitable for administering a bolus dose of actives for dermal or transdermal delivery [101]. This simple one-step application process avoids the problem of formulation misalignment with microneedle perforated skin as seen with the "poke-and-patch" strategy with solid microneedles.

However, such microneedle strategy is not without its disadvantages. One of the downsides of such strategies is that only limited amount of drug could be coated onto the tip and shaft of the microneedles [101]. Additionally, concerns have been raised on how well the coating adheres to the microneedle upon insertion into the skin as such coating may flake off prematurely before piercing

the skin leading to the unwanted loss of therapeutics. However, several strategies have been explored to ameliorate such drawbacks. For instance, Gill *et al*. found that increasing the insertion speed and tailoring the microneedle design (by fabricating a pocketed microneedle) may help improve coated microneedle delivery of therapeutics while reducing the propensity of coat flaking during insertion [101].

1.4.2.3 Hollow microneedles

These microneedles are reminiscent of hypodermic injection as it facilitates the flow of therapeutics via the microneedle bore into the skin. This approach permits more control over drug delivery rate by pressure driven flow [87]. Through the use of hollow microneedles, one may attach the microneedle system to an already available injectable formulation. This would allow pneumatic-driven delivery of formulation similar to conventional hypodermic injection.

However, this approach limits the selection of therapeutic to a liquid formulation. The use of liquid formulation in hollow microneedles also introduces the risk of leakage which can contribute to concerns with regards to payload delivery. Also, the presence of a hollow bore in the design reduces the mechanical strength of hollow microneedle, leading to an increased risk of fracture upon insertion into the skin [102]. In addition, hollow microneedles may be blocked by compressed dermal tissue which limits the available outlets for the formulation to flow out [103]. Nevertheless, such problem has been resolved via partial microneedle retraction post-insertion which induce tissue relaxation thus enhancing fluid infusion [104,105]. However, the retraction of microneedles to promote fluid infusion has been associated with increased pain sensation [106].

1.4.2.4 Dissolving microneedles

This category of microneedles involves encapsulating drugs within a polymeric matrix that forms the bulk of the microneedles. Unlike coated microneedles, the entire microneedle shaft dissolves upon insertion into the skin. The complete dissolution of dissolving microneedle results in no biohazardous sharps post insertion which is an advantage of using dissolving microneedles over solid, coated and

hollow designs. Also, meticulous design of the microneedle matrix permits drug delivery profile to be tuned for bolus or even sustained release over several weeks [107–109].

However, in meeting such requirements, the microneedle need to be inserted into the skin for a specified period before being removed. Such insertion time may vary from as quick as 1 min to as long as an hour for effective dissolution [107,110]. Furthermore, the deposition of polymer within the skin post-insertion has raised safety concerns. This is particularly true if such systems are to be used in the management of chronic conditions. However, this issue may be circumvented via utilising a regulatory approved biodegradable polymer which degrades via hydrolysis into innocuous molecules overtime [4]. In addition, another limitation of dissolving microneedles is that the microneedle arrays may not possess sufficient mechanical strength to pierce the skin causing the needle to fracture or buckle under pressure. Besides that, some dissolving polymeric microneedles may have a heating step in the manufacturing process that may lead to degradation of the therapeutic [107,111]. In order to eliminate this limitation, most dissolving microneedles are now made from aqueous polymer blends rather than hot polymer melts [112–114].

1.4.2.5 Hydrogel forming microneedles

Developed by Donnelly and co-workers, this is the latest class of microneedle which consist of microneedles fabricated from hydrogel-forming polymeric matrices. Upon skin application, this class of microneedles absorb interstitial fluid from surrounding skin tissue leading to hydrogel swelling [115]. This leads to the formation of continuous, unblocked hydrogel channels which therapeutic could diffuse into and across the skin. Additionally, the rate of drug delivery can be tuned by the density of crosslinking within the hydrogel network permitting controlled drug delivery kinetics. Also, such microneedles have also been utilised for biodiagnostic purposes through the analysis of interstitial fluid that is absorbed by the microneedles upon insertion into the skin [115–117].

This class of microneedle technology has been proposed to overcome the limitation associated with other classes of microneedles. The one-step application of hydrogel-forming microneedle linked to a

drug-loaded patch overcomes the cumbersome two-step application process associated with solid microneedle skin pre-treatment. It has frequently been reported that the rate of pore closure after solid microneedle pre-treatment differs considerably leading to considerable variation in drug delivery. Hydrogel-forming microneedles have the advantage of resisting pore closure while in place. This class of microneedle also has the added benefit of avoiding deposition of microneedle tip post-insertion. Deposition of such debris has been a contentious issue with regards to dissolving microneedles as well as solid microneedles that may fracture upon insertion. The ability of such needles to be removed intact post insertion is attributed to viscoelastic properties conferred by the hydrogel materials used to fabricate the microneedles [117]. However, due to the hydrophilic nature of the hydrogel conduit, this type of microneedle may not be suitable for the delivery of hydrophobic drug molecules. In addition, rapid delivery of actives may not be readily achieved with these hydrogel-forming microneedles due to the slow diffusion of actives from the reservoir into the skin through the hydrogel conduits.

There is no “one size fits all” microneedle system for the delivery of drug across and into the skin. Judicious selection of microneedle system tailored to the nature of the disease and physiochemical properties of the drug is paramount in the design of an effective microneedle system to deliver the payload. As an emerging pharmaceutical technology, microneedles display considerable advantages such as being patient friendly, easy to apply and remove, minimally invasive and painless. The versatility and diversity in microneedle designs allow the device to be tailored to nature of the disease intended to be treated. Such advantages may have a significant clinical impact in the foreseeable future. However, before such transition could occur, careful characterisation and evaluation of the microneedle system developed must be done in order to understand if the delivery system fits the intended purpose.

1.4.3 Characterisation and evaluation of microneedles

Microneedles vary in their dimensions and materials depending on their desired applications and needs. The characteristics and performance of these microneedles in drug delivery need to be assessed by the appropriate selection of experimental setups and analytical techniques in order to understand if the microneedle systems are suitable for the intended use.

1.4.3.1 Visual Inspection and Microscopy

The design of microneedles is dictated by a multitude of interdependent materials and fabrication parameters. Such micron scale needles need to possess appropriate mechanical strength, toughness and hardness to pierce the *stratum corneum* whilst at the same time be able to resist fracture and buckling failure. Before highlighting the methods and techniques used in evaluating the performance of microneedles, it would be worthwhile to illustrate the common terms which are frequently used to describe the architecture of a microneedle patch as shown in Figure 1-7.

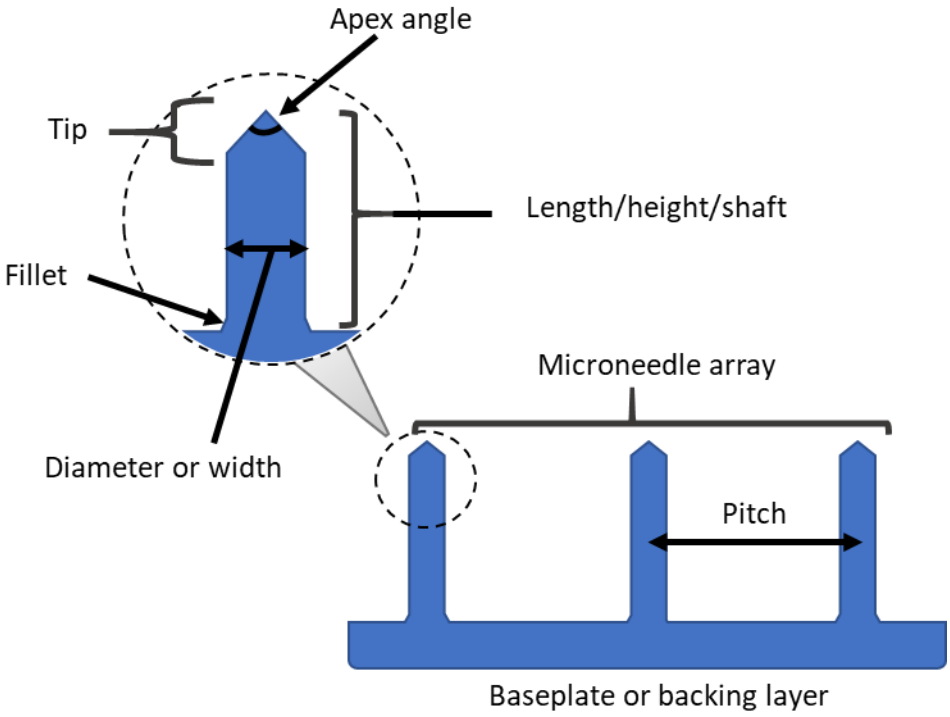

Figure 1-7 Common terminologies used in describing the architecture of a microneedle patch.

It is widely reported in the literature that microneedle geometry post-fabrication are evaluated through visual inspection, stereo microscopy and scanning electron microscopy (SEM) [101,118,119]. Such characterisation permits researchers to visualise the microneedle dimension, shape, surface morphology and needle distribution pattern on the array post-fabrication. This inspection also permits the experimenter to visualise the geometry of the microneedle fabricated and estimate the radius of curvature (tip radius), an integral characteristic in microneedle design which dictate the efficiency of insertion [120,121]. In addition, such examination of microneedle geometry is also critical in determining if the fabrication process produces needles of uniform geometry with sharp tips. The ability to clearly visualise microneedle geometry is illustrated in Figure 1-8 . Any heterogeneity in the microneedle architecture may result in poor penetration of the microneedle devices in some region of the skin.

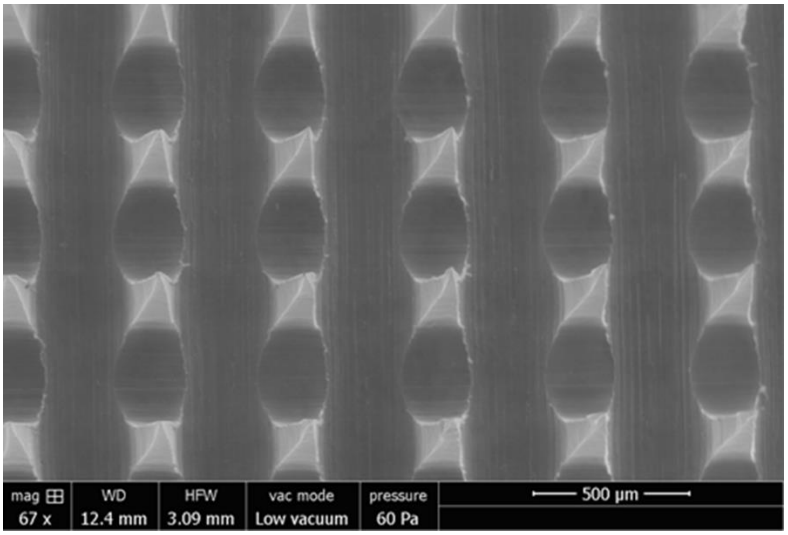

Figure 1-8 An example of a scanning electron microscopy (SEM) image of microneedle fabricated from starch-gelatine. Microneedle and SEM image were prepared by the PhD candidate himself, Mr Akmal H Sabri.

Microneedle tip geometry plays a pertinent role in the performance of microneedle. Early microneedle geometries consist mostly of cones and pyramids. Davis *et al*. were the first to explore how hollow microneedle tip design and geometry play an essential role in microneedle insertion. The group, through experimental measurements along with analytical and finite element modelling, identified that efficient microneedle insertion may be achieved by using microneedle with a small tip

radius. This is attributed to a smaller contact area between microneedle and the skin, thus generating a higher pressure at the tip which permits improved penetration. Additionally, the group also discovered that a hollow microneedle tip with a thick wall endows robustness to the microneedle patch against fracture upon insertion [102].

Aoyagi *et al.* extended the knowledge on how microneedle tip geometry influences insertion by systematically exploring the effect of tip geometry and needle width on the performance of biodegradable microneedles. The group found that biodegradable microneedles possessing low tip angle (15-30 ^{o}) and thin needle shaft (of 120 µm) were effective in enhancing microneedle insertion without causing tensile failure [122]. Furthering this, Li *et al.* through drawing lithography and laser-cutting techniques have fabricated microneedles of varying bevel angel (15 $^{\circ}$, 45 $^{\circ}$ and 90 $^{\circ}$) of similar wall thickness (30 µm). In their work, they have shown that hollow microneedles possessing a low angle bevel tip of 15° required the least force to pierce the skin, which is in agreement with what was originally reported by Davis *et al.* [123].

Additionally, the geometry of the microneedle itself has been shown to impact the insertion behaviour. Bediz *et al*. have shown that solid microneedles with an obelisk design were more effective in enabling deeper and more reproducible insertion in comparison to pyramidial shaped microneedle. This was attributed to the increase in insertion force with increasing depth for pyramidial microneedle, an issue which was not apparent in obelisk shaped microneedles [108]. However, such design parameters resulted in an opposite effect with hollow microneedles. This was highlighted in insertion studies by Chua *et al.* where they found that tapered/pyramidal hollow microneedle resulted in improved penetration in comparison to obelisk/straight hollow microneedles. In addition, the lumen of straight hollow microneedles were more likely to be occluded than that of tapered hollow microneedles as skin materials are displaced during insertion [121].

Additionally, the use of fluorescently labelled molecules and dyes may aid the identification of molecules that have been successfully incorporated into the microneedle patch [124–126]. Successful

incorporation of fluorescently labelled molecules and dyes may be visualised through the use of confocal laser scanning microscopy (CLSM), fluorescent microscopy or even visual inspection. Such inspection is pertinent as this provides the investigator with preliminary information with regards to the location of the incorporated molecules along the microneedle structures-tip, shaft or even the backing layer [127]. In addition, such inspection also provides information regarding the reproducibility and consistency of incorporating the molecule of interest into the microneedle structure during the fabrication process. Figure 1-9 illustrated the use of different dyes and fluorescence in elucidating the location of the incorporated molecules throughout the microneedle structures.

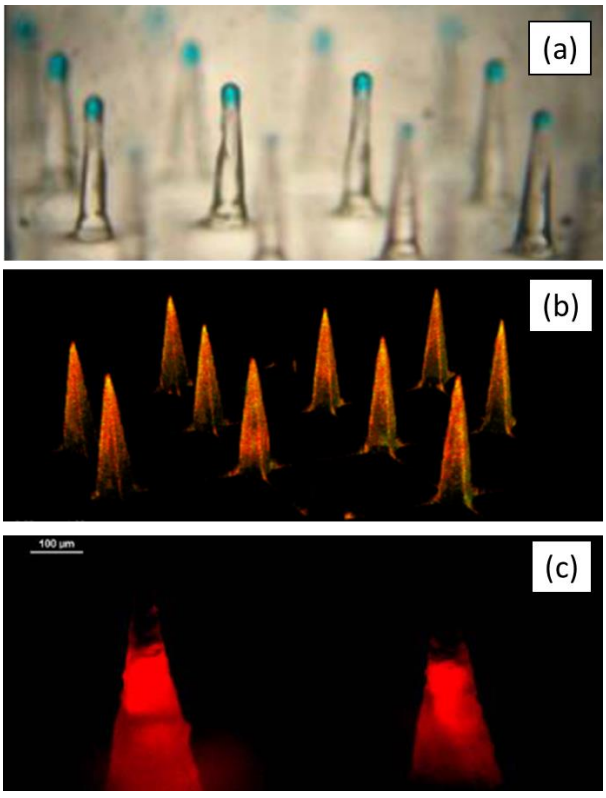

Figure 1-9(a) Utilisation of brilliant blue dye to visualise the successful and reproducible coating of microneedle array during fabrication process. Reproduced from Liu et al. [125]*. (b) An example of microneedle patch incorporated with fluorescently labelled inactivated polio vaccine particles and N-trimethyl chitosan chloride to visualise the localisation of labelled biomolecules within the patch using CLSM. Reproduced from Maaden et al.* [127] *(c) Using fluorescent microscopy to visualise the successful incorporation of Nile-red loaded nanoparticles into microneedle shafts with the absence of nanoparticles at the tip of the microneedles. Reproduced from Maaden et al.* [126]*.*

1.4.3.2 Strength test

In order for microneedle to perforate the skin and promote the permeation profile of therapeutics and cosmeceuticals, the device ought to possess sufficient mechanical strength to pierce the skin. The skin is well known for its inherent viscoelastic property which reduces the piercing capabilities of microneedles [128]. Should a microneedle device possess poor mechanical property, this will result in skin folding around the needle tips leading to poor penetration and microneedle tip buckling [105].

Thus, it is of great importance that strength test coupled to insertion studies are performed to evaluate the penetration capability of microneedles. The failure force per needle needs to exceed the force required for successful microneedle insertion into the skin to result in successful microneedle application. The successful insertion force for microneedles into skin barrier is approximately 0.098 N/needle [129,130] to penetrate the stratum corneum. However, a study by Donnelley *et al.* in 2012 have indicated that an insertion force as low as 0.03 N per needle may suffice in piercing the stratum corneum [115].

The most common test typically employed in evaluating the mechanical strength of microneedle is the axial compression test or the needle failure test [131]. Common instrument includes the TAXT analyser. This analysis involves a microneedle array attached to a test probe which then presses the microneedle at a pre-determined speed onto a flat metal block of aluminium until a peak maximum is registered in the force-distance curve. This is also known as the fracture force of the microneedle [131].

The test is frequently carried out to ascertain the mechanical strength that a microneedle could withstand before it deforms. This is done by measuring the maximum force registered by the texture analyser before microneedle is deformed. An example of a force displacement curve during a microneedle compression test is shown Figure 1-10. The distance travelled by the microneedles during the axial compression test is plotted on the *X*-axis while the force recorded by the probe is plotted on the *Y*-axis. It is apparent that there is a slight non-linearity to the force-displacement graph which is attributed to the slight inadvertent movement of the microneedles over the metal block during

compression as well as the minimal buckling of the microneedle itself. In the graph, the peak incident force is assumed to correspond the moment when all microneedles on a patch have fully fractured or collapsed [131]. The mechanical strength of microneedles is frequently reported as "force per needle". This property is calculated from the maximum force registered on the texture analyser divided by the number of needles per array. When performing this form of tensile strength measurement, it is imperative that the whole microneedle patch is flat. This is because the presence of any curvature on the microneedles patch may lead to uneven force distribution during the tensile strength measurement resulting inaccurate tensile strength measurements [131].

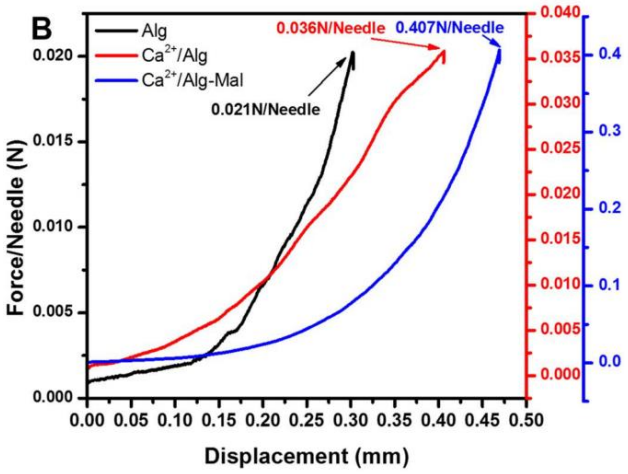

Figure 1-10 Example of a force displacement curve during a microneedle compression test. Reproduced from Zhang et al. [132]

This method of evaluating the tensile strength of microneedle using the whole patch, also known as bulk compression, only provide an average fracture force for the microneedle with the assumption that all the microneedles fracture simultaneously at the peak incident force. Such assumption may not be accurate as some needles in an array may buckle or break prematurely during the compression test. This may lead to an overestimation of the microneedle tensile strength. Recently, Romgens *et al.* highlighted the importance of estimating the mechanical strength of microneedles using single needle compression test relative to evaluating a whole microneedle patch. This allows the investigator

to circumvent the erroneous assumption made when performing a compression test on a microneedle patch [133].

In addition, the bulk compression method does not provide any insight into the variability in the fracture force across individual microneedles across the patch. Due to this limitation, Du *et al* explored the use of micromanipulation as a method for precise and comprehensive evaluation of the mechanical properties of individuals polymeric microneedles within a patch. Du *et al* discovered that indeed the mechanical strength of microneedles across one patch may vary significantly which would not be detected by the conventional tensile strength test currently used [134]. Another limitation worth highlighting with the conventional tensile strength test is the difference in the force distribution along the length of the microneedles during test relative to actual skin insertion. When conducting the tensile strength test, the microneedles are pressed on a flat and rigid surface that result in most of the force applied to be focussed on the tip of the microneedles. In contrast, during the skin insertion the force are distributed over the length of the microneedles due to elastic nature of the skin that causes the tissue to fold around the needles as the patch is applied to the skin [135].

In addition, most method used to evaluate the mechanical strength of microneedles only measures the tensile strength via axial compression. The values obtained from these tests are also known as the axial fracture force which represent the force needed to break the microneedles via vertical compression during skin insertion. It was later discovered by Gittard *et al* that the force experienced by microneedles during skin insertion is much lower than axial fracture force obtained from the conventional tensile strength test [135]. Despite the force required to puncture the skin being much lower than the axial fracture force recorded, incomplete microneedle insertion into the skin have been reported. This may be attributed to the heterogenous contour of the skin causing unintentional needle slippage during insertion that ultimately result in microneedle breakage due to shear force rather than axial compression [136]. Therefore, another limitation of the tensile strength test is the inability of the test to account for the shear force needed to fracture the needles. Several research group have modify

the test by placing the microneedles perpendicularly to the test probe as a method to estimate the shear force needed to fracture the microneedles [136,137]. However, a notable limitation for this variant of the test is the need for the investigator to manually align the probe on the microneedle during experiment. Such requirement is indeed challenging considering the micron scale of the needles which would inadvertently introduce experimental inaccuracies during the test [138].

Nevertheless, it is worth noting that the mechanism of compression for a single needle is very different from the insertion profile of a microneedle array. When an array of microneedles is subjected to a compression test, the force applied is likely to be distributed among the needles on the array leading to a phenomenon known as the 'bed of nail effect' which reduces the force experienced by a single needle on the array. Such effect is not apparent during a single needle compression test. Regardless of the approach taken in measuring the microneedle tensile strength, it could be agreed that the microneedle compression test is the most commonly employed in microneedle characterisation. This is because the test permits the investigator to predict should the fabricated needles possess sufficient strength to breach the *stratum corneum* during insertion studies.

1.4.3.3 Insertion studies

It is well known in the microneedle community that complete insertion of the whole microneedle length is difficult to achieve due to the inherent viscoelastic properties of the skin. The depth of microneedle insertion falls under two categories. True depth and estimated depth. Methods which provide true depth include confocal microscopy, X-ray transmission computational tomography and optical coherence tomography (OCT). On the other hand, method such as histological cross sectioning and staining provide estimated depths of microneedle insertion.

Conventionally, microneedle insertion studies are frequently carried out using excised animal skins [109,139,140] or human skins [101,141]. This involves placing an excised skin with the *stratum corneum* face up on a flat surface such as parafilm or a wooden cork to mimic the underlying soft tissue. The desired treatment site is then gently stretched to even out any skin folds while microneedles are

manually applied into the skin. After the microneedles are inserted and removed, the investigator will then apply a dye to the treatment site. Common dyes used to stain microneedle channels include gentian violet [118], methylene blue [120] and trypan blue [141]. Should successful microneedle insertion take place, one may observe the staining of microneedle channels. Such staining arises from the ability of the dye to selectively bind to the nucleus of the underlying epidermal and dermal cells over the anucleated *stratum corneum*. Alternatively, this study may be carried out *in vivo* using healthy human volunteer or animal such as nude mice models. Furthering this, the penetration success ratio of microneedles may be calculated by counting the number of dye-stained spots observed to the total number of microneedles per array [142] .

When performed *ex vivo*, microneedle insertion studies may be accompanied with histological sectioning that allows the investigator to visualise the depth of microneedle pores and estimate the length of microneedle penetration. Should the fabricated microneedle contain fluorescently labelled molecules, the microneedle insertion site may be visualised using fluorescent or confocal microscopy [143–145]. Examples of microneedle insertion sites visualised via microscopy post histological sectioning are shown in Figure 1-11. Despite the popularity of visualising microneedle channels using histological sectioning and microscopy, this process is quite lengthy and cumbersome, with the propensity of altering the skin structure during the freezing and sectioning steps [146].

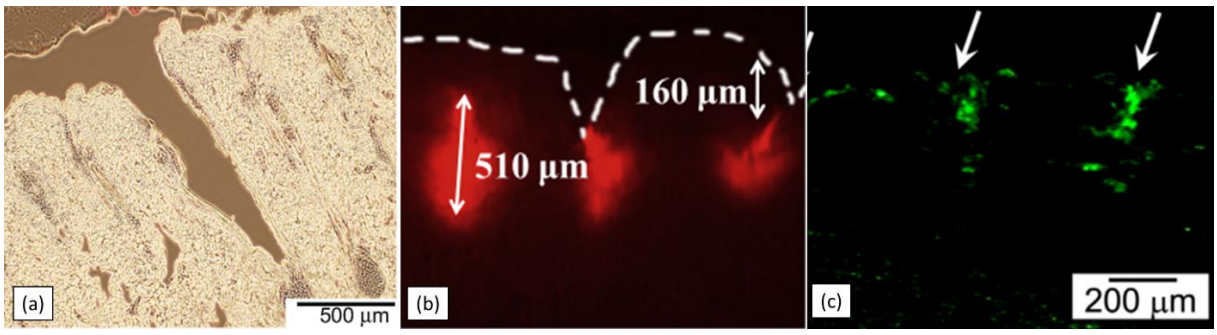

Figure 1-11(a) Example of microneedle insertion site visualised by microscopy after skin cross sectioning. Image reproduced from Lee et al. [147] *Microneedle insertion site imaged via fluorescent microscopy after sulforhodamine*

B was deposited into the skin post insertion. Reproduced from Zhu et al. [148]*. Microneedle insertion site containing FITC-dextran visualised via fluorescent microscopy. Reproduced from Ling et al.* [144]

Due to the limitation of histological sectioning in investigating microneedle insertion, alternative techniques have been explored in an effort to elucidate the true depth of microneedle insertion into the skin in a non-invasive manner. Insertion of microneedles may be observed in real time using optical coherence tomography (OCT) which is a non-invasive method for characterising skin structure. In addition, this technique permits real time monitoring of microneedle insertion into the skin [149]. Non-invasive diagnostic techniques such as OCT on human volunteers may be the most reliable method to study microneedle penetration as this overcomes the issue of architectural and biological differences between animal and human skin [150].

In addition, more advance analytical technique such as computerised X-ray tomography have been employed to study the penetration profile of microneedles. This was first carried out by Loizidou *et al*. This non-destructive technique utilises a series of X-ray scans taken at different rotation angles that generate 3D volumetric data. Such techniques allow researchers to visualise microneedle insertion in a 3D manner. However, the method is limited for microneedle materials that display X-ray contrast properties such as gold [146]. Examples of X-ray tomography and OCT images showing microneedle insertion into the skin is shown in Figure 1-12.

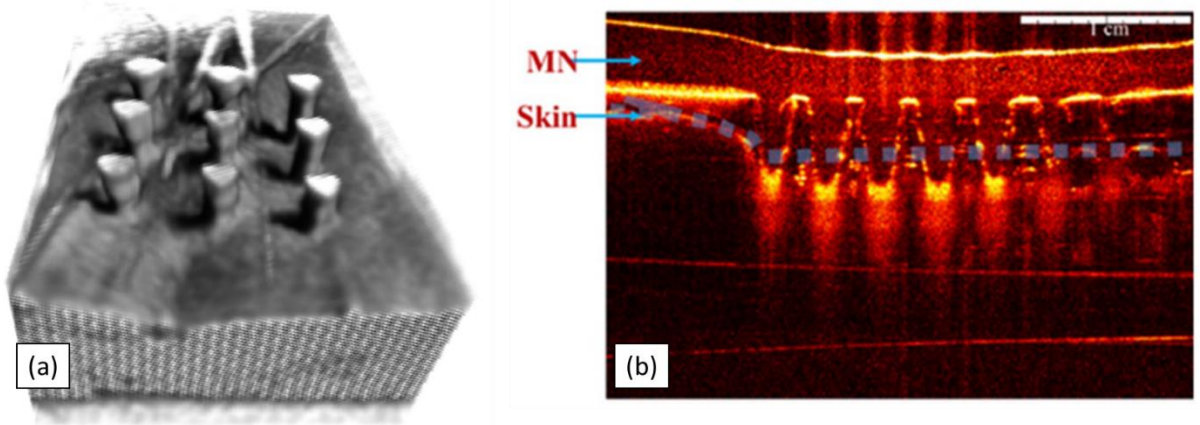

Figure 1-12 (a) An example of a X-ray computer tomography of a gold coated microneedle inserted into porcine skin which was imaged using Bruker microCT SkyScan 1174. Reproduced from Loizidou et al. [146]*. (b) An optical coherence tomography image of microneedle inserted in neonatal porcine skin. Reproduced from Vora et al.* [151]*.*

Additionally, Larrañeta *et al.* have developed a simple and validated insertion model for microneedles using thermoplastic sheet made of olefin-type polymer. Such polymer have been shown to simulate the elasticity and mechanical properties of the skin allowing researchers to evaluate the insertion depth of various microneedles in a fast and rapid manner [151]. The insertion depth may be estimated by multiplying the number of layers penetrated by the microneedle to the thickness of each Parafilm M® layer (127 µm). Additionally, a more accurate penetration may also be evaluated using optical coherence tomography. The simplicity of this test that obviates the use of biological material have slowly gained popularity within the microneedle community [131].

1.4.3.4 Permeation studies

The most common *in vitro* method employed in studying microneedle-enhanced dermal permeation of compounds is through the use of diffusion cells. In general, these diffusion cells consist of a donor compartment and receptor compartment that is separated by a membrane (typical *ex vivo* human or animal skin, or an artificial polymeric membrane). Formulations containing the permeants of interest is typically introduced into the donor compartment that diffuse across the membrane of choice and into the receptor compartment. The permeant that has diffused into the receptor compartment are then analysed by means of analytical techniques such as high-performance liquid chromatography (HPLC). Typically, diffusion cells are classified into two main types: static (Franz-type) and flow-through (Bronaugh-type) as shown in Figure 1-13.

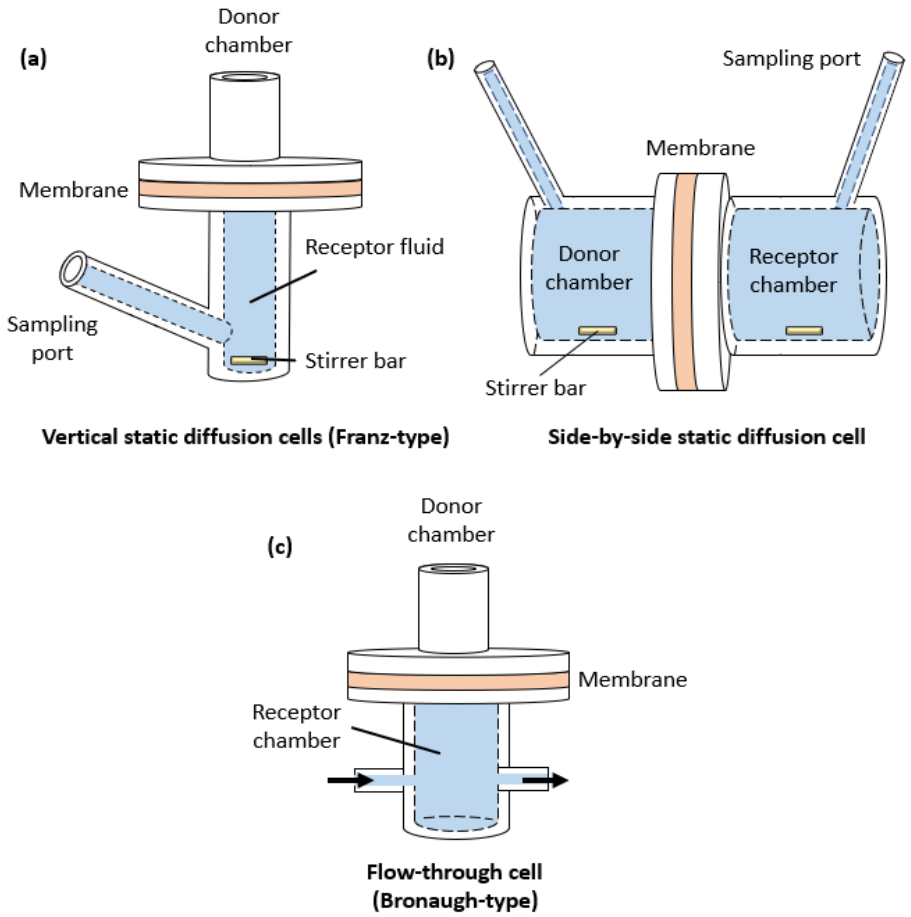

Figure 1-13 Types of diffusion cells used in studying skin permeation (a) vertical static diffusion cell (b) side-by-side static diffusion cell (c) flow through cell.

In static diffusion cells, permeants partition into a fixed volume receptor compartment that is thermostatically controlled. In addition, the receptor media is continuously mixed via a magnetic stirrer bar in order to maintain a sink condition within the receptor compartment [152]. Besides that, a defined volume of the receptor media is manually sampled at predefined intervals and replaced with an equal volume of fresh receptor media. Such a sampling procedure allows the investigator to plot the permeation profile of the investigated compound over time. Alternatively, the receptor compartment may be sampled at the end of the experiment to determine the cumulative amount of compound of interest that has permeated.

Franz-type diffusion cells can be further sub-classified into side-by-side or upright based on how the skin is orientated in the diffusion cell. The earliest type of diffusion cell used in percutaneous

absorption studies was the side-by-side static diffusion cells. In these diffusion cells both skin surfaces-*stratum corneum* and dermis are fully immersed in donor solution and receptor media, respectively, with both solutions being stirred simultaneously by means of stirrer bars. However, the side-by-side diffusion cells is rarely used in skin permeation study nowadays as the skin is more susceptible to damage with such experimental set up. In addition, there is the possibility of overestimating the permeation profile of compounds due to excessive and prolonged hydration of the *stratum corneum* by the donor compartment. In addition, the selection of formulations that are suitable to be investigated in side-by-side diffusion cells is limited to simple drug solutions. Nevertheless, the side-by-side static diffusion cells are occasionally used when evaluating drug delivery systems such as electroporation, iontophoresis and sonophoresis.

Due to the limitation of the side-by-side diffusion cells, another variant of the static diffusion cells known as the upright diffusion cell emerged in 1975. This type of diffusion was known as the Franz diffusion cell which was named after Thomas James Franz who invented the apparatus [153]. In this setup, the skin is clamped between a receptor compartment that contains the receptor media while the *stratum corneum* side faces the donor compartment and is open to the ambient laboratory environment. Such experimental set up aims to mimic the typical environment that the *stratum corneum* experiences [152,154].

The second type of diffusion cells is the flow-through cells which was introduced Robert Bronough and Raymond Stewart in 1984. Unlike the static diffusion cells, the flow-through cells maintain a sink condition by utilising a peristaltic pump that ensure continuous flow of the receptor media through the receptor chamber. Such continuous flow beneath the skin attempts to mimics the dermal blood circulation that carries exogenous compound away from the absorption site. In addition, these type of cells employs automatic sampling that overcome labour intensive sampling time points while enabling continuous monitoring of absorption profile [155]. Despite these advantages, the Franz-type

static diffusion is more commonly used in percutaneous studies as the flow-through cells are inherently more complex and costly thus limiting their utility [152].

In the field of microneedle research, the Franz-type diffusion cells are the most commonly employed experimental setup used to study the permeation of pharmaceuticals and cosmeceutical into and across the skin. However, compared to the conventional way of performing *in vitro* Franz cell permeation study, microneedle application is typically applied to skin first before the donor compartment is mounted onto the receptor compartment [119,126,156,157]. It is worth noting that a different set up should be adopted when designing a microneedle mediated Franz cell permeation study. Some may opt to exclude the process of dermatoming the skin prior to setting up the Franz cells as the action of dermatoming the skin may results in loss of skin tension and elasticity [158]. Such alteration in skin biomechanical properties during the dermatome process may lead to over-penetration of microneedle into the dermal tissue. Therefore it is of no surprise that some researchers opt to conduct *in vitro* microneedle mediated permeation study using full skin thickness in order to preserve the biomechanical properties of skin [66,126,151].

In general, *ex vivo* human skin provides the best model to study and estimate the permeation profile of drug molecules across the skin [159]. Nevertheless, access to *ex vivo* human skin is very scarce and expensive. This is further complicated by large sample variability in *ex vivo* human skin due to race, age, gender as well as the anatomical location where the skin was sourced. Furthermore, as large number of studies are typically required to access, develop and optimise pharmaceutical formulations means that *ex vivo* animal skins are usually used as surrogates to evaluate permeation of drug into and across the skin. Despite being more readily available than human skin, rodent skin is considered unsuitable as a surrogate to *ex vivo* human skin. This is because rodent skins have an epidermal thickness of less than 25 µm which is much thinner than that of human skin which have an epidermal thickness of 72 µm [160]. Besides that, the presence of *panniculus carnosus*, a muscular layer in rodent skin that is absent in human skin leads to differences in the mechanical properties of rodent skin

relative to human skin. Such anatomical differences between rodent and human skin can lead to an overestimation in drug permeability [161]. On the other hand, porcine skin is deemed to be the most histologically similar to human skin and thus is widely used as a surrogate to study the permeation of compounds into and across the skin [162]. The comparison in properties and anatomy of human and porcine skin can be summarised in the Table 1-1.

Table 1-1 Comparison between the properties of ex vivo human and porcine skin as reported by Jacobi et al [162], Ranamukhaarachchi et al [163] and Netzlaff et al[164]

Properties	Human skin	Porcine skin
Average thickness of *stratum corneum,* µm	19	21
Average thickness of viable epidermis, µm	76	72
Average thickness of dermis, mm	1.86	1.85
Average hair follicle density per cm^2	≈20	≈23
Average depth of extension of hair follicle into the dermis, mm	1.20	1.00-3.00
Average diameter of the orifice of hair follicle, µm	≈ 200 µm	≈ 170 µm
Mechanical properties measured as Young's modulus for full skin thickness, N/m^2	1.88 ± 1.23	1.74 ± 1.28
Arrangement of lipid within the *stratum corneum*	orthorhombic lattice	hexagonal lattice
Percent of dry weight of cholesterol from full thickness skin, (w/w) %	0.63 ± 0.15	0.62 ± 0.42
Percent of dry weight of cholesterol ester from full thickness skin, (w/w) %	0.56 ± 0.09	0.12 ± 0.07
Percent of dry weight of fatty acids from full thickness skin, (w/w) %	0.68 ± 0.16	0.34 ± 0.25

Percent of dry weight of triglycerides from full thickness skin, (w/w) %	5.48 ± 2.42	1.37 ± 1.02
Percent of dry weight of ceramide from full thickness skin, (w/w) %	0.65 ± 0.10	0.18 ± 0.07

It can be seen that there are some similarities of between human and porcine skin as shown in Table 1-1. This is true in terms of *stratum corneum*, epidermal and dermal thickness as well as the overall mechanical properties of the skin. Nevertheless, there are also some differences between human and porcine skin that is worth noting such as the differences in lipid profile (e.g cholesterol ester, triglycerides, fatty acid and ceramide) as well as the overall lipid arrangement within the *stratum corneum*. Despite these differences, there are a number of studies that have shown that both *ex vivo* porcine and human skin display similar permeability for both hydrophilic and lipophilic compound that justify the use of porcine skin as a surrogate to human skin [164,165].

However, it is also worth highlighting that the permeation results obtained from either *ex vivo* human or porcine skin should be carefully interpreted as it has been shown that the process of freeze-thawing the skin samples may result in some degree of damage to the skin through the formation of ice crystal within the *stratum corneum* [166]. Such damage to the *stratum corneum* may lead to an enhancement and overestimation in the permeation of compound across the skin when compared to *in vivo* conditions. However, a study by Barbero and Frasch found no significant difference in the steady steady-state flux of diethyl phthalate across fresh and previously frozen *ex vivo* skin (stored up to 18 months), suggesting that the effect of freeze-thawing in some instance might not be significant on the barrier properties of the skin [167]. On the other hand, it is worth highlighting that one of the major limitation of using freeze-thawed *ex vivo* skin is the inability to use these models to predict dermal drug metabolism as these skin samples are rendered metabolically inactive once the skin are frozen due to ischaemic necrosis [168]. Nevertheless, the use of frozen skin after thawing indeed provide some level of convenience in early formulation development studies in screening the permeation of

compound across the skin before such formulation are evaluated further *in vivo* using a suitable animal model.

1.4.4 Application of microneedles in skin cancers

Research in utilising microneedles for delivery of therapeutics for the treatment of skin cancers was pioneered by Donnelly *et al.* in 2008. Through the use of solid silicon microneedles and bioadhesive patches containing 19 mg aminolaevulinic acid (ALA) cm^{-2}, the group employed the 'poke and patch' strategy on a nude mouse model to enhance ALA delivery into the skin. This was the first study to demonstrate microneedles enhanced localised delivery of a photosensitiser to the skin. In addition, such a strategy also showed a reduced application time, and a reduction in the dose of ALA needed to elicit high-level of photosensitiser in targeted skin lesions [169]. Following these studies, various groups have explored different microneedle designs to deliver a range of anticancer drugs to the skin. Examples of such drugs include methyl aminolevulinic acid (MAL) [170], meso-tetra (N-methyl-4-pyridyl) porphinetetratosylate (TMP) [171], itraconazole [172] and 5-FU [66]. A summary of these studies is presented in Table 1-2.

Table 1-2 Summary of microneedle studies focussed on intradermal delivery of therapeutics for skin cancer. Abbreviations: ALA (aminolaevulinic acid), TMP (meso-tetra (N-methyl-4-pyridyl) porphinetetratosylate), MAL (methyl aminolaevulinic acid), protoporphyrin IX (PIX), 5-Fluorouracil (5-FU) programmed cell death protein 1 (PD1). The table is a simplified and updated version from the table that was published in the original manuscript.

Microneedle Type	Delivered therapeutics	Model to evaluate microneedle performance	Ref
Hydrogel forming.	ALA and TMP	*Ex vivo* (neonatal porcine skin)	Donnelly *et al.* (2014) [173]
Solid.	ALA	*Ex vivo* (murine and porcine skin) In vivo (murine model)	Donnelly *et al.* (2008) [169]
Solid.	TMP	*Ex vivo* (murine and porcine skin) and *in vivo* (murine model)	Donnelly *et al.* (2009) [171]
Dissolving.	ALA and MAL	*In vivo* healthy human volunteer (n=14)	Mikolajewska *et al.* (2010) [170]

Microneedle Type	Delivered therapeutics	Model to evaluate microneedle performance	Ref
Solid.	ALA	*In vivo* human with actinic keratosis or Bowen's disease (n=3)	Kolde *et al.* (2013) [174]
Coated.	ALA	*Ex vivo* (porcine skin) using Franz cell set up *In vivo* (murine model)	Jain *et al.* (2016) [175]
Dissolving.	anti-PD1 antibody	*In vivo* B16F10 murine model of melanoma	Wang *et al.* (2016) [176]
Dissolving.	anti-PD1 antibody	*In vivo* B16F10 murine melanoma model	Ye *et al.* (2016) [177]
Solid and hollow.	Itraconazole	*In vivo* human basal cell carcinoma murine model	Zhang *et al.* (2016) [172]
Solid.	Melanoma vaccine microparticle	Tumour challenge study using *In vivo* murine model	Bhowmik *et al.* (2011) [178]
Solid.	Nanoparticles containing DNA vaccine for malignant melanoma (MM) therapy	Tumour challenge study using *In vivo* murine model	Hu *et al.* (2015) [179]
Coated.	human melanoma antigens and adjuvant	*In vitro* cell culture using dendritic and T cells. *In vivo* murine model	Zeng *et al.* (2017) [180]
Solid.	5-FU	*In vitro* Franz Cell setup using mouse skin *In vivo* B16F10 murine model of melanoma	Naguib *et al.* (2014) [66]
Solid.	ALA	*In vivo* hairless murine model with SCC induced through UV irradiation	Wang *et al.* (2015) [181]
Dissolving.	Lanthanum hexaboride nanoparticles and Doxorubicin	*In vitro* drug release into (porcine cadaver skin). *In vivo* severe combined immunodeficient (SCID) murine model bearing 4T1 tumours.	Chen *et al.* (2016) [182]
Dissolving.	Doxorubicin and gold nanocage	*In vitro* B16F10 mouse melanoma cell line. *In vivo* B16F10 murine model of melanoma	Dong *et al.* (2018) [183]

Microneedle Type	Delivered therapeutics	Model to evaluate microneedle performance	Ref
Dissolving.	STAT3 siRNA encapsulated with polyethylenimine	*In vitro* B16F10 melanoma cells line. *In vivo* B16F10 murine model of melanoma	Pan *et al.* (2018) [184]
Dissolving.	Redaporfin™	In vitro Franz Cell setup using porcine skin In vivo biodistribution studies	Hamdan *et al.* (2018) [185]
Coated.	octaarginine/ BRAF siRNA nanocomplexes	*In vitro* A375 human melanoma cells line. *In vivo* A375 murine model of melanoma	Ruan *et al.* (2018) [186]
Coated.	PEGylated gold nanorod and doxorubicin	*In vivo* Release study in murine model *In vivo* A431 murine model of melanoma	Hao *et al.* (2018) [187]
Solid.	mesoporous organo-silica nanoparticles covalently linked with dabrafenib and trametinib	*Ex vivo* (porcine skin) *In vivo* A375 murine model of melanoma	Tham *et al.* (2018) [188]
Dissolving.	Mesoporous silica nanoparticles loaded with doxorubicin hydrochloride and indocyanine green	*In vitro* viability of MG-63 osteosarcoma cell line. *In vivo* murine model of osteosarcoma.	Pei *et al.* (2018) [189]

Microneedle Type	Delivered therapeutics	Model to evaluate microneedle performance	Ref
Solid.	Vismodegib	*In vitro* Franz Cell setup using porcine skin. *In vitro* skin irritation test using reconstructed human epidermis model.	Nguyen and Banga, (2018) [128]
Dissolving.	5-FU and indocyanine green	*In vivo* A375 murine model of melanoma and A431 human squamous carcinoma model	Hao *et al.* (2020) [190]
Coated.	Cisplatin	*In vitro* Franz Cell setup using porcine skin. *In vivo* A431 murine model of human squamous carcinoma	Uddin *et al.* (2020) [191]
Dissolving.	Doxorubicin and indocyanine green	*Ex vivo* (porcine skin) insertion and drug release *In vivo* B16F10 murine model of melanoma	Song *et al.* (2020) [192]
Dissolving.	Curcumin	*Ex vivo* (porcine skin) insertion and drug release	Abdelghany *et al.* (2019) [193]
Dissolving.	Cytotoxic T-cell epitope peptide	*In vivo* B16F10 murine model of melanoma	Kim *et al.* (2019) [194]

Microneedle Type	Delivered therapeutics	Model to evaluate microneedle performance	Ref
Dissolving	HA15, an emerging antimelanoma drug	*In vitro* Franz Cell setup using murine skin *In vivo* B16F10 murine model of melanoma	Chen *et al.* (2020) [195]

For example, Jain *et al.* developed a 5-ALA coated microneedle to improve dermal delivery of the photosensitizer to treat skin tumours. The group showed that the 5-ALA coated microneedle patch allowed improved delivery of 5-ALA deeper into the tumour lesion in comparison with topical application of 5-ALA cream. Interestingly, the coated microneedle also displayed better efficacy in the *in vivo* murine skin tumour model despite delivering a lower dose relative to topical cream application [175].

On the other hand, Naguib *et al.* demonstrated, using a murine model, the feasibility of using solid microneedles to enhance the intradermal delivery of 5-FU to treat skin tumours. In their *in vitro* work, the group demonstrated that 5-FU flux increased by 4.5-fold when 5-FU cream was applied on microneedle-perforated murine skin compared to cream application on intact skin. *In vivo* work using a mouse model with B16-F10 melanoma tumour showed that topical application of 5-FU cream (5% w/w) on microneedle-perforated skin showed significant tumour inhibition relative to intact skin [66]. Although preliminary in nature, these studies highlight that microneedles hold great potential in improving intradermal delivery of antineoplastic agents to improve the treatment efficacy of skin cancer. More recently, several groups began to explore the strategy of delivering anti-melanoma vaccines as a method to treat and prevent the development of metastatic melanoma [178,179,196]. Recently, it has been proposed that delivery of anticancer agents into superficial skin tumours via

dissolving microneedles may be more efficacious than nanosized carriers as microscale structures of microneedles enable long term retention of chemotherapeutics at tumour sites [182].

However, it is worth highlighting that due to the metastatic nature of metastatic melanoma, microneedles may not be a suitable standalone intradermal therapy, unless they are used for transdermal delivery of antineoplastic agents for systemic management of metastatic melanoma. In such a setting, microneedle-based treatment for melanoma ought to be used as an adjuvant to the standard metastatic melanoma care plan. Therefore, should research on utilising microneedles for the treatment of melanoma continue, researchers in the area ought to aware of the systemic nature of the disease and evaluate how microneedles may be able to be used to treat the metastatic melanoma that has invaded to other sites of the body. If such a strategy is deemed ineffective, research on microneedle-based skin cancer therapy should focus on more localised tumours such as BCC or some variants of SCC.

1.5 Time of flight secondary ion mass spectrometry (ToF-SIMS) in skin permeation analysis

1.5.1 Limitations of current methods to track dermal distribution of therapeutics

Detailed analysis of the dermal distribution of pharmaceuticals within the skin strata is paramount in order to evaluate the permeation enhancement effect conferred by microneedles for targeted skin delivery. Traditionally, chromatographic analysis (e.g., high-performance liquid chromatography, HPLC) is frequently implemented in microneedle permeation studies in order to evaluate the delivery of drugs into and across the skin. However, the tissue manipulation steps and extraction procedures lead to the loss of valuable spatial information regarding drug localisation within the skin tissue [197].

In order to overcome this limitation, microneedle permeation studies frequently use fluorescently-tagged molecules in order to track their distribution within the skin [104]. This method of tracking dermal distribution can be achieved via the use of confocal laser scanning microscopy (CLSM). CLSM utilises point illumination via the use focused laser beam that is rastered across the sample of interest. The emitted fluorescence from the in-focus plane is passed through a pinhole onto a detector, which the

measures the fluorescence from the site of analysis. Any out-of-focus fluorescence is blocked by the pinhole, which is said to be confocal with the focal point of the objective lens. CLSM has been used to tracked the permeation of compounds delivered using microneedle-based delivery systems [129,132,144]. Although this approach allows the experimenters to track drug localisation within the skin, the use of fluorescent tagging with this method alters the physiochemical properties of molecules leading to erroneous estimation of drug distribution in biological tissues [198]. In addition, the need for different fluorescent tagging to track the dermal distribution of multiple molecules complicates the method even further.

Some of the techniques that offer label-free imaging of dermal drug distribution include confocal Raman microscopy and stimulated Raman scattering microscopy. These techniques have been used to visualise the dermal distribution of several pharmaceuticals such as 5-fluorouracil [199], ketoprofen [200], and terbinafine [200]. In addition, Confocal Raman microscopy and stimulated Raman scattering microscopy offer the advantage of being non-destructive techniques that require minimal sample preparation prior to analysis [201]. Although these methods offer researchers the ease and feasibility to visualise dermal drug distribution in a label-free manner, some compounds may not have a diagnostic Raman signal, thus limiting the range of molecules which could be tracked by the technique. Furthermore, the molecule of interest which do have a diagnostic Raman signal should be present at sufficient concentration to allow detection. Another issue associated with Raman-based imaging is the high level of autofluorescence from biological tissue which can mask the weak Raman signal thus limiting the utility of these techniques to map dermal drug distribution [202]. Hence, there is a clear need for advanced analytical techniques to be utilised in the field of microneedle research to allow researchers to track drug distribution within skin tissues in a label-free manner with high chemical sensitivity for a wider range of drug molecules.

1.5.2 Principle of ToF-SIMS Analysis

Time-of-flight secondary ion mass spectrometry (ToF-SIMS) is a powerful surface analytical technique that confers excellent mass resolution, chemical sensitivity and high spatial resolution [203,204]. Analysis of samples using ToF-SIMS permits us to chemically map the spatial distribution of a compound of interest as well as providing information on how such distribution changes with depth. The general component of a ToF-SIMS instrument is illustrated in Figure 1-14.

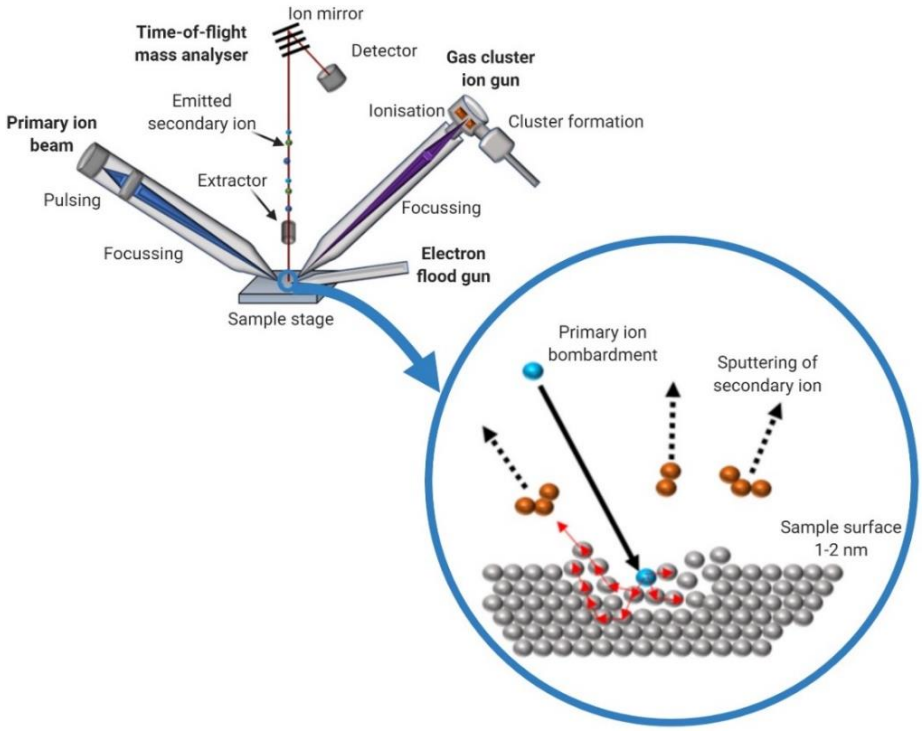

Figure 1-14 A general schematic of the ToF-SIMS instrument. The inset shows a close up of the sample analysis taking place as a result of the collision cascade (red arrows) caused by primary ion bombardment onto the sample surface. Adapted from Saleem & Galla 2010 [205]

ToF-SIMS employs the use of a focussed primary ion beam that is rastered across the samples surface. Sample analysis is conducted under ultra-high vacuum (~ 10^{-7} Torr) as this ensure the ion beam is focussed leading to high spatial resolution. The bombardment of the primary ion beam on the sample will lead to an energy transfer process from the primary ion beam to the target surface leading to molecular fragmentation. In addition, such energy transfer known as the collision cascade, shown in

red arrows in Figure 1-14, endows the molecular species at the target surface with the ability to overcome the surface binding energy leading to the emission of secondary particles through a process known as sputtering. These desorbed secondary ions are then then extracted through a time-of-flight tube which separates and detects the particles based on their mass-to-charge (*m/z*) ratio [205,206]. The recorded ion can be represented as a single spectrum of the analysed surface or a mass spectral image where each pixel is a complete mass spectrum. Such mass spectral images are of heuristic value in identifying how ions of interest are distributed across the analysed surface [207].

ToF-SIMS may be operated under two different modes: static and dynamic. In static SIMS, the ion dose delivered is low (< 10^{12} cm^{-2}) with a low flux (10 pA^{-5} nA) [208]. The low primary-ion dose delivered results in approximately less than 1 % of the uppermost surface monolayer being sampled [209]. With this operational mode, the primary ion dose delivered is below the static limit and ensures that statistically no region on the sample will be rastered twice during the acquisition period. This mode of analysis also ensures only the surface (1-2 nm) of the samples are analysed [210].

On the other hand, dynamic SIMS describes the operation of the primary ion beam at high current flux while delivering the primary ions at a dose which is above the static limit. This operating parameter leads to sample surface erosion. This operation mode is frequently used to elucidate changes in a sample's chemical composition and distribution as a function of depth [208].

Depth profiling using ToF-SIMS may be carried out using either monoatomic ions or cluster ions. However, monatomic ions sources such as Ga^+ and Cs^+ cause much deeper damage into the sample upon impact with low sputter yield compared to cluster ion sources. In addition, subsurface mixing may ensue followed by substantial topography development. These drawbacks severely reduce the depth resolution that could be achieved during depth profiling [211,212]. In contrast, cluster ions do not penetrate deep into the sample. Upon impact, the energy from cluster ions is deposited within the first few nanometer of the surface. This leads to high sputtering yields with minimal subsurface damage as well as preserving larger molecular species which may be of interest [213,214].

Research in the area of primary ion beams has led to development of several polyatomic ion sources. This includes Bi_n^+, C_{60}^+ and Ar_n^+. Unlike monoatomic primary ion sources, the energy associated with polyatomic ion source are distributed evenly between all the atoms that forms the polyatomic cluster. Such energy dispersion between the atoms results in low energy impacts between the primary ion source and the samples. Such low energy impact results in an increase in the overall secondary ions yield sputtered from the samples. In addition, such impacts also improved the desorption of larger secondary ion fragments that contain greater chemical complexity and information. Such enhancement in the secondary ion emitted was more noticeable in the higher mass region (i.e., *m/z* > 200) of the spectrum [215]. This improvement in secondary ion yield detected from the use of cluster primary ion beam was of great importance as it permitted the analysis of biological samples which do not ionise as readily as inorganic materials.

1.5.3 Application of ToF-SIMS imaging in drug delivery to the skin

Since the development of cluster primary ion beams there are substantial amount of studies that have utilised ToF-SIMS in analysing a range of biological materials ranging from proteins [216], lipids [217] and even diseased tissues [218–221]. Subsequently, the application of ToF-SIMS in the area of skin tissue analysis have also been explored [222–225]. The utilisation of ToF-SIMS in the area of skin permeation research emerged in 2006 and was pioneered by Okamoto *et al*. who studied the permeation of pseudo ceramide into *ex vivo* porcine skin [226]. However, it was not until seven years later that Judd *et al.* utilised ToF-SIMS as a method to track the permeation of drug molecules such as chlorhexidine digluconate into *ex vivo* skin as shown in Figure 1-15 highlighting that most of the drug is localised within the *stratum corneum* post permeation [223].

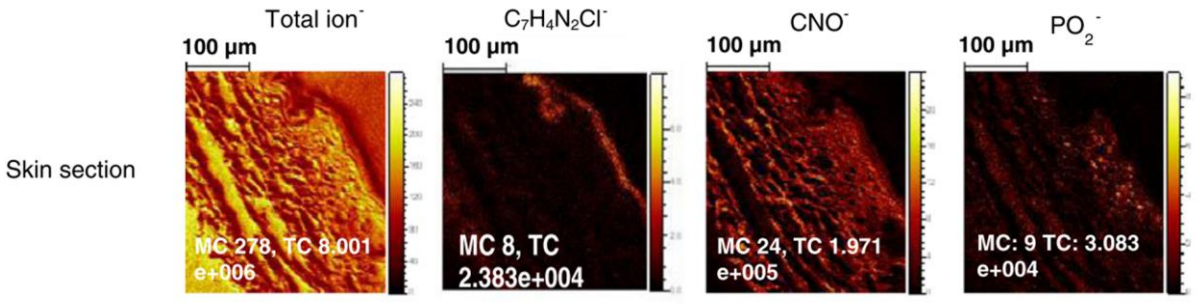

Figure 1-15 ToF-SIMS images of various ions fragments from ToF-SIMS analysis of skin cross-sections treated with 2% chlorhexidine (w/v) treated onto ex vivo porcine skin. $C_7H_4N_2Cl^-$ is the fragment ion for chlorhexidine and was used to track the permeation of the drug into the skin. Phosphate ion, PO_2^- was used to map the viable epidermis while CNO^- is generic fragment ion for biological tissue such as skin. Field of view is 400 × 400 µm. Adapted from Judd et al. [223]

The most common sample types that are analysed via ToF-SIMS from a majority of skin permeation studies are tape strips and cross-sections. Tape strips are widely analysed using ToF-SIMS as this type sample allow us to gauge the permeation of compound into the *stratum corneum*. This form of sample analysis via ToF-SIMS allows us view the lateral distribution of compounds within the *stratum corneum* at a layer-by-layer level [227]. In addition, tape stripping also allows us to collect *in vivo* human samples in a minimally invasive manner relative to punch biopsies. On the other hand, ToF-SIMS analysis of skin cross-section from *ex vivo* tissues enable researcher to gauge the permeation profile of a compound as a function skin depth following permeation experiments [68]. Following the early works by Okamoto *et al*. and Judd *et al*. there have been an increasing number of publications in the field that have utilised ToF-SIMS as an analytical tool to track the permeation of compounds into the skin through the analysis of samples such as skin cross-sections and tape strips. Table 1-3 summarise the list of publication which have utilised ToF-SIMS as analytical method to track the permeation of compound into the skin.

Table 1-3 Utilisation of ToF-SIMS analysis in skin permeation studies.

Samples	Primary ion beam used for analysis	Permeant(s) investigated	Reference
Cross sections from *ex vivo* porcine skin	25 keV Au^+	Sphingolipid E and pseudo-sphingosine	Okamoto *et al*. (2006) [226]
Cross sections and tape strips from *ex vivo* porcine skin	25 keV Bi_3^+	Chlorhexidine digluconate	Judd *et al*. (2013) [223]
Cross sections from *ex vivo* human skin	25 keV Bi_3^+	Oleic, linoleic, lauric and capric acid	Kezutyte *et al*. (2013) [228]
Cross sections from *in vivo* mouse skin	60 keV Bi_3^{2+}	Chromium ions	Kubo *et al*. (2013) [225]
Cross sections from *in vivo* mouse skin	25 keV Bi_3^+	Roflumilast, tofacitinib and ruxolitinib	Sjövall *et al*. (2014) [224]
Cross sections from *ex vivo* human skin	25 keV Bi_3^+	Linoleic, oleic, palmitoleic, palmitic, and stearic fatty acid	Cizinauskas *et al*. (2017) [229]
Cross sections from *ex vivo* human skin	25 keV Bi_3^+	Dihydroquercetin	Cizinauskas *et al*. (2017) [230]
Cross sections and tape strips from *ex vivo* porcine skin	25 keV Bi_3^+	Chlorhexidine digluconate	Holmes *et al*. (2017) [227]
Cross sections from *ex vivo* human skin	25 keV Bi_3^+	Exogenous ceramide Carvacrol	Sjövall *et al*. (2018) [231]

Full thickness *ex vivo* porcine skin	25 keV Bi_3^+ (with 20 keV Ar_{1900} for depth profiling)	Ascorbic acid and ascorbyl glucoside	Starr *et al*. (2019) [197]
Tape strips and cross sections from *ex vivo* porcine skin	25 keV Bi_3^+	Imiquimod	Al-Mayahy *et al*. (2019) [68]
Tape strips from *in vivo* human volunteers	30 keV Bi_3^{2+} (with 5 keV Ar_{1000} for depth profiling	Collagen tripeptide	Kawashima *et al*. (2020) [232]
Cross sections from *in vivo* rat skin	50 keV Bi_3^{2+}	Metal oxide nanoparticles	Matter *et al.* (2020) [233]

It can be seen from Table 1-3 that the utilisation of ToF-SIMS analysis in the area of skin permeation research has slowly grown over the years. Nevertheless, the use of ToF-SIMS in skin research is associated with some drawbacks. One of the limitations of ToF-SIMS analysis is the inability of the technique to provide fully quantitative results due to a phenomenon known as the matrix effect. The matrix effect is a situation in which the components of the analysed sample, other than the compound of interest, influences the yield and intensity of the detected secondary ions [234]. The matrix in this instance would be the surrounding skin tissue while the compound of interest would be the permeants that are investigated. In order to circumvent this limitation, some of the reported permeation studies would employ chromatographic methods such as HPLC-UV and LC-MS to support the ToF-SIMS analysis [68,227,231].

Nevertheless, analysis of samples using ToF-SIMS allows chemical mapping of the distribution of a compound of interest by tracking the mass-to-charge ratio (*m/z*) of specific molecular ions from the mass spectra. This analytical approach allows us to track the distribution of compounds, both

exogenous and endogenous, within a biological milieu in a label-free manner. In addition, the ability of the instrument to track the topical permeation of pharmaceuticals and cosmeceuticals such as dihydroquercetin [230], ascorbic acid [197], fatty acids [235], carvacrol [231] and roflumilast [224] highlights the value of the technique in skin research.

Following the growing body work in the area of skin permeation analysis via ToF-SIMS, Al-Mayahy *et al*. was the first and only publication to date at the time of writing this thesis that reported the application of ToF-SIMS imaging as an analytical tool to monitor microneedle-based drug delivery strategy to the skin. Al-Mayahy *et al.* demonstrated for the first time using ToF-SIMS imaging of tape strips that the application of Aldara™ cream on microneedle pre-treated skin resulted in enhanced the permeation of the drug within the *stratum corneum*. However, ToF-SIMS analysis of the skin cross-sections revealed that the drug was mostly localised on the skin surface and to some degree into the microneedle channels within the upper epidermis as shown in Figure 1-16 [68]. It was apparent that this strategy does enhance the delivery of the drug into the skin but not to the depth needed in managing nodular BCC. However, this study highlights the value of ToF-SIMS imaging in understanding the dermal drug distribution following microneedle-based drug delivery strategies. Despite the powerful analytical capabilities offered by this form of mass spectrometry imaging, Al-Mayahy *et al*. did not fully explore and demonstrate the utility of ToF-SIMS imaging in evaluating the effectiveness of microneedle-based drug delivery systems. For instance, Al-Mayahy *et al*. did not evaluate if the instrument could detect the presence of other components of the formulation (e.g., excipients) in the skin following administration. In addition, there is yet any work that have evaluated the dermal distribution of the formulation in skin tumours in a label-free fashion using ToF-SIMS imaging.

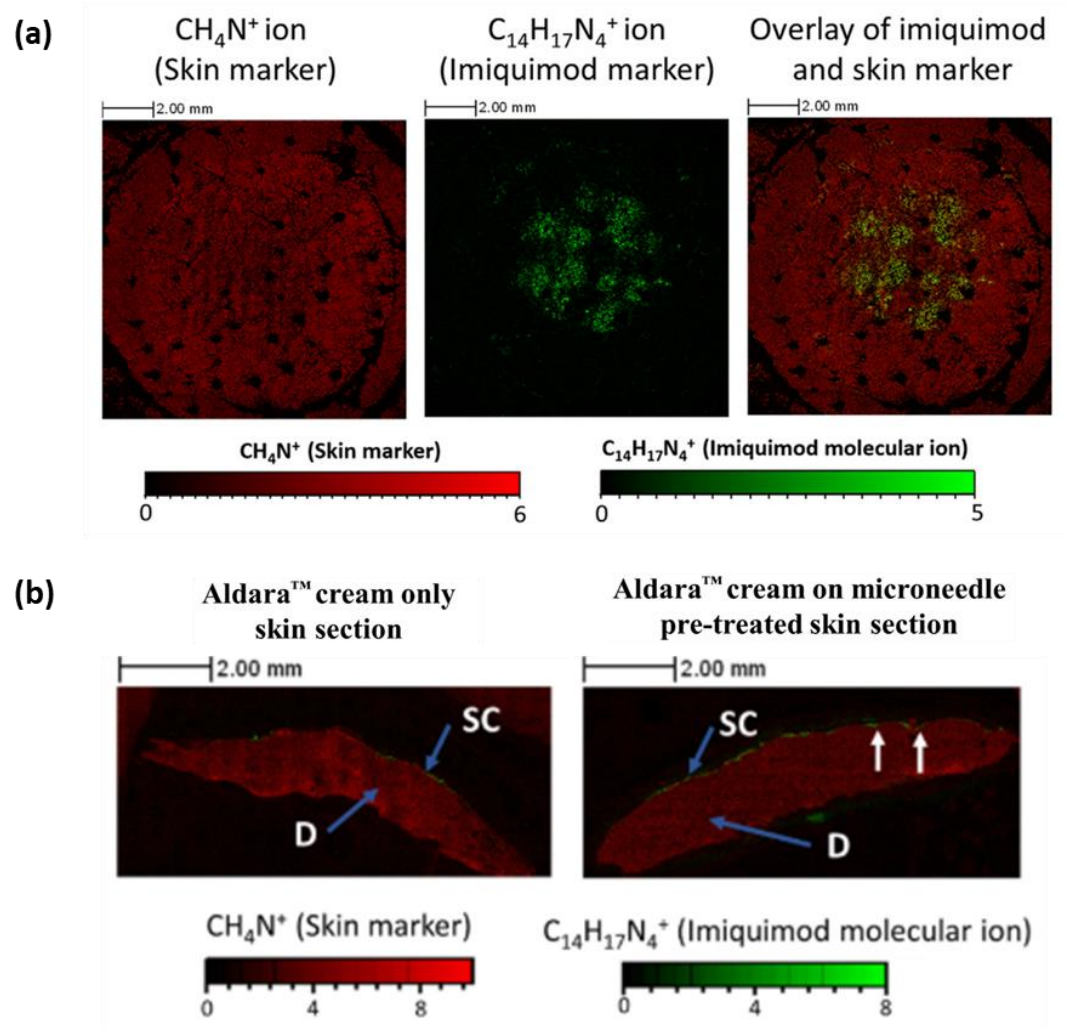

Figure 1-16 (a) ToF-SIMS ion images of tape strip from ex vivo porcine skin treated with Aldara™ cream following microneedles pre-treatment. This figure shows enhances lateral permeation of imiquimod across the stratum corneum when Aldara™ cream is applied on microneedle pre-treated skin. The skin marker (CH_4N^+), the imiquimod marker ($C_{14}H_{17}N_4^+$). (b) ToF-SIMS ion distribution map of porcine skin cross sections from Aldara™ cream on intact skin and microneedles pre-treated skin. The overlay image of the skin marker (CH_4N^+) with imiquimod marker ($C_{14}H_{17}N_4^+$) indicates the localisation of imiquimod within the stratum corneum for the Aldara™ cream only treated skin. White arrows indicate microneedle indentations and delivery of imiquimod into the epidermis that still persisted after 24 h. The skin cross-section covers the microneedle-treated part of the skin. SC indicates stratum corneum, D indicates dermis. Reproduced from Al-Mayahy et al. [68]

1.6 Thesis aims

Given the impact of BCC and limitation of the current therapies, the over-arching goal of this thesis is to explore and develop a targeted drug delivery strategy using microneedles to improve the intradermal delivery of imiquimod for the treatment of nodular BCC.

The first aim of this thesis was to investigate the utility of two commercial microneedle systems, the Dermapen® and the Dermastamp™ in improving the intradermal delivery of imiquimod into the skin. In order to achieve this aim, the mechanical insertion of the two commercial microneedle system was first evaluated using *in vitro* skin simulant and *ex vivo* porcine as highlighted in Chapter 2 of the thesis. Following this, the microneedle system that displayed an insertion profile capable of reaching depths at which nodular BCC resides was explored further. This involved investigating the effectiveness of using the microneedle system in combination with Aldara™ cream in order to deliver the drug into the dermis. This will demonstrate whether the combination existing commercial products may provide an elegant synergy to enhance the intradermal localisation of imiquimod for the treatment of BCC. This combination strategy was explored and discussed in Chapter 3 of the thesis.

The second aim of this thesis was to develop dissolvable polymeric microneedle patches loaded with imiquimod to promote the intradermal delivery of the immunomodulator for BCC treatment. The simple and straightforward one-step application using dissolving polymeric microneedle patches relative to the two-step application process using solid microneedles and Aldara™ cream may be a more preferred treatment option for patients. Therefore, Chapter 4 of this thesis explores the fabrication, characterisation and evaluation of dissolving microneedles prepared using the commercial polymer, Kollidon® VA 64 as drug delivery system for nodular BCC. Furthering this, a range of polymers that have never been used in manufacturing polymeric microneedles were synthesised. These polymers were then evaluated and fabricated into dissolving microneedles to produce a library of microneedle patches of different polymeric chemistries and designs. These polymeric microneedles were characterised for their capability to puncture the skin and deliver imiquimod intradermally. The

best dissolvable polymeric microneedle system was then evaluated further *in vivo* using a mouse model for skin tumours coupled with *ex vivo* delivery into patients' BCC tumours. The development and screening of this library of microneedle patches is presented in Chapter 5 of this thesis.

Chapter 2 Characterisation of mechanical insertion of commercial microneedles

Akmal H Sabri [a], Zachary Cater [b], Jane Ogilvie [c], David J Scurr [a], Maria Marlow [a] Joel Segal [d]

[a.] Division of Advanced Materials and Healthcare Technologies, School of Pharmacy, The University of Nottingham, NG7 2RD, UK

[b.] Department of Mechanical, Materials and Manufacturing Engineering, Faculty of Engineering, University of Nottingham, Nottingham, NG8 1BB

[c.] Walgreens Boots Alliance, Thane Road, Nottingham, NG90 1BS

[d] Advanced Manufacturing Technology Research Group, Faculty of Engineering, University of Nottingham, Nottingham, NG8 1BB

This chapter has been published in the following research article:

A.H. Sabri, Z. Cater, J. Ogilvie, D. Scurr, M. Marlow, J. Segal, 2020. *Characterisation of mechanical insertion of commercial microneedles*, Journal of Drug Delivery Science and Technology doi: https://doi.org/10.1016/j.jddst.2020.101766

Acknowledgement of research work done by co-authors

- Zachary Cater: An undergraduate Mech Eng. student supervised by A.H. Sabri and J. Segal. Zachary Cater developed the biaxial stretch rig used in the experimental work within this chapter. The work done by Zachary Cater is in **Section 2.4.1 Biaxial Stretch Rig Development** In addition, Zachary Cater also Assisted A.H. Sabri in conducting the insertion studies in **Section 2.4.2 Biaxial strain on microneedle skin insertion force**.
- J. Ogilvie, D. Scurr, M. Marlow, J. Segal: Supervisors to A.H. Sabri and supervised him during the writing of the article. Critically reviewed the manuscript and editing.

Keyword: Microneedle, skin strain, microchannels, biaxial stretch, skin insertion

2.1Abstract

The protection provided by the human skin is mostly attributed to the *stratum corneum.* However, this barrier also limits the range of molecules that can be delivered into and across the skin. One of the methods to overcome this physiological barrier and improve the delivery of molecules into and across the skin is via the use of microneedles. This work evaluates the mechanical insertion of two different commercially available microneedle systems, Dermapen® and Dermastamp™. The influence of biaxial skin strain on the penetration of the two microneedle systems was evaluated *ex vivo* using a biaxial stretch rig. From the skin insertion study, it was apparent that for all levels of biaxial strain investigated, the Dermapen® required less force than the Dermastamp™ to puncture the skin. In addition, it was observed that the oscillating microneedle system, the Dermapen®, resulted in deeper skin insertion *ex vivo* in comparison to the Dermastamp™. The use of this new biaxial stretch rig and the *ex vivo* skin insertion depth study highlights that the oscillating Dermapen® required less force to perforate the skin at varying biaxial strain whilst resulting in deeper skin penetration *ex vivo* in comparison to the Dermastamp™. Although the Dermapen® punctured the skin deeper than the Dermastamp™, such difference in penetration did not influence the permeation profile of imiquimod, a drug used in the management of basal cell carcinoma, into and across the skin as evidenced from a 24-hour *ex vivo* permeation study.

2.2 Introduction

The human skin is the largest organ in the human body and is comprised of three layers; the epidermis, dermis and hypodermis. The epidermis is a multilayer compartment of the skin that comprises of the *stratum corneum, stratum granulosum, stratum spinosum* and *stratum basale* [236]. The outermost layer of the epidermis, the *stratum corneum,* is avascular and has evolved to provide protection against physical and chemical insults. The protection provided by the *stratum corneum* has also resulted in a barrier to the delivery of compounds across the skin either for therapeutic or cosmetic purposes [68].

Microneedles are one of the strategies explored to improve the delivery of compounds into and across the skin. These are minimally-invasive needles with lengths that ranging between 250-1000 µm capable of perforating the *stratum corneum* in order to promote the delivery of compound into and across the skin [237]. Due to their size, microneedles offer painless skin insertion as they are unlikely to stimulate the dermal pain receptors upon application [238]. The ability of microneedles to puncture the skin may of great clinical utility in managing skin condition where the target disease site resides deep within the skin tissues such as nodular basal cell carcinoma (BCC).

Some of the microneedle products available on the market, licensed for cosmetic use, include the Dermastamp™ and Dermapen®. The Dermastamp™ consists of a stamp with an array of microneedles arranged at the base of the device. The microneedles are inserted into the skin in one vertical motion, creating micron sized channels in the skin. The Dermapen® is a motor driven microneedling device that inserts its needles into the skin in a continuous oscillating motion at one of five programmed frequency levels. The use of a motor helps circumvent the issue of varying insertion force between users. It also features an adjustable dial to control the needle's depth of penetration during use. However, little research exists evaluating the effectiveness of such a motor driven device or the associated advantages or disadvantages in its use in comparison to the Dermastamp™ and its single stamping motion.

In order to effectively generate microneedle channels, the skins topology must also be considered. The human skin features a roughened surface due to the variation in structure of the keratinocytes on the *stratum corneum* [239,240]. This surface is undulating in nature, being up to 150 microns from peak to trough for those aged over 60 [240], thus clearly demonstrating the need to smooth the skin as far as possible to maximise depth of penetration by the needles. To achieve smoothing, the skin must be stretched. It is understood that when skin is uniaxially stretched, the skin acts in a compressive fashion in the perpendicular direction to maintain the area of the surface, causing micro-furrows to develop [241].This highlights the need for biaxial stretching to mitigate against this and ensure microneedle insertion into the skin. Biaxial skin stretching has been performed in several studies [242–244] with a non-linear stiffening of skin being found as a function of strain. This relationship has been supported by a simulation study by Flynn and Rubin [245] however little other data appears to exist regarding how increase in strain affects the penetration of microneedle into the skin.

In this work, we compare the insertion force profiles of two commercially available microneedle systems; Dermastamp™ and Dermapen®. This study evaluates the influence of biaxial skin strain on the insertion force of two different commercial microneedling systems into the skin. Besides that, the influence of microneedle oscillation during microneedle application was evaluated using an *in vitro* and an *ex vivo* set up. Lastly, the impact of these microneedle systems on the permeation profile of imiquimod, a compound used in the management of basal cell carcinoma, was also investigated.

2.3 Materials

Dermapen® (ZJChao, China) and Dermastamp™ (Teoxy Beauty, Wuhan, China). The Dermapen® is an oscillating microneedling pen featuring a 36-needle removable array, with tip radius of 44-68 µm and conical geometry. In order to mimic how the Dermapen® would be used by a patient in a real-world setting, the plastic ring around the microneedle cartridge was not removed for all skin insertion and permeation study. The Dermastamp™ is a non-oscillating microneedle stamp featuring a 42-needle array of 1mm length, tip radius of 21-25 µm and curved conical geometry. The geometry of the

microneedles from respective devices are visualised using Leica DM4000B (Leica Microsystem, Germany). The geometry of the microneedles is shown in Figure 2-1

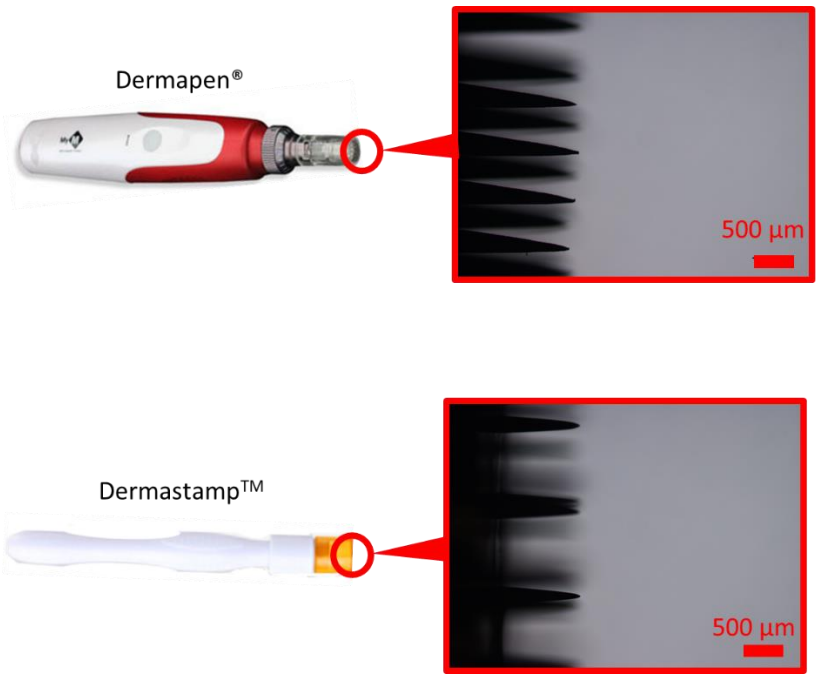

Figure 2-1 Close up microscopy image showing the geometry of microneedles from Dermapen® and Dermastamp™

Porcine skin was used to study the insertion force profile of commercial microneedles instead of ex-vivo human skin due to its limited availability and the ethical difficulties associated with its use. Various studies have highlighted that porcine skin is a suitable alternative to human [246]. Porcine flank skin samples from six-month old animals were obtained from a local abattoir, reared specifically for food. Skin samples were collected prior to any steam cleaning, and then prepared. The skin was washed with distilled water and dried using tissue. Full thickness skin was used to avoid altering the skins biomechanical properties, which may lead to over-penetration of microneedles into the dermal tissue [66]. After that, the skin samples were stored at -20 °C and used within six months. Gentian violet solution 1% w/v (De La Cruz products, USA) was used as a dye to highlight the microneedle channels created in porcine skin. Parafilm M® (Brand Bermis, Wertheim, Germany) of 127 µm thickness was used as a skin simulant in the in-vitro insertion study. Imiquimod was purchased from Cayman

Chemicals, USA. 5% w/w imiquimod cream (Aldara™), MEDA Company, Sweden was purchased from Manor Pharmacy, UK. Sodium acetate was purchased from Sigma-Aldrich, UK. Acetonitrile (HPLC grade) and glacial acetic acid were obtained from Fisher Scientific, UK. Teepol solution (multipurpose detergent) was ordered from Scientific Laboratory Supplies, UK. D-Squame standard sampling discs (adhesive discs) were purchased from Cuderm corporation, USA. Deionised water was obtained from an ELGA reservoir, PURELAB® Ultra, ELGA, UK. All reagents were of analytical grade, unless otherwise stated.

2.4 Methods

2.4.1 Biaxial Stretch Rig Development

Following two designs presented in literature [243,244], a low cost biaxial skin stretching rig was produced. The rig consists of four manual linear stages arranged as shown in Figure 2-2 on an 8 mm laser cut acrylic base. Further laser cut components permit clamping to be achieved using M4 Cap Head Bolts and 5 mm acrylic plates. Friction between the clamping plates was improved using 40 grit emery cloth, double sided taped to the plates. The centre of the rig, over which the microneedle array is inserted, consists of an acrylic block topped with a 6mm layer of natural cork to simulate the stiffness of skeletal muscle [247] . Aluminium foil was overlaid on the cork with a thin covering of detergent. This was performed to reduce the friction experienced by the skin on the cork mat during stretching thus aiding the amount of strain that could be achieved within the skin. In addition, a laser cut jig for locating the biaxial stretch rig on the bed of a Texture Analyser (TA), (Stable Micro Systems, Surrey, UK) was also prepared to ensure consistency of the location of insertion of the microneedle array. Zero strain was assumed for each piece of skin when initially clamped.

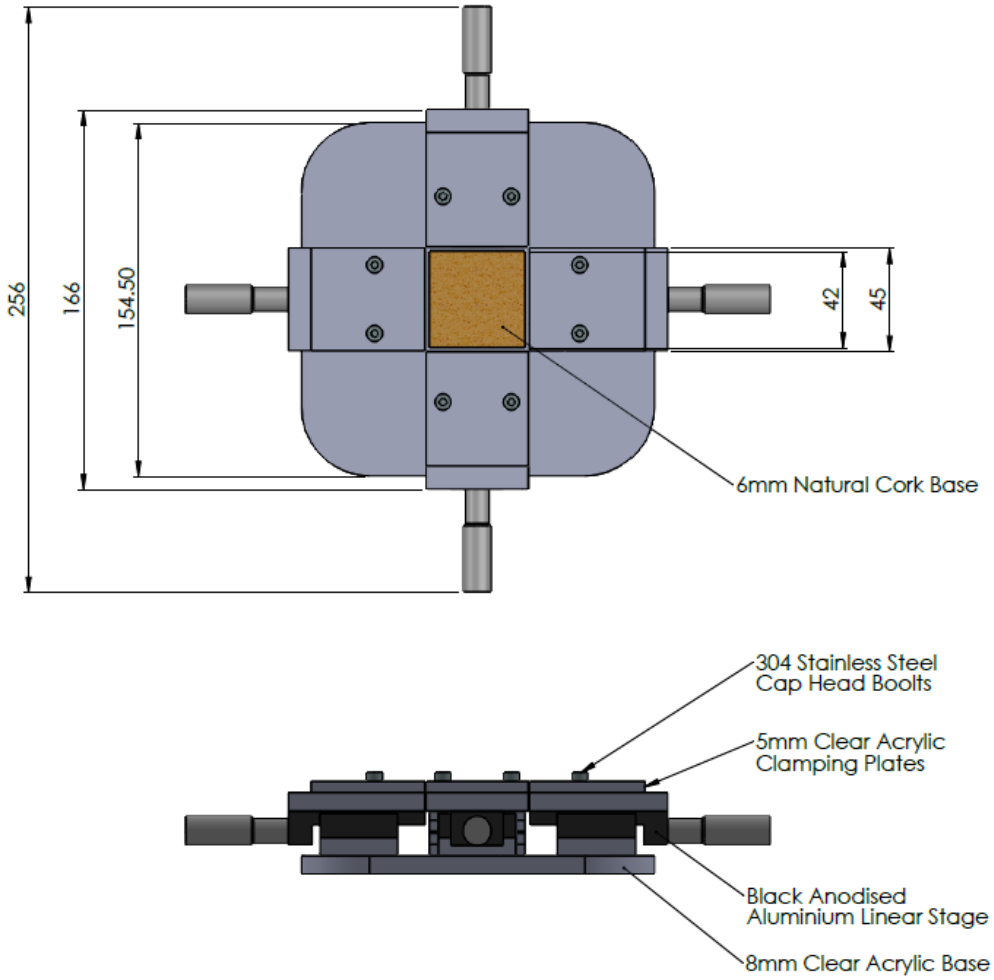

Figure 2-2 A schematic of the conceived manual biaxial stretch rig

2.4.2 Biaxial strain on microneedle skin insertion force

In order to investigate the effect of biaxial stretching on microneedle puncture performance of the Dermapen® and Dermastamp™, an insertion experiment was performed. The prepared porcine skin was inserted into the biaxial stretch rig and clamped, Figure 2-3 **(a)**. The skin samples were then subjected to five levels of biaxial strain; 1.00, 1.0625, 1.125, 1.875 and 1.25 (i.e., a biaxial stretch of 0mm, 2.5mm, 5mm, 7.5mm and 10mm of a 40x40 mm grid). The level of biaxial strain was measured using a 40x40 mm grid of 5 mm squares ink-stamped onto the skin samples, Figure 2-3 **(a)**. The skin sample was biaxially stretched and a pair of Vernier callipers used to measure the level of stretch i.e., 0mm, 2.5mm, 5mm, 7.5mm and 10mm. Strain in each direction was calculated using Equation 2-1.

$$\varepsilon = \Delta l / l$$

Equation 2-1 Equation for strain where ε is strain, l is length, and Δl is the change in length of skin. ε strain, has no unit as the units from Δl and l cancel each other out.

The skin-loaded rig was then placed under the probe of the TA, using a laser cut jig to align a quadrant with the probe's central position. A microneedle-loaded probe, see Figure 2-3 **(b)**, was then attached to the TA. The following parameters were used for the TA program; 5kg Load Cell, Pre-Test Speed: 0.5mm/sec, Test Speed: 0.5mm/sec, Post-Test Speed: 10mm/Sec, Trigger Force: 0.01N. The microneedles were inserted into the skin sample by the TA and the force-displacement profile recorded. Following their removal, the Gentian Violet dye was applied to the skin, Figure 2-3 **(c)** to visualise the number of microneedle channels generated. The number of microchannels generated were counted to measure the percentage of successful microneedle insertion. The Dermastamp™ was housed in a custom mount that consist of a turned aluminium with a roll pin used to hold the microneedle array in place. An M6 grub screw was used in the rear of the mount as an attachment to the TA. For the Dermapen®, a 3D printed (Fused Deposition Modelling) jacket was designed to house the device within an aluminium tube and stub assembly via a tapered interference fit. The assembly was then attached to the TA again by an M6 grub screw. The Dermapen®'s adjustable needle length was set to 1000 µm, the same length of the Dermastamp™ needles.

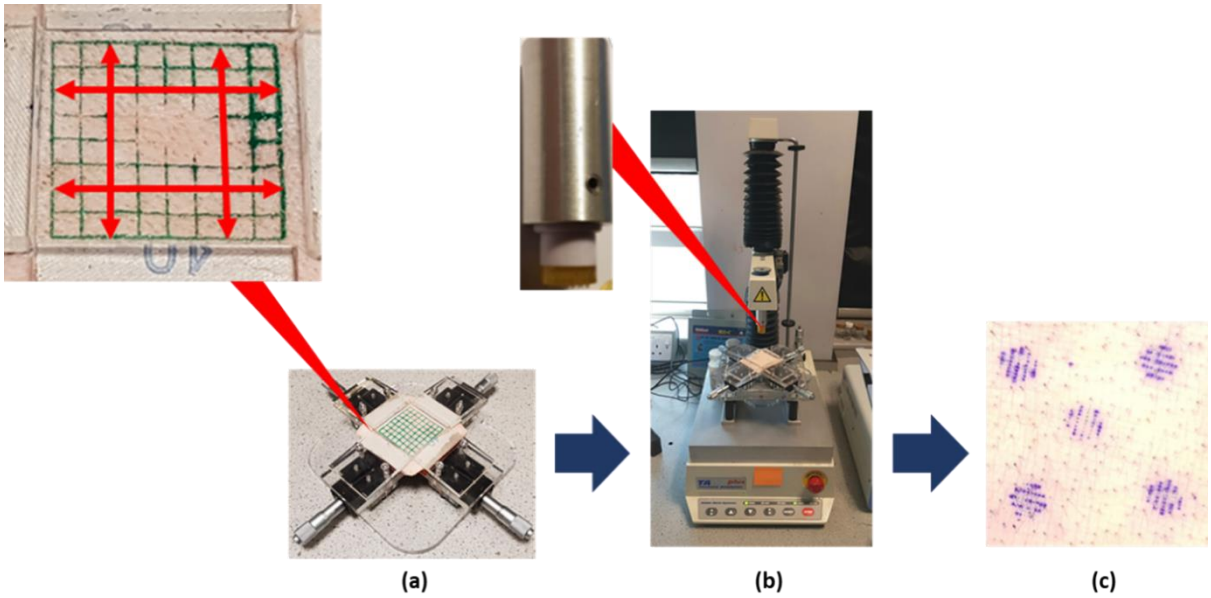

Figure 2-3 Schematic detailing the setup to investigate effect of biaxial strain on microneedle skin insertion. A 40x40 mm grid of 5 mm squares ink was stamped onto the skin samples in ***Step (a)*** *in order to measure the level of biaxial strain on the skin. Using a texture analyser (TA), respective microneedle systems were attached to the probe of the instrument to allow insertion into the skin as shown in* ***Step (b)****. Visualisation of microneedle channels using Gentian Violet dye as depicted in* ***Step (c)***

2.4.3 *In vitro* skin simulant insertion study

As an alternative method to determine the microneedle penetration depth, a polymeric film (Parafilm M®,) was used as a skin simulant. This insertion study was adopted from Larrañeta *et al.* [248]. In brief, eight layers of Parafilm M® were stacked onto each other on a cork layer. Both microneedle systems were applied onto the Parafilm M® stacks. Six replicates were performed, and the pores generated were investigated under an optical microscope. The percentage of holes created per layer for respective microneedle length was calculated using following Equation 2-2:

$$\%\ \text{hole generated} = \frac{N\ \text{microneedle channels observed}}{N\ \text{microneedles per array}} \times 100$$

Equation 2-2 Equation to establish the percentage of holes produced by the microneedle devices. Where N represents 'number of'

2.4.4 *Ex vivo* skin insertion study

In order to evaluate the penetration depth of the Dermapen® and Dermastamp™ needles into the skin, an *ex vivo* penetration study using porcine skin was conducted. The porcine flank skin was defrosted at room temperature for an hour prior to the experiment. Using scissors, excess hair was carefully trimmed from the skin. A 36-microneedle array tip was used, and the vibration speed was set to level 1 (412 cycles/min) [249]. The microneedle skin pre-treatment was applied by gently stretching the skin and placing the Dermapen® vertically upon the skin for 10 seconds. A microneedle length of 1000 µm was used in this study. After treating the skin with the microneedle pen, 10 µl of 1 % Gentian Violet Dye was applied to the surface of the skin and left at room temperature for 60 minutes. Excess dye was removed and the skin was then visually inspected to identify microneedle pores. The skin samples were then cryo-sectioned (Leica CM3050 S Research Cryostat, UK) and the depth of microneedle penetration was measured under an optical microscope (Zeta Profilometer, KLA-Tencor, US). The same procedure was repeated to evaluate the depth of Dermastamp™ penetration into the skin.

2.4.5 Skin permeation study

In order to investigate the influence of the different microneedle system on skin permeation, an *ex vivo* skin permeation study using a Franz-type diffusion cell was conducted using a model compound, imiquimod. Imiquimod was selected as a model compound as the molecule displayed poor permeation across the skin [68]. The application of microneedle system to skin is hypothesised to improve the permeation of imiquimod into the skin. Prior to the permeation study, skin samples were defrosted for at least an hour at room temperature. The skin was trimmed into small pieces according to the surface area of the donor chamber of the Franz diffusion cell (Soham Scientific, Cambridgeshire, UK). The trimmed skin samples were equilibrated by placing them above the receptor compartment for 15 minutes prior to skin treatment. The porcine skins were subjected to the following treatment modalities: i) application of 5% w/w of imiquimod cream alone as a control ii) application of 1000 µm microneedles to the skin as a pre-treatment using Dermapen® followed by 5% w/w of imiquimod cream iii) application of 1000 µm microneedles to the skin as a pre-treatment using Dermastamp™

followed by 5% w/w of imiquimod cream. Next, the porcine skins were placed on top of the receptor compartment filled with 3 ml of degassed 100 mM acetate buffer pH 3.7. This buffer was selected as the receptor phase in order to maintain a sink condition throughout the permeation study. This is due to the insolubility of imiquimod at neutral or basic pH values. Various groups have reported the use of acetate buffer pH 3.7 as the receptor phase in imiquimod permeation studies as this ensure imiquimod is soluble at this pH while maintaining a sink condition in the receptor chamber [53–55]. The skin was then secured between the donor and receptor compartment of the diffusion cell using a metal clamp, with the stratum corneum side facing the donor compartment. Upon assembling the Franz diffusion cell, the permeation experiment was conducted over a period of 24 hours in a thermostatically controlled water bath set at 36.5 ^{o}C.

After a 24-hour permeation experiment, the excess cream was removed and collected from the skin surface by careful application of sponges soaked with 3% v/v Teepol® solution. The sponges were pooled for imiquimod HPLC analysis as a total skin wash. Any formulation which might have spread to the donor chamber was collected by the sponges and stored for imiquimod analysis by HPLC as a donor chamber wash. Upon removing excess formulation from the skin surface, 15 sequential tape strips were collected from the skin. The amount of imiquimod from the different Franz cell elements (skin wash, donor chamber wash, pooled tape strips and remaining skin after tape stripping) were extracted by the addition of 5, 5, 10 and 5 mL of methanol extraction mixture (methanol 70%: acetate buffer pH 3.7 100 mM 30%) respectively using a previously reported method [52]. Samples were then vortexed for 1 minute and sonicated for 30 minutes before being left overnight. Subsequently, samples were vortexed again and sonicated for a further 30 minutes. 1000 µl of the extracts were collected and spiked with 100 µl of 100 µg/ml propranolol as an internal standard. The samples were then filtered through 0.22 µm membrane. For the receptor fluid, 1000 µl of the solution from each Franz cells were collected and spiked with 100 µl of 100 µg/ml propranolol as an internal standard before being filtered through 0.22 µm membrane. HPLC analysis was carried out using an Agilent 1100 series instrument (Agilent Technologies, Germany) equipped with degasser, quaternary pump, column

thermostat, autosampler and UV detector. System control and data acquisition were performed using Chemostation software. The details of the HPLC chromatographic conditions are as follow: column C18 (150 × 4.6 mm) ACE3/ACE-HPLC with a particle size of 5 µm, pore size of 100 Å, pore volume of 1.0 ml/g and a surface area of 300 m^2/g, Hichrom Limited, UK. The mobile phase composition for analysis of extracts from skin wash, donor chamber wash, pooled tape strips and remaining skin consists of 10 mM acetate buffer: acetonitrile (79:21). Whilst, the mobile phase composition for analysis of receptor fluid consists of 10 mM acetate buffer: acetonitrile (70:30). The system operated at a flow rate of 1.0 mL/minute, UV detection at λ_{max}= 226 nm, injection volume of 40 µL and column temperature of 25 °C.

2.4.6 Statistical analysis

Results were reported as mean with standard deviation (SD) (n≥5). Statistical calculations were performed in Prism (IBM, USA), a software package. The Student's t-test and One-Way ANOVA followed by a Tukey post-hoc test was applied to compare the results of different groups. Statistically, a significant difference was denoted by *p* value < 0.05.

2.5 Results and Discussion

2.5.1 Influence of biaxial strain on commercial microneedle perforation.

A biaxial skin stretching experiment was conducted in order to investigate the effect of skin strain on the insertion of two commercial microneedle systems. From Figure 2-4 it can be seen that the force needed by the Dermapen® to perforate the skin was significantly lower than the Dermastamp™ for the range of strain rates investigated. It was also found that an increase in force was needed for the Dermastamp™ to puncture the skin as the strain increased, however this force plateaued at a biaxial strain of circa 1.1. In contrast, a linear relationship is presented for the Dermapen® suggesting that insertion force increases with a higher strain rate.

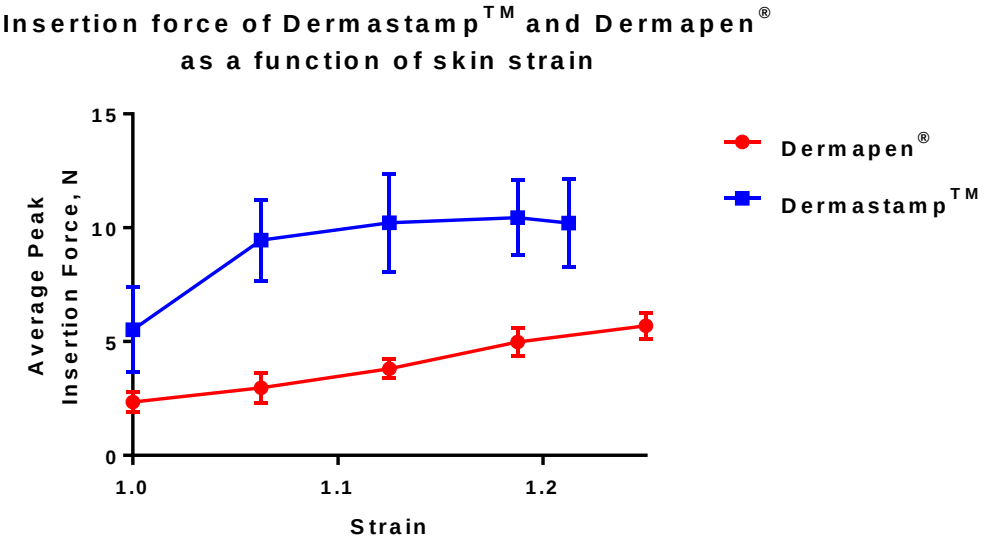

Figure 2-4 Biaxial skin strain and insertion force relationship for commercial microneedle systems Dermapen® and Dermastamp™. Data expressed as means ± SD, n=5.

The relationships shown in Figure 2-4, an increase in force with increases in biaxial strain, align with Lanir & Fung's work that showed skin as a non-linear material that exponentially stiffens when biaxially stretched [244]. As stiffness is defined as the resistance to bending or deformation, it is proposed that as skin exponentially stiffens with an increase in strain. This results in the force needed to deform the skin and insert the needles will increase significantly with biaxial stretching.

Following microneedle insertion, the formed puncture sites were visualised by application of Gentian Violet Dye. The percentage of successful microneedle insertions is shown in Figure 2-5 for the two microneedle systems. It is evident that as the biaxial strain of the skin sample increases, an increase in the number of successful microneedle insertions was observed for the Dermapen®, which then plateaus as the skin was subjected to further biaxial strain. For the Dermastamp™, as the biaxial strain of the skin increases, we observed a rise in the percentage of successful microneedle insertion. However, as biaxial strain of the skin was increased further, the percentage of successful microneedle insertion into the skin decreased.

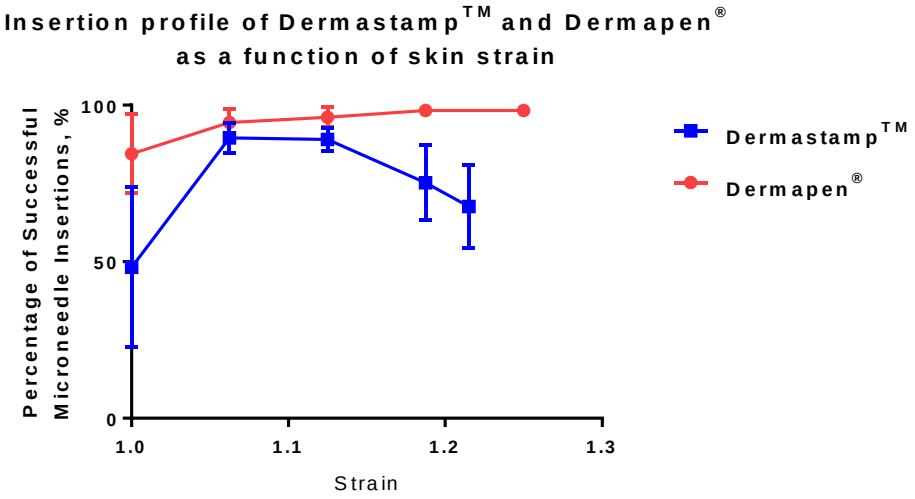

Figure 2-5 Averaged percentage of maximum number of dyed microneedle insertion holes generated for each level of stretch. Data expressed as means ± SD, n=5.

Previous work by Maiti *et al.* has shown that subjecting the skin to strain may help smooth its surface [250]. Such topographical change in skin structure may help mitigate the presence of micro-furrows on the skin which fold around the microneedles and can present resistance to microneedle insertion [157]. One of the ways to achieve skin smoothening is via subjecting the skin to strain or stretching [251]. However, the current work suggests that smoothening the skin by subjecting the skin to biaxial strain may help improve microneedle insertion up to an optimum strain (1.0625 and 1.125) as shown with the Dermastamp™ in Figure 2-5. Beyond this optimum strain, the percentage of successful microneedle penetration decreases due to increased skin stiffness with increasing strain as shown by previous investigators [244].

For the Dermapen®, the increase in the percentage of successful microneedle insertions with increasing strain is attributed to the observation that the skin smooths upon stretching [251]. Subjecting the skin to biaxial strain results in flattening of the micro-furrows and permits an increased probability of the needles puncturing through the *stratum corneum*. This is due to the linear motor, that oscillates the microneedle array, providing a secondary force to assist with insertion into the skin, irrespective

of the rise in skin stiffness with the increasing strain. These results demonstrate that the Dermapen® is more effective than the Dermastamp™ in generating microneedle channels across the skin.

Unlike the Dermastamp™, the presence of plastic shoulders at the tip of microneedle cartridge of the Dermapen® imposes an additional surface tension to the skin during microneedle application. This helps to further mitigate the propensity of the skin to fold around the needles while mitigating the variability in puncture force. This is evidenced by the smaller standard deviation error bar for Dermapen® relative to Dermastamp™ for the level of skin strain investigated shown in Figure 2-4. The combination of these physical factors mimics the insertion mechanism of a mosquito's proboscis. The shoulder of the cartridge of the Dermapen® plays a similar role to that of the mosquito labium which applies lateral strain to the skin prior to puncture. This ultimately focusses the force at the tip of the Dermapen® permitting a more effective insertion [122]. The microneedles in this case are equivalent to the mosquito's labrum which insert itself at defined frequency in a stamping manner allowing deeper insertion with repeated insertion.

2.5.2 *In vitro* skin simulant insertion depth study of commercial microneedle

An in-vitro skin simulant study, using Parafilm M®, was performed to compare the percentage of successful microneedle channels against depth for the two commercial microneedle systems being considered; the Dermapen® and Dermastamp™. The insertion profiles of the commercial microneedle systems were established using a methodology developed and validated by Larraneta *et al.* [248]. The experiment involves the insertion of the microneedle devices into a stack of eight Parafilm M® layers, followed by the separation of the layers and their visualisation under an optical microscope to evaluate the number of microneedle channels formed, leading to the insertion profiles in Figure 2-6.

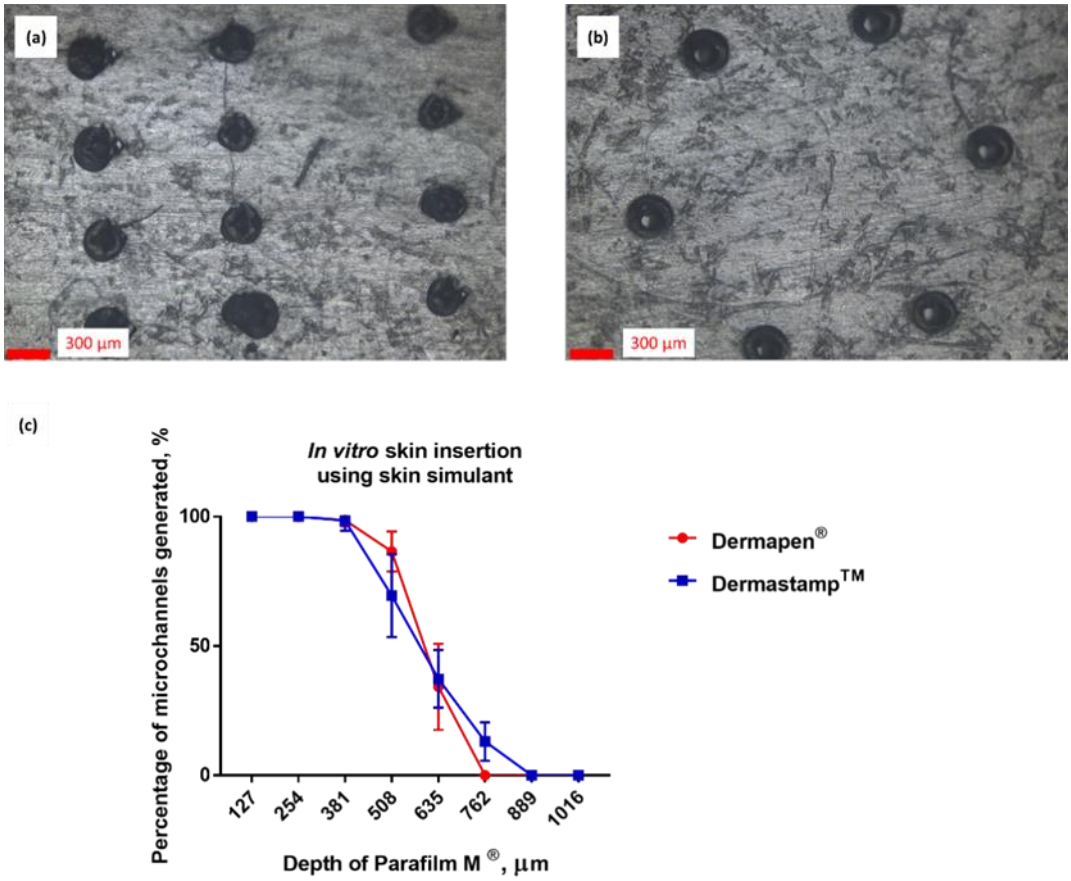

Figure 2-6 Microscopic images of first layer of Parafilm M® stack punctured by stainless steel microneedles by (a) Dermapen®, (b) Dermastamp™ Scale bar:300 µm (c) Insertion profile of different commercial microneedle systems, Dermapen® and Dermastamp™ into Parafilm M® layers, data expressed as means ± SD, n=6.

The two microneedle systems typically pierce the first five layers, with approximately 100% of the needles piercing the first three layers before the percentage of microchannels generated begins to decrease. The generated channels displayed uniform geometry as shown in Figure 2-6 **(a)** and **(b).** However, less than 50% of the microneedles successfully pierced the fifth and sixth layer.

Hutton *et al.* showed that microneedle patches fabricated from a copolymer of methyl vinyl ether and maleic acid were capable of penetrating the Parafilm M® layers to a depth of approximately 60% of the microneedle height [252]. Vora *et al.* also showed that microneedles fabricated from poly(vinyl pyrrolidone) (PVP) loaded with nano- and microparticles were capable of penetrating the Parafilm layers up to 60% of the microneedle length [151]. This work aligns with our findings that the commercial

microneedle systems were capable of penetrating Parafilm M® layers up to circa 60% of the microneedle length. Furthermore, the results in Figure 2-6 **(c)** suggest that for an *in vitro* skin simulant model, the insertion profiles are similar for both microneedle systems. In a follow up study, Larraneta *et al.* discovered that the insertion profile of microneedle arrays was more dependent on needle density and design rather than the material used [131]. Such observations may explain the similar insertion profiles of the two commercial microneedles systems, as both microneedles are made from the same material; stainless steel.

2.5.3 *Ex vivo* skin insertion study

An *ex vivo* penetration study was conducted to ascertain the microneedle penetration depth of the two different commercially available microneedle systems in actual skin tissue. Figure 2-7 shows that successful penetration of microneedles into *ex vivo* porcine flank skin evidenced from the visualisation of microneedle channels from cryo-sectioned skin samples. From Figure 2-7 it was apparent that the region surrounding the microneedle pore retained a normal structure with intact stratum corneum. However, the microneedle channels displayed a deep indentation with disrupted *stratum corneum*.

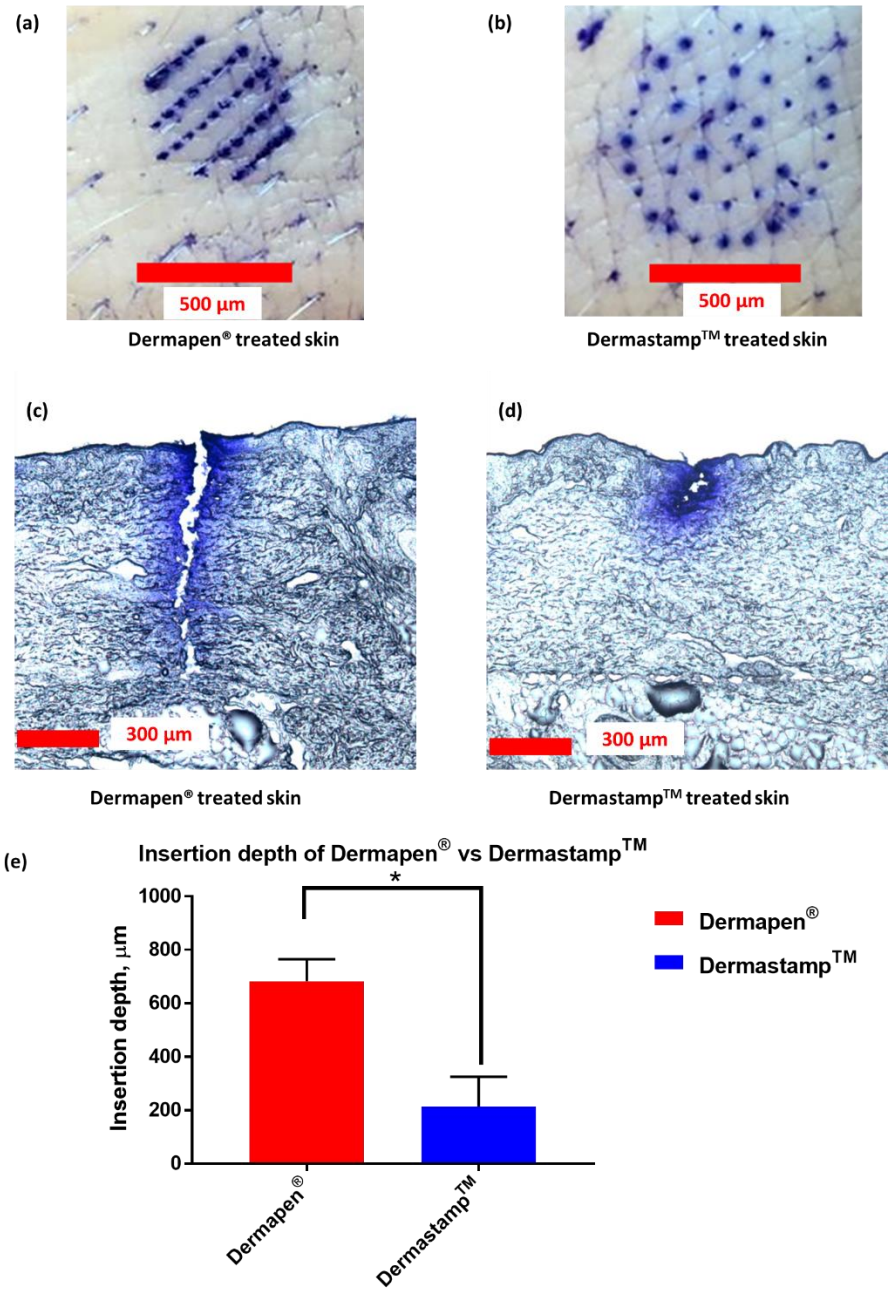

Figure 2-7 Visual image of porcine flank skin surface after gentian staining following (a) Dermapen® and (b) DermastampTM application. Optical microscopy images of porcine flank skin cross sections after application of (c) Dermapen and (d) Dermastamp. The skin was stained with 1% gentian violet solution to allow visualisation of microneedle channels formed after microneedle treatment. n=10, data is expressed as mean ± SD. Differences were determined using a two-tailed Student's t test, and deemed significant at $p<0.05$

In the context of drug delivery, it has been shown by Andrews *et al.* that drug entry into and across the skin is not just limited by the outermost layer of the skin, the *stratum corneum,* but the penetration of molecules is limited by the overall epidermis itself [253]. This would suggest that both microneedle systems were capable of perforating the skin to generate microneedle channels which could be used by drug molecules to enter deeper layers of the skin.

It was evident that the microneedle penetration depth by the Dermapen® was significantly deeper in comparison to the Dermastamp™. Such observation may be attributed to the oscillating motion of the device during skin application which has been suggested to improve skin penetration [254]. Previous work by Izumi *et al.* investigated the influence of vibration on the penetration of microneedles into an *in vitro* silicone skin model. The group observed that the application of vibrating microneedles at 30 Hz during skin application resulted in a reduction in the force needed to penetrate the skin [255]. This reduction in puncture force is attributed to the reduction in effective frictional forces experienced by microneedles under vibration [256]. The rapid vibration of the microneedles also mitigates the likelihood of viscoelastic materials such as skin from attaching to the microneedle during the insertion step. This reduction of effective frictional forces experienced by oscillating microneedles may also serve as an explanation as to why the Dermapen® displayed lower peak insertion force in comparison to the Dermastamp™, shown in Figure 2-4.

Another factor that may influence microneedle insertion into the skin is the different organization of the microneedles on the Dermastamp and Dermapen systems. From Figure 2-7 **(a)** and **(b)** along with microscopy image from Figure 2-6 **(a)** and **(b)** it is evident that the 36 microneedles on the Dermapen® are organised in rows whereas the 42 microneedles on the Dermastamp™ are organised in concentric circles. The needles on Dermapen® are closely distributed to one another in comparison to the needles on the Dermastamp™. Previous work by Olatunji *et al.* highlighted that insertion force increases when microneedle interspacing decreases [257]. In contrast to the finding by Olatunji *et al.,* we observed that although the needle interspacing on the Dermapen® are closer than the Dermastamp™, the

Dermapen® still required less insertion than the Dermastamp™. By comparing our findings to that of Olatunji *et al.*, it can be postulated that the method (oscillating vs non-oscillating) in which the microneedle is applied to the skin overrides the influence of microneedle interspacing on insertion force and penetration depth.

By comparing the penetration data for both microneedle systems from Figure 2-6 and Figure 2-7, it is evident that the insertion of microneedles into *in vitro* skin simulant, Parafilm M® stacks, were significantly deeper than that of *ex vivo* skin tissue. Such disparity in results suggest that the *in vitro* test developed by Larraneta *et al.* may have some limitations when the insertion data is translated to *ex vivo* tissues and potentially *in vivo.* Both Parafilm M® and skin are inherently viscoelastic materials which display both elastic and viscous properties under deformation. Unlike skin, which is an elastic biological tissue that returns to its normal state after mild stretching or compression [258], Parafilm M® exhibits irreversible plastic deformation when stretched or compressed [259].

2.5.4 Skin permeation study

A permeation study was conducted to investigate the effect of different commercial microneedle systems on the permeation of imiquimod, a drug used in the management of BCC, that displayed poor cutaneous permeation [68]. One of the strategies to overcome the limited permeation of imiquimod is to employ permeation enhancing strategy such as microneedle. Upon microneedle application, transient microchannels are generated within the skin that promote the delivery of the drug across the skin. The amount of imiquimod (µg) recovered from the various Franz cell components following the 24-hour permeation study is displayed in Figure 2-8.

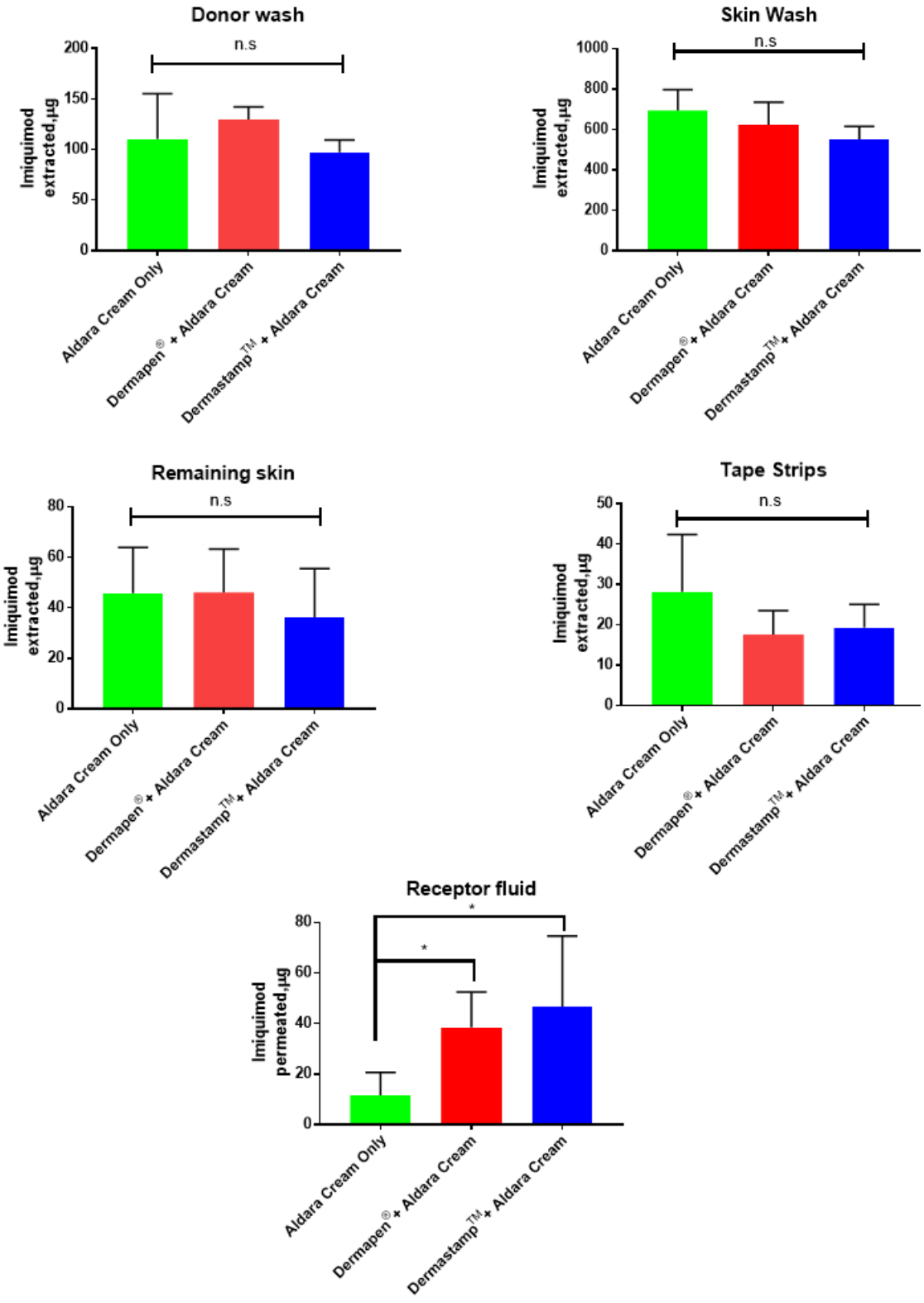

Figure 2-8 HPLC analysis of the mean amount of imiquimod recovered from the different Franz cell components (donor chamber wash, skin wash, tape strips, remaining skin and receptor fluid) post-permeation study. Data is presented as the mean ± SD (n = 6). Differences were calculated using one-way ANOVA, followed by Tukey's post hoc test, and deemed significant at $p<0.05$. n.s = not statistically significant at $p>0.05$.

For all treatment modalities, we observed no statistical difference (*p>0.05*) in the amount of imiquimod recovered from different Franz cell components (donor wash, skin wash, tape strips and remaining skin) except for the receptor fluid. With regards to receptor fluid, it was seen that when the skin was pre-treated with either microneedle systems, a strategy known as poke-and-patch, we observed enhanced delivery of imiquimod across the skin relative to the cream only control. However, it was worth noting we observed no statistical difference in the permeation of imiquimod into the receptor fluid between Dermapen® and Dermastamp™. In addition, it is also observed that the amount of imiquimod that was delivered into the remaining skin using the poke-and-patch strategy were statistically similar between all three treatment strategies. This highlights that using a poke-and-patch strategy with these commercial microneedle systems only enhanced the amount of drug delivered across the skin but not into the skin. As the intended target site for imiquimod is the dermis where nodular BCC resides, this suggest that the poke-and-patch strategy with these commercial microneedle systems may not be a suitable strategy for managing this type of skin tumour as we did not observe any enhancement in intradermal delivery of imiquimod into the skin relative to the commercial cream Aldara™.

One possibility for the similarity in permeation profiles for the two microneedle systems is attributed the fact that both systems successfully breached the *stratum corneum*, epidermis and down to superficial dermis as highlighted in Figure 2-7 **(c)** and **(d)**. It has been reported that the thickness of porcine epidermal layer varies between 30-140 µm [260] and it was shown that both microneedle system penetrated into the porcine skin to a depth of at least 200 µm, reaching the superficial dermal layer of the skin. This layer of the skin is viscoelastic due to the presence of a dense network of collagen and elastin [105,133,261]. Although the Dermapen® may puncture the skin deeper than the Dermastamp™, immediately upon microneedle removal the channels generated in the dermal layer of the skin immediately recoils and reseals conferring similar resistance in permeation for imiquimod across the dermis for both microneedle systems. A limitation which is frequently highlighted when a poke-and-patch strategy is adopted for solid microneedles systems [262].

2.6 Conclusion

In conclusion, this work expands our knowledge on the mechanical insertion of microneedles into the skin. Applying biaxial strain on the skin indeed influences the penetration of microneedles into the skin. It was apparent that the two commercially available microneedle systems, Dermapen® and Dermastamp™ have very different insertion force profiles with increasing strain. For all the skin strain levels investigated, it was evident that the Dermapen® required less insertion force than the Dermastamp™. Interestingly, the percentage of successful insertion continues to increase before plateauing with increasing skin strain for the oscillating Dermapen®. In contrast for the Dermastamp™, the percentage of successful microneedle insertions increases with strain before decreasing at higher strain rate. In terms of insertion depth, it was apparent that the penetration of the Dermapen® was much deeper than that of the Dermastamp™. Such a difference was not detected when the microneedle systems were evaluated using the commonly used Parafilm M® stack insertion study but only became apparent when the devices were evaluated *ex vivo*. The lower insertion force and deeper penetration provided by the Dermapen® was attributed to the oscillating feature of the microneedle system which mitigates the effective frictional force experienced by the needle during skin insertion. Lastly, although the Dermapen® may puncture the skin deeper than the Dermastamp™, such difference in penetration did not affect the permeation profile of imiquimod into and across the skin when a poke-and-patch drug delivery strategy was used as shown in the *ex vivo* permeation study.

Chapter 3 Intradermal delivery of an immunomodulator for basal cell carcinoma; expanding the mechanistic insight in solid microneedle enhanced delivery of hydrophobic molecules

Akmal Sabri [a], Jane Ogilvie [b], John McKenna [c], Joel Segal [d], David Scurr [a], and Maria Marlow [a]

[a] School of Pharmacy, University of Nottingham, Nottingham NG72RD, United Kingdom.

[b] Walgreens Boots Alliance, Thane Road, Nottingham, NG90 1BS

[c] Leicester Royal Infirmary University Hospitals Leicester Dermatology Department, Infirmary Square, Leicester LE1 5WW

[d] Department of Mechanical, Materials and Manufacturing Engineering, Faculty of Engineering, University of Nottingham, Nottingham, NG8 1BB

This chapter has been published in the following research article:

A.H. Sabri, J. Ogilvie, J. McKenna, J. Segal, D. Scurr, M. Marlow, 2020. Intradermal Delivery of an Immunomodulator for Basal Cell Carcinoma; Expanding the Mechanistic Insight into Solid Microneedle-Enhanced Delivery of Hydrophobic Molecules, Molecular Pharmaceutics https://doi.org/10.1021/acs.molpharmaceut.0c00347

Acknowledgement of research work done by co-authors

- J. Ogilvie, D. Scurr, M. Marlow, J. Segal: Supervisors to A.H. Sabri and supervised him during the writing of the article. Critically reviewed the manuscript and editing.

Keyword: Microneedles, imiquimod, basal cell carcinoma, time-of-flight secondary ion mass spectrometry.

3.1 Abstract

Basal cell carcinoma (BCC) is the most common cutaneous malignancy in humans. One of the most efficacious drugs used in the management of basal cell carcinoma BCC is the immunomodulator, imiquimod. However, imiquimod has physiochemical properties that limit its permeation to reach deeper, nodular tumour lesions. The use of microneedles may overcome such limitations and promote intradermal drug delivery. The current work evaluates the effectiveness of using an oscillating microneedle device Dermapen® either as a pre or post-treatment with 5% w/w imiquimod cream application to deliver the drug into the dermis. The effectiveness of microneedles to enhance the permeation of imiquimod was evaluated *ex vivo* using a Franz cell set up. After a 24-hour permeation experiment, sequential tape strips and vertical cross-sections of the porcine skin were collected and analysed using time-of-flight secondary ion mass spectrometry (ToF-SIMS). In addition, respective Franz cell components were analysed using high performance liquid chromatography (HPLC). Analysis of porcine skin cross-sections demonstrated limited dermal permeation of 5% w/w imiquimod cream. Similarly, limited dermal permeation was also seen when 5% w/w imiquimod cream was applied to the skin that was pre-treated with the Dermapen®, this is known as poke-and-patch. In contrast, when the formulation was applied first to the skin prior to Dermapen® application, this is known as patch-and-poke, we observed a significant increase in intradermal permeation of imiquimod. Such enhancement occurs immediately upon microneedle application, generating an intradermal depot that persists for up to 24 hours. Intradermal colocalization of isostearic acid, an excipient in the cream, with imiquimod within microneedle channels was also demonstrated. However, such enhancement in intradermal delivery of imiquimod was not observed when the patch-and-poke strategy used a non-oscillating microneedle applicator, the Dermastamp™. The current work highlights that using the patch-and-poke approach with an oscillating microneedle pen may be a viable approach to improve the current treatment in BCC patients who would prefer a less invasive intervention relative to surgery.

3.2 Introduction

Basal cell carcinoma (BCC) is the most common skin cancer in humans [263]. Despite having a low tendency to metastasize, BCC may result in substantial peripheral tissue destruction if left untreated [264]. The two most common BCC subtypes are superficial and nodular [31]. Superficial BCC generally manifests and proliferates parallel to the epidermis [32,33]. On the other hand, nodular BCC typically resides deep within the papillary and reticular dermis [36]. Despite the effectiveness of surgical interventions which display a 95% cure rate [43], accurate detection of tumour margins prior to surgery is pivotal in ensuring complete tumour resection. Such prerequisites are both time-consuming and technical, which limits the use of such treatments [61]. In addition, not all BCC patients are suitable for surgical intervention and some may opt for non-surgical treatment due to lower overall cost and better cosmetic outcomes [63-64]. This is further corroborated by the findings of Tinelli *et al.* who reported that patients generally preferred topical therapy over surgical intervention [265]. One of the most efficacious drugs used in topical therapy for BCC is the immunomodulator, imiquimod [59].

Recently, William *et al.* reported that topical imiquimod therapy for nodular BCC resulted in a cure rate significantly less than surgical intervention [34]. The lower cure rate of imiquimod in treating BCC, particularly the nodular variant is due to the location of the tumour that resides deeper within the dermis [266]. This tumour location provides an anatomical barrier for imiquimod to permeate in sufficient quantity to eradicate the tumour [267].

One of the methods to improve the delivery of therapeutics for the treatment of BCC is via the use of microneedles. Microneedles are biomedical devices that consist of arrays of fine needles with lengths ranging between 250 and 1000 µm. Upon application to the skin, these devices generate transient channels that provide a route across the *stratum corneum* into the deeper layers of the skin [262]. The application of microneedle-based drug delivery for the management of BCC was pioneered by Donnelly *et al.* [169]. Donnelly *et al.* demonstrated that microneedles enhanced the localised delivery of aminolaevulinic acid into the skin for BCC treatment. Further to this Naguib *et al.* demonstrated, via a

murine model, the feasibility of using solid microneedles to enhance the intradermal delivery of 5-fluorouracil to treat skin tumours. Following these studies, various groups have explored different microneedle designs to deliver a range of anticancer agents such as methyl aminolevulinic acid [170], meso-tetra(N-methyl-4-pyridyl)orphinetetratosylate [171], and itraconazole [172].

Detailed analysis of the dermal distribution of pharmaceuticals within the skin strata is paramount in order to evaluate the permeation enhancement effect conferred by microneedles for targeted skin delivery. Traditionally, chromatographic analysis (e.g. high-performance liquid chromatography, HPLC) is frequently implemented in microneedle permeation studies in order to evaluate the delivery of drugs into and across the skin. However, this analytical method is dependent on efficient drug extraction and effective column separation from co-extracted endogenous components of the skin. Furthermore, the tissue manipulation steps and extraction procedures lead to the loss of valuable spatial information regarding drug localisation within the skin tissue [197]. In order to overcome this limitation, microneedle permeation studies frequently utilise fluorescently-tagged molecules in order to track their distribution within the skin [104]. This method of tracking dermal distribution can be achieved via the use of confocal laser scanning microscopy (CLSM). CLSM utilises point illumination via the use of focused laser beam that is rastered across the sample of interest. The emitted fluorescence from the in-focus plane is passed through a pinhole onto a detector, which measures the fluorescence from the site of analysis. Any out-of-focus fluorescence is blocked by the pinhole, which is said to be confocal with the focal point of the objective lens. CLSM has been used to tracked the permeation of compounds delivered using microneedle-based delivery systems [129,132,144]. Although this approach allows the experimenters to track drug localisation within the skin, the use of fluorescent tagging with this method alters the physiochemical properties of molecules leading to erroneous estimation of drug distribution in biological tissues [198]. In addition, the need for different fluorescent tagging to track the dermal distribution of multiple molecules complicates the method even further. Hence, there is a clear need for advanced analytical techniques to be utilised in the field of

microneedle research to allow researchers to track drug distribution within skin tissues in a label-free manner.

Some of the techniques that offer label-free imaging of dermal drug distribution include confocal Raman microscopy and stimulated Raman scattering microscopy. These techniques has been used to visualise the dermal distribution of several pharmaceuticals such as 5-fluorouracil [199], ketoprofen [200], and terbinafine [200]. Although these methods offer experimenters the ability to visualise dermal drug distribution in a label-free manner, the Raman signal is normally a weak. This necessitates that the molecule of interest should be present at sufficient concentration to allow detection. In addition, the drug molecules also need to possess Raman active chemical groups that are different from native skin biomolecules to permit differentiation and detection. Another issue associated with Raman-based imaging is the high level of autofluorescence from biological tissue which can mask the weak Raman signal thus limiting the utility of these techniques to map dermal drug distribution [202].

Time-of-flight secondary ion mass spectrometry (ToF-SIMS) on the other hand is a powerful surface analytical technique that confers excellent mass and spatial resolution along with chemical sensitivity [203,204]. Analysis of samples using ToF-SIMS allows chemical mapping of the distribution of a compound of interest by tracking the mass-to-charge ratio (*m/z*) of specific molecular ions from the mass spectra. This analytical approach allows us to track the distribution of compounds, both exogenous and endogenous, within a biological milieu in a label-free manner. Such analytical power conferred by ToF-SIMS has led to the use of the technique to analyse a range of biological materials such as insulin and even cancerous tissue [216–221]. In addition, the ability of the instrument to track the topical permeation of pharmaceuticals and cosmeceuticals such as chlorhexidine [227,268], ascorbic acid [197], dihydroquercetin [230], fatty acids [235], carvacrol [231] and roflumilast [224] highlights the value of the technique in skin research. Despite the powerful analytical capability offered by this form of mass spectrometry imaging, the utility of ToF-SIMS in evaluating the effectiveness of microneedle-based drug delivery system has yet to be fully demonstrated.

A previous study demonstrated the limited permeation of imiquimod into the skin when the drug is administered as a topical cream [68]. This work also demonstrated that solid microneedles provided a solution to deliver imiquimod beyond the *stratum corneum* and into the viable epidermis. However, such delivery depth was not sufficient to reach the dermal depth in which nodular BCC typically resides. In the present work, we explore further the application of solid microneedles as a physical permeation enhancement strategy to deliver imiquimod deeper into the dermis for BCC treatment. In addition, the microneedle system should deliver imiquimod to a depth of approximately 400 µm below the skin surface which is the target region in which nodular BCC typically manifests [34]. The current study highlights that the approach in which microneedles are used in combination with an imiquimod cream, can lead to the successful intradermal delivery of imiquimod. The concept of using a patch-and-poke strategy with solid microneedles was initially conceptualized in a review published by McCaffrey *et al.* as a method to deliver genes into the skin [269]. Patch-and-poke is defined at the application of formulations onto the skin prior to solid microneedle application. However, research on the effectiveness of the patch-and-poke approach using solid microneedle is limited. This is because research on solid microneedles focuses mostly on a poke-and-patch strategy to deliver drug into or across the skin. Furthermore, using the poke-and-patch strategy results in the generation of hydrophilic/aqueous microneedle channels post application that act as a barrier to the permeation of hydrophobic drugs into the skin [247,270]. Therefore, there is a lacuna in the knowledge about the effectiveness of using the patch-and-poke approach with solid microneedles.

In this work, it is demonstrated that a patch-and-poke strategy is more effective in delivering imiquimod intradermally than the conventional poke-and-patch approach. This work also demonstrated that microneedle oscillation during application plays an important role in the effective intradermal delivery of imiquimod using the patch-and-poke strategy.

3.3 Materials

Imiquimod was purchased from Cayman Chemicals, USA. Aldara™ topical cream (5% w/w imiquimiod), MEDA Company, Sweden was purchased from Manor Pharmacy, UK. Dermapen®, which is a microneedling pen, was purchased from ZJChao, China. The microneedles on the Dermapen® had a tapered conical structure. The microneedle had a base diameter of 370 µm with a tip radius of 53.4°. The distance between microneedles (pitch) was 620 µm. Microneedles were arranged in rows which formed an overall circular area. The Dermapen® has five different oscillation speeds- 8000, 10000, 12000, 14000 and 16000 RPM. In addition, the needle length could be adjusted between 250-1500 µm. For the purpose of the permeation study, we selected a microneedle length 1000 µm and an oscillation speed of 8000 RPM. During application, the pen was held by one hand with gentle pressure while the hand was used to hold the skin in place. The Dermastamp™ which was a microneedle stamp, was purchased from Teoxy Beauty, Wuhan, China. The microneedles on the Dermastamp™ also had a tapered conical structure. The microneedle had a base diameter of 210 µm with a tip radius of 22.8°. The distance between microneedles (pitch) was 1050 µm. Microneedles were arranged in an annular fashion which formed an overall circular area. The Dermastamp™ had no oscillating function and the needle length of the Dermastamp used was fixed to 1000 µm. During application, the Dermastamp™ was held by one hand with and applied by one swift stamping motion with gentle pressure. Sodium acetate was purchased from Sigma-Aldrich, UK. Acetonitrile (HPLC grade) and glacial acetic acid were obtained from Fisher Scientific, UK. Teepol solution (multipurpose detergent) was ordered from Scientific Laboratory Supplies, UK. D-Squame standard sampling discs (adhesive discs) were ordered from Cuderm corporation, USA. OCT media was obtained from VWR International Ltd. Belgium. Deionised water was obtained from an ELGA reservoir, PURELAB® Ultra, ELGA, UK. All reagents were of analytical grade, unless otherwise stated. *Ex vivo p*orcine skin was used to investigate the permeation of imiquimod due to the similarities in histology, thickness and permeability to human skin [246]. Skin samples were prepared from ears of six-month-old pigs obtained from a local abattoir prior to steam cleaning. Full skin thickness was used to prevent altering the skin

biomechanical properties which may lead to over-penetration of the microneedles into the skin [66]. The porcine skin samples were stored at -20 °C until analysis. The integrity of the skin samples prepared via this method was assessed by electrical resistance, using the method and guidelines described by Davies *et al.* using EVOM2 Voltohmmeter (World Precision Instruments, U.S.A). Only skin that produced an electrical resistance reading of greater than 10 kΩ was used. [271].

3.4 Methods

3.4.1 Permeation study of 5% w/w imiquimod cream through porcine skin

Imiquimod dermal permeation with and without microneedle treatment was evaluated *ex vivo* using a Franz-type diffusion cell. Prior to the permeation study, skin samples were defrosted for at least an hour at room temperature. The skin was trimmed into small pieces according to the surface area of the donor chamber of the Franz diffusion cell (Soham Scientific, Cambridgeshire, UK). The trimmed skin samples were equilibrated by placing them above the receptor compartment for 15 minutes prior to skin treatment. The Franz cells used in this study had a receptor compartment volume of 3 ml.

The porcine skins were subjected to the following treatment modalities: i) application of 20 mg Aldara™ cream alone ii) application of 1000 µm microneedles to the skin as a pre-treatment using Dermapen® followed by 20 mg Aldara™ cream. 1000 µm refers to the length of the microneedles. This is known as the poke-and-patch approach. 12-microneedle array cartridges were used for this treatment. iii) Application of 20 mg Aldara™ cream followed by 1000 µm microneedle treatment using Dermapen®. This is known as the patch-and-poke approach. Either a 12-microneedle or a 36-microneedle array cartridge were used for this treatment. All the arrays used in the microneedle treatment groups have similar surface area of application which is 0.64 cm^2.

The choice of microneedles selected for this permeation were based on several reasons. Firstly, the microneedle selected were manufactured from stainless steel which displayed good biocompatibility with biological tissues such as skin [272,273]. In addition, the high mechanical strength of stainless-steel microneedles overcome the issues of microneedle tip breakage and deposition within the skin upon

application. Such problems are frequently encountered with microneedles fabricated from brittle materials such as ceramics and silica [74]. Furthermore, the higher mechanical strength of stainless-steel microneedles ensure relative to polymeric microneedles ensures that these microneedles would have higher insertion efficiency into the skin while thus generating more microneedle channels for drug permeation into the skin [274]. The microneedle length selected was 1000 µm as this microneedle length gave an insertion depth of 600 µm as shown in Figure S3 1**.** This depth at which nodular BCC typically grows within the skin [34,35]. Guided by these information and insertion data, stainless-steel microneedles with lengths of 1000 µm (Dermapen®) were selected for the skin permeation study.

Next, the porcine skins were placed on top of the receptor compartment filled with 3 ml of degassed 100 mM acetate buffer pH 3.7. This buffer was selected as the receptor phase in order to maintain a sink condition throughout the permeation study. This is due to the insolubility of imiquimod at neutral or basic pH values. Various groups have reported the use of acetate buffer pH 3.7 as the receptor phase in imiquimod permeation studies [53–55]. The skin was then secured between the donor and receptor compartment of the diffusion cell using a metal clamp, with the stratum corneum side facing the donor compartment. Upon assembling the Franz diffusion cell, the permeation experiment was conducted over a period of 24 hours in a thermostatically controlled water bath set at 36.5 ^{o}C.

3.4.2 Quantification of imiquimod post-permeation study

After a 24-hour permeation experiment, the excess cream was removed and collected from the skin surface by careful application of sponges soaked with 3% v/v Teepol® solution. The sponges were pooled for imiquimod HPLC analysis as a total skin wash. Any formulation which might have spread to the donor chamber was collected by the sponges and stored for imiquimod analysis by HPLC as a donor chamber wash. Upon removing excess formulation from the skin surface, 15 sequential tape strips were collected from the skin as detailed in Section 3.4.3.

The amount of imiquimod from the different Franz cell elements (skin wash, donor chamber wash, pooled tape strips and remaining skin after tape stripping) were extracted by the addition of 5, 5, 10

and 5 mL of methanol extraction mixture (methanol 70%: acetate buffer pH 3.7 100 mM 30%) respectively using a previously reported method [52]. Samples were then vortexed for 1 minute and sonicated for 30 minutes before being left overnight. Subsequently, samples were vortexed again and sonicated for a further 30 minutes. 1 ml of the extracts were collected and spiked with 100 µl of 100 µg/ml propranolol as an internal standard. The samples were then filtered through 0.22 µm membrane. For the receptor fluid, 1 ml of the solution from each Franz cells were collected and spiked with 100 µl of 100 µg/ml propranolol as an internal standard before being filtered through 0.22 µm membrane. HPLC analysis was carried out using an Agilent 1100 series instrument (Agilent Technologies, Germany) equipped with degasser, quaternary pump, column thermostat, autosampler and UV detector. System control and data acquisition were performed using Chemostation software. The details of the HPLC chromatographic conditions are as follow: column C18 (150 × 4.6 mm) ACE3/ACE-HPLC with a particle size of 5 µm, pore size of 100 Å, pore volume of 1.0 ml/g and a surface area of 300 m^2/g, Hichrom Limited, UK. The mobile phase composition for analysis of extracts from skin wash, donor chamber wash, pooled tape strips and remaining skin consists of 10 mM acetate buffer: acetonitrile (79:21). Whilst, the mobile phase composition for analysis of receptor fluid consists of 10 mM aqueous acetate buffer: acetonitrile (70:30). The system operated at a flow rate of 1.0 mL/minute, UV detection at λ_{max}=226 nm, injection volume of 40 µL and column temperature of 25 °C.

3.4.3 Tape stripping and cryo-sectioning of porcine skin post-permeation experiment for ToF-SIMS analysis.

After 24 hours, the skins were detached from the Franz diffusion cells. Excess Aldara™ cream was removed. 15 sequential tape strips were collected for each skin samples. Sequential removal of corneocytes was judged by the resistance felt during the stripping step and the change in opacity of the tape post stripping. The skin was rotated 180° for each tape strip. This ensures that the tape stripping would not result in premature removal of the whole *stratum corneum* during tape stripping. All tape strips collected were stored in a freezer at -20 °C until analysis.

In order to measure the depth of imiquimod permeation into the skin, the permeation experiments were repeated as described above in Section 3.4.1. After the permeation study, excess formulation was removed and a 1 cm x 1 cm of each microneedle application site was fresh frozen with liquid nitrogen. Skin cross-sectioning was performed using a cryostat (Leica CM3050 S Research Cryostat, UK). The skin slices were then thaw mounted on a glass slides and stored at -20 ^{o}C prior to ToF-SIMS analysis.

3.4.4 ToF-SIMS analysis

ToF-SIMS was used to analyse individual tape strips and cryo-sectioned porcine skin samples. ToF-SIMS analysis was performed using a ToF-SIMS IV instrument (IONTOF, GmbH) with a Bi_3^+ cluster source. A primary ion energy of 25 KeV was used, the primary ion dose was preserved below 1×10^{12} per cm^2 to ensure static conditions. Pulsed target current of approximately 0.3 pA, and post-acceleration energy of 10 keV were employed throughout the sample analysis. The mass resolution for the instrument was 7000 at *m/z* 28. The scanned area of the tape strips samples was (4 mm × 4 mm) encompassing the skin area exposed to Aldara™ cream during Franz cell diffusion experiments. On the other hand, an analysis area of (1.5 mm x 3 mm) was employed for the skin cross-sections. Both sample types were analysed at a resolution of 100 pixels/mm. An ion representing biological material and therefore indicative of skin (skin marker) was identified as CH_4N^+ and was used to threshold the data sets from tape strips. CH_4N^+ is a common fragment observed in organic materials such as biological specimens. Therefore, this secondary ion was used to track the presence of corneocyte extracted on the tape strips. The data was reconstructed to remove the data from the adhesive tape material found between the fissures in the stripped skin and therefore the data was only analysed from the skin material. Following this, each image of the individual tape strip (4 mm × 4 mm) was divided into four smaller data sets of (2 mm × 2 mm) which results in four repeats (n = 4) for each sample and their intensities were normalised to the total ion intensity. All ToF-SIMS data were acquired in positive ionisation mode as this gave the best ionization intensity for imiquimod based on our previous work [68]. In addition, pure imiquimod, pure isostearic acid and Aldara™ cream

reference spectra were obtained by analysing the pure drug, pure fatty acid and the cream on silicon wafers using ToF-SIMS.

3.4.5 Understanding the effect of vibration of Dermapen® on the intradermal permeation of imiquimod

One of the features of the Dermapen® is the ability of the device to vibrate the microneedles at the tip of the device. In order to understand the role of oscillation on the intradermal delivery of imiquimod into the skin, the permeation study was repeated as detailed in Section 3.4.1. However, porcine skins were subjected to the following treatment modalities: i) Application of 20 mg Aldara™ cream followed by 1000 µm microneedle treatment using Dermapen®. A 36-microneedle array cartridge was used for this treatment ii) Application of 20 mg Aldara™ cream followed by 1000 µm microneedle treatment using a non-vibrating Dermastamp™. The Dermastamp™ consists of 40-microneedle array per stamp. The Dermastamp™ was similar to the Dermapen® in terms of microneedle length used (which is 1000 µm) and the material used to manufacture the needle, which was stainless steel. The only main difference was that the Dermastamp™ did not have any vibration function. After a 24-hour permeation study, the skin samples were cryo-sectioned and analysed by ToF-SIMS using the same conditions outlined in Section 3.4.4. In addition, a time point study (0, 1, 6, 12 and 24 hours) was conducted to evaluate how the dermal distribution of imiquimod changes over the course of 24 hours with the patch-and-poke approach using the Dermapen®.

3.5 Results and discussion

3.5.1 Skin insertion and dye binding study

An *ex vivo* skin insertion study was conducted to establish the microneedle length needed to reach the skin strata where nodular BCC typically resides. From the supplementary data, Figure S3 1, it can be seen that when the length of Dermapen was adjusted to 1000 µm, an insertion depth of approximately 600 µm was observed. Such penetration depth is sufficient to reach beyond the epidermis layer and into the dermis layers. As nodular BCC typically manifests from the *stratum basale*

at the dermoepidermal junction and grows deeper into the dermis, this suggests that adjusting the Dermapen® to 1000 µm would provide sufficient penetration to reach nodular BCC tumours [4]. Therefore, guided by the skin insertion study data, we selected the 1000 µm length microneedles (Dermapen®) for the skin permeation study.

3.5.2 HPLC analysis of imiquimod from Franz cell components post-permeation study.

HPLC analysis was performed in order to quantify the amount of imiquimod that has remained or permeated into respective Franz cell compartments over the course of the permeation study. The mean amount of imiquimod (µg) recovered from the various Franz cell components following the 24-hour permeation study is shown in Figure 3-1. The amount of imiquimod extracted from the applied dose from cream alone was highest in the skin wash relative to other Franz cell components. This suggests that when imiquimod is delivered as a topical cream, the drug displayed limited permeation into the skin. Such findings agree with previous work that showed that application of imiquimod as a topical cream resulted in the majority of the dose being recovered from the skin surface [68]. However, the amount of imiquimod recovered contradicts the finding by Stein *et al.,* who found that only 19% of the applied Aldara™ cream remained on the skin surface highlighting sufficient dermal permeation of imiquimod [275]. Such enhanced permeation reported by Stein and co-worker is likely due to the use of murine skin which is more permeable and thinner in comparison to human and porcine skin [276].

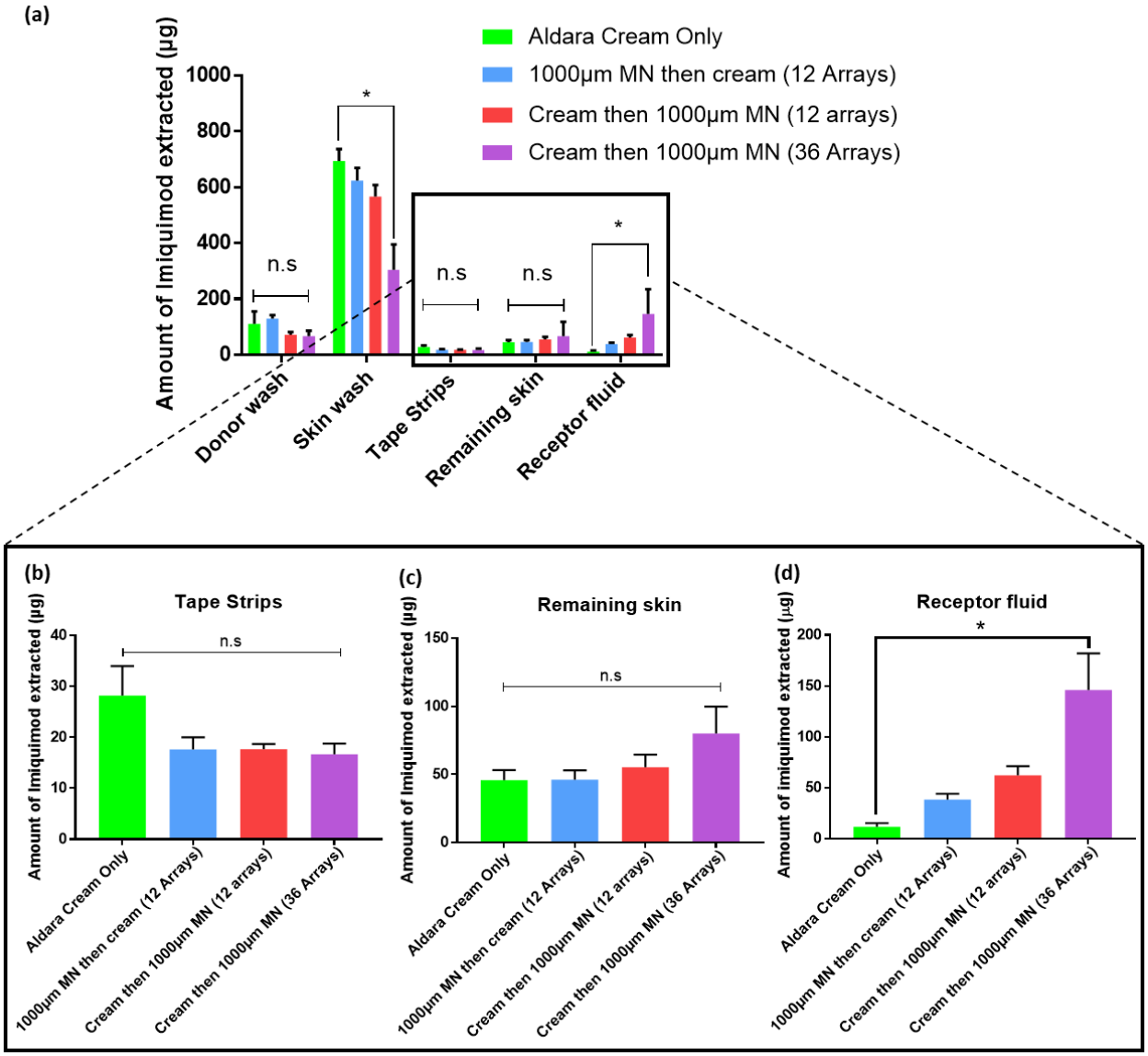

Figure 3-1 HPLC analysis of the mean amount of imiquimod recovered from the different Franz cell components (donor chamber wash, skin wash, tape strips, remaining skin and receptor fluid) post-permeation study. Data is presented as the mean ± SD (n = 6). The inset details the amount of imiquimod that has permeated into (b) tape strips (c) remaining skin and (d) receptor fluid. Differences were calculated using one-way ANOVA, followed by Tukey's post hoc test, and deemed significant at $p<0.05$. n.s = not statistically significant at $p>0.05$. MN refers to microneedles.

One of the ways to circumvent the limited dermal permeation of imiquimod is to utilise a physical permeation enhancer such as microneedles to promote the delivery of the drug into the skin. Thus, in this study, we utilised a microneedling device, Dermapen® in order to enhanced imiquimod delivery

into the skin. One of the earliest and simplest microneedle-based approaches to promote intradermal drug delivery is via the poke-and-patch method [247]. However, when we conducted an *ex vivo* skin permeation study, we observed that the delivery profile of imiquimod with the poke-and-patch approach was similar to topical cream application as shown in Figure 3-1.

One of the possible explanations for the similar permeation profile of imiquimod into and across *ex vivo* skin between these two strategies (cream alone vs poke-and-patch) is due to the formation of hydrophilic microneedle channels from the outflow of dermal interstitial fluid upon microneedle application [247,270]. Such channels may act as a barrier for the effective permeation of a hydrophobic drug such as imiquimod [277]. Therefore, we also investigated if the application of topical Aldara™ cream (5% w/w imiquimod) followed by microneedling, a patch-and-poke approach, as an alternative strategy to improve the delivery of imiquimod into the skin. When the *ex vivo* skin permeation study was carried out using the patch-and-poke strategy, we observed a decrease in the amount of imiquimod recovered from the skin wash. This was statistically significant when the patch-and-poke approach used a 36-needle cartridge.

Although not statistically significant, the HPLC analysis of imiquimod extracted from remaining skin showed an increasing trend in the amount of imiquimod delivered into the skin with the patch-and-poke approach in comparison to the poke-and-patch approach. However, the difference in the amount delivered across the skin was most prominent from the analysis of receptor fluid. Analysis of receptor fluid indicates an increase in the amount of imiquimod delivered into and across the skin. However, such differences were only statistically significant when the patch-and-poke approach was adopted using the 36-microneedle array Dermapen®.

In addition, we have established that sink condition was maintained throughout our study as will be described. The saturation solubility of imiquimod, which is a weak base, in the receptor compartment, acetate buffer 100 mM, has been reported by De Paula *et al.* is 1360.2 (µg/mL) at pH 4.0 [52]. Therefore, as we used a lower pH acetate buffer, pH 3.7, which has been used in by other investigators [53–55], we

predicted that the solubility of the drug at pH 3.7 would be comparable if not higher than that reported by De Paula *et al*. Data for the receptor fluid that has been converted into µg/mL in the Supplementary Information (Figure S3 2) indicates that the highest concentration detected was on average 48.7 µg/ml. This indicates that after 24 hours, the highest average concentration imiquimod within the receptor fluid was 3% of its saturation solubility concentration reported. Ng *et al.* have indicated that in order for sink conditions to be maintained, the penetrant concentrations in the receptor solution should not be more than 10% of their saturation solubility concentration [278]. Based on this information, we can confirm that sink conditions were indeed maintained throughout the permeation study.

The increase in amount of imiquimod delivered across into the receptor fluid may be attributed to the enhanced amount of imiquimod delivered into the dermis using the patch and poke approach. Imiquimod is known to have low aqueous solubility such as in the interstitial fluid within the dermal microenvironment, but displays higher solubility in acidic pH due the molecule being a weak base [52]. Based on the physiochemical property of the drug, it is likely that imiquimod delivered into the dermis may have partitioned into the acidic acetate buffer within the receptor solution over time as the drug has higher solubility in the acidic buffer. In addition, it is worth noting that the dermis receives a rich blood supply that is derived from the hypodermis. Therefore, it is postulated that any drug that reaches this layer of the skin, after traversing the tortuous epidermal layers, has the potential to be rapidly absorbed into the systemic circulation [4]. Based on Figure 3-1 **(c)** and **(d)**, it can be inferred that the patch-and-poke strategy may result in improved delivery into the dermis which is target region for nodular BCC. The partitioning of the drug into the receptor fluid may provide some indication of potential systemic exposure. Based on Figure 3-1 it can be inferred that although the patch-and-poke strategy may result in improved delivery into the dermis, such mode of delivery may lead to increased systemic exposure of imiquimod which could result is side effects such as flu-like symptoms [279]. Therefore, in order to limit the likelihood of such side effects arising, it could be suggested that

reducing dosing frequency for the patch-and-poke strategy relative to the dosing frequency of Aldara™ cream application may mitigate the likelihood of such side effects arising.

3.5.3 ToF-SIMS analysis of tape strips post-permeation study

Despite the quantitative results provided by HPLC analysis, the method does not confer any information detailing imiquimod distribution within individual layers of skin. Therefore, an additional analytical technique was used to provide spatial information regarding imiquimod permeation. Analysis of samples using ToF-SIMS allows a chemical map of the distribution of a compound of interest to be acquired as well as providing information on how such distribution changes with depth. It has been mentioned in Section 3.4.3 that the skin was washed 3 % Teepol solutions followed by subsequent wash with deionised water to remove excess Aldara™ cream from the skin surface. Where sensitive analyses are done on these samples by ToF-SIMS, concerns may arise of potential interfering chemicals from the Teepol solutions on the samples. Additional validation has been done to show that the main surfactants present in Teepol which are sodium dodecylbenzene sulphonate, sodium lauryl sulfate and Pareth-10 (polyethylene glycol ether) are not present in detectable amount via ToF-SIMS analysis following subsequent wash with deionised water. This can be seen in the supplementary data, Figure S3 3

In previous work, it has been found that the permeation of the imiquimod across the skin could be tracked by monitoring the molecular ion $C_{14}H_{17}N_4^+$ [68]. ToF-SIMS secondary ion images of the analysed tape stripped area, which represents the exposed area of the skin to Aldara™ cream during Franz cell diffusion experiment, are illustrated in Figure 3-2. An ion representative of skin tissue (CH_4N^+) and a diagnostic imiquimod ion ($C_{14}H_{17}N_4^+$) ion image for tape strips no. 6 is shown in Figure 3-2 **(a)**. It was apparent that the signal from the skin marker (CH_4N^+) was much lower in the two top ion images. However, should there be a reduction or increase in the ions collected, each ToF-SIMS image collected is normalised to the total ion collected. As all the ion images collected have been scaled to the same value as shown with scale bars, we attributed the signal reduction from the skin marker (CH_4N^+) for

the two top ion images is due to biological variation as the porcine skin used is from different pigs' ears.

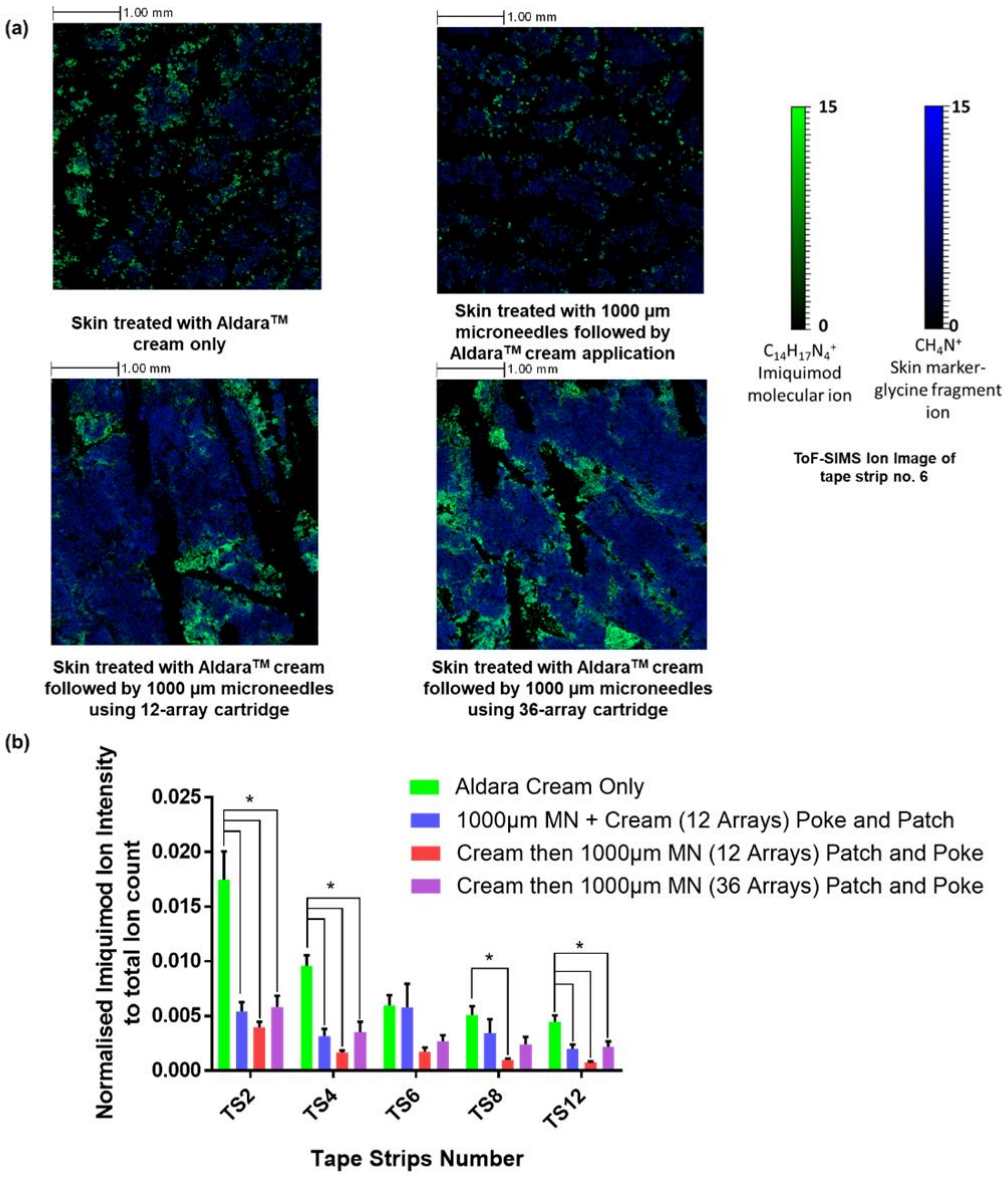

Figure 3-2 (a) ToF-SIMS 4 mm × 4 mm secondary ion distribution maps on tape strip surfaces. The scale bar represents 1 mm, and the images have been normalized to the total ion image. The distribution maps are from tape strip no. 6, showing the distribution of the imiquimod molecular ion ($C_{14}H_{17}N_4^+$), and biological marker for corneocytes (CH_4N^+) (b) ToF-SIMS exported peak intensities (normalized to total ion intensity) for imiquimod molecular ion peak as a function of increasing tape strip number from porcine skin. The skin was either treated with AldaraTM cream only, pre-treated with microneedles (1000 µm) before AldaraTM cream application or treated with microneedles (1000 µm) of different array size after cream application. Data are expressed as

mean ± SEM for n=12 analytical repeats. MN-refers to microneedles, Differences were calculated using one-way ANOVA, followed by Tukey's post hoc test, and deemed significant at p<0.05.

Figure 3-2 (b) highlights how imiquimod ion intensity changes with stratum corneum depth as a function of tape strip number. The decrease in permeation of imiquimod from tape strips no. 2 to no. 12 is due to an increase in water content with stratum corneum depth which limits the permeation of imiquimod [280]. The poor water solubility and lipophilicity of imiquimod resulted in limited dermal permeation when the drug is applied to the skin as a topical cream. Specifically, as imiquimod is a lipophilic molecule, when the drug is only applied as a topical cream it is likely that the molecule mostly permeates from the cream and into the superficial layer of the stratum corneum. As the superficial layer of the stratum corneum are known to be lipid rich, imiquimod would partition into this lipid matrix and remain there relative to permeating deeper into the skin. This may serve as an explanation for the higher imiquimod ion intensity observed from tape strips obtained from skin samples treated with Aldara™ cream alone relative to skin subjected to microneedle application.

In contrast, it can be seen from Figure 3-2 **(b)** that perforating the skin with microneedles either before or after cream application results in a decrease in the measured imiquimod ion intensity from ToF-SIMS analysed tape strips in comparison to tape strips from skin samples treated with Aldara™ cream alone. This finding agrees with the trend observed from the HPLC results in Figure 3-1 **(b)** that showed lower imiquimod concentration in the pooled tape strips from skin samples subjected to microneedle perforation relative to Aldara™ cream only treated skins. This observation may be attributed to the generation of microneedle channels within the *stratum corneum* with microneedle application. When the microneedle was applied as a pre-treatment using the 12 arrays via the poke-and-patch strategy, the *stratum corneum* is now perforated with aqueous microneedle channels. As the drug is poorly water soluble these aqueous channels may hinder the permeation of the drug into the *stratum corneum* resulting in lower imiquimod ion intensity relative to Aldara™ cream. Without any aqueous microneedle channels in the cream only treated group, the drug will be able to partition and remain in the lipid rich matrix of the *stratum corneum*. However, when the microneedle was applied after

cream application using either the 12 or 36 arrays, via the patch-and-poke strategy we also observed lower imiquimod ion intensity relative to Aldara™ cream. In this instance, the microneedle application is now mechanically inserting the drug across the *stratum corneum* and directly into the epidermis and dermis. Therefore, there will be less cream available on the skin surface as evidenced from the HPLC data in Figure 3-1 **(a)** for skin wash. As there is less cream on the skin surface, there will now be less drug to partition from the skin surface and into the *stratum corneum* resulting in lower imiquimod ion intensity relative to Aldara™ cream.

On the other hand, the current finding contradicts our previous report that showed higher imiquimod ion intensity from ToF-SIMS analysed tape strips obtained from the poke-and-patch approach relative to topical cream application alone [68]. In the previous work, a shorter microneedle length (250 µm) was employed while 1000 µm was used in this study. The shorter needles used in the previous work may generate shallower microneedle channels that remained mostly within the viable epidermis layer. These shallower microneedle pores are more likely to promote the permeation of imiquimod into the superficial layer of the skin rather than flowing deeper into the dermis. These shallower drug-filled microneedle channels may act as focal points for the drug to radiate out to surrounding corneocytes, resulting in higher imiquimod intensity when a shorter microneedle length is used with the poke-and-patch approach relative to topical cream alone.

3.5.4 ToF-SIMS Analysis of Skin Cross-sections

3.5.4.1 Effect of microneedle pre-treatment "poke-and-patch" versus post-treatment "patch-and-poke" on the delivery of imiquimod.

It was apparent from ToF-SIMS analysis of tape strips as shown in Figure 3-2 **(b)**, that using either the poke-and-patch or patch-and-poke approach, we observed a similar trend in the permeation of imiquimod through the *stratum corneum*. This suggests that both microneedle application strategies, either before or after cream application may not influence the permeation of imiquimod through the *stratum corneum.* In order to investigate if the two solid microneedle application strategies may

influence the intradermal delivery of imiquimod deeper into the skin, we employed ToF-SIMS analysis of skin cross-sections in addition to tape strip analysis. Understanding the spatial distribution of molecular species is paramount in elucidating the effectiveness of drug delivery systems within a biological tissue. Conventional liquid chromatography mass spectrometry (LC-MS) is traditionally employed to understand the effectiveness of a drug delivery strategy, however the extraction process employed leads to loss in spatial information [281]. ToF-SIMS has the capability to simultaneously map molecular ion of the dosed compound in tandem with the native fragment ions from skin tissue [268]. Examples of ion signals used to distinguish respective skin strata are $C_5H_{15}NPO_4^+$ (a fragment ion for phosphatidylcholine) and $C_{17}H_{32}N^+$ (a fragment ion for ceramide) [224]. The *stratum corneum* displays high levels of ceramide whilst being devoid of phospholipids [282]. Therefore, phosphatidylcholine ion fragments were used to map the viable epidermis and dermis while ceramide fragment ions were used to identify the *stratum corneum*.

From Figure 3-3, it is evident that there is limited availability of imiquimod within deeper skin layers when applied either through topical cream alone **(i)** or via the poke-and-patch **(ii)** approach. However, when Aldara™ is applied via the patch-and-poke approach in Figure 3-3 **(iii)** and **(iv)**, we observed enhanced imiquimod delivery into the dermis. This observation agrees with the trend observed from the HPLC analysis from Figure 3-1 **(c)** that shows an increase in imiquimod concentration in the skin with the patch-and-poke approach using 36-needle array Dermapen®. In addition, the delivered drug is localised within microchannels formed during microneedle insertion. Typically nodular BCC presents 400 µm below the skin surface [34]. The ToF-SIMS analysis of skin cross-sections from Figure 3-3 suggest that the patch-and-poke approach may be a suitable strategy to enable enhanced imiquimod delivery into the dermis for the treatment of nodular BCC.

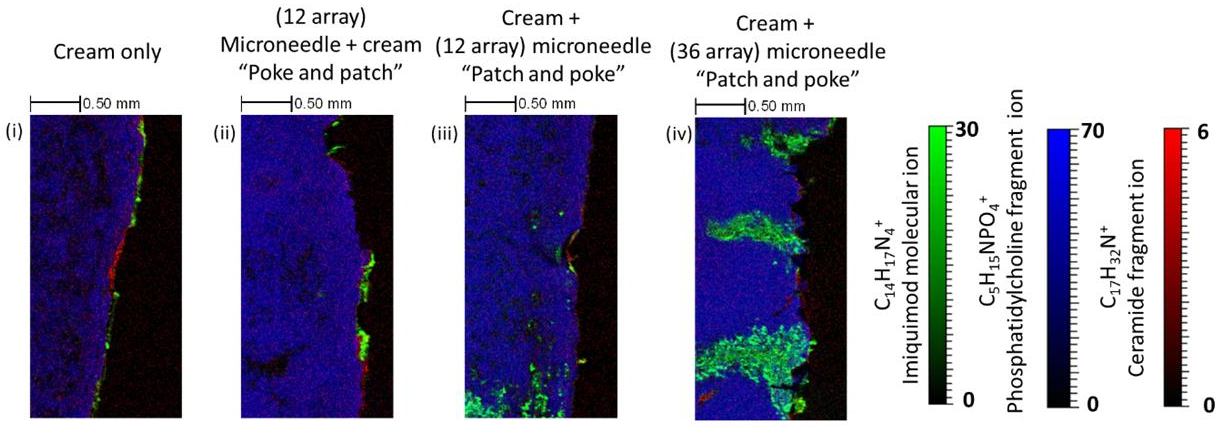

Figure 3-3 ToF-SIMS secondary ion distribution map of skin cross sections from porcine skin that were treated with (i) Aldara™ cream (5% w/w imiquimod) alone (ii) in combination with Dermapen (1000 µm) using the 'poke-and-patch' approach (iii)-(iv) in combination with Dermapen (1000 µm) using the 'patch-and-poke' approach with different needle arrays. This resulted in improved drug delivery into the lower layer of the skin (dermis) with the 'patch and poke' strategy.

It has been demonstrated previously that ToF-SIMS can chemically image drug permeation through microneedle channels in the *stratum corneum* and upper epidermis [68] . However, these studies adopted a poke-and-patch approach that showed localisation of imiquimod within the *stratum corneum* which agrees with the current findings [68]. One of the possible explanations for the limited drug permeation with the poke-and-patch approach is the viscoelastic property of the skin that causes some regions of the skin to recoil and close over time after microneedle application. In some instances, the closure can be as rapid as 5 minutes [95,97]. This rapid closure of microneedle pores may limit dermal permeation of imiquimod via the poke and patch approach. Additionally, perforating the skin with microneedles prior to cream application promotes the flow of more interstitial fluid into the microneedle channels. This results in the formation of hydrophilic pores that act as a barrier to the entry of hydrophobic drugs, such as imiquimod, deeper into the dermis [247,270]. This phenomenon does not affect the intradermal delivery of imiquimod using the patch-and-poke approach, as the drug is mechanically driven into the skin during repeated microneedle insertion circumventing the effect of microneedle pore closure.

Another possible limitation of the poke and patch approach with solid microneedles is limited drug flux from highly viscous formulations through microneedle perforated skin. This hypothesis was evaluated by Milewski *et al*. The group observed that as the viscosity of a formulation increases, the flux of naltrexone hydrochloride decreased across microneedle pre-treated *ex vivo* mini-pig skin [283]. Pharmaceutical creams, such as Aldara™ (5% w/w imiquimod) are inherently viscous formulations relative to gels and lotions [284]. The rapid closure of microneedle channels coupled with slow permeation of the drug from the highly viscous Aldara™ cream into the skin may only limit the drug distribution into the *stratum corneum* with the poke-and-patch approach.

Owing to the parallel detection capability, ToF-SIMS analysis can simultaneously map the presence of excipients within biological tissues as well as the drug. One example of an excipient that is present in Aldara™ cream is isostearic acid. Conventionally, isostearic acid has been incorporated in various topical and cosmetic products as a permeation enhancer [285]. However, Walter *et al.* have shown that isostearic acid also displayed active pharmacological properties which are independent of the immune mediated response induced by imiquimod [286]. Isostearic acid plays a critical role in inflammasome activation, which is pertinent for the overall efficacy of Aldara™ cream. It is also therefore of interest to chemically map the presence of isostearic acid in the microneedle channels. Through monitoring the molecular ion peak at *m/z* 285.3 indicated in Figure 3-4 **(a),** we were able to detect the co-localisation of the excipient within the microneedle channels as shown in Figure 3-4 **(b)** and **(c)**. The peak assignment for isostearic acid was validated by referring to fragmentation pattern at *m/z* 285 with the reference spectra of pure isostearic acid on silicon wafer as shown in the supplementary data (Figure S3 4).

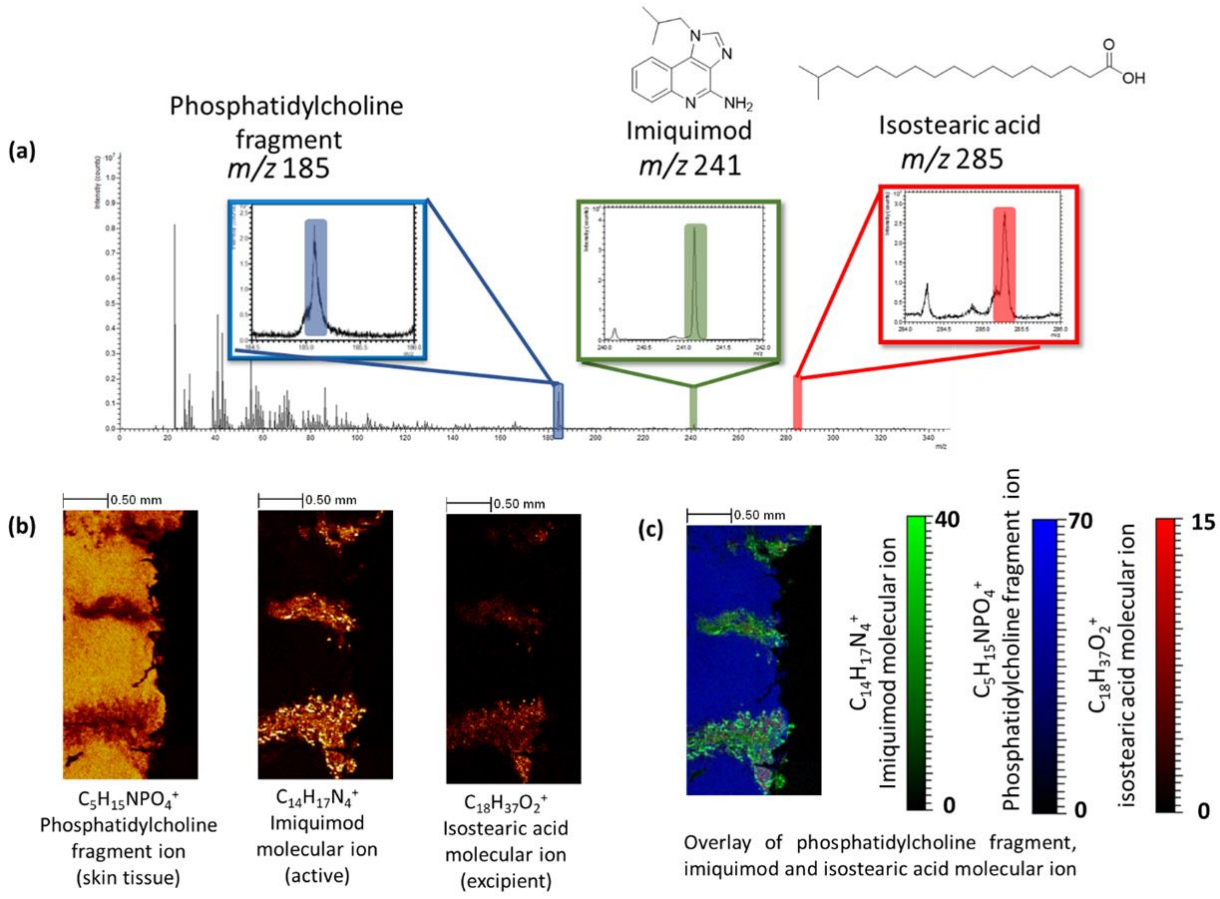

Figure 3-4 (a) Positive polarity ToF-SIMS spectra of ex vivo porcine skin treated with 5% w/w imiquimod topical cream using patch and poke approach, where the inset spectrum shows the peak of the $[M+H]^+$ of imiquimod at m/z=241 and $[M+H]^+$ of isostearic acid at m/z=285.3 (b) ToF-SIMS 2D chemical ion maps of phosphatidylcholine (biological tissue), imiquimod (active) and isostearic acid (excipient) acquired from cross section analysis of ex vivo porcine skin tissue after a 24 hour permeation experiment. Chemical ion map shows location of skin tissue along with the biodistribution of active and excipient. (c) an overlay image of the excipient isostearic acid marker ($C_{18}H_{37}O_2^+$) in red, imiquimod ($C_{14}H_{17}N_4^+$) in green and the skin marker ($C_5H_{15}NPO_4^+$) in blue. The overlay indicates the ability ToF-SIMS to detect the colocalisation of imiquimod (active) and isostearic acid (excipient) within the microneedle channel within the ex vivo skin tissue.

Traditional methods to study microneedle-enhanced permeation require the use of fluorescently-labelled drug molecules to track the intradermal localisation of pharmaceuticals within the skin. This approach may alter the physiochemical properties of the drug leading to erroneous estimation of drug permeation into the skin [198]. In addition, such methods only allow the tracking of the active drug

molecule which limits our understanding of the dermal distribution of the other components in the formulation such as polymers and fatty acid-based surfactants. The current work, highlights that the patch-and-poke strategy using oscillating solid microneedles may be a simple strategy to enable co-localised intradermal delivery of a poorly water soluble active and an excipient as evidenced by ToF-SIMS analysis. Similar to imiquimod, isostearic acid also has low water solubility which limits the penetration of the fatty acid into the more aqueous dermis [287]. The co-delivery of these compounds into the dermis ensures that isostearic acid may execute a synergistic action along with imiquimod in stimulating an effective inflammatory response for the treatment of nodular BCC.

3.5.4.2 Effect of vibration on the delivery of imiquimod into the dermis using patch-and-poke approach with Dermapen

One of the features of the Dermapen® is the vibration of microneedles at the tip of the device. This generates a stamp-like motion overcoming the issue of varying pressure of application by end-users [288]. Hence, we attempted to understand if vibration plays a functional role in the intradermal delivery of imiquimod using the patch and poke approach. We repeated the experiment using an *ex vivo* porcine skin permeation study followed by ToF-SIMS analysis of skin cross-section. As a comparator to the vibrating Dermapen®, we treated the skin with a Dermastamp™. The Dermastamp™ perforates the skin in a single stamp motion without the assistance of a vibrating electric motor. Both microneedle devices used were 1000 µm in length. It can be seen from Figure 3-5 that generation of imiquimod filled microneedle channels within the dermis with the patch-and-poke strategy only occurred when the skin was treated with the oscillating Dermapen® following cream application.

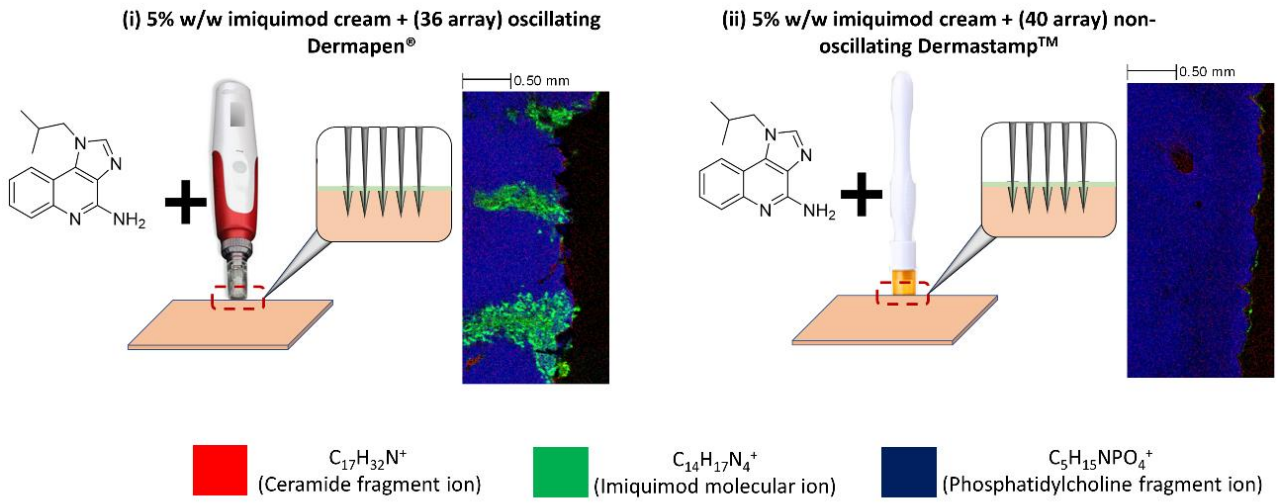

Figure 3-5 ToF-SIMS secondary ion distribution map of skin cross sections for ex vivo porcine skins that were treated with (i) Aldara cream (5% w/w imiquimod) followed by Dermapen® (1000 µm) application and (ii) Aldara cream (5% w/w imiquimod) application followed by 1000 µm Dermastamp™

The ability of the Dermapen® to efficiently penetrate the skin relative to other microneedle systems is attributed to the vibrating-stamping motion of the device during device application [254,289]. Izumi *et al.* explored the effect of vibration on the penetration of microneedles into artificial silicone rubber skin. The group found that applying a vibration of 30 Hz to a microneedle array during skin insertion resulted in a reduction in the force needed to penetrate the skin [255]. The reduction in puncture force is attributed to the reduction in frictional forces experienced by microneedles under vibration [256]. The rapid vibration of the microneedles also mitigates the likelihood of viscoelastic materials such as skin and topical cream from attaching to the microneedle during the insertion step. This phenomenon provides an explanation as to why the patch-and-poke motion using Dermastamp™ was unsuccessful in delivering imiquimod into the dermis. The topical cream along with superficial skin tissues (i.e., *stratum corneum*) may attach to the tip of the needles during microneedle application resulting in poor penetration profile. Aoyagi *et al.* also showed that that vibration indeed plays a critical role in microneedle insertion. However, Aoyagi and co-workers also demonstrated that a reduction in puncture force is also achievable when the skin is stretched prior to microneedle application [122]. Unlike the Dermastamp™, the presence of shoulders at the tip of microneedle cartridge of the Dermapen®

generates tension on the skin during microneedle application. This helps to reduce the propensity of the skin to fold around the needles while decreasing the puncture force needed to perforate the skin.

As it was apparent that the patch and poke approach using the Dermapen® provided the most effective intradermal delivery of imiquimod into skin, we then attempt to understand how imiquimod dermal distribution changes over 24 hours with this strategy. Subsequently, we repeated the *ex vivo* Franz cell permeation experiment using the patch-and-poke approach and performed ToF-SIMS analysis on the skin at five different time points. From Figure 3-6, we can see that using the patch-and-poke approach, the generation of imiquimod filled channels took place immediately (0 hours) post microneedle application on the skin after cream application. It is well known that the conventional poke-and-patch strategy is reliant on passive diffusion for the entry of drug molecules across aqueous microneedle channel to achieve intradermal delivery [283]. Such a process is both slow and ineffective for the delivery of hydrophobic molecules due to their poor solubility in the aqueous channels. Coupled with the rapid closure of microneedle channels, this renders the poke-and-patch approach a poor strategy for the delivery of hydrophobic drugs. On the other hand, the patch-and-poke approach is dependent on the mechanical insertion of drug directly into the skin during microneedle application which overcomes the issues of solubility and pore closure.

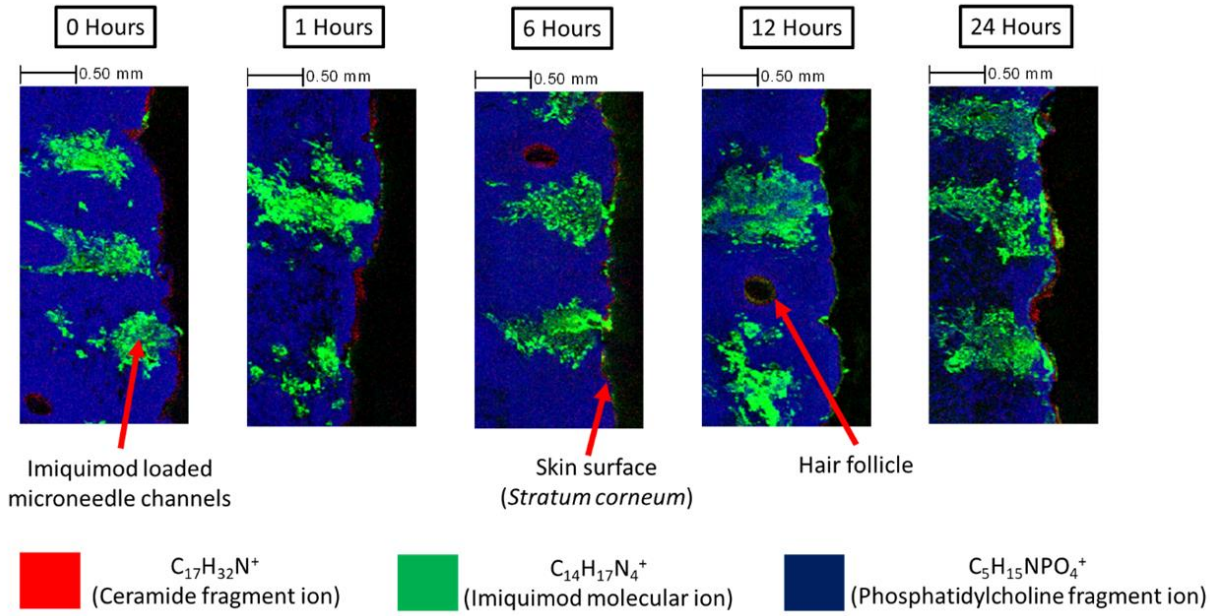

Figure 3-6 ToF-SIMS secondary ion distribution map of porcine skin cross sections from different time points. These images highlight improved drug delivery into the lower layer of the skin (dermis) that persisted in the skin up to 24 hours. In addition, the formulation was immediately present in the deeper layers of the skin upon microneedle application. Phosphatidylcholine highlights the viable epidermis and dermis while ceramide highlights the top layer of the skin. Black circles indicate areas filled by hair follicles.

The presence of imiquimod loaded channels within the dermis that persisted for 24 hours was attributed to the poor water solubility of the drug [290]. The limited water solubility of imiquimod coupled with the fact that the water composition increases with dermal depth serves as possible explanation as to why imiquimod channels remained in the *ex vivo* skin tissues up to 24 hours [291]. The application of imiquimod cream followed by Dermapen® application generates localised regions of imiquimod within the skin which resemble the structure of the microneedle channels. This shows that using a patch-and-poke strategy with oscillating microneedles provide an elegant synergy of existing products to enhance localisation of imiquimod intradermally. Such a drug delivery strategy may help prevent the requirement for surgical intervention for the treatment of deep-rooted basal cell carcinoma.

3.6 Conclusion

This work expands current understanding on the application of solid microneedles as a physical permeation enhancement strategy to promote the delivery of imiquimod into the skin for the treatment for BCC. The approach in which microneedles are used in combination with Aldara™ cream plays a critical role for the successful intradermal delivery of imiquimod into the skin. It has been demonstrated that in order to successfully deliver a hydrophobic molecule such as imiquimod into the dermis, a patch-and-poke approach is superior to the conventional poke-and-patch approach. Furthermore, it has also been demonstrated that an oscillating microneedle system, such as the Dermapen® for the patch-and-poke strategy, is a critical factor in providing successful intradermal delivery of imiquimod into the skin. Using this novel patch-and-poke approach hydrophobic drugs are mechanically inserted into the microneedle channels within the dermis upon microneedle application. This avoids the generation of hydrophilic/aqueous microneedle channels formed using the traditional poke-and-patch which can pose as a barrier to drug permeation. In summary, this work suggests that the combination of Aldara™ cream in combination with the oscillating Dermapen® provides an elegant synergy to enhance localised intradermal delivery of imiquimod. Such a strategy may provide a less invasive intervention to patients who would prefer an alternative treatment to surgery for the treatment of nodular BCC.

3.7 Supplementary Figures

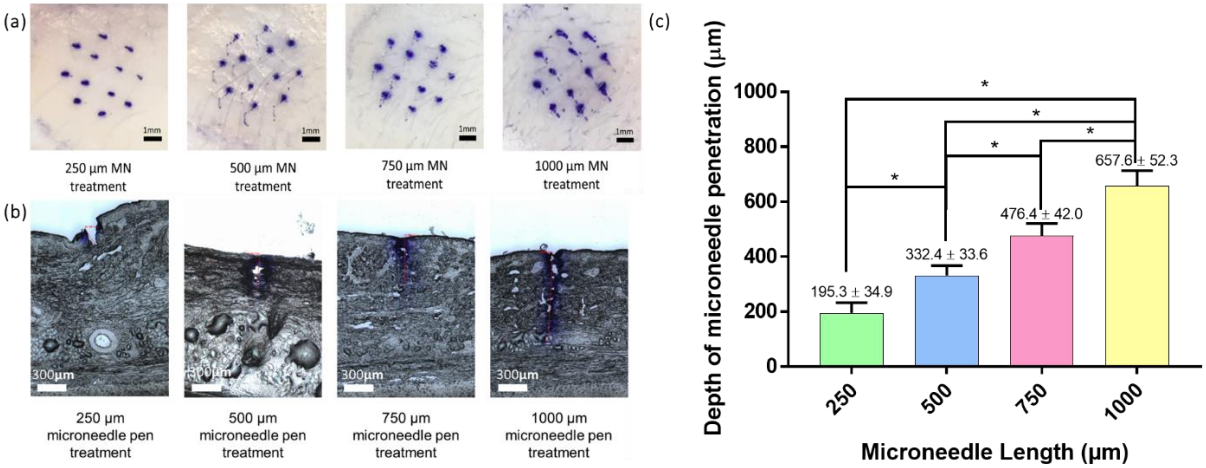

Figure S3 1 (a) Gentian violet staining of microneedle channels formed after microneedle application of different length followed by gentian violet staining (b) Optical microscopy images of porcine skin histological cross sections after application of microneedle pens of differing lengths. Microneedle channels were visualised and tracked by monitoring region of the skin stained by gentian violet solution. (c) Microneedle penetration depth measured from the length of microneedle channels from skin cross-sections. Data are expressed as mean ± SD, n=8. Differences were calculated using one-way ANOVA, followed by Tukey's post hoc test, and deemed significant at p<0.05. n.s = not statistically significant at p>0.05.

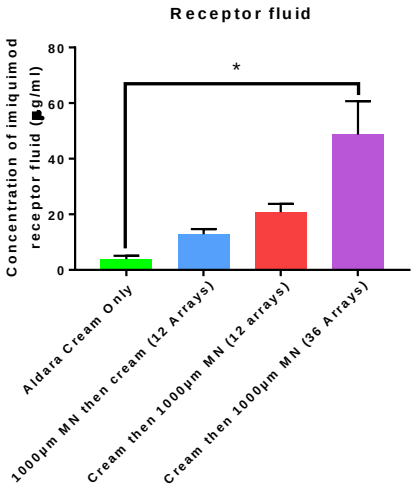

Figure S3 2 HPLC analysis of imiquimod concentration in receptor fluid post-permeation study. Data is presented as the mean ± SD (n = 6). Differences were calculated using one-way ANOVA, followed by Tukey's post hoc test, and deemed significant at p<0.05. n.s = not statistically significant at p>0.05.

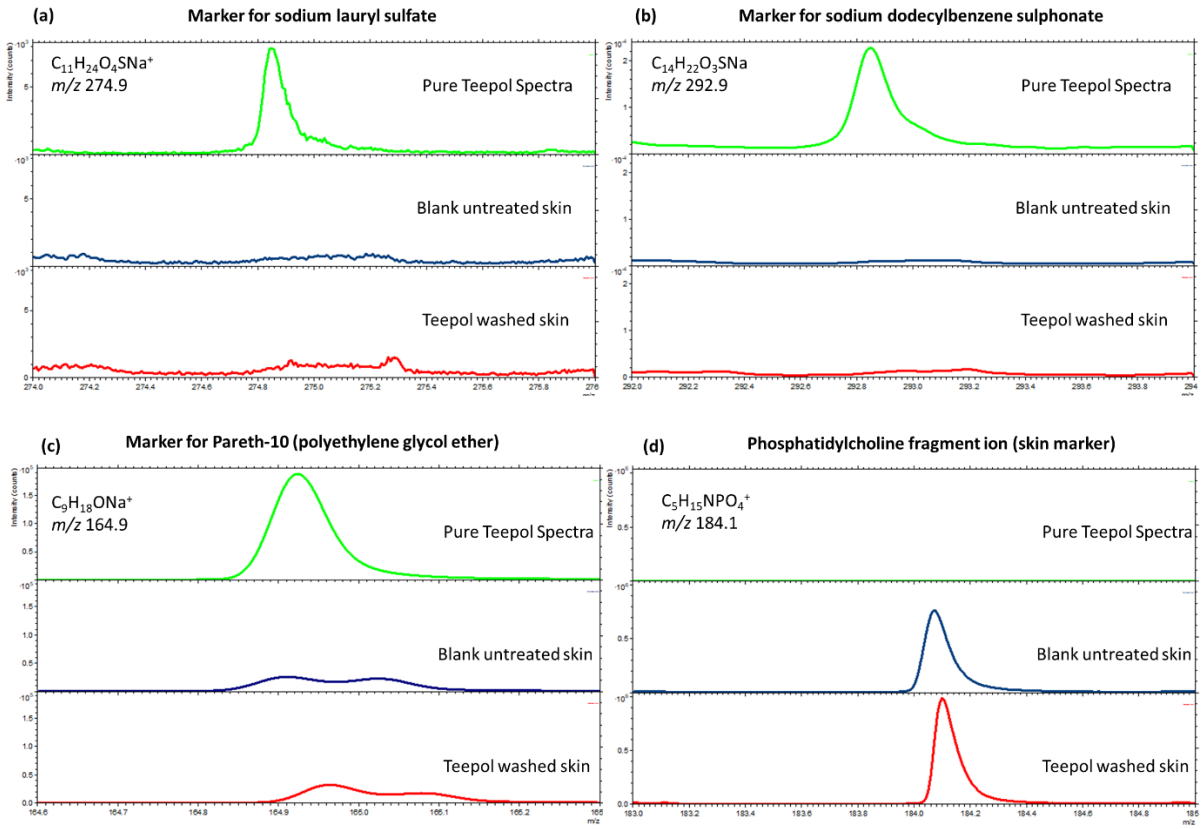

Figure S3 3 ToF-SIMS spectra of pure concentrated Teepol solution, blank untreated skin and skin that has been washed with Teepol followed by subsequent wash with deionised (similar to how skin samples were treated in the experimental chapter post permeation). The control spectra highlight the absence of (a) sodium lauryl sulfate (b) sodium dodecylbenzene sulphonate and (c) Pareth-10 (polyethylene glycol ether) from the Teepol washed skin following subsequent wash with deionised water. In addition, Figure (d) showed that the phosphatidylcholine fragment ion $C_5H_{15}NPO_4^+$ which is used as a marker to identify the skin was absent from the Teepol solution. Collectively this control spectra showed that there was minimal chemical interference from the washing step post permeation on the ToF-SIMS analysis of the samples.

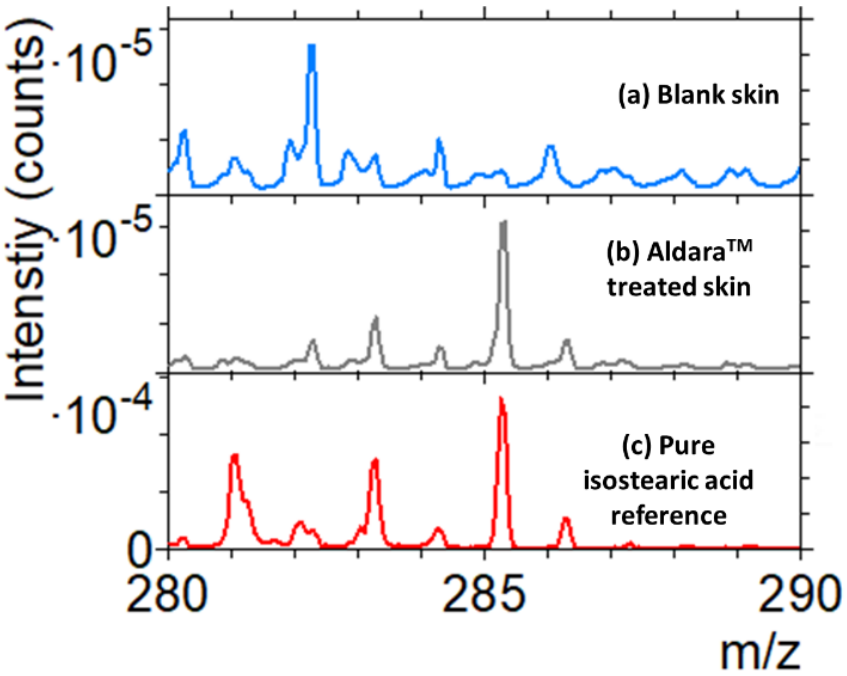

Figure S3 4 Overlaid ToF-SIMS spectra of (a) blank untreated skin (b) skin treated with Aldara™ cream using the patch and poke approach (c) pure isostearic acid reference, showing the peak of the $[M+H]^+$ of isostearic acid ($C_{18}H_{37}O_2^+$) at m/z = 285.

Chapter 4 Intradermal delivery of imiquimod using polymeric microneedles for basal cell carcinoma

Akmal H. Sabri [a], Zachary Cater [b], Pratik Gurnani [a], Jane Ogilvie [c], Joel Segal [b], David J. Scurr [a] and Maria Marlow [a]*

[a] School of Pharmacy, University of Nottingham, Nottingham NG72RD, United Kingdom.

[b] Advanced Manufacturing Technology Research Group, Faculty of Engineering, University of Nottingham, Nottingham, NG8 1BB

[c] Walgreens Boots Alliance, Thane Road, Nottingham, NG90 1BS.

This chapter has been published in the following research article:

A.H. Sabri, Z. Cater, P. Gurnani, J. Ogilvie, J. Segal, D. Scurr, M. Marlow, 2020. *Intradermal delivery of imiquimod using polymeric microneedles for basal cell carcinoma*, Int J. Pharmaceutics https://doi.org/10.1016/j.ijpharm.2020.119808

Acknowledgement of research work done by co-authors

- Zachary Cater: An undergraduate Mech Eng. student supervised by A.H. Sabri and J. Segal. Zachary Cater assisted Akmal Sabri with the computer aided design (CAD) for the microneedle master structures along with its subsequent production at the University of Nottingham Institute for Advanced Manufacturing. The work done by Zachary Cater formed part of **Section 4.4.1 Design and production of microneedle master structure and microneedle PDMS moulds.** In addition, Zachary Cater was also involved in critically reviewing the manuscript for publication.
- Pratik Gurnani: Assisted Akmal Sabri in PVPVA polymer characterisation by assisting Akmal in running the differential scanning calorimetry for the polymer. The data for the differential scanning calorimetry is in **Section 4.7 Supplementary Figures**. In addition, Pratik Gurnani was also involved in critically reviewing the manuscript for publication.

- J. Ogilvie, D. Scurr, M. Marlow, J. Segal: Supervisors to A.H. Sabri and supervised him during the writing of the article. Critically reviewed the manuscript and editing.

Keyword: Microneedles, Imiquimod, Basal cell carcinoma, Time-of-flight secondary ion mass spectrometry, Polyvinylpyrrolidone-co-vinyl acetate

4.1 Abstract

Despite being one of the most efficacious drugs used in the treatment of basal cell carcinoma (BCC), imiquimod has limited cutaneous permeation. The current work presents the development of polyvinylpyrrolidone-co-vinyl acetate (PVPVA) microneedles loaded with imiquimod for improving intradermal delivery of imiquimod for the treatment of nodular BCC. *In vitro* permeation studies, using full thickness *ex vivo* porcine skin were used to evaluate the effectiveness of these imiquimod loaded polymeric microneedles in comparison to the topical application of commercial Aldara™ cream. HPLC analysis demonstrated similar intradermal permeation of imiquimod from Aldara™ cream and imiquimod-loaded microneedles despite the microneedle having a six-fold lower drug loading than the clinical dose of Aldara™ used for BCC management. In addition, ToF-SIMS analysis of skin cross sections demonstrated intradermal localisation of imiquimod following microneedle-based delivery while the Aldara™ treated skin showed the drug localised predominantly within the *stratum corneum*. ToF-SIMS analysis also demonstrated intradermal co-localisation of the PVPVA polymer, used in fabricating the microneedle, with imiquimod within the microneedle channels in a label-free manner. This study demonstrates that a polymeric microneedle system with a lower drug loading may be a viable approach in improving the intradermal delivery of imiquimod for the treatment of nodular BCC.

4.2 Introduction

Basal cell carcinoma (BCC) is the most prevalent type of skin cancer, with the number of individuals affected by the disease escalating worldwide. For instance, a large US sex-stratified cohort study by Wu *et al.* highlighted that the incidence rate of BCC in both men and women have doubled over the past 20 years [27]. In addition, similar trends have been reported in Canada, Asia, Australia and Europe [28]. Furthermore, it is anticipated that the incident rate will continue to escalate due to the rise in an aging population coupled with historical UV exposure [29]. Given that UV exposure is a risk factor in developing BCC, it therefore quite common that BCC typically manifests on sun exposed regions of the body such as the face, arms and necks [30]. The two most common BCC subtypes are superficial and nodular [31]. Superficial BCC generally manifests as flat red patches on the skin on the skin surface and proliferates parallel to the epidermis [32,33]. On the other hand, nodular BCC manifests as a translucent pearly nodule that resides within dermis at approximately 400 µm below the skin surface [34,35]. In addition, it has been reported that at least one-third of nodular BCC coexists with superficial BCC [36]

Despite displaying low metastasis rates of 0.0028 %, this form of skin cancer can lead to considerable local tissue destruction (nose, ears and eyelids) leading to poor cosmetic outcomes and disfigurement at the disease site [37,38]. The high incidence rate of the disease also forms a considerable proportion of a dermatologist's workload [39]. Therefore, there is a need to develop a simple and efficacious treatment strategy, which patients could simply administer by themselves in the management of BCC. Although surgical intervention is effective in treating BCC, such treatment is both time-consuming and technical [61]. In addition, some patients may opt for non-surgical alternatives that offer lower

overall treatment costs and improved cosmetic outcomes [64,265]. One of the most effective non-surgical interventions is the topical application of the immunomodulator, imiquimod [59].

Imiquimod is a potent immune response modifier that induces its immunomodulation through Toll-like receptors (TLR) located on antigen presenting cells. Upon binding to these receptors, imiquimod induces the release of pro-inflammatory cytokines which culminate in its antitumoral activity [58]. Imiquimod is marketed as Aldara™ cream (5% w/w) by 3M Pharmaceuticals for the treatment of anogenital warts, actinic keratosis and superficial BCC. Despite its potency, the drug has limited dermal permeation thus reducing its therapeutic value to superficial BCC [67]. However, in the case of nodular BCC, it has been found that topical therapy with imiquimod typically has a lower cure rate than surgical intervention [34]. Such a finding is attributed to the efficient barrier function of the *stratum corneum* which limits the permeation of imiquimod into the skin [68]. In addition, the location of nodular BCC that resides deep within the aqueous dermis presents another barrier for imiquimod delivery. This is because imiquimod is poorly water soluble and thereby has limited permeation into the dermis [267,292]. The poor permeation properties of imiquimod deeper into the skin is attributed to the various physiochemical properties of the drug. It is suggested some of the ideal characteristics for a drug to permeate deeper into the skin include a Mw < 600 Da, a Log P 1.0 to 3.0, a low melting point, and ≤2 hydrogen bonding groups [237]. Although imiquimod meets some of these criteria, the drug has a high melting point of 292 °C and a total of 4 hydrogen bonding groups. The presence of such hydrogen bonding groups, especially the primary amine that may interact with the anionic components of the stratum corneum, contribute to the poor permeation profile of imiquimod deeper into the skin [68]. Furthermore, the drug has poor aqueous solubility which precludes the drug from permeating deeper into the aqueous and water rich dermal layers [35] .The combination of these factors presents a challenge in

delivering imiquimod in a concentrated and localised fashion into the dermis for the treatment of nodular BCC.

It has been reported by patients that topical treatment such as creams are often unfavorable as this drug delivery vehicle typically has poor cosmetic feel upon administration as well as exuding an unpleasant scent once applied. In addition, the restriction in daily activities post application may result in poor compliance [69]. Also, the likelihood of the cream spreading onto clothes and healthy skin also raises the issue of unwanted side effects.

One of the drug delivery platforms that could be utilised to improve the delivery of imiquimod into the dermis for the management of basal cell carcinoma are microneedles. Microneedles consist of arrays of fine micro-projections that generate transient channels when applied to the skin. The accepted view is that microneedles breach the outermost layer of the skin, *stratum corneum*, generating channels which promote the entry of molecules into and across the skin [293]. Microneedles have been widely investigated as a drug delivery platform for skin cancer therapy, as such systems provide more localised delivery of therapeutics. In the context of skin tumours, microneedle-based drug delivery systems can locally mediate the release of drugs and increase their permeation into deeper tumour regions within the skin [237]. Several researchers have investigated the utility of using solid microneedles, as a skin pre-treatment via the poke-and-patch strategy, to improve the utility of delivering anticancer compounds into the skin for the treatment of skin cancer. Naguib *et al.* demonstrated, via a murine model, the feasibility of using solid stainless-steel microneedles to enhance the intradermal delivery of 5-fluorouracil, 5-FU to treat skin tumours. In their *in vitro* work, the group demonstrated that 5-FU flux increased by 4.5-fold when 5-FU cream was applied on microneedle perforated murine skin compared to cream application on intact skin [66]. More recently, Al-Mayahy *et al.* showed that using a two-step

application process involving pre-treating the skin with solid stainless-steel microneedles followed by Aldara™ cream application, they were able to enhance the permeation of imiquimod deeper into the skin [68].

However, the utility of using solid stainless-steel microneedles is limited by the short duration

(< 15 min) than the channels remain open, due to the regeneration of skin, ultimately reducing the amount of drug delivered [95]. Given these limitations of topical cream application, there is an impetus to reformulate imiquimod into a dissolving microneedle system which could offer a more effective and patient friendly treatment strategy for the management of nodular BCC. The simple and straightforward one-step application using dissolving polymeric microneedle patch loaded with imiquimod relative to the two-step application process via the poke-and-patch strategy using solid microneedles and Aldara™ may be a more preferred treatment option for patients. However, there are no studies to date that have evaluated improving the delivery of imiquimod into the dermis via the use of dissolving polymeric microneedles for the management of nodular BCC.

The aim of this study is to fabricate and characterize polymeric microneedles as a drug delivery system to achieve the localised intradermal delivery of imiquimod for nodular BCC treatment. Polyvinylpyrollidone-co-vinyl acetate (PVPVA) microneedles loaded with imiquimod were developed through a microfabrication and micromoulding technique. PVPVA is a biocompatible polymer that is widely used in the pharmaceutical industry as a dry binder in tableting, as a film-forming agent in tablet coating, as well as a film-forming agent in topical drug delivery systems [294,295]. Besides that, being a derivative of PVP, PVPVA is a chemically and biologically inert polymer which obviates the issues of polymer-drug compatibility along with biological toxicities [296,297]. A series of experiments were performed to characterise the

PVPVA microneedle formulation. In addition, an *in vitro* permeation study, using full thickness *ex vivo* porcine skin was used to evaluate imiquimod delivery into and across the skin. HPLC and ToF-SIMS analysis were utilised to illustrate the permeation and dermal distribution of imiquimod into skin following the application of imiquimod loaded microneedles versus Aldara™ cream. This study can serve as a basis for future *in vivo* and clinical studies with imiquimod loaded PVPVA microneedles for nodular BCC treatment.

4.3 Materials

Imiquimod was purchased from Cayman Chemicals, USA. Aldara™ topical cream (5% w/w imiquimod), MEDA Company, Sweden was purchased from Manor Pharmacy, UK. Polyvinylpyrollidone-co-vinyl acetate, PVPVA (Kollidon® VA 64 Mw 15-20 kDa), was kindly provided by BASF (Ludwigshafen, Germany). Polyethylene glycol, PEG 400 was purchased from Sigma Aldrich, Belgium. Sodium carboxymethyl cellulose, Mw 90,000 was purchased from Sigma Aldrich, USA. Glycerol was purchased from Sigma Aldrich, USA. Sodium acetate was purchased from Sigma-Aldrich, UK. Acetonitrile (HPLC grade) and glacial acetic acid were obtained from Fisher Scientific, UK. Teepol solution (Multipurpose detergent) was ordered from Scientific Laboratory Supplies, UK. D-Squame standard sampling discs (adhesive discs) were purchased from Cuderm corporation, USA. OCT media was obtained from VWR International Ltd. Belgium. Deionised water was obtained from an ELGA reservoir, PURELAB® Ultra, ELGA, UK. All reagents were of analytical grade, unless otherwise stated. *Ex vivo p*orcine skin was used in imiquimod permeation studies due to the similarities in histology, thickness and permeability to human skin [246]. Skin samples were prepared from ears of six-month-old pigs obtained from a local abattoir prior to steam cleaning. The skins were of full skin thickness to prevent altering the biomechanical properties of the tissue that may lead to over-penetration of the microneedles into the skin [66]. The porcine skin samples were stored at -20 °C until analysis.

4.4 Methods

4.4.1 Design and production of microneedle master structure and microneedle PDMS moulds

To produce the custom PDMS moulds, a stainless-steel microneedle master structure was designed in SolidWorks 2018 (Dassault Systèmes), consisting of a 10 x 10 array of 300 µm x 300 µm x 1000 µm (W x L x H) pyramidal microneedles with tip-to-tip spacing of 800 µm. This master structure, and a corresponding mould housing, Figure S4- 1, were then produced from stainless-steel using a Kern Evo CNC Micro Milling Machine at the University of Nottingham Institute for Advanced Manufacturing. A polydimethylsiloxane (PDMS) (Sylgard 184®, Dow Corning, Midland, MI) mould was then created from the stainless-steel microneedle master structure. A mixture of elastomer and curing agent, Sylgard 184®, were prepared at a ratio of 10:1 (elastomer: curing agent). The mixture was then degassed for 45 minutes to remove any trapped air in the mixture. After degassing the PDMS mixture was poured into the stainless-steel master mould structure and placed in an 80 ^{o}C oven for one hour to cure the PDMS. After curing, the mould along with the cured PDMS was plunged into an ice bath to allow ease of removal of the cured PDMS mould. The stainless-steel master structure was then cleaned with propan-2-ol before being reused to make further PDMS moulds.

4.4.2 Fabrication of blank and drug loaded polyvinylpyrrolidone-co-vinyl acetate (PVPVA) microneedles

Polymeric microneedles were prepared using a micromolding technique. The PDMS moulds produced as described in Section 4.4.1 were used to fabricate the blank microneedles. The microneedle matrix was prepared using 16.2 % w/v PVPVA (in water) by dissolving the polymer at room temperature and pressure for one hour. Then, 2% v/v of PEG 400 was added to the polymer solution. The polymer solution was then degassed for 30 minutes and 150 µl of the PVPVA solution was then pipetted using a positive displacement pipette into the PDMS mould and centrifuged at 4000 RPM for 15 min at room temperature to fill the needle cavities. Then, excess polymer was removed before leaving the needle

layer to dry overnight in a desiccator. The backing layer of the microneedle patch were prepared using 5.2 % w/w of carboxymethylcellulose, CMC (in water). The backing solution was made by dissolving CMC under stirring at 75 ^{o}C for 2 hours. In addition, 0.66 % v/w of glycerol was added to the backing solution as a plasticiser. Using a positive displacement pipette, 200 µl of the CMC solution was then pipetted on top of the needle layers and centrifuged at 3500 RPM for 10 minutes. The mould was dried at room temperature for 48 hours in a desiccator. The polymeric microneedles were then demoulded and stored in a desiccator until further use. For imiquimod loaded microneedles the fabrication process was repeated in a similar fashion and composition, however the drug, PEG 400 and PVPVA were dissolved in 0.05 M of hydrochloric acid under stirring for 1 hour.

4.4.3 Characterisation of PVPVA microneedles (SEM, tensile strength, skin insertion properties)

4.4.3.1 Microscopy

Polymeric microneedle images were captured using an optical microscope (Zeiss Axioplan, Germany) and an environmental scanning electron microscopy (ESEM) (FEI Quanta 650) in low vacuum mode to visualize the shape and dimensions of the microneedles. For ESEM imaging, the microneedles were mounted on a metal stub using double-sided carbon tape prior to imaging.

4.4.3.2 Measurement of needle fracture force

The needle fracture force of the polymeric microneedles was determined using a texture analyser (Stable Microsystems, UK) following a previously reported method [137]. This is to investigate the effect of applying an axial force parallel to the microneedle vertical axis, similar to the force encountered by the needles during application to the skin. The polymeric microneedles were visually inspected before and after application of the compression force. For this, the force required for compression of the polymeric microneedle to a specified distance was measured. The polymeric microneedles were attached to a 10 mm cylindrical Delrin probe (part code P/ 10) using double-sided adhesive tape. The probe is connected to a 50-kg load cell and was set at the same distance from the platform for all the

test measurements. The TA XT Plus Texture Analyser was set to compression, the pre-test speed was set at 2 mm/s and post-test speed at 10 mm/s. The trigger type was set to auto (force) with a trigger force of 0.009 N. The test station compresses the polymeric microneedle against a flat block of aluminium of dimensions 10.0 × 9.0 cm. Compression force versus displacement curves were plotted to calculate the fracture force. A total of five microneedle patches were used to evaluate the fracture force of the microneedles.

4.4.3.3 In vitro skin simulant insertion

As an alternative method to determine the microneedle penetration depth as a function of length, a polymeric film (Parafilm M®, a blend of a hydrocarbon wax and a polyolefin) was utilised as a skin model. This insertion study was adapted from Larrañeta *et al.* [248]. In brief, 8 layers of Parafilm M® were stacked onto each other on a cork mat that mimics underlying muscles. The PVPVA microneedle patch was applied under thumb pressure for 10 seconds. Six replicates were generated and observed under the Zeta Profilometer (KLA-Tencor, US) for the number of micropores created.

4.4.3.4 Dye binding study

In order to evaluate if the microneedle patch is capable of penetrating the skin and to visualise the depth of microneedle penetration into the skin, a dye binding study using *ex vivo* porcine skin was conducted. The porcine ear skin was defrosted at room temperature for an hour prior to the experiment. Using clippers, excess hair was carefully trimmed from the skin. Regions of the skin were then selected for microneedle treatment. The skin was treated with PVPVA microneedles loaded with methylene blue dye (1% w/v), which is a hydrophilic dye. The microneedle was left in the skin for one hour before removing the microneedle patch. Upon removing the patch, the skin was visually inspected to see if any microneedle channels have been generated in the skin. In order to gauge the depth of microneedle penetration into the skin, skin cross-sectioning was performed. In brief, each microneedle application site was cut into 1 cm × 1 cm and fresh frozen on a metal block that was cooled with liquid nitrogen. Skin cross-sections were performed using a cryostat (Leica CM3050 S

Research Cryostat, UK). The depth of microneedle penetration as visualised by methylene blue permeation was measured using an optical microscope (Zeta Profilometer, KLA-Tencor, US).

4.4.4 Measurement of imiquimod permeation from PVPVA microneedles

Imiquimod skin permeation was evaluated *ex vivo* using a Franz-type diffusion cell. Prior to the permeation study, skin samples were defrosted and carefully trimmed into small pieces according to the area of the donor chamber of the Franz diffusion cell (Soham Scientific, Cambridgeshire, UK). The *ex vivo* porcine skins were subjected to the following treatments: i) application of 20 mg Aldara™ cream. This is in accordance with clinical dose approved by the FDA for the treatment of BCC. ii) imiquimod loaded PVPVA microneedles. Next, the treated porcine skins were placed on top of the receptor compartment filled with 3 ml of degassed 100 mM acetate buffer pH 3.7. This buffer was chosen as the receptor phase in order to maintain sink conditions throughout the permeation study. This is due to the insolubility of imiquimod at neutral or basic pH values. Various researchers have reported using acetate buffer pH 3.7 as the receptor phase in imiquimod permeation studies [53–55]. The skin was then secured between the donor and receptor compartment of the diffusion cell using a metal clamp, with the stratum corneum side facing the donor compartment. Upon assembling the Franz diffusion cell, the permeation experiment was conducted over a period of 24 hours in a thermostatically controlled water bath set at 36.5 ^{o}C. 1000 µl of the receptor fluid at designated time points (0.5, 1, 3, 6, 12 and 24 hours) was sampled and then replaced with equal volume of fresh 100 mM acetate buffer pH 3.7. Upon sampling, 1000 µl of the solution from each Franz cell after collection was then spiked with 100 µl of 100 µg/ml propranolol as an internal standard before being filtered through 0.22 µm membrane prior to HPLC analysis.

After the 24-hour permeation experiment, the excess cream was removed from the Aldara™ cream treated skin surface by careful application of sponges soaked with 3% v/v Teepol® solution. For the microneedle patch treated skin, the remaining microneedle patch was removed from the skin. Upon removing excess formulation from the skin surface, 15 sequential tape strips were collected from the

skin. The amount of imiquimod from the pooled tape strips and remaining skin after tape stripping were extracted by the addition of 10 and 5 mL of methanol extraction mixture (Methanol 70%: Acetate Buffer pH 3.7 100 mM 30%) respectively using a previously reported method [52]. Samples were then vortexed for 1 minute and sonicated for 30 minutes before being left overnight. Subsequently, samples were vortexed again and sonicated for a further 30 minutes. After sonication, 1000 µl of the extracts were collected and spiked with 100 µl of 100 µg/ml propranolol as an internal standard. The samples were then filtered through 0.22 µm membrane prior to HPLC analysis.

4.4.5 High performance liquid chromatography (HPLC) analysis

HPLC analysis was carried out using an Agilent 1100 series instrument (Agilent Technologies, Germany) equipped with degasser, quaternary pump, column thermostat, autosampler and UV detector. System control and data acquisition were performed using Chemostation software. The details of the HPLC chromatographic conditions are as follow: column C18 (150 × 4.6 mm) ACE3/ACE-HPLC with a particle size of 5 µm, pore size of 100 Å, pore volume of 1.0 ml/g and a surface area of 300 m^2/g, Hichrom Limited, UK. The mobile phase composition for analysis of extracts from skin wash, donor chamber wash, pooled tape strips and remaining skin consists of 10 mM acetate buffer: acetonitrile (79:21). Whilst, the mobile phase composition for analysis of receptor fluid consists of 10 mM acetate buffer: acetonitrile (70:30). The HPLC was operated at a flow rate of 1.0 mL/minute, UV detection at λ_{max}=226 nm, an injection volume of 40 µL and a column temperature of 25 °C.

4.4.6 ToF-SIMS analysis of skin cross-sections

In order to evaluate the depth of imiquimod permeation into the skin, the permeation experiments were repeated as described above Section 4.4.4. After the permeation study, excess formulation was removed from skin samples treated with cream and microneedles. Then, 1 cm × 1 cm of each application site was fresh frozen with liquid nitrogen. Skin cross-sectioning was performed using a cryostat (Leica CM3050 S Research Cryostat, UK). The skin slices were then thaw mounted on a glass slides and stored at -20 °C prior to ToF-SIMS analysis. ToF-SIMS was used to analyse the cryo-sectioned

porcine skin samples. ToF-SIMS analysis was performed using a ToF-SIMS IV instrument (IONTOF, GmbH) with a Bi_3^+ cluster source. A primary ion energy of 25 KeV was used, the primary ion dose was preserved below 1×10^{12} per cm^2 to ensure static conditions. Pulsed target current of approximately 0.3 pA, and post-acceleration energy of 10 keV were employed throughout the sample analysis. The mass resolution for the instrument was 7000 at *m/z* 28.

4.4.7 Statistical analysis

Statistical analysis was conducted using GraphPad Prism 7.02 software. Data are shown as mean ± standard error of mean. When comparing two groups an unpaired t-test analysis was used, while one-way analysis of variance (ANOVA) with Tukey's multiple comparisons tests was used to compare multiple groups. *p* values < 0.05 were considered statistically significant.

4.5 Results and Discussion

4.5.1 Microneedle fabrication

In this work, polymeric PVPVA microneedles of pyramidal geometry were fabricated through four manufacturing stages; structure design via CAD, micromachining, PDMS mould production and casting as shown in the schematic of Figure S4- 1. Micro-milling was used to fabricate the designed stainless-steel master structures with minimal surface imperfections as evidenced in Figure S4- 1. Micro-milling was used as the technique enables simplicity in the design process while offering low manufacturing cost in generating complex geometry with high accuracy and repeatability [298].

Next, the PDMS moulds were produced by micromoulding followed by microneedle patch fabrication via casting, centrifugation and drying. The resulting polymeric microneedle patch is shown in Figure 4-1. Upon visual inspection as shown in Figure 4-1 **(a)**, we found that the microneedle array consists of 100 uniformly distributed pyramidal microneedles. Each microneedle array had a slightly opaque and off-white appearance. The microneedle patch displays micro projections, pyramidal in structure with a length of 992.3 ± 45.3 µm (mean ± SD, *n*=10) and a tip diameter of 32.3 ± 3.1 µm (mean ± SD, *n*=4) as visualised by optical microscopy images shown in Figure 4-1 **(b)** and **(c)**. With

regards to the production method used in this study, which involved centrifugation and micromoulding, such methodology is most suited for lab-based research. However, this method of microneedle fabrication would not be ideal for the manufacture of patches at a commercial scale. However, the use of aqueous drug-polymer blend casting could be potentially be translated into the scalable roller system manufacturing method developed by Lutton *et al.* [299]. The use of the roller system manufacturing method would provide a potential scale-up manufacturing method at a commercial scale, enabling the transition from laboratory to industry and subsequent clinical practice.

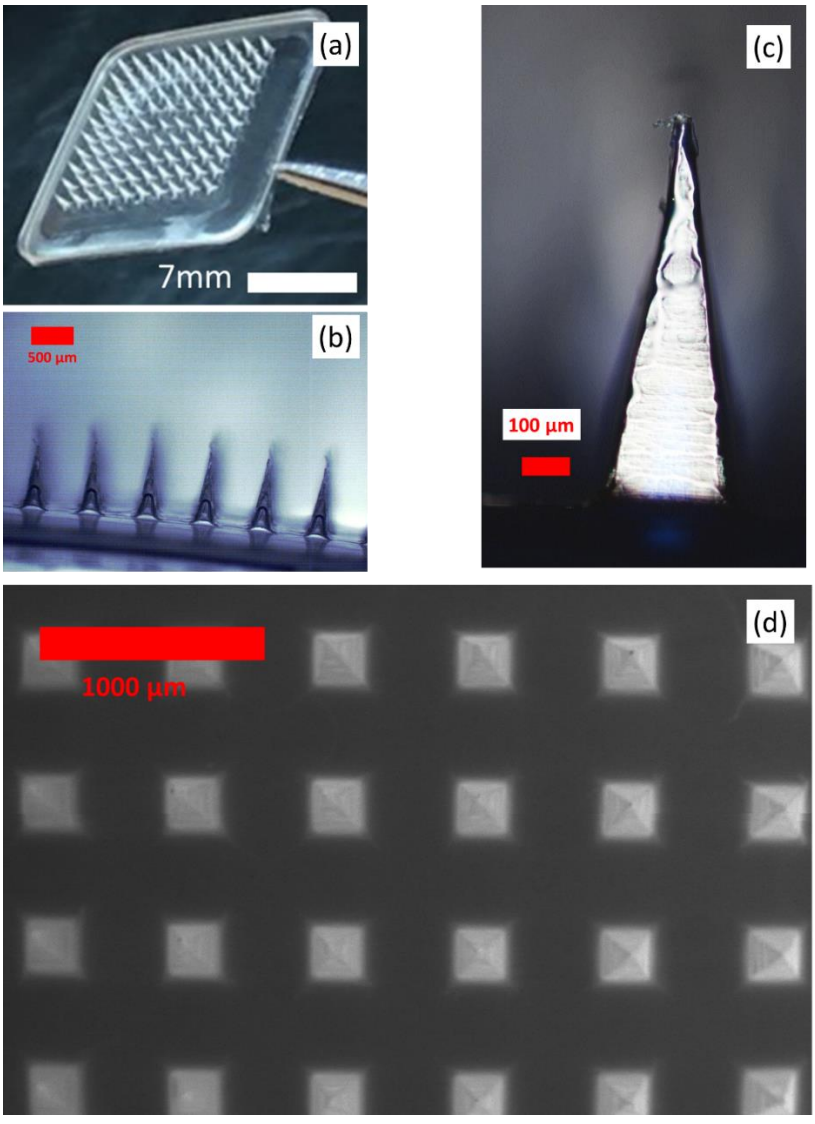

Figure 4-1a) Photograph image of PVPVA microneedles post-fabrication (b) Optical microscopy image of PVPVA microneedles at 12.5x magnification (c) close up microscopy image - of a single PVPVA polymeric microneedle at 50x magnification (d) SEM images of PVPVA microneedles at 39x magnification

An analysis by SEM, as shown in Figure 4-1 **(d)**, revealed equally spaced, sharp pyramidal microneedles, on a clean and smooth base. This clearly indicates that the copolymer PVPVA was a suitable material for fabricating polymeric microneedles. Although, PVPVA has not been used previously for microneedle fabrication, the homopolymer PVP has been widely used. In addition, the hydrophilic nature of both of these polymers makes it easy to use them for fabricating microneedles via casting and micromoulding aqueous solutions of the polymers into the PDMS moulds. This overcomes the need for organic solvents which could damage the PDMS moulds with repeated use [300]. Previous work has shown that PVP microneedles are capable of delivering a range of therapeutics such as sumatriptan, polymyxin B, atorvastatin, aspirin, and lisinopril [301–303]. In addition, although PVPVA has never been used previously in microneedle fabrication, the extensive biocompatible and cytocompatible data on the polymer strongly suggest that the PVPVA microneedles are safe for this biomedical application [304].

Preliminary microneedle fabrication without the use of PEG 400 as a plasticiser resulted in microneedles with fractured tips as shown in Figure S4- 2. A lack of consistency in microneedle length and tip formation may result in complications such as failure to penetrate the skin as well as inconsistent drug release from the individual microneedles within the same patch. The presence of fractured tips is attributed to the formation of brittle polymeric microneedles post-drying. The brittleness of the preliminary PVPVA microneedles was due to the high T_g of the polymer at 107 ^oC as shown in Figure S4- 3. Since the microneedles were demoulded at room temperature, the polymer is well below its T_g and is in a glassy and brittle state making it prone to fracture [12]. In order to overcome this issue, PEG 400 was introduced into the needle matrix as a plasticiser. The use of PEG 400 falls under the category of an external plasticiser which has been used in several other microneedle formulations [302,303,305].

Due to the rigid but brittle nature of PVPVA, we discovered that using the same PVPVA and PEG 400 polymer solution as a backing layer resulted in microneedle patches that fractured during the

demoulding stage as shown in Figure S4- 4. A microneedle backing layer ought to be flexible to enable easy demoulding while allowing the microneedle patch to adapt to the skin curvature during administration [306]. In order to meet these criteria, we used a different polymer blend consisting of CMC and glycerol to fabricate the backing. CMC is one of the most commonly used polymer solutions in fabricating the backing layer of microneedle patches [307,308].

4.5.2 Microneedle characterisation

The mechanical properties of the needles were determined using a texture analyser. The polymeric microneedle arrays were subjected to an axial compression test to measure the fracture force of the polymeric microneedles. Profiles of force versus displacement (analogous to stress-strain curves), based on average force values (n = 5), were generated for the PVPVA polymeric microneedle patch. This force versus displacement curve was then used to determine the average fracture force per needle. From the microneedle fracture test, the PVPVA microneedles displayed a fracture force of 0.106 ± 0.003 N/needle (mean ± SD, *n*=5). The required fracture force that microneedles need to possess in order to puncture the skin without fracturing is 0.098 N/needle [129,130]. In addition, Donnelley *et al.* has even reported successful skin insertion with microneedles that possess a fracture force as low as 0.03 N/needle [115]. Therefore, it can be inferred that the fabricated microneedles displayed sufficient mechanical strength above the reported threshold needed to puncture the skin without fracturing.

It is of great importance that fracture test is coupled to insertion studies in order to evaluate the penetration capability of the fabricated microneedles. The insertion of PVPVA microneedle patch into a stack of Parafilm® layers was used as an *in vitro* skin model. This was performed by applying the patches onto the Parafilm® stacks under thumb pressure. Upon application, each Parafilm layer was separated and visualised using an optical microscope to evaluate the pore uniformity as a function of penetration depth. Figure 4-2 **(a)** shows that square shaped pores, which follows the shape of the square pyramidal PVPVA microneedle, were created on the Parafilm layers upon microneedle patch

application. In addition, it can be seen that the number of microneedle channels generated decreased as a function of Parafilm layer number with the deepest layer penetrated by the microneedle patch being the fourth layer as shown in in the insertion profile of Figure 4-2 **(b)**. In addition, it was apparent that all replicates resulted in complete microneedle insertion in the first parafilm layer as shown in Figure 4-2 **(b)**. The Parafilm® insertion test was developed by Larrañeta *et al.* as an *in vitro* test to predict the insertion capabilities of microneedles in actual skin tissues [248]. Collectively, Figure 4-2 **(a)** along with the insertion profile from Figure 4-2 **(b)**, suggests that fabricated PVPVA microneedle patch is capable breaching the *stratum corneum* permitting microneedle insertion into the skin.

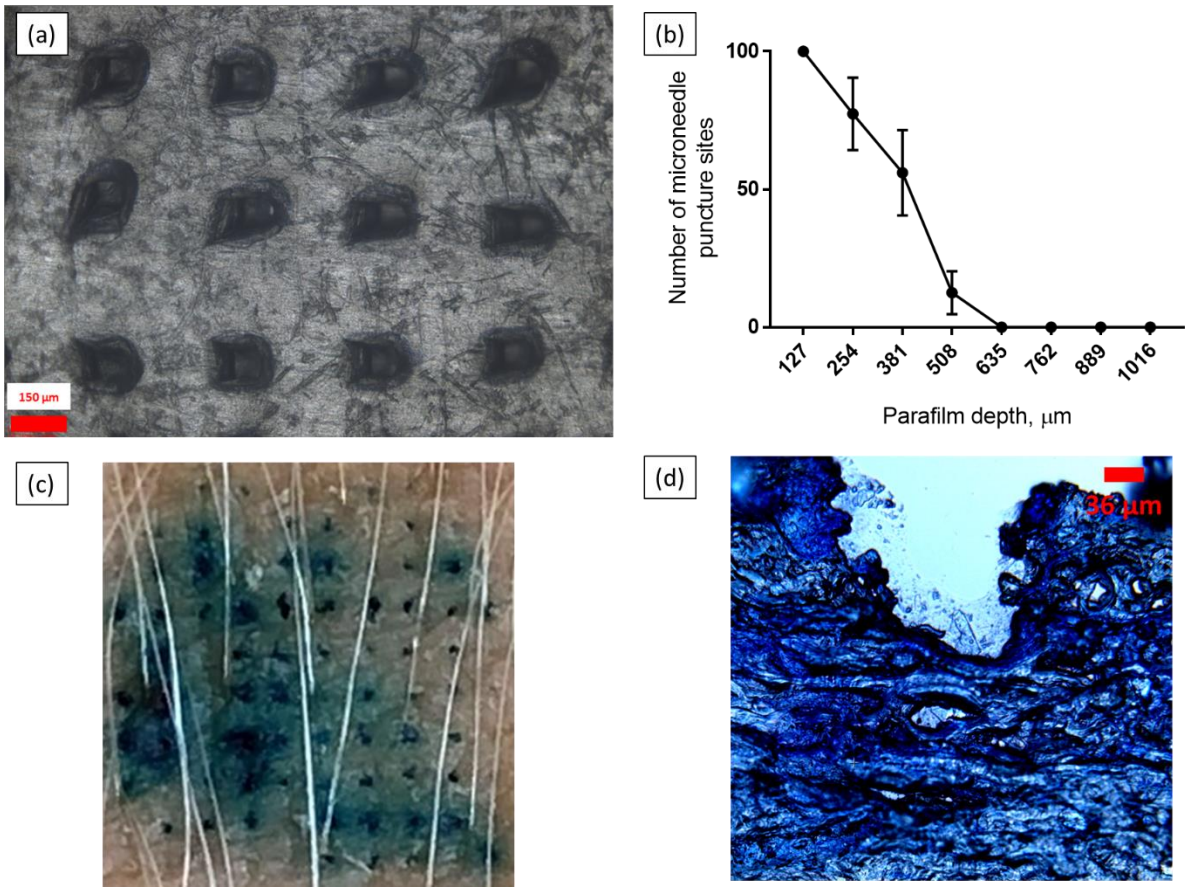

Figure 4-2 (a) Microscopic images of first Parafilm® treated by PVPVA microneedles (b) Insertion profile of PVPVA microneedle into Parafilm® layers, data is expressed as mean± SD for n=6 (c) Microchannels created in ex vivo porcine skin visualised via the release of methylene blue from PVPVA microneedles (d) Optical microscopy image of microneedle channels created when the skin is treated with PVPVA microneedles

A dye release study was then performed to evaluate the ability of the microneedle patches to puncture the skin. Methylene blue loaded microneedle patch was applied onto porcine cadaver skin, which upon application resulted in the release of the hydrophilic dye to the surrounding skin tissue upon PVPVA dissolution. This results in the formation of blue microneedle channels within the porcine skin that follows the distribution of PVPVA microneedles on the patch as shown in Figure 4-2 **(c)**. The histological image of the vertical section of microneedle treated skin, shown in Figure 4-2 **(d)** provides an estimate into the depth of microneedle penetration into the skin. The application of PVPVA microneedles loaded with methylene blue breached the *stratum corneum* and epidermis layers as shown in Figure 4-2 **(d)**. The average depth of microneedle penetration was 426 ± 72 µm (mean ± SD, *n*=10). The penetration depth of the microneedles is of approximately the same depth as that observed with the Parafilm insertion study. With regards to clinical translation of the technology, reproducible insertion of microneedles by patients and carers is an important factor to consider. Various strategies have emerged over the years to ensure effective and reproducible insertion of microneedle patches into the skin. One of the strategies could be the use of microneedle applicators. Some examples of the microneedle applicator that could be used include MicroCor™ and Macroflux® [289]. Alternatively, the use of pressure-indicating sensor film such as Pressurex-micro® Green may be an alternative, might be an option in providing feedback to patient and carers that they had pressed the microneedle with sufficient force into the skin [309]

It was apparent that the microneedle penetration depth into *ex vivo* skin was shorter than the length of the microneedle. This observation agrees with earlier findings by Martanto *et al.* who reported partial microneedle insertion into the skin [105]. Such an observation is attributed to the inherent elastic nature of the skin which resists microneedle penetration. However, since it has been reported that the thickness of the porcine epidermal layer varies between 30-140 µm [260] it can be seen that from the vertical cross-sectional data Figure 4-2 **(a)** the microneedle application in this case has reached the dermis. In comparison, the human skin is reported to have an epidermal thickness of 800-1500 µm for thick skin (palm of the hands and sole of the feet) and 70-150 µm for thin skin (face,

eye lids, neck and arm) [310]. Importantly in this instance, as BCC mainly manifests on thin skin surfaces such as the face, neck and eyelid [311], it can be postulated that application of the PVPVA microneedle patch would bypass the epidermis and reach the dermis which is the target site for the treatment of nodular BCC. Besides that, in regions where there are curvatures such as the facial cheeks, nose and eyelids the application of microneedle would still be viable. However, in this instance, the use of a very flexible backing layer such as those fabricated from polyethylene glycol diacrylate (PEGDA) would allow the microneedle patch to adapt to skin curvature whilst permeating effective skin insertion [306].

The hygroscopic nature of PVPVA could have an adverse effect on the needle architecture along with its insertion capabilities on long term storage. Hence in order for this technology to be translated into clinical practice stability studies will need to be carried out to verify the needle structure. With respect to the hygroscopicity of PVPVA, relative to PVP which is widely used in microneedle research, PVPVA is less hygroscopic that PVP. The work by Shamblin and Zografi showed that the amount of water absorbed by PVPVA was one-third of that absorbed by PVP when stored at humidity levels similar to that of ambient room conditions. Such an observation is attributed to the carbonyl group of the vinyl acetate moiety which is less basic and hence less prone to hydrogen bonding than the carbonyl group in the pyrrolidone ring [312]. Therefore, the use PVPVA which is a less hygroscopic polymer than the widely used PVP, may produce microneedles which are less susceptible to moisture than the commonly fabricated PVP microneedles. Nevertheless, one of the manufacturing and distribution challenges will be the need to manufacture, distribute and store the microneedles in a low humidity environment to reduce the exposure to moisture that may affect the architecture of the needle and ultimately the insertion of the needle into the skin. One possible suggestion to overcome this is to pack the microneedle patches in nitrogen flushed sterile packets that demonstrate protection against water ingress.

Considering the fact that microneedle dosage forms penetrate the stratum corneum rather than adhere to the surface of the skin as in a conventional transdermal patch, sterility will potentially be a

key requirement by regulatory bodies. Previous work by Mccrudden *et al.* 2014 have shown that endotoxin levels in dissolving microneedles can achieve levels below set by the Food and Drug Administration (FDA) guidelines for medical devices that are in direct contact with lymphatic tissue (20 units/device) using the appropriate sterilisation techniques [313]. As PVPVA microneedles may be susceptible to moisture due to the hygroscopic nature of polymeric microneedle, the use of heat/steam sterilisation may damage this type of microneedle necessitating microneedle production under aseptic conditions. The use of gamma irradiation may be an alternative, however previous work has shown that this method of terminal sterilisation alters the release profile of dissolving microneedles [313].

4.5.3 Drug release study from PVPVA microneedles

4.5.3.1 HPLC analysis

In vitro permeation studies utilising Franz diffusion cells are widely used to study the intradermal and transdermal delivery of drugs across the skin. In this work, we investigated the delivery of imiquimod from drug loaded microneedle patches into and across the skin in comparison to the commercial imiquimod cream, Aldara™. Imiquimod was loaded into the microneedles by dissolving both the polymer (PVPVA) and the drug into a polymer blend, casting the solution into the PDMS micromoulds, centrifugation and finally drying. Imiquimod-loaded polymeric PVPVA microneedles dissolved gradually in a limited volume of the skin's interstitial fluid to release drug into and across the skin layer. It was apparent that both drug delivery systems were capable of delivering imiquimod into the *stratum corneum*, remaining skin and into the receptor fluid as shown in Figure 4-3.

From Figure 4-3 **(a)** we observed that the mean amount of imiquimod delivered into the *stratum corneum* as evidenced from HPLC analysis of tape strips are 23.2 µg for microneedle treated and 8.6 µg for Aldara™ cream treated skins. The differences in amount of imiquimod delivered into the *stratum corneum* was of statistical significance ($p<0.05$). Such enhanced permeation into the *stratum corneum* with imiquimod loaded microneedles may be attributed to the generation of microneedle

channels within the skin. These channels act as focal points for imiquimod to permeate laterally and localise to the surrounding corneocytes, thus enhancing delivery to the upper layer of the skin.

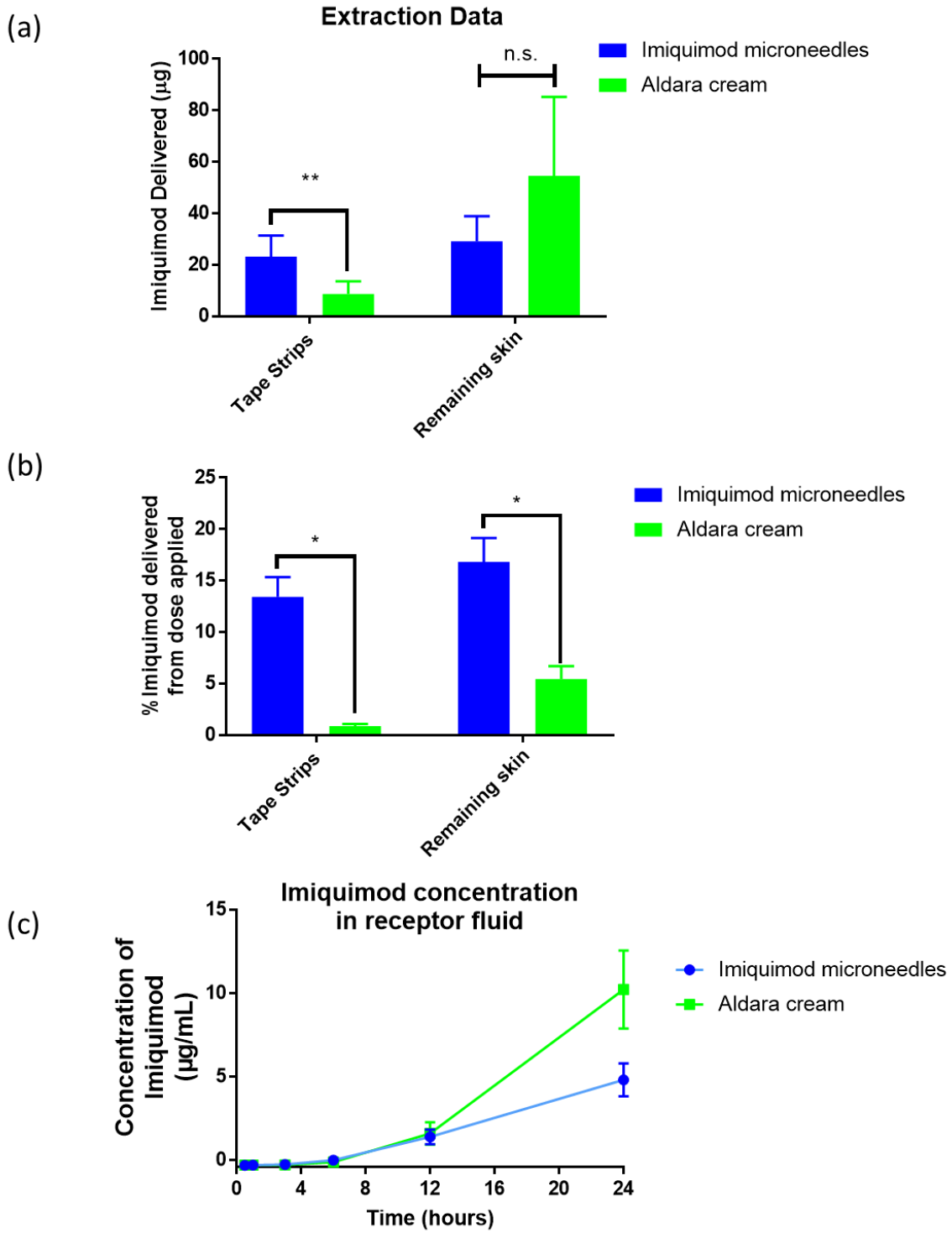

Figure 4-3 Amount of drug extracted from skin (a) tape strips and (b) remaining skin after 24 hours in the permeation study. (c) Drug concentration within receptor fluid as a function of time during permeation study

from Aldara™ and imiquimod microneedles. Data are expressed as mean± SEM for n=6. Differences were determined using a two-tailed Student's t test, and deemed significant at p<0.05. n.s = not statistically significant at p>0.05

However, in the case of nodular BCC the drug delivery system must be capable of delivering the drug beyond the *stratum corneum* and deeper into the skin [34]. Therefore, in order to gauge the amount of drug delivered deeper into the skin, HPLC analysis was conducted on remaining skin after tape stripping. Figure 4-3 **(a)** also shows that the mean amount of imiquimod delivered into the remaining skin from both treatment groups. It was observed that the amount drug extracted from the remaining skin treated with the microneedles was lower than the amount of drug delivered by the commercial cream, Aldara™ although such differences were not statically significant (*p>0.05*). This would suggest that the overall amount delivered per application of both delivery system are similar. From a dose delivered perspective, it may appear that the microneedle patch does not offer any additional benefits. However, when the two systems are viewed in terms of ease of application, the microneedle patch offers a simple one-step application to insert the microneedles into the skin under thumb pressure. This avoids the issues of dosing accuracy with the amount of cream applied and problems associated with the cream spreading to non-diseased skin which are associated with Aldara™ cream. With regards to the amount of imiquimod delivered for the management of BCC, it would be more preferable to use the Aldara™ cream in the management of superficial BCC as we would mitigate the unnecessary exposure of underlying healthy skin tissue to imiquimod. However, given the fact that at least one-third of nodular BCC coexist with superficial BCC [36], the use of imiquimod loaded microneedles in such instances would be useful as the drug could deliver equal amounts of imiquimod to tumour located at the skin surface and underlying skin tissues.

In addition, Figure 4-3 **(b)** shows the amount of imiquimod delivered into the *stratum corneum* and remaining skin when calculated as a percentage of the applied dose. In this instance the percentage of the drug successfully delivered into the *stratum corneum* and remaining skin is significantly higher with imiquimod microneedles than that of Aldara™ cream. The drug loading in the microneedle patch

was 165.6 ± 21.4 µg (mean ± SD, *n*=8). Whilst, ≈20 mg of Aldara cream (1000 µg of imiquimod) was applied to the skin area of 3.8 cm^2, in the Franz cell, which is based on clinical dose for Aldara™ cream for the treatment of BCC [314]. Figure 4-3 **(b)** highlights that we are able to deliver similar amounts of imiquimod into the remaining skin using a different delivery system despite a 6-fold lower drug loading with the microneedle patch.

Figure 4-3 **(c)** shows the concentration of imiquimod detected in the receptor fluid over time. It can be seen that the concentration of imiquimod in the receptor fluid overtime, was similar between Aldara™ cream and imiquimod microneedle treated skin for up to 12 hours. However, at 24 hours, the concentration of imiquimod within the receptor fluid is less for skin treated with imiquimod microneedles relative to Aldara™ cream. This highlights that over the course of 24 hours, the microneedle patch resulted in less imiquimod delivery across the skin while delivering similar quantity of the drug into the remaining skin. It is understood the amount of drug detected in receptor fluid following an *in vitro* Franz cell permeation study provide a an indicator on the likelihood of systemic exposure [1]. Hence, it could be postulated that the likelihood for systemic exposure to imiquimod following microneedle treatment is lower in comparison to Aldara™ application. This may limit the likelihood of influenza-like symptoms, an undesirable side effect associated with imiquimod systemic exposure [315]. Based on the current work, it is suggested that the microneedle is left in the skin for 24 hours to allow comparative application and delivery of imiquimod into the skin as to that of Aldara™ cream. In terms of practical delivery of imiquimod using microneedle relative to other routes of administrations such as oral delivery, a microneedle based intradermal delivery would be more practical as it enables more targeted delivery and avoids the likelihood of systemic side effects arising from oral delivery of imiquimod which could give rise to flu-like symptoms and result in a poor overall quality of life for the patient.

In terms of enhancing imiquimod permeation, several groups have considered alternative drug delivery systems such as the use of an emulsion gel [275], transethosomes [67] and a hydrogel/oleogel

colloidal mixture [316]. However, these types of formulations are typically associated with poor sensory and cosmetic issues (e.g., tackiness and stickiness) upon application. In addition, these semisolid dosage forms could potentially stain patients' clothes as well as spread to healthy skin regions leading to unwanted side effects [69,317]. This may ultimately limit patient compliance to the overall treatment. These limitations are not encountered with microneedle formulations as the patches are anchored in place by the micro-projections ensuring precise localised delivery at the site of application. In addition, with regards to disposal of the patch upon skin insertion, as the PVPVA microneedles are dissolving microneedles, the microneedles will dissolve in the skin leaving behind the backing layer. Therefore the microneedle patch is self-disabling post-insertion overcoming the issues of dangerous sharp waste disposal in resource-poor settings [318].

4.5.3.2 ToF-SIMS analysis

It was apparent that HPLC analysis provided quantitative results that permit us to compare the delivery efficiency of both formulations. However, HPLC does not provide any spatial information pertaining to the dermal distribution of imiquimod. In order to complement the HPLC data, ToF-SIMS was utilised to provide insight into the dermal distribution of imiquimod.

Figure 4-4 shows ToF-SIMS secondary ion images from skin cross-sections analysed after a 24-hour permeation study. Due to the parallel detection capabilities of the ToF-SIMS, secondary ions originating from both the skin tissue, polymer and drug were detected and analysed. By carefully monitoring the ion peaks from the ToF-SIMS spectra (Figure S4- 5), we are able to visualise the localisation and distribution of these secondary ions. The fragment ion for phosphatidylcholine, $C_5H_{15}NPO_4^+$ was used to identify the dermis and viable epidermis. Additionally, the fragment ion for ceramide, $C_{17}H_{32}N^+$ is utilised to distinguish the *stratum corneum* from the viable epidermis and dermis [224]. This is because, the *stratum corneum* displays high levels of ceramide whilst being devoid of phospholipids which makes $C_{17}H_{32}N^+$ a good marker for the stratum corneum [197,282]. In a previous work, it has been found that the permeation of the imiquimod across the skin could be tracked by

monitoring the molecular ion $C_{14}H_{17}N_4^+$ [68]. Through monitoring the fragment ion peak $C_6H_{10}NO^+$ we were able to detect the localisation of the PVPVA polymer within the microneedle channels as shown in Figure 4-4. The peak assignment for PVPVA was validated by referring to fragmentation pattern at *m/z* 112 with the reference spectra of pure PVPVA on silicon wafer as shown in the supplementary data (Figure S4- 6). It is worth noting that, that the parallel detection capability of the ToF-SIMS also enabled the detection of Si^+ marker -an inorganic ion of silicon -indicated in yellow in Figure S4- 7 and Figure S4- 8 used to identify the glass slide (the substrate used to mount the cross-sections) as silicon is a common fundamental constituent of glass. Figures Figure S4- 7 and Figure S4- 8 also shows the total ions image collected from the ToF-SIMS sample analysis.

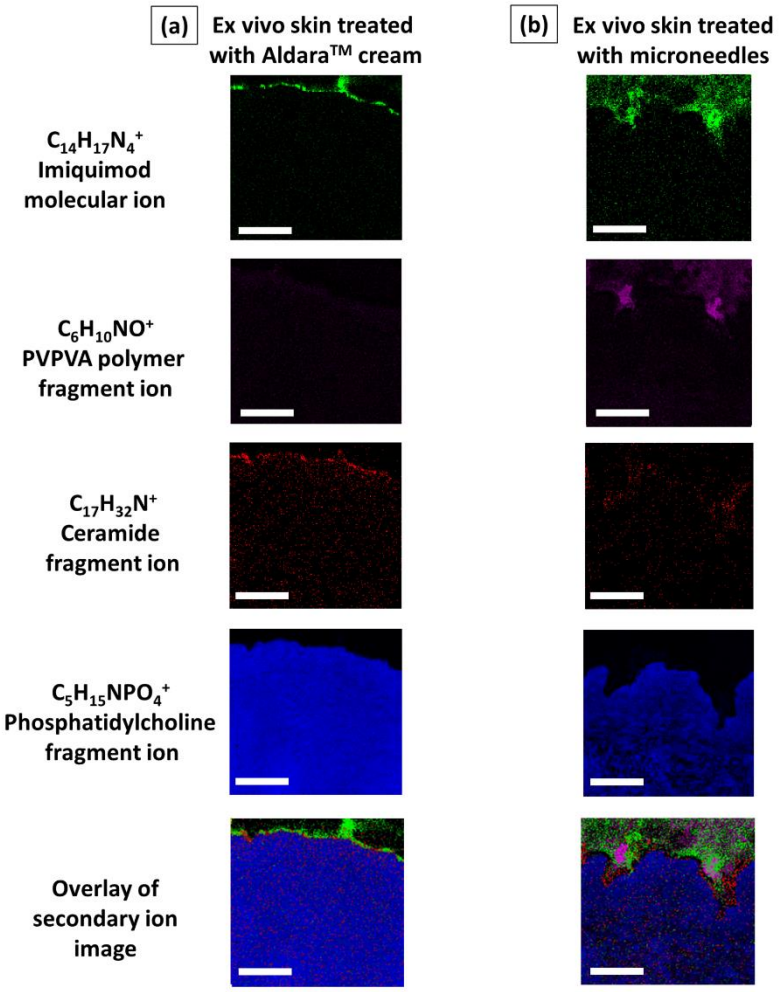

Figure 4-4 ToF-SIMS image of skin cross sections from ex vivo porcine skin that were treated with (a) Aldara™ cream (5% w/w imiquimod) alone (b) PVPVA microneedles loaded with imiquimod after a 24-hour permeation study. Figure (b) shows localisation of semi-dissolved polymeric microneedles within the dermis with skin treated imiquimod loaded microneedles. $C_{14}H_{17}N_4^+$inidicated in green is the molecular ion for imiquimod, $C_5H_{15}NPO_4^+$ indicated in blue is the fragment ion for phosphatidylcholine used to identify the viable epidermis and dermis. $C_{17}H_{32}N^+$ indicated in red is the fragment ion for ceramide used to identify the stratum corneum. $C_6H_{10}NO^+$ indicated in pink is the fragment ion for PVPVA polymer. Scale bar: 500 µm

It is apparent from Figure 4-4 **(a)** that there is limited availability of imiquimod within deeper skin strata when the molecule was delivered as a topical cream, Aldara™. When the drug is applied as a topical cream, imiquimod is localised in the *stratum corneum* as evidenced from overlay of imiquimod molecular ion, $C_{14}H_{17}N_4^+$ with the fragment ion for ceramide, $C_{17}H_{32}N^+$. However, when imiquimod is

delivered as a polymeric microneedle patch, we observed delivery of imiquimod into the dermis within microchannels as shown in Figure 4-4 **(b)**. It is clear from the ceramide fragment ion, $C_{17}H_{32}N^+$ in Figure 4-4 **(a)** that the *stratum corneum* looks intact when the drug is administered as a topical cream. In contrast, when the drug is delivered as a polymeric microneedle patch, we observed disruption in the ceramide fragment ion, $C_{17}H_{32}N^+$ distribution within top layer of the skin as shown in Figure 4-4 **(b)** that suggest that the microneedles have disrupted the *stratum corneum* permitting the insertion of the drug loaded polymeric microneedles into the skin. Typically, nodular BCCs are much harder to treat effectively as the tumour typically manifests 400 µm below the skin surface [34]. The ToF-SIMS analysis of skin cross-sections from Figure 4-4 suggests that the microneedle patch penetrated the skin to a depth of approximately 450 µm resulting in imiquimod delivery into the dermis. With regards to penetrating the BCC tumours with microneedles, concerns may be raised on the likelihood of aggravating the tumour which may lead to unintended side effects. However, there is little to no clinical concerns with regards to penetrating BCC tumour as the tumours are routinely penetrated via punch biopsy and intraoperative incisional biopsy. Such surgical procedures do not lead to any localised or distant spread of the BCC tumour. In fact, microneedle insertions are minimally invasive, therefore the damage inflicted from penetrating the BCC tumour with microneedles is less relative to these routine surgical procedures. In addition, many BCC lesions are also frequently traumatised accidentally by the patients themselves which causes localised bleeding but again no serious consequences [319,320].

With regards to the dermal distribution of the various components of a microneedle system, several research groups have employed techniques such as fluorescently tagging the molecule of interest in order to visually track the delivery of compound into the skin [129,321]. This method results in modification of the physiochemical properties of the drug leading to potentially inaccurate estimation of drug permeation into the skin [198]. However, there is no work in the field that has demonstrated the capability to simultaneously detect the deposition of both drug and polymer from a dissolving microneedle patch in a label free manner. ToF-SIMS analysis also provides the capability to perform

parallel detection of both endogenous and exogenous chemistry present in the analysed samples, thus permitting simultaneous mapping the presence of polymer within biological tissues as well as the drug. The polymer that is used in fabricating the microneedle patch is PVPVA. Through monitoring the fragment ion peak at *m/z* 112 we were able to detect the co-localisation of the polymer and imiquimod within the microneedle channels as shown in Figure 4-4.

By comparing this finding with the ToF-SIMS analysis of skin cross-section from samples treated imiquimod loaded microneedles in Figure 4-4 **(b)**, it was observed that imiquimod was colocalised in the presence of PVPVA polymer within the dermis following skin application. This leaves imiquimod which is embedded in a polymer matrix within skin. It has been previously postulated that embedded drug-polymer matrix slowly undergoes dissolution; generating localised regions of enhanced viscosity within the skin that slows the rate of drug release to surrounding tissues [72,73]. However, in the current work we are able to demonstrate via ToF-SIMS analysis the existence of such semi-dissolved polymeric regions within the dermis that retains drug from permeating across the skin and into the receptor fluid. From a clinical perspective, the reduction in imiquimod permeation across the skin may limit the likelihood of systemic side-effects. The ability of a microneedle patch to deliver the drug to a desired location despite having lower drug loading may serve as a possible explanation for the dose sparing advantage conferred by dissolving polymeric microneedles. To the best of our knowledge, this is the first report of the dose sparing advantage conferred by microneedles for small molecule therapeutics.

Although a PVPVA polymer depot was observed, there is evidence based on this commercial polymer's Mw i.e 15-20 kDa that it would be eventually excreted. Indeed, based on the findings from Kagan *et al.* on the elimination of macromolecules from the skin, it is estimated that a majority of the polymer will be drained into the dermal blood capillaries with some drainage into the dermal lymphatics before reaching the systemic circulation [322]. Furthermore, as the PVPVA has a Mw less than 60 kDa, the polymer will be excreted through the kidneys once it reaches the systemic circulation [323,324].

The HPLC analysis data for Aldara™ cream treated skin shown in Figure 4-3 **(a)** appears to contradict the ToF-SIMS analysis of skin cross-section with regards to amount drug delivered into the superficial layer of the skin, i.e., the *stratum corneum*. In order to elucidate this discrepancy, we performed a closer analysis of skin cross-sections of Aldara™ cream treated skin as shown in Figure 4-5. As discussed earlier, the fragment ion for phosphatidylcholine ($C_5H_{15}NPO_4^+$) was used to identify the dermis and viable epidermis while the fragment ion for ceramide, $C_{17}H_{32}N^+$ is now utilised to distinguish the *stratum corneum* from the viable epidermis and dermis. Closer analysis of the Aldara™ cream treated skin showed that the majority of the molecule of interest, imiquimod resides within the *stratum corneum*.

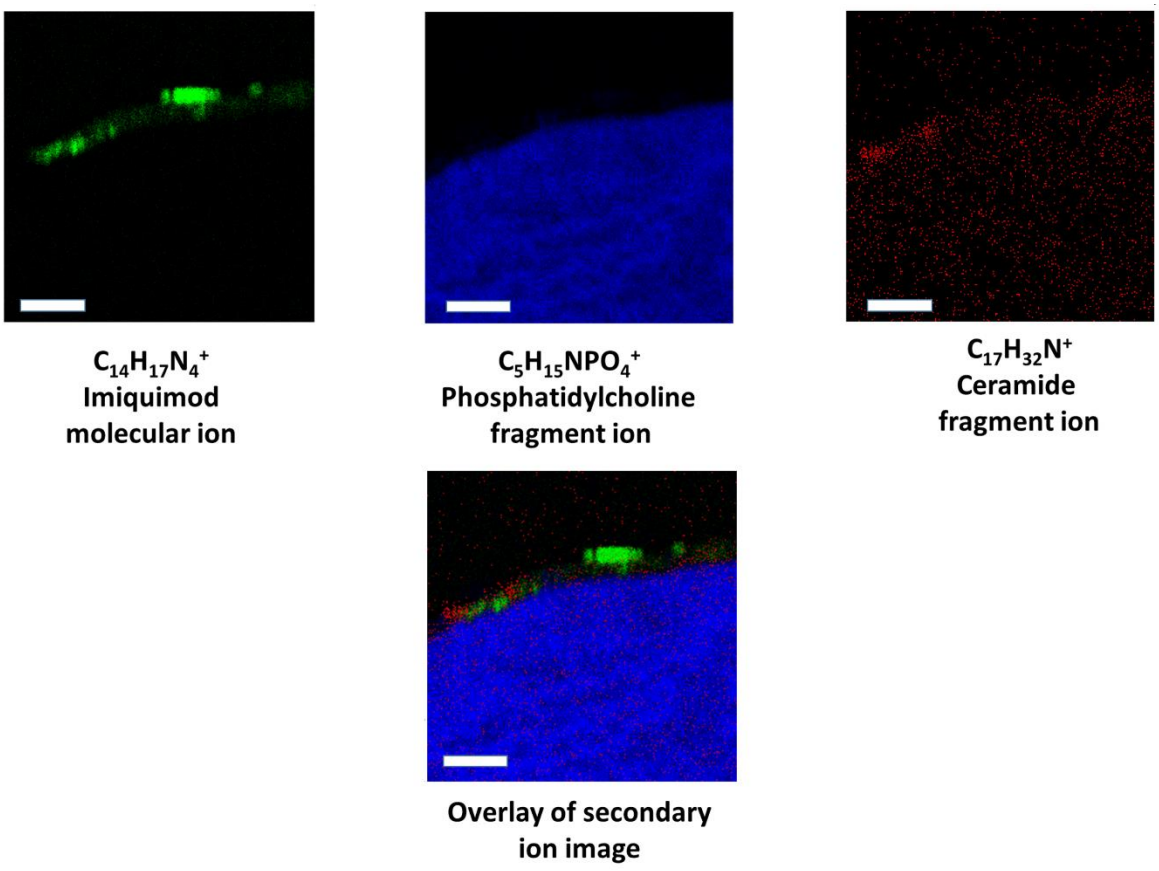

Figure 4-5 ToF-SIMS image of skin cross sections from porcine skin that were treated with Aldara™ cream (5% w/w imiquimod) alone. This analysis was conducted at a higher resolution closer to the skin surface to image the localisation of imiquimod near the stratum corneum and epidermis junction. $C_{14}H_{17}N_4^+$ the molecular ion for

imiquimod indicated in green is, $C_5H_{15}NPO_4^+$ the fragment ion for phosphatidylcholine used to identify the viable epidermis and dermis indicated in blue. $C_{17}H_{32}N^+$ is the fragment ion for ceramide used to identify the stratum corneum indicated in red. The overlays highlights imiquimod localisation within the stratum corneum and some near the epidermis just below the stratum corneum. Scale bar: 100 µm

With regards to tape stripping as a method to quantify drug permeation into the superficial layer of the skin, various groups have observed a reduction in corneocytes removed with tape strip number. Such reduction in corneocyte extraction is attributed to the increase in corneocyte cohesion with *stratum corneum* depth [325–327]. In addition, the increase in skin hydration with skin depth also reduces the ability of the tape adhesive to remove the corneocyte during the stripping process [291]. When analysing the distribution of imiquimod on the Aldara™ treated skin from Figure 4-4, it may appear that most imiquimod is with the top layer of the skin. However, upon closer cross-sectional analysis of Figure 4-5 the majority of the molecule of interest, imiquimod resides within the deeper layer of the *stratum corneum*. These layers are not so easily removed by tape stripping and thus are extracted with the remaining skin.

4.6 Conclusions

In conclusion, the current work highlights the design, fabrication, evaluation and application of drug loaded polymeric microneedles as a drug delivery platform for the intradermal delivery of imiquimod for the treatment of nodular BCC. Permeation studies utilising Franz diffusion cells demonstrated that the imiquimod loaded polymeric microneedles were capable of delivering similar quantities of imiquimod to the region of tumours, despite a 6-fold lower drug loading, relative to the current clinical dose of Aldara™ cream used in BCC treatment. This ability of the polymeric microneedle to deliver the drug to the right target site despite lower drug loading may be of economic benefit while also limiting the likelihood of side effects. Using a microneedle patch, imiquimod loaded polymeric microneedles are mechanically inserted and embedded within the dermis upon application which is the target site for the treatment of nodular BCC. ToF-SIMS analysis of skin cross-sections highlighted the presence of the embedded drug-polymer matrix within the skin, which retains the drug in the dermis while

reducing the permeation of the drug across the skin. This provides evidence to support the mechanistic understanding of how the embedded drug-polymer matrix following polymeric microneedles administration controls the release of drugs. In summary, this work suggests that imiquimod loaded polymeric microneedles may be of clinical utility for localised intradermal delivery of imiquimod. Such formulations may provide a less invasive intervention to patients who would prefer an alternative treatment to surgery for the treatment of nodular BCC.

4.7 Supplementary Figures

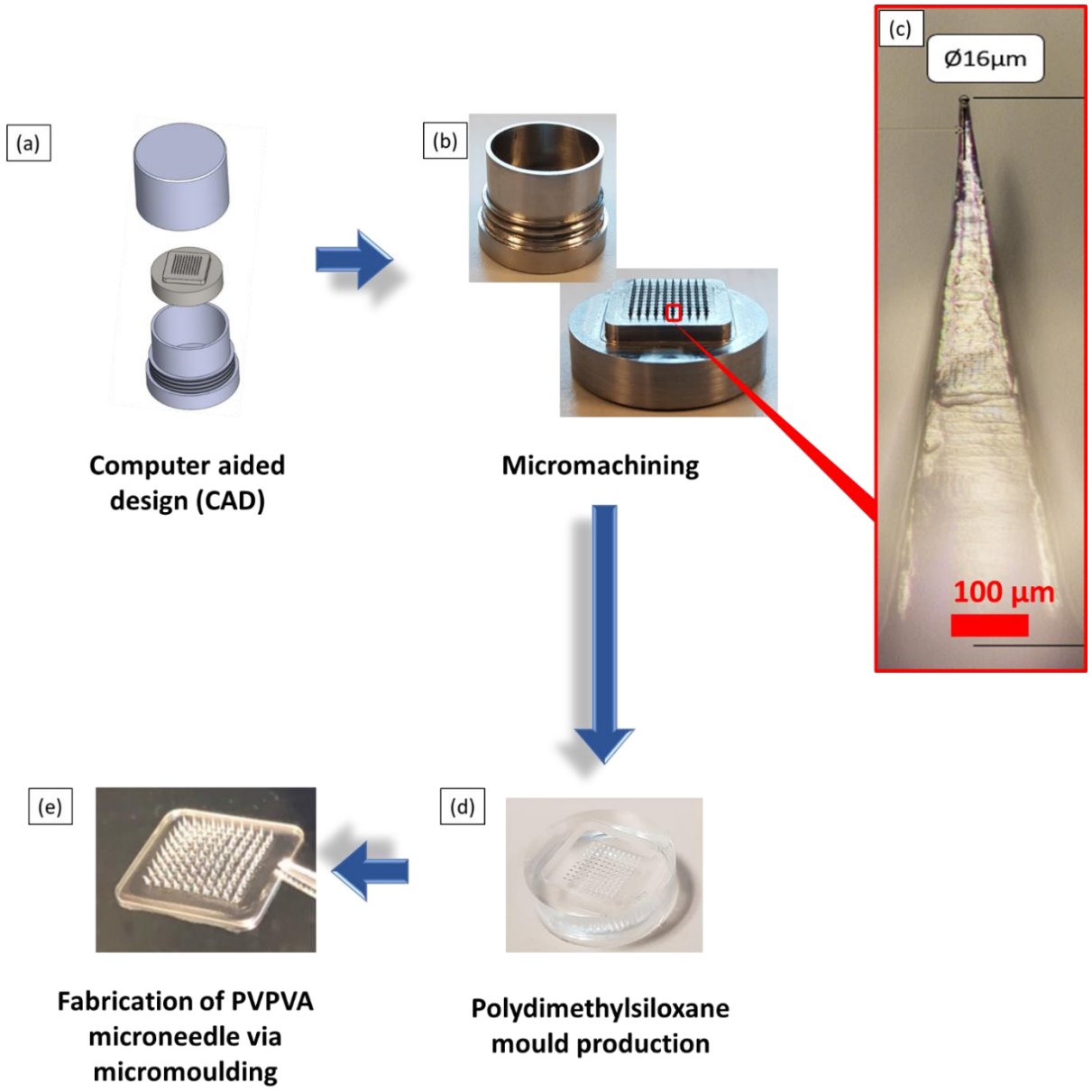

Figure S4- 1 Representation schematics of PVPVA microneedle production process. (a) Microneedle structure was first engineered using computer aided design (CAD). (b) Micromachining technique is utilized to produce the master structure. (c) microscopy image of a machined pyramidal microneedle from the stainless-steel master structure. (d) PDMS mould were then producted via micromoulding. (e) Afterwards, PVPVA microneedles were fabricated through casting and micromoulding PVPVA polymer drug mixture using the PDMS moulds.

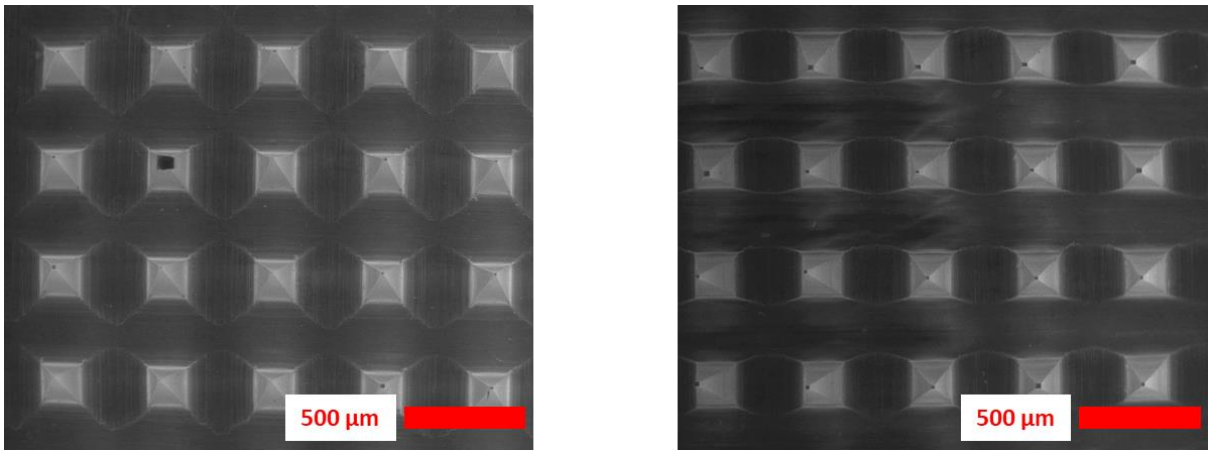

Figure S4- 2 Pyramidal PVPVA microneedle fabricated without using the plasticiser PEG 400 resulting in microneedles with fractured tips post demoulding.

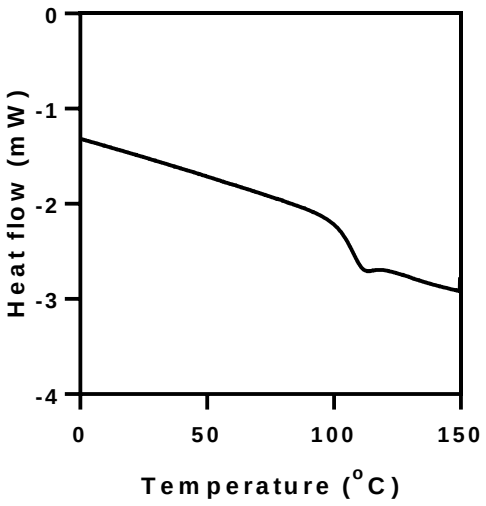

Figure S4- 3 Differential scanning calorimetry thermogram of pure PVPVA showing the glass transition temperature (Tg) at approximately 107 °C.

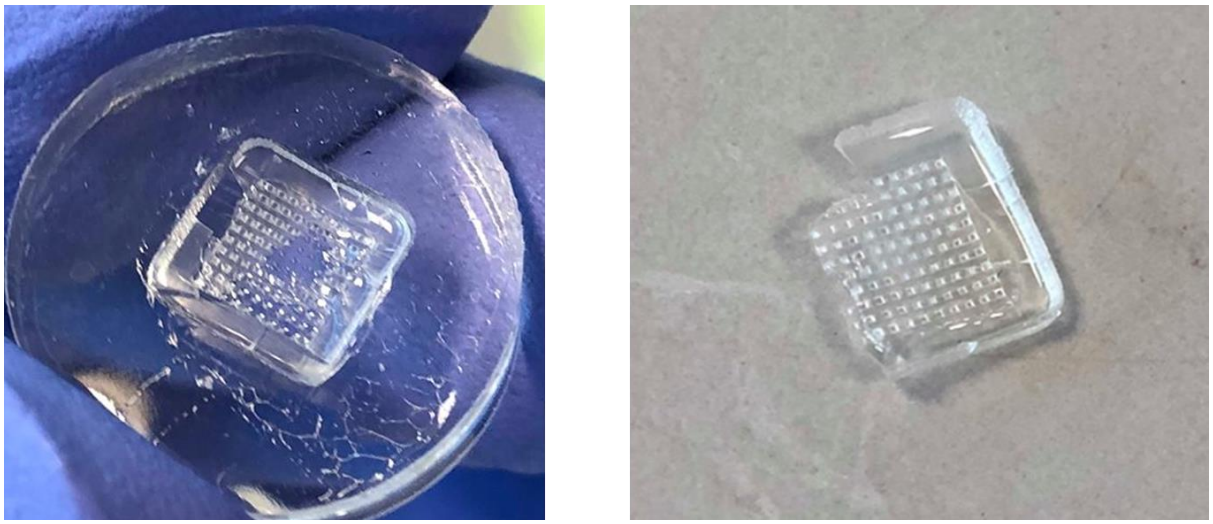

Figure S4- 4 Pyramidal PVPVA microneedle patches fabricated with PVPVA and PEG 400 for both the needle and backing layer. The backing layer shattered as it was too rigid and brittle during the demoulding step.

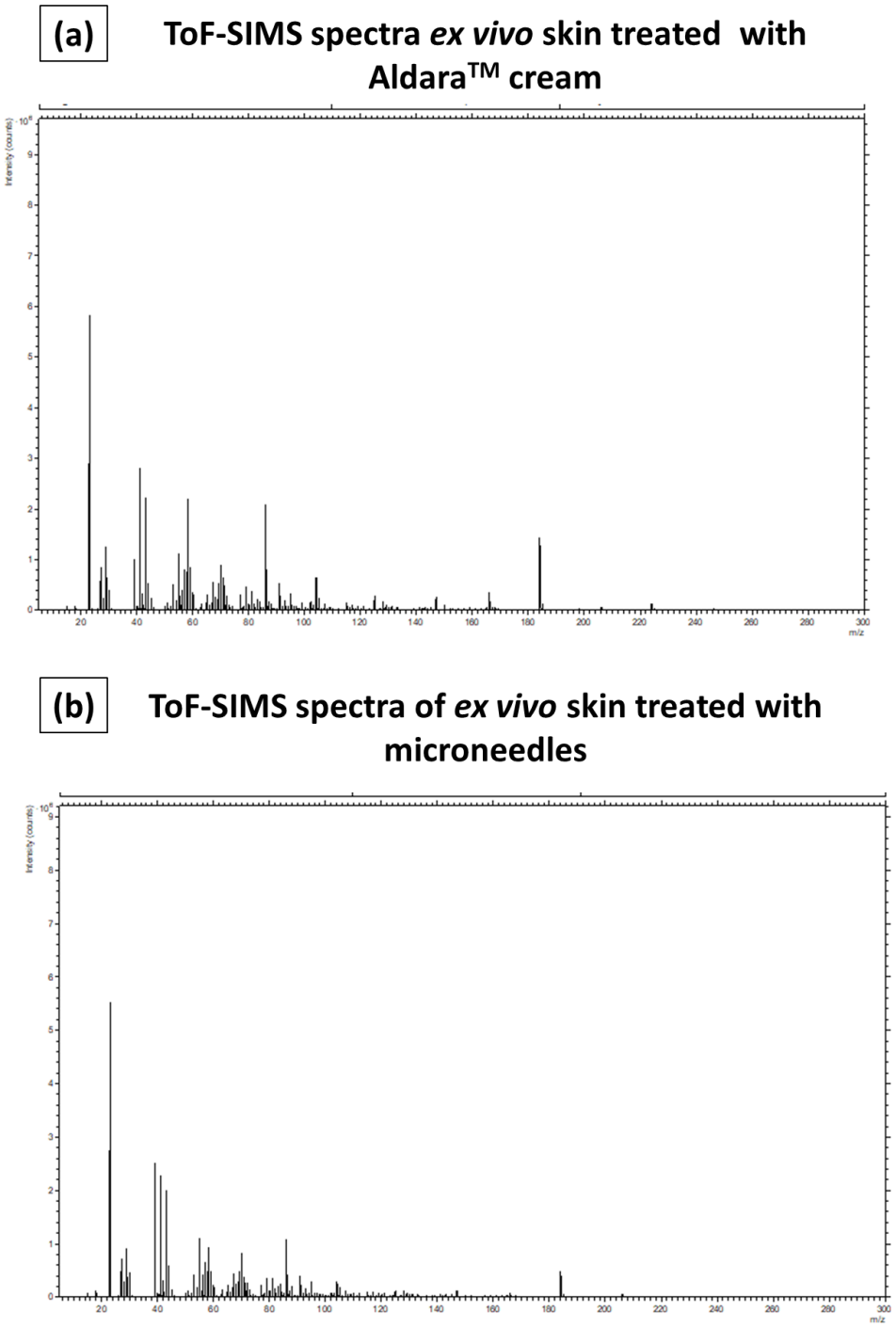

Figure S4- 5 ToF-SIMS spectra of (a) skin treated with AldaraTM cream (5% w/w imiquimod) (b) skin treated with imiquimod loaded PVPVA polymeric microneedles.

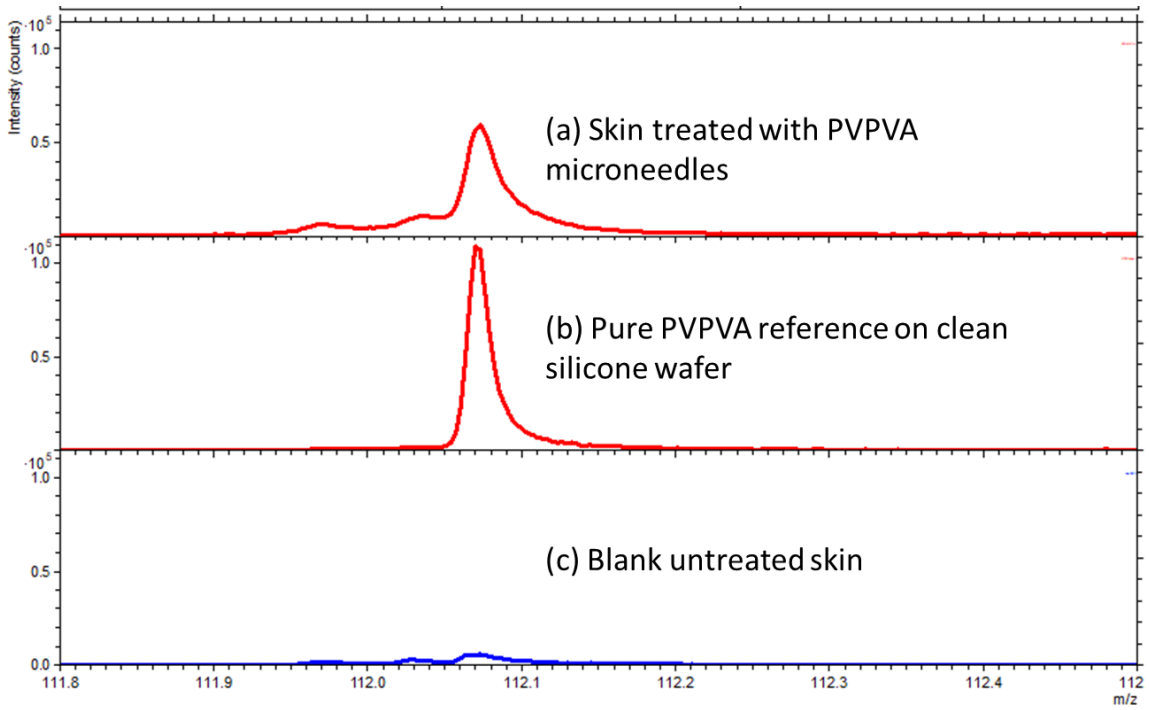

Figure S4- 6 Overlaid ToF-SIMS spectra of (c) blank untreated skin (b) skin treated with PVPVA polymeric microneedles (c) pure PVPVA reference, showing the fragment peak of PVPVA ($C_6H_{10}NO^+$) at m/z = 112 as suitable marker to track the dermal distribution of the polymer within the skin.

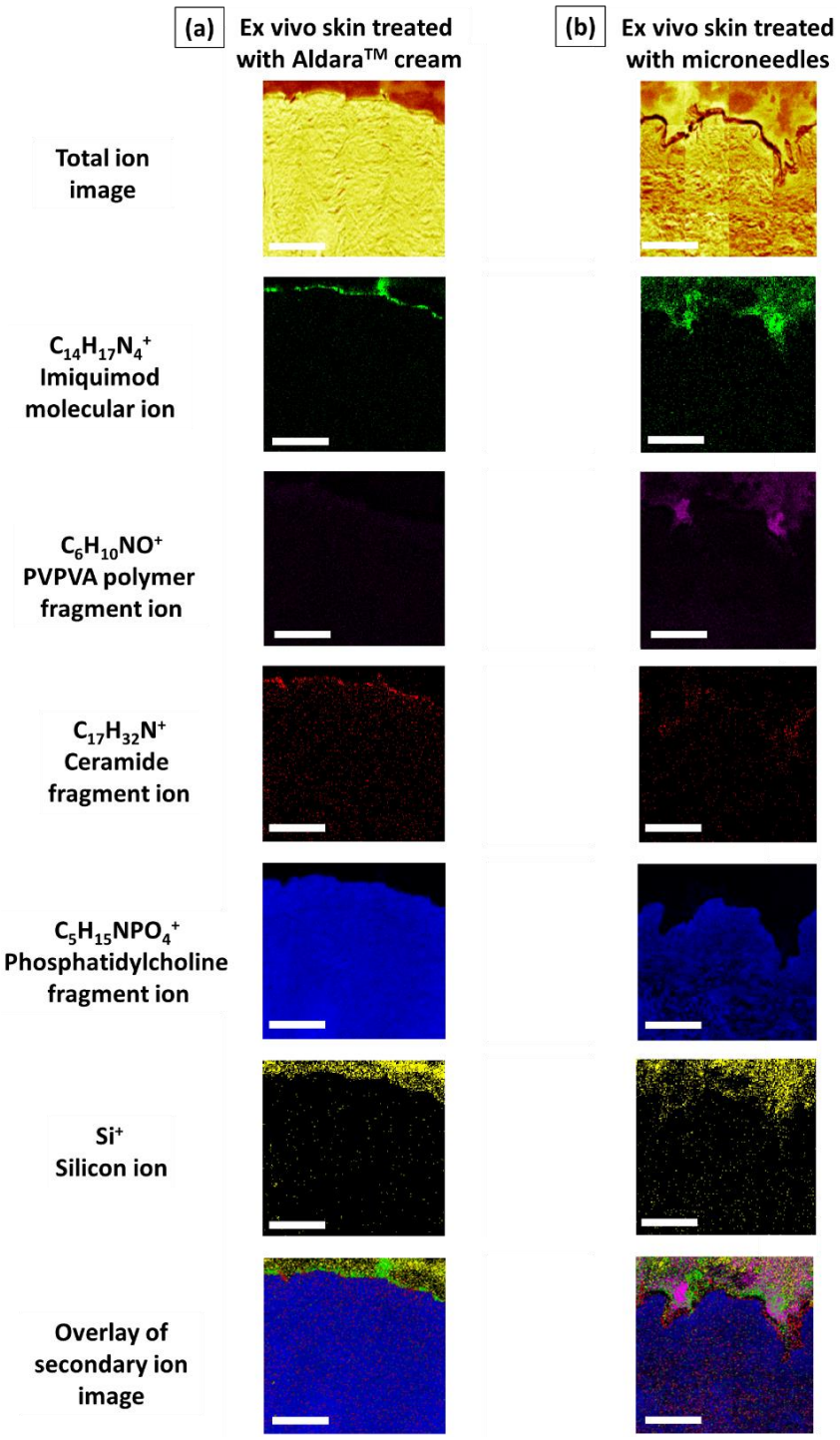

Figure S4- 7 ToF-SIMS secondary ion image of skin cross sections from ex vivo porcine skin that were treated with (i) Aldara™ cream (5% w/w imiquimod) alone (ii) PVPVA microneedles loaded with imiquimod after a 24-hour permeation study. Localisation of semi-dissolved polymeric microneedles within the dermis with skin treated imiquimod loaded microneedles. $C_{14}H_{17}N_4^+$inidicated in green is the molecular ion for imiquimod, $C_5H_{15}NPO_4^+$ indicated in blue is the fragment ion for phosphatidylcholine used to identify the viable epidermis and dermis. $C_{17}H_{32}N^+$ indicated in red is the fragment ion for ceramide used to identify the stratum corneum. $C_6H_{10}NO^+$

indicated in pink is the fragment ion for PVPVA polymer. Si^+ is an inorganic ion marker indicated in yellow is used to identify the glass slide. Scale bar: 500 µm.

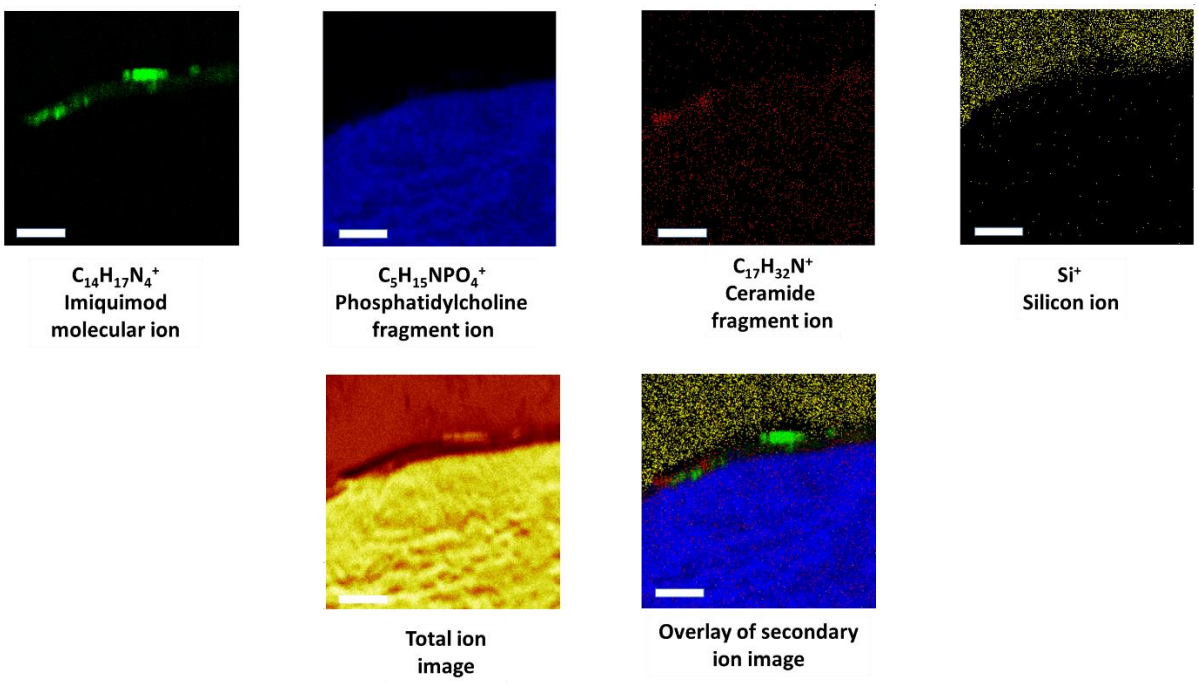

Figure S4- 8 ToF-SIMS analysis of skin cross sections from porcine skin that were treated with Aldara™ cream (5% w/w imiquimod) alone. This analysis was conducted at a higher resolution closer to the skin surface to image the localisation of imiquimod near the stratum corneum and epidermis junction. $C_{14}H_{17}N_4^+$ the molecular ion for imiquimod indicated in green is, $C_5H_{15}NPO_4^+$ the fragment ion for phosphatidylcholine used to identify the viable epidermis and dermis indicated in blue. $C_{17}H_{32}N^+$ is the fragment ion for ceramide used to identify the stratum corneum indicated in red. Si^+ is an inorganic ion marker used to identify the glass slide. The overlays highlights imiquimod localisation within the stratum corneum and some near the epidermis just below the stratum corneum. Scale bar: 100 µm.

Chapter 5 Development and characterisation of a series of dissolving polymeric microneedles for targeted drug delivery for basal cell carcinoma.

Akmal H. Sabri [a], Zachary Cater [b], Pratik Gurnani [a], Victoria Brentville [c], Lindy Durrant [c], Jane Ogilvie [d], J. McKenna [e], Joel Segal [b], David J. Scurr [a] and Maria Marlow [a]*

[a] School of Pharmacy, University of Nottingham, Nottingham NG72RD, United Kingdom.

[b] Advanced Manufacturing Technology Research Group, Faculty of Engineering, University of Nottingham, Nottingham, NG8 1BB

[c] Scancell Ltd, University of Nottingham Biodiscovery Institute, Nottingham, UK

[d] Walgreens Boots Alliance, Thane Road, Nottingham, NG90 1BS.

[e] Leicester Royal Infirmary University Hospitals Leicester Dermatology Department, Infirmary Square, Leicester LE1 5WW, United Kingdom

Acknowledgement of research work done by co-authors

- Zachary Cater: An undergraduate Mech Eng. student supervised by A.H. Sabri and J. Segal. Zachary Cater assisted Akmal Sabri with the computer aided design (CAD) for the microneedle master structures along with its subsequent production at the University of Nottingham Institute for Advanced Manufacturing. The work done by Zachary Cater formed part of **Section 5.4.1 Design and production of microneedle master structure and microneedle PDMS moulds.**
- Pratik Gurnani: Supervised and assisted Akmal Sabri during the polymer synthesis that forms section **5.4.2 Polymer synthesis** for this chapter. Pratik Gurnani also conducted gel permeation chromatography for the polymers due to the restricted access of the instrument

to trained personnel. This form **Section 5.4.3 Polymer characterisation by gel permeation chromatography (GPC)/size exclusion chromatography (SEC)**.

- Victoria Brentville and Lindy Durrant: *In vivo* study co-ordination and planning. Victoria Brentville was directly involved setting up the animal model and conducting the in vivo study on behalf of Akmal Sabri that formed Section **5.4.10 *In vivo* Tumour study**.
- John McKenna. John is a consultant dermatologist who supervised Akmal during his PhD and helped recruit patients for human clinical study. John was the surgeon who performed Mohs surgery and shipped patient samples to Akmal Sabri. The samples were used in section **5.4.9 ToF-SIMS analysis of microneedles and human BCC skin cross-sections**
- J. Ogilvie, D. Scurr, M. Marlow, J. Segal: Supervisors to A.H. Sabri and supervised him during the writing of the article. Critically reviewed the manuscript and editing.

Keyword: pNAM, Microneedles, imiquimod, basal cell carcinoma, time-of-flight secondary ion mass spectrometry

5.1 Abstract

Imiquimod is one of the most efficacious drugs used in the treatment of superficial basal cell carcinoma (BCC). Nevertheless, imiquimod possesses physicochemical properties that limit its permeation to deeper tumour lesions such as those seen in nodular BCC. The current work presents the development, characterisation and evaluation of a series polymeric microneedles of different designs and polymeric chemistries as a drug delivery platform for nodular BCC. The polymeric microneedles were manufactured from the commercial PVPVA polymer, Kollidon® VA 64 as well as pAMPS, pNAM and pHEAM that were synthesised via free radical polymerisation reactions. The microneedles fabricated from pAMPS, pNAM and pHEAM displayed superior mechanical strength relative to the commercial PVPVA polymer. In addition, microneedle insertion studies highlighted that microneedles formulated out of pHEAM and pNAM displayed the highest insertion efficiency and penetration profile out of all the microneedle formulations evaluated. However, drug release studies into *ex vivo* skin tissues demonstrated that only the pNAM obelisk microneedle patch was capable of achieving higher intradermal delivery of imiquimod relative to the commercial cream, Aldara™, and the PVPVA microneedles that was manufactured in our previous study. This was further corroborated by ToF-SIMS analysis of *ex vivo* patient BCC tumours treated with imiquimod loaded microneedle patches that demonstrated significant intradermal delivery of imiquimod within the tumour relative to the commercial cream Aldara™. In addition, an *in vivo* tumour mouse efficacy study for skin tumours highlighted that the pNAM microneedles were capable of delivering the drug into the skin tumour which ultimately slowed down tumour growth. This study demonstrates that the pNAM obelisk microneedle system developed may be a viable approach in improving the intradermal delivery of imiquimod for the treatment of nodular BCC for patients who would prefer a less invasive treatment relative to surgical interventions. Furthermore, the pNAM microneedle system may be simple and viable delivery system for the administration of other therapeutics into and across the skin.

5.2 Introduction

Basal cell carcinoma (BCC) is the most common cutaneous malignancy that accounts for approximately 70-80 % of all skin cancers [328]. Data from epidemiology studies indicate that the overall incidence of BCC is growing at steady rate of 1-3 % annually and it is predicted that this incidence will continue to rise globally due to the rise in the aging patient population coupled with an increase in UV exposure [25,29]. Nevertheless, this cancer is not regarded as life threatening as BCC typically have a very low metastasis rate of 0.0028 % resulting an overall mortality rate of less than 0.1 % [28,329]. However, should BCC be left untreated the tumour can cause considerable local tissue damage (nose, ears and eyelids), leading to poor cosmetic outcomes and skin site disfigurement [37,38]. The high incidence rate of the disease forms a considerable burden to the healthcare system. In the US, direct treatment costs for the management of BCC are estimated to amount to US$1.8–3.4 billion annually [39]. Such high treatment costs are attributed to the use of Mohs micrographic surgery in the management of BCC, which imposes a financial burden of over US$2.0 billion annually as well as being a considerable burden to the workload of dermatologists [39,330]. Therefore, the development of a simple and effective treatment that patients could self-administer themselves for the treatment of BCC is needed. Furthermore, some patients may prefer a non-surgical intervention that offers lower overall treatment costs with improved cosmetic outcomes [64,265].

One of the most effective non-surgical interventions used in the management of BCC is the topical application of the immunomodulator, imiquimod [59]. The drug is marketed as Aldara™ cream (5% w/w imiquimod) by 3M Pharmaceuticals and was initially approved by the FDA for the management of external genital and perianal warts in 1997. However, in 2004 Aldara™ was approved for the management of actinic keratosis and superficial BCC. Imiquimod belongs to a class of drugs known as imidazoquinoline which is an immunomodulator that stimulates toll-like receptors 7 (TLR-7) on dendritic cells, macrophages and monocytes when applied topically. Upon binding to the TLR-7 receptor on these immune cells, imiquimod stimulates downstream processes which leads to the production of pro-inflammatory cytokines culminating in its antitumoral activity [58]. However, topical

therapy with Aldara™ has been met with low cure rates when the formulation was administered to patients presenting with cases of nodular BCC [34]. This finding is attributed to efficient barrier of function of the *stratum corneum* as well as the location of nodular BCC that resides deep within the aqueous dermis, thus presenting a formidable challenge for the delivery of imiquimod in a concentrated and localised fashion into the dermis for the treatment of nodular BCC [68].

One of the drug delivery strategies that could be used to improve the delivery of imiquimod into the dermis for the treatment of nodular basal cell carcinoma are microneedles. Microneedles consist of arrays of fine micro-projections that upon application the skin produce micron size channels within the skin. The general consensus is that these microneedles channels can then be utilised to promote the delivery of therapeutics into and across the skin [293]. As microneedles provide direct application and administration of drug into the skin, this drug delivery platform has gained interest as a strategy to provide more localised delivery of therapeutics in the treatment of skin cancer [237].

Several researchers have investigated the utility of using solid microneedles, as a skin pre-treatment strategy prior to formulation administration, to improve the utility of delivering anticancer compounds into the skin for the treatment of skin cancer. For instance, Al-Mayahy *et al.* showed that using a two-step application process involving pre-treating the skin with solid stainless-steel microneedles followed by Aldara™ cream application, they were able to provide some degree permeation enhancement of imiquimod into the skin although [68]. However, it was apparent from the imaging mass spectrometry data, that the permeation of imiquimod into skin pre-treated with solid stainless-steel microneedles was mainly localised in the epidermis and did not reach the deeper dermal layer where some skin cancers such as nodular BCC resides. Furthering this, we have explored and demonstrated that by switching the application step of the oscillating solid microneedle, using the Dermapen® device, from pre-treatment to post-treatment, we were able to enhance the delivery of imiquimod deep into the dermal layers to the depth where nodular BCC resides [35].

Nevertheless, the utility of using solid stainless-steel microneedles with either pre-treatment of post-treatment strategies are limited by the two step application process which may not be favourable

by some patients as they would prefer formulations that they can administer in a single step with ease [331]. Given these limitations, we have recently explored the strategy of reformulating imiquimod into dissolvable polymeric microneedles for the treatment of nodular BCC. We have shown that by reformulating imiquimod into dissolving pyramidal polymeric microneedles using poly (vinylpyrrolidone/vinyl acetate) PVPVA, we were able to deliver the drug deeper into the skin relative to Aldara cream. Nevertheless, quantitative analysis using HPLC highlights that the amount delivered into the remaining skin layers were similar between the imiquimod loaded PVPVA microneedles and Aldara cream, indicating that there is still room to improve the delivery strategy even further [332].

The current work highlights the fabrication and evaluation of a series of polymeric microneedles patches of different geometries and polymeric chemistries as a drug delivery system to achieve the localised intradermal delivery of imiquimod for the management of nodular BCC. Microneedle moulds of different microneedle architectures were produced using micromachining. The moulds were then used to manufacture dissolving microneedles from the commercial PVPVA polymer, Kollidon® VA 64 as well as poly N-acryloylmorpholine (pNAM), poly N-hydroxyethyl acrylamide (pHEAM) and poly 2-acrylamido-2-methyl-1-propanesulfonic acid (pAMPS) that were synthesised via free radical polymerisation reactions. pNAM, pHEAM and pAMPS are biocompatible polymers that have been utilised to some degree, although their use is not as widespread as other pharmaceutical polymers, for various applications either as a hydrogel for wound healing [333], drug delivery [334], or as a system to control cellular adhesion[335]. Nevertheless, the utility of these polymers in fabricating polymeric microneedle systems have yet to be explored. Using polymer casting and micromoulding, polymeric microneedles of pyramidal and obelisk architecture with different polymer chemistries were manufactured. A series of experiments were performed to characterise the range of polymeric microneedle formulations developed. In addition, *in vitro* permeation studies utilising using full thickness *ex vivo* porcine skin was performed to evaluate imiquimod delivery from these polymeric microneedle patches into and across the skin. Subsequently, the formulation that provides the greatest enhancement in intradermal delivery of imiquimod with minimal transdermal release was

then evaluated in an *ex vivo* human BCC tumour in order to gauge if the polymeric microneedle formulation was capable delivering imiquimod into the tumour. Lastly, the efficacy of the formulation was also evaluated *in vivo* using a rodent model for skin tumours in order to determine if the delivered imiquimod was capable of slowing down tumour growth. This study can serve as a basis for the future development of polymeric microneedles therapies for the management of nodular BCC as well as other skin cancers alike.

5.3 Materials

Imiquimod was purchased from Cayman Chemicals, USA. Aldara™ topical cream (5% w/w imiquimod), MEDA Company, Sweden was purchased from Manor Pharmacy, UK. Polyvinylpyrollidone-co-vinyl acetate (PVPVA), was kindly provided by BASF (Ludwigshafen, Germany). Polyethylene glycol, PEG 400 was purchased from Sigma Aldrich, Belgium. Sodium carboxymethyl cellulose, Mw 90,000 was purchased from Sigma Aldrich, USA. N-acryloylmorpholine (97%), N-hydroxyethyl acrylamide (97%) and 2-acrylamido-2-methyl-1-propanesulfonic acid (99%) were purchased from Sigma Aldrich, USA and the inhibitor removed by passing the monomers through a column of aluminium oxide. Thermal initiators 4,4'-azobis(4-cyanovalericacid) (ACVA, > 98%) was purchased from Sigma-Aldrich while 2,2'-azobis[2-(2-imidazolin-2-yl) propane] dihydrochloride (VA-044, > 98%) was purchased from Wako Pure Chemical Industries Ltd. Glycerol was purchased from Sigma Aldrich, USA. Dimethyl sulfoxide (DMSO), tetrahydrofuran (THF) and diethyl ether were of reagent grade and were purchased from Fisher Chemical, UK. Deuterium oxide (99.9% D atom), DMSO-d_6 (99.5% D atom), and Chloroform-d (99.8% D atom) were obtained from Sigma-Aldrich and used for ^{1}H NMR spectroscopy. Sodium acetate was purchased from Sigma-Aldrich, UK. Acetonitrile (HPLC grade) and glacial acetic acid were obtained from Fisher Scientific, UK. Teepol solution (multipurpose detergent) was ordered from Scientific Laboratory Supplies, UK. D-Squame standard sampling discs (adhesive discs) were purchased from Cuderm corporation, USA. OCT media was obtained from VWR International Ltd. Belgium. Deionised water was obtained from an ELGA reservoir, PURELAB® Ultra, ELGA, UK. All reagents were of analytical grade, unless otherwise stated. *Ex vivo p*orcine skin was used in imiquimod permeation studies due to

the similarities in histology, thickness and permeability to human skin [246]. Skin samples were prepared from ears of six-month-old pigs obtained from a local abattoir prior to steam cleaning. The skins were of full skin thickness to prevent altering the biomechanical properties of the tissue that may lead to excessive penetration of the microneedles into the skin [66]. The porcine skin samples were stored at -20 °C until analysis.

5.4 Methods

5.4.1 Design and production of microneedle master structure and microneedle PDMS moulds

To produce the custom polydimethylsiloxane (PDMS) moulds, a stainless-steel microneedle master structure was designed in SolidWorks 2018 (Dassault Systèmes), consisting of a 10 x 10 array of 300 µm x 300 µm x 1000 µm (W x L x H) of either pyramidal or obelisk microneedles with tip-to-tip spacing of 800 µm. This master structure, and a corresponding mould housing were then produced from stainless-steel using a Kern Evo CNC Micro Milling Machine at the University of Nottingham Institute for Advanced Manufacturing. PDMS (Sylgard 184®, Dow Corning, Midland, MI) moulds were then created from the stainless-steel microneedle master structure. A mixture of elastomer and curing agent, Sylgard 184®, were prepared at a ratio of 10:1 (elastomer: curing agent). The mixture was then degassed for 45 minutes to remove any trapped air in the mixture. After degassing the PDMS mixture was poured into the stainless-steel master mould structure and placed in an 80 ^{o}C oven for one hour to cure the PDMS. After curing, the mould along with the cured PDMS was plunged into an ice bath to allow ease of removal of the cured PDMS mould. The stainless-steel master structure was then cleaned with propan-2-ol before being reused to make further PDMS moulds.

5.4.2 Polymer synthesis

Polymers were synthesized using the following general procedure from the conditions described in Table 5-1. Monomer, initiator and solvents were added to a 50 mL round bottomed flask equipped with a magnetic stirrer. The flask was sealed, the solution purged with argon gas for 10 min and then

immersed in an oil bath at 70 °C for two hours. Polymerisations were monitored by ^{1}H NMR spectroscopy and quenched by removing from the reaction mixture from heat and exposing it to air. Polymers were purified and isolated either by precipitation or dialysis in water followed by lyophilisation.

Table 5-1 Concentration and monomer and initiator used for polymer synthesis along with purification method post-synthesis. [M] refer to molar concentration, [mM] refer to millimolar concentration, MWCO refer to molecular weight cut-off.

Polymer	Solvent	Monomer concentration [M]	Initiator	Initiator concentration, [mM]	Purification method
pHEAM	DMSO	1.0	ACVA	1.0	Dialysis against water (25 kDA MWCO)
pNAM	H_2O	1.0	VA-044	1.0	Polymer was dissolved in THF and precipitated in diethyl ether
pAMPS	H_2O	0.5	VA-044	1.0	Dialysis against water (25 kDA MWCO)

5.4.3 Polymer characterisation by gel permeation chromatography (GPC)/size exclusion chromatography (SEC)

SEC analysis for PVPVA and pHEAM were determined was performed using a Polymer Laboratories PL-50 instrument fitted with a differential refractive index detector. The system was equipped with 2×

PLgel Mixed D columns (300 × 7.5 mm) and a PLgel 5 µm guard column. The eluent used was 0.1% LiBr in dimethylformamide (DMF). Samples were eluted at 1 mL min−1 with the column oven heating to 50 °C. PMMA standards (Agilent EasyVials) were used for conventional calibration between 500−955,550 g mol−1. Experimental molar mass (Mn,SEC) and dispersity (Đ) values of synthesized polymers were determined by using Cirrus GPC software.

SEC analysis for pNAM was performed using a Shimadzu Prominence instrument fitted with a differential refractive index detector. The system was equipped with 2× PLgel Mixed D columns (300 × 7.5 mm) and a PLgel 5 µm guard column. The eluent used was 2% (w/w) triethylamine and 0.01% butylated hydroxytoluene (w/w) in THF. Samples were eluted at 1 mL min−1 with the column oven heating to 50 °C. PMMA standards (Agilent EasyVials) were used for conventional calibration between 500−955,550 g mol−1. Experimental molar mass (Mn,SEC) and dispersity (Đ) values of synthesized polymers were determined by using Shimadzu GPC software.

SEC analysis for pAMPS was performed using an Agilent GPC instrument fitted with a differential refractive index detector and UV detector. The system was equipped with 2x PL Aquagel-OH columns (300 × 7.5 mm) and a PL Aquagel-OH guard column. The eluent used was an aqueous solution of $NaNO_3$ (0.1 M). Samples were eluted at 1 mL min^{-1} . PEG standards (Agilent EasyVials) were used for conventional calibration between 500 − 955,550 g mol^{-1}. Experimental molar mass (Mn,SEC) and dispersity (Đ) values of synthesized polymers were determined by using ASTRA software

5.4.4 Differential scanning calorimetry of polymers

In order to understand the physical properties of PVPVA polymer, DSC measurements were conducted. Dry polymer samples (~10 mg) were assessed using a Mettler Toledo DSC1 using a scan rate of 10 K/min in a temperature range of -100 to 150 °C. The glass transition temperature (T_g) was recorded as the midpoint of the glass transition observed in the second heating run.

5.4.5 Fabrication of blank and drug loaded polymeric microneedles

Polymeric microneedles were prepared using a micromolding technique. The PDMS moulds produced as described in Section 5.4.1 were used to fabricate the blank microneedles. The microneedle matrices of different polymers were prepared by dissolving respective polymer and additive in water under stirring for one hour. The optimised compositions of different microneedle formulations are shown in Table 5-2.

Table 5-2 Optimised microneedle formulation composition for respective polymers

Microneedle formulation	**Polymer concentration, % w/v**	**Additive**	
		PEG 400, % v/v	PVA, % w/v
pHEAM Pyramidal	6.25	n/a	2.0
pHEAM Obelisk	6.25	n/a	2.0
pNAM Pyramidal	6.25	n/a	2.0
pNAM Obelisk	6.25	n/a	2.0
pAMPS Pyramidal	6.25	n/a	2.0
pAMPS Obelisk	5.42	n/a	2.9
PVPVA Pyramidal	16.2	2.0	n/a
PVPVA Obelisk	16.2	4.0	n/a

The polymer solution was then degassed for 30 minutes before 150 µl of the polymer solution was pipetted into the PDMS mould and centrifuged at 4000 RPM for 15 min at room temperature, to fill the needle cavities. Then, excess polymer was removed before leaving the needle layer to dry

overnight in a desiccator. The backing layer of the microneedle patches were prepared using 5.2 % w/w of carboxymethylcellulose, CMC (in water). The backing solution was made by dissolving CMC under stirring at 75 ^{o}C for 2 hours. In addition, 0.66 % v/w of glycerol was added to the backing solution as a plasticiser. Using a positive displacement pipette, 200 µl of the CMC solution was then pipetted on top of the needle layer and centrifuged at 3500 RPM for 10 minutes. The mould was dried at room temperature for 48 hours in a desiccator. The polymeric microneedles were then demoulded and stored in a desiccator until further use. For imiquimod loaded microneedles the fabrication process was repeated in a similar fashion with the addition of 1 % w/v of imiquimod for all formulation composition, however the drug and polymer were dissolved in 0.05 M of hydrochloric acid under stirring for 1 hour.

5.4.6 Characterisation of polymeric microneedles (SEM, tensile strength, skin insertion properties)

5.4.6.1 Microscopy

Polymeric microneedle images were captured using an optical microscope (Zeiss Axioplan, Germany) and an environmental scanning electron microscopy (ESEM) (FEI Quanta 650) in low vacuum mode to visualize the shape and dimensions of the microneedles. For ESEM imaging, the microneedles were mounted on a metal stub using double-sided carbon tape prior to imaging.

5.4.6.2 Measurement of needle fracture force

The needle fracture force of the polymeric microneedles was determined using a texture analyser (Stable Microsystems, UK) following a previously reported method [137]. Needle fracture force was measured to investigate the effect of applying an axial force parallel to the microneedle vertical axis, similar to the force encountered by the needles during application to the skin, on the mechanical properties of the needles. The polymeric microneedles were visually inspected before and after application of the compression force. For this, the force required for compression of the polymeric microneedle to a specified distance was measured. The polymeric microneedles were attached to a

10 mm cylindrical Delrin probe (part code P/ 10) using double-sided adhesive tape. The probe was connected to a 50-kg load cell and was set at the same distance from the platform for all the test measurements. The TA XT Plus Texture Analyser was set to compression, the pre-test speed was set at 2 mm/s and post-test speed at 10 mm/s. The trigger type was set to auto (force) with a trigger force of 0.009 N. The test station compresses the polymeric microneedle against a flat block of aluminium of dimensions 10.0 × 9.0 cm. Compression force versus displacement curves were plotted to calculate the fracture force. A total of five microneedle patches were used to evaluate the fracture force of the microneedles.

5.4.6.3 In vitro skin simulant insertion

As an alternative method to determine the microneedle penetration depth as a function of length, a polymeric film (Parafilm M®, a blend of a hydrocarbon wax and a polyolefin) was utilised as a skin model. This insertion study was adapted from Larrañeta *et al.* [248]. In brief, 8 layers of Parafilm M® were stacked onto each other on a cork mat that mimics underlying muscles. The polymeric microneedle patches were applied under thumb pressure for 10 seconds. Six replicates were generated and observed under the Zeta Profilometer (KLA-Tencor, US) for the number of micropores created.

5.4.6.4 Dye binding study

In order to evaluate if the microneedle patch was capable of penetrating the skin and to visualise the depth of microneedle penetration into the skin, a dye binding study using *ex vivo* porcine skin was conducted. The porcine ear skin was defrosted at room temperature for an hour prior to the experiment. Using clippers, excess hair was carefully trimmed from the skin. Regions of the skin were then selected for microneedle treatment. The skin was treated with polymeric microneedles loaded with methylene blue dye (1% w/v), which is a hydrophilic dye. The microneedle was left in the skin for one hour before removing the microneedle patch. Upon removing the patch, the skin was visually inspected to see if any microneedle channels had been generated in the skin. In order to gauge the depth of microneedle penetration into the skin, skin cross-sectioning was performed. In brief, each

microneedle application site was cut into 1 cm × 1 cm and fresh frozen on a metal block that was cooled with liquid nitrogen. Skin cross-sections were performed using a cryostat (Leica CM3050 S Research Cryostat, UK). The depth of microneedle penetration, as visualised by methylene blue permeation, was measured using an optical microscope (Zeta Profilometer, KLA-Tencor, US).

5.4.7 Measurement of imiquimod permeation from polymeric microneedles

Imiquimod skin permeation was evaluated *ex vivo* using a Franz-type diffusion cell. Prior to the permeation study, skin samples were defrosted and carefully trimmed into small pieces according to the area of the donor chamber of the Franz diffusion cell (Soham Scientific, Cambridgeshire, UK). The *ex vivo* porcine skins were subjected to the following treatments: i) application of 20 mg Aldara™ cream, in accordance with clinical dose approved by the FDA for the treatment of BCC. ii) imiquimod loaded polymeric microneedles. Next, the treated porcine skins were placed on top of the receptor compartment filled with 3 ml of degassed 100 mM acetate buffer pH 3.7. The skin was then secured between the donor and receptor compartment of the diffusion cell using a metal clamp, with the *stratum corneum* side facing the donor compartment. Upon assembling the Franz diffusion cell, the permeation experiment was conducted over a period of 24 hours in a thermostatically controlled water bath set at 36.5 ^{o}C. 1000 µl of the receptor fluid at designated time points (0.5, 1, 3, 6, 12 and 24 hours) was sampled and then replaced with equal volume of fresh 100 mM acetate buffer pH 3.7. Upon sampling, 1000 µl of the solution from each Franz cell after collection was then spiked with 100 µl of 100 µg/ml propranolol as an internal standard before being filtered through 0.22 µm membrane prior to HPLC analysis.

After the 24-hour permeation experiment, excess cream was removed from the Aldara^{TM} treated skin surface by careful application of sponges soaked with 3% v/v Teepol® solution. For the microneedle patch treated skin, the remaining microneedle patch was removed from the skin. Upon removing excess formulation from the skin surface, 15 sequential tape strips were collected from the skin. The amount of imiquimod from the pooled tape strips and remaining skin after tape stripping were

extracted by the addition of 10 and 5 mL of methanol extraction mixture (Methanol 70%: Acetate Buffer pH 3.7 100 mM 30%) respectively using a previously reported method [52]. Samples were then vortexed for 1 minute and sonicated for 30 minutes before being left overnight. Subsequently, samples were vortexed again and sonicated for a further 30 minutes. After sonication, 1000 µl of the extracts were collected and spiked with 100 µl of 100 µg/ml propranolol as an internal standard. The samples were then filtered through 0.22 µm membrane prior to HPLC analysis.

5.4.8 High performance liquid chromatography (HPLC) analysis

HPLC analysis was carried out using an Agilent 1100 series instrument (Agilent Technologies, Germany) equipped with degasser, quaternary pump, column thermostat, autosampler and UV detector. System control and data acquisition were performed using Chemostation software. The details of the HPLC chromatographic conditions are as follow: column C18 (150 × 4.6 mm) ACE3/ACE-HPLC with a particle size of 5 µm, pore size of 100 Å, pore volume of 1.0 ml/g and a surface area of 300 m^2/g, Hichrom Limited, UK. The mobile phase composition for analysis of extracts from skin wash, donor chamber wash, pooled tape strips and remaining skin consists of 10 mM acetate buffer: acetonitrile (79:21). Whilst, the mobile phase composition for analysis of receptor fluid consists of 10 mM acetate buffer: acetonitrile (70:30). The HPLC was operated at a flow rate of 1.0 mL/minute, UV detection at λ_{max}=226 nm, an injection volume of 40 µL and a column temperature of 25 °C.

5.4.9 ToF-SIMS analysis of microneedles and human BCC skin cross-sections

The chemical composition of the microneedles manufactured was established by ToF-SIMS analysis. Prior to the analysis, the microneedles were carefully removed from the backing layer using a pair of micro-scissors. Following the removal of the microneedles from the backing layer, the microneedles were adhered on a glass slide that was coated with 5% w/v poly (hydroxyethylmethacrylate) and left to dry overnight before analysis under room temperature and pressure. ToF-SIMS analysis was performed under delayed extraction mode which is set to 90 ns using the Hybrid-SIMS instrument (IONTOF, GmbH) with a Bi_3^+ cluster source. A primary ion energy of 30 keV was used, the primary ion

dose was preserved below 1×10^{12} per cm^2 to ensure static conditions. A pulsed target current of approximately 0.12 pA, and post-acceleration energy of 10 keV were employed throughout the sample analysis. In order to visualise the sub-surface chemical composition of the microneedle glass cluster ion beam (GCIB) sputtering was conducted on the microneedles using a 20 keV GCIB (Ar_{1500}^+) with a target current of 3 nA. Non-interlaced sputtering was employed, whereby the sputter and analysis ion beams do not operate simultaneously but at regular alternating intervals, with a single cycle consisting of 10 s sputtering, a 1.0 s pause and 3.25 s of analysis. After sputtering, the microneedles were analysed using the same analysing parameter with Bi_3^+ cluster source.

In order to evaluate the depth of imiquimod permeation into the skin, the permeation experiments were repeated as described above Section 5.4.7. However, in this instance *ex vivo* human BCC samples were utilised in the permeation experiment instead. Samples were obtained from patients attending Mohs micrographic surgery for the removal of nodular BCC at the dermatology clinic at Leicester Royal Infirmary. Patients' informed consent were first sought before samples were collected for the investigation. The study protocol was approved by the East of Scotland Research Ethics Service (EoSRES) Board and the NHS Health Research Authority (NHS HRA approval ID: 130880). After the permeation study, excess formulation was removed from skin samples treated with cream and microneedles. Subsequently, 1 cm × 1 cm areas of each application site were fresh frozen with liquid nitrogen. Skin cross-sectioning was performed using a cryostat (Leica CM3050 S Research Cryostat, UK). The skin slices were then thaw mounted on a glass slides and stored at -20 ^oC prior to ToF-SIMS analysis. ToF-SIMS was used to analyse the cryo-sectioned porcine skin samples. ToF-SIMS analysis was performed using a ToF-SIMS IV instrument (IONTOF, GmbH) with a Bi_3^+ cluster source. A primary ion energy of 25 KeV was used, the primary ion dose was preserved below 1×10^{12} per cm^2 to ensure static conditions. Pulsed target current of approximately 0.3 pA, and post-acceleration energy of 10 keV were employed throughout the sample analysis.

5.4.10 *In vivo* tumour study

Female HHDII/HLA- DP4 (DP*0401) mice (EM:02221, European Mouse Mutant Archive), aged between 8 and 12 weeks old, were used. All work was carried out at Nottingham Trent University under a Home Office approved project license. For the tumour study mice were randomized into different groups and not blinded to the investigators. The three treatment groups were (i) mice that received imiquimod loaded polymeric microneedle patches, (ii) mice that received unloaded polymeric microneedle patches and (iii) mice that did not receive any treatment which was selected as a negative control (n=10 per cohort). In the tumour study mice were challenged with 4×105 B16 HHDII DP4 melanoma cells on the right flank. The fur on the right flank was shaved prior to microneedle application. Microneedle patches were applied to the melanoma tumour site on the right flank and secured using a kinesiology tape to avoid the microneedle from being dislodged by the mice during the study. The patch was applied to the melanoma tumour site for 24 hours before removal. The imiquimod loaded microneedle patch were administered on days 4, 8, 11 and 15 post tumour implantations. Tumour growth was monitored at 3 to 4-day intervals and mice were humanely euthanized once the tumour reached 10 to 15 mm in diameter. Tumour volume was estimated using the following formula, volume = $(\pi/6) \times (L \times W^2)$, where L is length and W is width of the tumour.

5.4.11 Statistical analysis

Statistical analysis was conducted using GraphPad Prism 7.02 software. Data are shown as mean ± standard error of mean. When comparing two groups an unpaired t-test analysis was used, while one-way analysis of variance (ANOVA) with Tukey's multiple comparisons tests was used to compare multiple groups. p values < 0.05 were considered statistically significant.

5.5 Results and Discussion

5.5.1 Polymer synthesis

Three hydrophilic polymers, polyNAM, polyHEAM and polyAMPS were synthesised via free radical polymerisation reaction followed by purification either through precipitation or dialysis to remove

impurities left from the polymerisation reaction, such as unreacted monomer and initiators. The successful conversion of monomer into polymer is evidenced by ^{1}H-NMR shown in Figure S5- 1. The reaction scheme for respective polymers is shown in Figure 5-1. These polymers were chosen as they have yet to be explored as a material for microneedle fabrication despite being used elsewhere the field of drug delivery and tissue engineering [333–335].

Free radical polymerisation was chosen as the method for polymer synthesis due to the simplicity in the synthesis route, low cost and applicability to a wide range of monomer chemistries [336]. In addition, this form of polymerisation reaction can be carried out in solution, emulsion, or suspension and bulk monomer, highlighting the versatility of this polymerisation reaction. Furthermore, as this form of polymerisation reaction is one of the most common methods employed in polymer synthesis in the industry, there is a possibility for the polymer synthesised in this work to be produced at commercial scale [337]. Prior to polymer reaction, all the reaction medias were purged with $Ar_{(g)}$. The purpose of this step was to remove any oxygen molecules from the reaction vessel as oxygen molecules will scavenge the radicals produced from thermolysis of the thermoinitiators in addition to the propagating macroradicals. This could lead to the production of stable peroxyl radicals, which are less reactive, leading to inhibition in the polymerisation reaction [338].

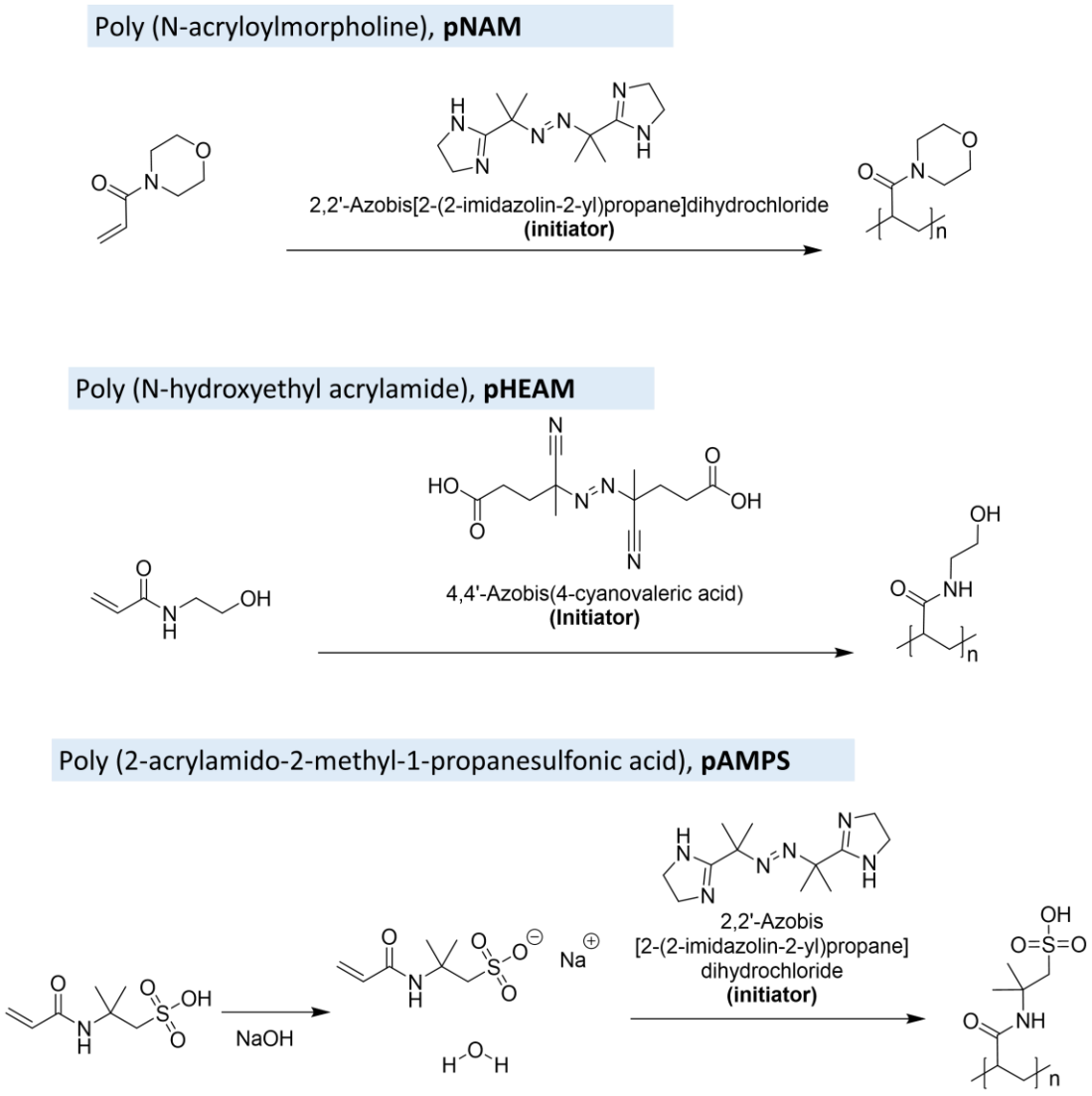

Figure 5-1 Reaction scheme for the synthesis of poly (N-acryloylmorpholine), poly (N-hydroxyethyl acrylamide) and poly (2-acrylamido-2-methyl-1-propanesulfonic acid)

From Table 5-3 it is clear that all the polymers synthesised displayed a broad dispersity, *Đ* ranging from 1.80 for pAMPS up to 3.10 for pNAM. Within polymer chemistry, polymers are consider to have broad dispersity when the molecular weight distribution displays a dispersity of *Đ* >1.4 [339]. Some of the hallmarks of the polymer synthesis by free radical polymerisation are high monomer to polymer conversion rate, as well as the presence of broad polymer dispersity. Such broad dispersity is attributed to the lack of control over chain propagation as well as premature and irreversible chain termination via recombination or disproportionation during the polymerisation reaction [340,341]. It is also worth noting that the commercial polymer, PVPVA used in a previous study also displayed *Đ* of

2.23 suggesting that the commercial polymer was also synthesised by a free radical polymerisation reaction [332].

Table 5-3 Summary of the characterisation and properties of the polymers synthesised via free radical polymerisation along with the commercial polymer PVPVA used in the study

Polymers	**Conversion, %**	**number average molecular weights M_n ($g\ mol^{-1}$)**	**Dispersity, *Đ***	**Glass transition temperature, Tg, °C**
PVPVA	n/a	16, 900	2.23	106
pNAM	94	55, 800	3.10	117
pHEAM	>99	126, 900	2.72	127
pAMPS	>99	43, 700	1.80	143

Despite similar reaction temperatures and times for all the polymers synthesised, it can be seen that there were differences in the molecular weight of the polymers synthesised, with pHEAM displaying the greatest molecular weight. This is attributed to the Trommsdorff–Norrish effect that took place during the synthesis of pHEAM, leading to enhanced localised viscosity of polymerisation media, which slows down the polymer termination step. In contrast, the propagation step in the free-radical polymerisation reaction is insensitive to the increase in viscosity. This ultimately causes the polymer chains to grow with minimal termination thus culminating in pHEAM exhibiting the highest molecular weight relative to the other polymers synthesised [342]. Such observations in which polymers exhibit Trommsdorff–Norrish have been reported for the synthesis of methacrylate and styrene-based polymers [343,344] as well as acrylamide-based polymers[345,346]. However, such an effect has never been reported before for homopolymers of polyacrylamides.

It is worth noting that the synthesised polymers, pNAM, pHEAM and pAMPS displayed a higher glass transition temperature, T_g relative to the commercial polymer PVPVA. Such high glass transition temperatures are attributed to the greater molecular weight of the synthesised polymers relative to PVPVA. Such an observation is corroborated by the findings by other research groups that showed that the T_g of polymers increased with increasing polymer molecular weight [347–349]. This observation can be explained by the Flory-Fox theory that describes how the glass transition temperature, T_g of a polymer increases with an increase in molecular weight, M_n. With higher molecular weight polymers, there is a decrease in the concentration of the more molecularly mobile polymer end chains, but a rise in the concentration of the less molecularly mobile polymer middle chain. This results in a lower excess free volume and slower molecular mobility, resulting in greater intermolecular interaction between polymers that culminates in a rise in T_g [350]. However, in the case of pAMPS the increase in T_g is not only attributed to a rise in the polymer molecular weight but also to the presence of the highly ionisable propanesulfonic acid side group. This can form strong intermolecular ionic interactions between polymer chains giving rise to higher T_g, relative to the other polymers. Such an observation is corroborated by the work by Shibata *et al.* in which they discovered that poly(4-vinylpyridine) polymers with a higher degree of ionic interactions, through the incorporation of disulfonic acid moiety into the polymer, exhibit a rise in T_g. [351]. Therefore, despite pAMPS having a lower molecular weight relative to pHEAM and pNAM, the presence of strong ionic interaction between polymer chains in pAMPS reduces the polymer molecular mobility resulting in the polymer with the highest T_g out of the four polymers evaluated. Following synthesis and purification, the polymers synthesised along with the commercial polymer PVPVA were then used to fabricated polymeric microneedles for the delivery of imiquimod.

5.5.2 Microneedle fabrication

In this work, eight different polymeric microneedles of varying geometries and chemistries were fabricated following polymer synthesis. First the dimensions of the master structures were designed via computer aided design (CAD), then manufactured by micromachining. Two different microneedle

geometries were chosen i.e., pyramidal and obelisk. The stainless-steel master structures were used to manufacture PDMS moulds which were subsequently used for microneedle production. Micro-milling was used to fabricate the designed stainless-steel master structures as this method produced has been shown to produce minimal surface imperfections [332]. In addition, it has been described that micro-milling offers low manufacturing cost in generating complex architecture at a micron scale with high accuracy and repeatability [298].

The polymeric microneedles were fabricated via casting, centrifugation and drying. The resulting polymeric microneedle patch is shown in Figure 5-2. Upon inspection via microscopy as shown in Figure 5-2 **(a)-(d)**, the microneedle patch displays visible micro projections, which were either pyramidal or obelisk depending on the mould which the polymer blend was casted into. All microneedle formulations gave a needle length of ≈ 980 µm as shown in Figure S5- 2. The pyramidal microneedle displayed a tip radius of 32.3 ± 3.1 µm (mean ± SD, *n*=4) while the obelisk microneedles showed a tip radius of 22.3 ± 2.5 µm (mean ± SD, *n*=4) as observed via optical microscopy Figure 5-2 **(e)**.

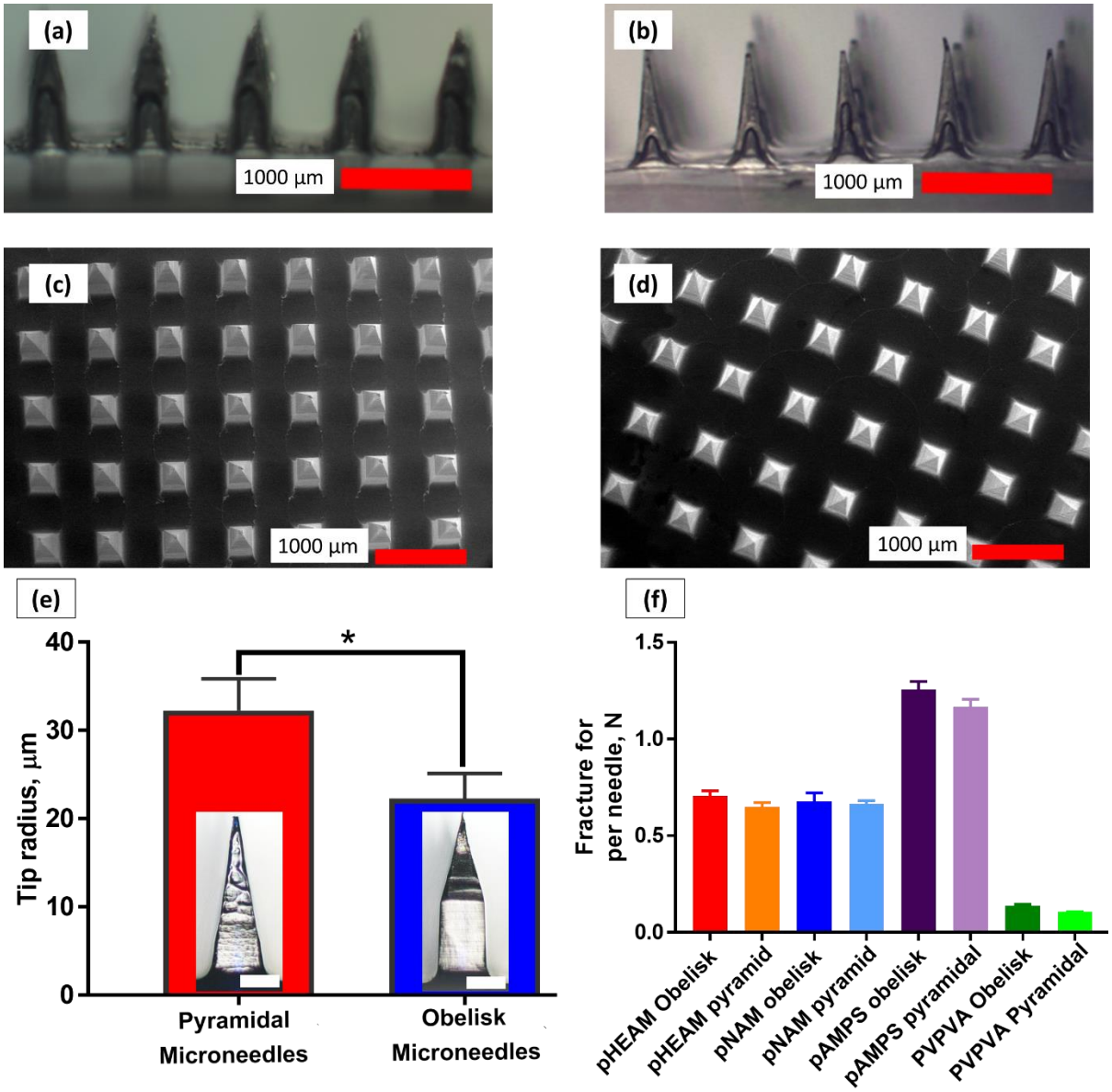

Figure 5-2 Optical microscopy image of (a) obelisk pNAM microneedles and (b) pyramidal pNAM microneedles at 12.5× magnification. SEM images of (c) obelisk an (d) pyramidal pNAM microneedles at 39× magnification. (e) Measurement of microneedle tip radius for obelisk and pyramidal PVPVA microneedles data are expressed as mean ± SD, n=4 Inset within the bar charts highlights a closeup microscopy image - of a single pyramidal and obelisk polymeric microneedle at 50× magnification, scale bar: 250 µm. Differences were determined using a two-tailed Student's t test, and deemed significant at $p<0.05$. (f) Measurement of microneedle fracture force for different microneedle formulations data are expressed as mean ± SD, n=6.

SEM analysis, as shown in Figure 5-2 **(c)-(d)**, revealed that equally spaced, sharp pyramidal and obelisk microneedles, on a clean and smooth baseplate were formed when the polymer blends were casted, dried and demoulded from the respective PDMS moulds. This was true for all the polymers used in fabricating the microneedles as shown in Figure S5- 3. This clearly indicates that the copolymer PVPVA along with the homopolymers pNAM, pHEAM and pAMPS were suitable materials for fabricating polymeric microneedles. We have previously demonstrated for the first time that PVPVA was a suitable material for fabricating dissolvable microneedles for the delivery of imiquimod [332]. However, the current work has explored and expanded the range of polymers that could be used as a material for microneedle fabrication by introducing the use of pNAM, pHEAM and pAMPS. Additionally, these polymers are hydrophilic which permitted formulation of these polymers into an aqueous blend for casting and micromoulding for microneedle production. The use of water as a solvent to dissolve these polymers is an advantage as this avoids the use of organic solvents. The use of organic solvents in formulation production may be an issue especially during commercial manufacture, due to an inability to completely remove the solvent from the formulation. This will ultimately lead to trace amounts of organic solvents in the formulation, which are sometimes known as residual solvent. Despite meeting the standards set out in pharmacopeias, these solvents may accumulate in patients' body over time with repeated application, which may lead serious side effects over time [352]. Furthermore, the absence of organic solvents also mitigates the swelling the PDMS moulds used in microneedle production [300]..

We have previously reported that in order to prepare microneedles using Kollidon® VA 64, the formulation necessitates the incorporation of PEG 400 as a plasticiser. PEG 400 in this case may act as a plasticiser which reduces the brittleness of the microneedle post manufacture by imparting some degree of flexibility to permit ease of handling during demoulding [332]. Similarly, in the current work it was observed that microneedles prepared from the use of pure aqueous blend of pNAM, pHEAM and pAMPS (without the presence of any other additive) also resulted in microneedle formation with poor mechanical properties, such as fractured tips as shown in Figure S5- 3. Nevertheless, such a limitation

was ameliorated by the incorporation of PVA as an additive during the fabrication of the microneedle layer. PVA is a water-soluble, synthetic, semi-crystalline polymer has previously been used as an additive in the manufacture of microneedle fabrication [353]. When incorporated into a microneedle formulation PVA does not act as a plasticiser directly with the polymer that it is mixed with but instead act as a carrier in which it retains some water molecules. Indeed, water was used as a solvent to dissolve the polymers during for the casting and micromoulding stage. However, upon drying not all of these water molecules are completely removed as some are retained in the amorphous region of the PVA structure [354]. These water molecules form hydrogen bonds with the hydroxyl group of PVA and the hydrogen bond forming groups of other incorporated hydrophilic polymers, forming a structural water layer. In this instance, the remaining water molecules, which are retained in the presence of PVA, behave as an internal plasticiser thus reducing the brittleness of the needle layer during the demoulding stage and handling post-manufacture.

The mechanical properties of the fabricated microneedles formulation were determined using a texture analyser. The polymeric microneedle arrays were subjected to an axial compression test to measure the fracture force of the polymeric microneedles. From the microneedle fracture test as shown in Figure 5-2, the PVPVA based microneedle formulations, which were manufactured from the commercial polymer Kollidon® VA 64, displayed the lowest fracture force out of all the eight formulations evaluated. Nevertheless it has been highlighted that on average, a microneedle ought to display a fracture force of approximately 0.098 N/needle in order for the needle to display effective insertion into the skin without fracturing [129,130]. The superior fracture force from the microneedle patches fabricated from pNAM, pHEAM and pAMPS may be attributed to the higher molecular weight of the polymer used in making the microneedle patches relative to the PVPVA microneedles as it has been shown that polymers with higher molecular weight display a greater tensile strength relative to lower molecular weight polymers [355]. Secondly, such enhanced fracture force can be attributed to the additive added during the microneedle manufacturing stage. In the case of pNAM, pHEAM and pAMPS microneedles, PVA was added into the microneedle formulation to provide some degree of

plasticisation in order to mitigate microneedle fracture during the demoulding stage. However, there is a possibility for pNAM, pHEAM and pAMPS polymers to form polymer-polymer interactions with the high molecular weight PVA polymer (20kDa) via hydrogen bonding and chain entanglement within the microneedle. Such supramolecular interaction between polymers have been shown by Lamm *et al.* to significantly improve the tensile strength of polymers resulting in stronger microneedles [356,357]. In the case of pAMPS, these interactions were further reinforced by the presence of ionic hydrogen bonding between the charged sulfonic acid group on the polymer pendant with the oxygen group on the PVA polymer which resulted in pAMPS formulation displaying the highest tensile strength. In contrast, the addition of PEG 400, which with a lower molecular weight, was insufficient to cause any polymer-polymer entanglement in the PVPVA microneedles. Instead, the PEG 400 molecule would embed itself as an external plasticiser between the PVPVA polymer chain giving enhanced free polymer volume and thus weakening the polymer-polymer interaction that ultimately results in a weaker overall microneedle fracture force [358].

5.5.3 Microneedle insertion characterisation

It is of great importance that the microneedle fracture test is coupled with insertion studies to evaluate the penetration capability of the fabricated microneedle patches. The insertion of the microneedle patches into a stack of Parafilm® layers was used as an *in vitro* skin model. This was performed by applying the microneedle patches onto the Parafilm® stacks under thumb pressure. Upon application, respective Parafilm® layers were separated and observed using an optical microscope to evaluate the pore uniformity as a function of penetration depth. It can be seen from Figure 5-3 **(a)-(b)** that the number of microneedle channels generated decreased as a function of Parafilm® layer number with pyramidal microneedles displaying greater insertion relative to obelisk microneedles. This observation may be attributed to the surface area of different microneedle designs that are in contact with the Parafilm® layers during insertion, with the pyramidal design having a smaller surface area (0.6 mm^2 per needle) of contact relative to the obelisk design (0.9 mm^2 per needle). Therefore, the obelisk design will experience more effective frictional force relative to the

pyramidal design resulting in a lower insertion profile into the Parafilm® layers. In addition, it was clear that for all the formulation evaluated, complete microneedle insertion was observed in the first Parafilm® layer as shown in Figure 5-3 **(a)-(b)**. Collectively, the fracture force data from Figure 5-2 **(e)** along with the insertion profile from Figure 5-3 **(a)-(b)** would suggest that all of the microneedle patches fabricated were capable breaching the *stratum corneum* permitting microneedle insertion into the skin.

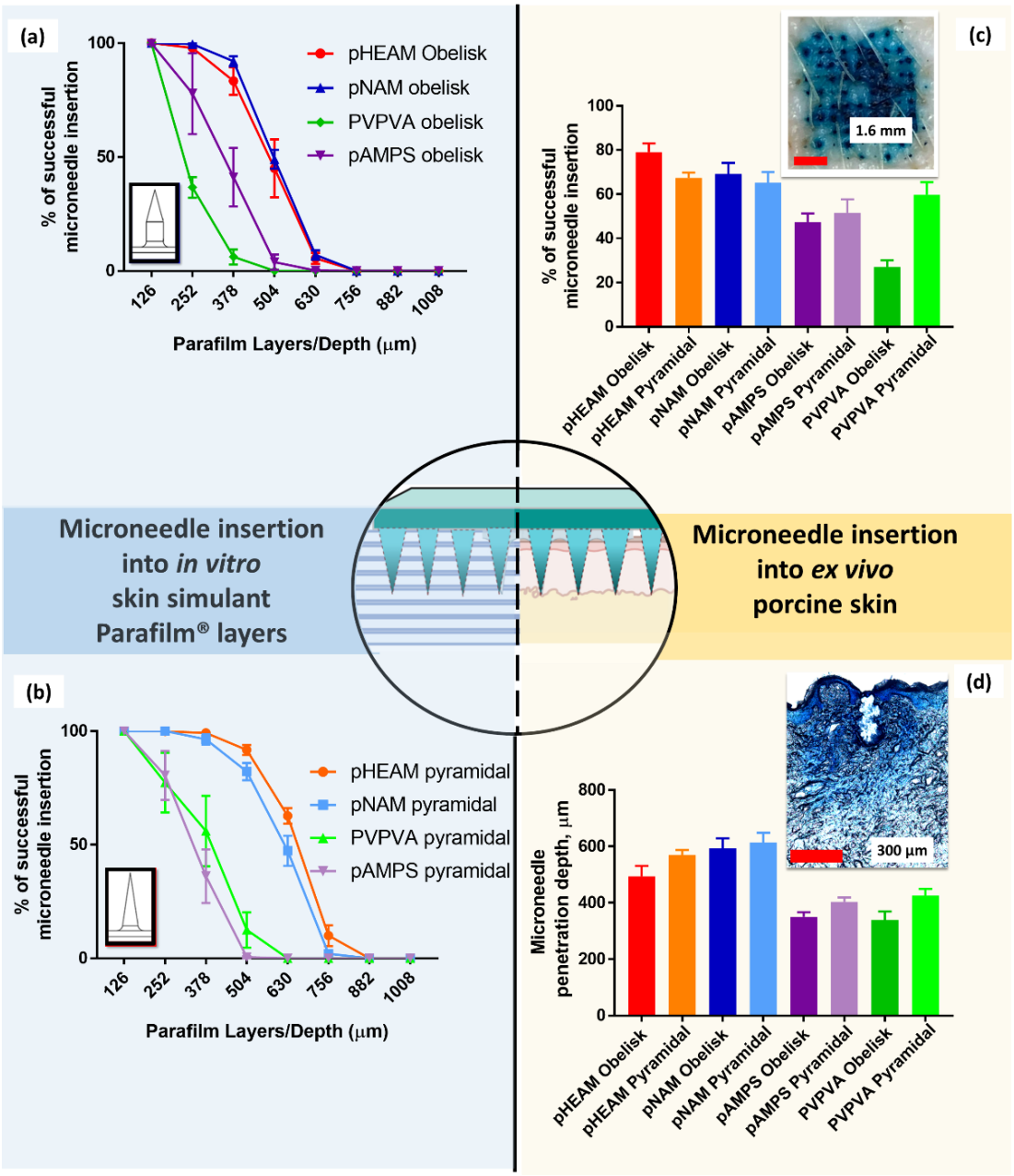

Figure 5-3 Insertion profile of different polymeric microneedle formulations into Parafilm® layers for microneedles with (a)obelisk design and (b) pyramidal design. (c) Percentage of successful microneedle insertion for different microneedle formulation into ex vivo porcine flank skin. Inset shows an example of an ex vivo porcine skin treated with methylene blue loaded polymeric microneedles (d) Microneedle penetration depth for different microneedle formulation into ex vivo porcine flank skin. Inset shows an example of an optical microscopy image of microneedle channels created when the skin is treated with polymeric microneedle patches. Data are expressed as mean ± SEM for n = 6.

The Parafilm® insertion experiment was then complemented with dye release study in order to evaluate the ability of the microneedle patches to puncture actual skin tissue *ex vivo*. Methylene blue loaded microneedle patches were administered onto porcine cadaver skin, which upon application resulted in the release of the hydrophilic dye into the surrounding skin tissue upon polymer dissolution. This ultimately resulted in the formation of blue pores within the porcine skin that followed the distribution of microneedles on the patch as shown in Figure 5-3 **(c).**

However, when the number of microneedles generated in the skin from the application of methylene blue loaded microneedles was evaluated, we observed that the number of channels in the skin was much lower than that observed from the Parafilm® insertion study. Such discrepancy in results suggests that the although the *in vitro* test developed by Larraneta *et al*. is useful in providing early estimation data of microneedle insertion, the test indeed has some limitations when the insertion data is translated into *ex vivo* skin tissues. This may be explained by the fact that Parafilm M® exhibits irreversible plastic deformation when stretched or compressed, thus providing a lower resistance to microneedle insertion [259]. In contrast, the skin is an elastic biological tissue that returns to its normal state under mild stretching or compression thus conferring greater level of resistance to microneedle insertion relative to the Parafilm® layers.

From Figure 5-3 **(c)** it was apparent that all microneedle formulations were unable to generate 100 % microneedle channels into the *ex* vivo porcine tissue. Such observations whereby incomplete insertion of all needles from microneedle patches has been observed previously by other researchers [359,360].

This observation can be attributed to the "bed of nail" effect, a situation where the force experienced by each microneedle is less than the overall force applied to the microneedle patch due to force redistribution between the needles [143]. When the fracture force of the microneedles was evaluated using the texture analyser it was assumed that the fracture force recorded was evenly distributed between needles. This assumption may not be the case when the patch is applied to the skin *ex vivo* or *in vivo* under thumb pressure as it has been shown in the work by Vicente-pérez *et al.* that force distribution across a microneedle patch as visualised via pressure-indicating sensor film was not entirely uniform, giving rise to heterogenous force redistribution [309]. This may lead to the situation where only some microneedles on the patch experience sufficient force to pierce the skin leading to poor insertion efficiency. In the case of PVPVA microneedles, the introduction of PEG 400 already resulted in mechanically weaker microneedles, which combined with the phenomenon of heterogenous force redistribution under manual application resulted in poor insertion efficiency especially with the obelisk design. In the case of pAMPS microneedles, although the polymer displayed a high fracture force, the poor insertion properties of this formulation was attributed to the brittleness of the pAMPS polymer. This is because the polymer is far below its T_g relative to the other polymers making it brittle and prone to fracture during needle insertion. In addition, the brittle nature of pAMPS have been reported by other researcher as well [361].

Although the Parafilm® insertion study is a poor predictor of the number of microneedle channels in *ex vivo* skin tissues, comparison between the penetration depth from the Parafilm® insertion data and *ex vivo* porcine skin insertion data suggested that the penetration depths of the microneedles were of approximately the same depth. This does suggest that the skin simulant, Parafilm® may have some value as an *in vitro* surrogate in estimating the penetration depth of the microneedle when *ex vivo* skin tissues are scarce. It worth noting from Figure 5-3 **(d)** that microneedles fabricated from pNAM polymer with either pyramidal or obelisk design resulted in the deepest microneedle insertion into the *ex vivo* skin with an insertion depth of approximately ≈ 600 µm.

Branski *et al.* have reported that the average thickness of the porcine epidermal layer varies between 30-140 µm [260]. It can be seen from Figure 5-3 **(d)** that all the microneedle formulations evaluated resulted in insertion depths that were greater than 200 µm, suggesting that all the formulations evaluated would reach the dermis. In comparison, the human skin is reported to have an epidermal thickness of around 70-150 µm for thin skin (face, eye lids, neck and arm); regions where BCC mainly manifests [310,311]. Therefore, it can be postulated that application of these microneedle patches would provide the insertion depth needed to bypass the epidermis and reach the dermis, the target site for the treatment of nodular BCC.

5.5.4 Chemical imaging and characterisation of microneedle via ToF-SIMS

ToF-SIMS analysis was conducted on the fabricated microneedles of different designs and chemistry in order visualise the chemical composition and distribution of imiquimod and the polymer used in fabricating the microneedles. It is apparent from Figure 5-4 that the micromoulding strategy using the drug polymer blend to fabricate the polymeric microneedles resulted in the formation of homogenous microneedles in terms of polymer and drug distribution. It can be observed that the choice of the polymers used, this case PVPVA, pNAM, pHEAM and pAMPS, did not result in any observable differences in the distribution of the drug or polymer along the microneedle length. Furthermore, this form of analysis provides a method of validating visually that both the drug and the polymer has been successfully loaded into the microneedle structure.

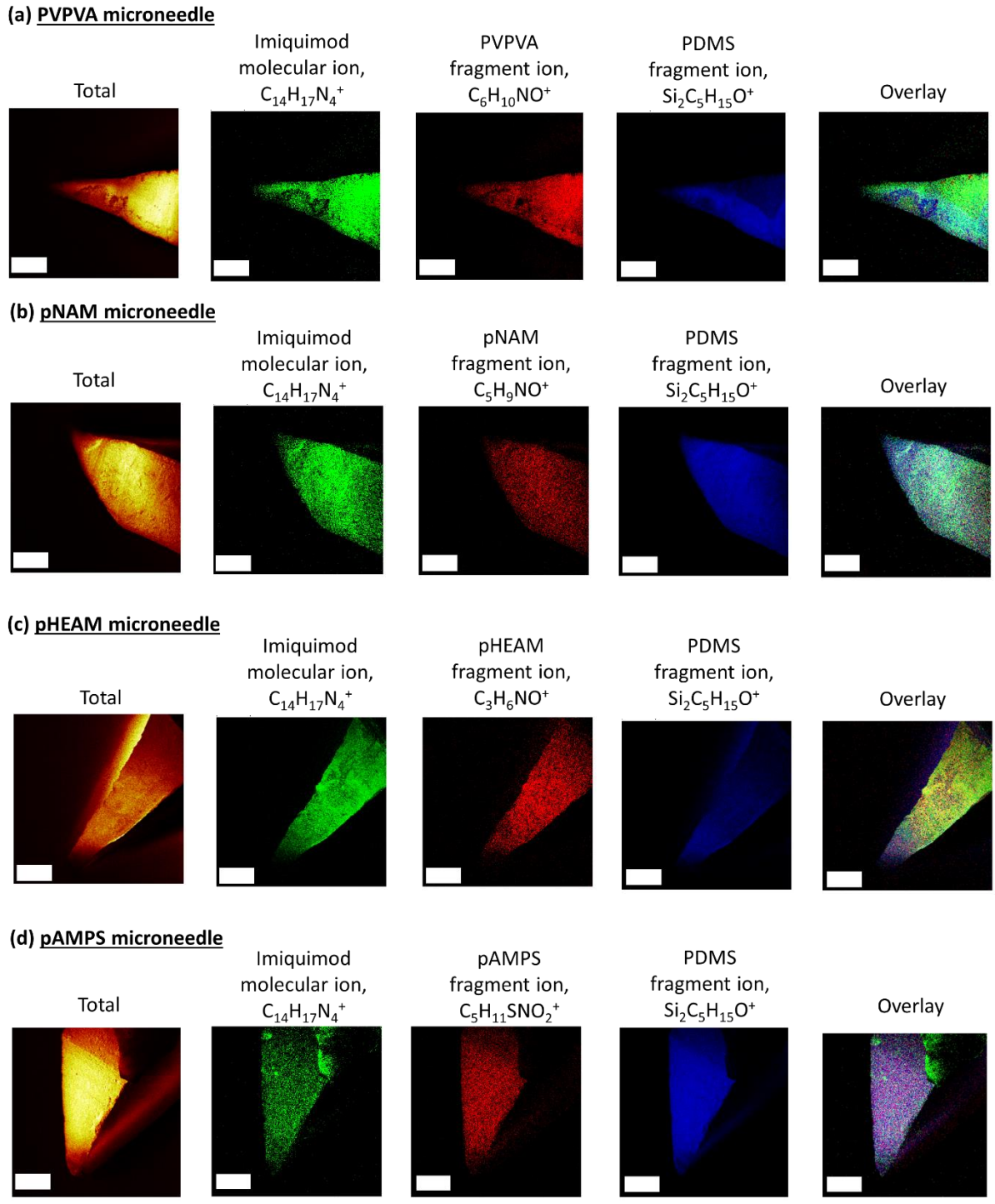

Figure 5-4 ToF-SIMS secondary ion image of imiquimod loaded microneedle of different polymeric chemistries showing the total ion images collected along with the respective ions used to track the presence of the drug, polymer and PDMS contaminant. $C_{14}H_{17}N_4^+$ indicated in green is the molecular ion for imiquimod. Indicated in red are the respective fragment ion for the different polymers used to fabricate the microneedle. $Si_2C_5H_{15}O^+$ indicated

in blue is the fragment ion for PDMS. Overlay images highlight the homogenous distribution of drug and polymer along the microneedle length for respective formulation.

Conventionally, dyes such as fluorescence isothiocyanate and Nile-red are frequently utilised either through conjugating with the payload or as a surrogate to the payload in order to gauge if the therapeutic has been successfully incorporated into microneedles [127,362]. This provides some degree of information on the spatial localisation of the therapeutic along the microneedles, but this approach introduces an additional step of conjugating the delivered therapeutic with the dye prior to microneedle fabrication. The conjugation process in some respects also presents the need of purifying the conjugated payload post synthesis, which can be time consuming. Furthermore, the use of these dyes also introduces the requirement of conducting these experiments in the absence of light to avoid photobleaching of the incorporated dye [363]. In addition, this approach only provides detail on the spatial localisation of the therapeutic along the needle but does not provide any visual information regarding the distribution of the other components of the microneedles, such as the polymer used, as well as the presence of potential contaminants arising from the fabrication process.

In order to obviate the limitation of this conventional approach, it has been demonstrated that mass spectrometry imaging using ToF-SIMS may serve as an alternative method to visualise the distribution of both drugs and polymer along the microneedle in a label free fashion. It was demonstrated for the first time as seen in Figure 5-4 that the conventional process of producing microneedles using PDMS moulds resulted in the deposition of PDMS on the microneedle itself. This was achieved by tracking the fragment ion, $Si_2C_5H_{15}O^+$ which is specific to PDMS. Nevertheless, such contamination is only superficial and is limited to the surface of the microneedle because it was shown that upon sputtering the microneedles with Ar_{1500} gas cluster ion beam to remove the first few nanometers of the microneedle surface of the microneedle there was no longer any PDMS signals observed within the microneedle as seen in Figure S5- 4**.**

This observation may be attributed to the leaching of the PDMS oligomers from the mould into the microneedle formulation when the drug polymer blends were casted into the moulds during production. PDMS is one of the most widely used synthetic polymers in daily life, ranging from household appliances to cosmetics and medical devices. Therefore, leaching and release of PDMS oligomer is not uncommon. For instance, Gross using direct analysis in real time-mass spectrometry (DART-MS) detected the release of low to medium molecular weight oligomers from PDMS based appliances used on a daily basis [364]. Similarly, Carter *et al.* have also reported the leaching of uncrosslinked PDMS oligomer from PDMS chips into microfluidic channels used in growing cells for organ-on-chip research. Such observations were attributed to the incomplete curing of the PDMS oligomers during microfluidic chip production [365]. From a patient perspective, the presence of PDMS on the microneedle formulation may be lead concerns regarding the health risks associated with the deposition of the PDMS oligomer into the skin. Such an issue would be exacerbated if the microneedle formulations are used in delivery of the therapeutic for the management of long-term conditions such as cardiovascular diseases and diabetes. However, in the case of the BCC the management of the disease is usually short term which mitigates the likelihood of PDMS accumulation in the skin. Furthermore, the wide spread use of PDMS in the biomedical field owing to its good biocompatibility further reduces the concern associated with superficial PDMS contamination on the microneedle surface [366].

5.5.5 Drug release study from microneedles into *ex vivo* porcine skin

In the present work, the delivery of imiquimod from different microneedle patches into and across the skin was evaluated in comparison to the commercial imiquimod cream, Aldara™. In order to gauge the delivery of imiquimod into and across the skin, *in vitro* permeation studies utilising Franz diffusion cells were carried out. Imiquimod was loaded into the microneedles by dissolving both the polymer and the drug along with the selected additive to form a polymer blend before casting the mixture into the PDMS micromoulds, followed by centrifugation and drying.

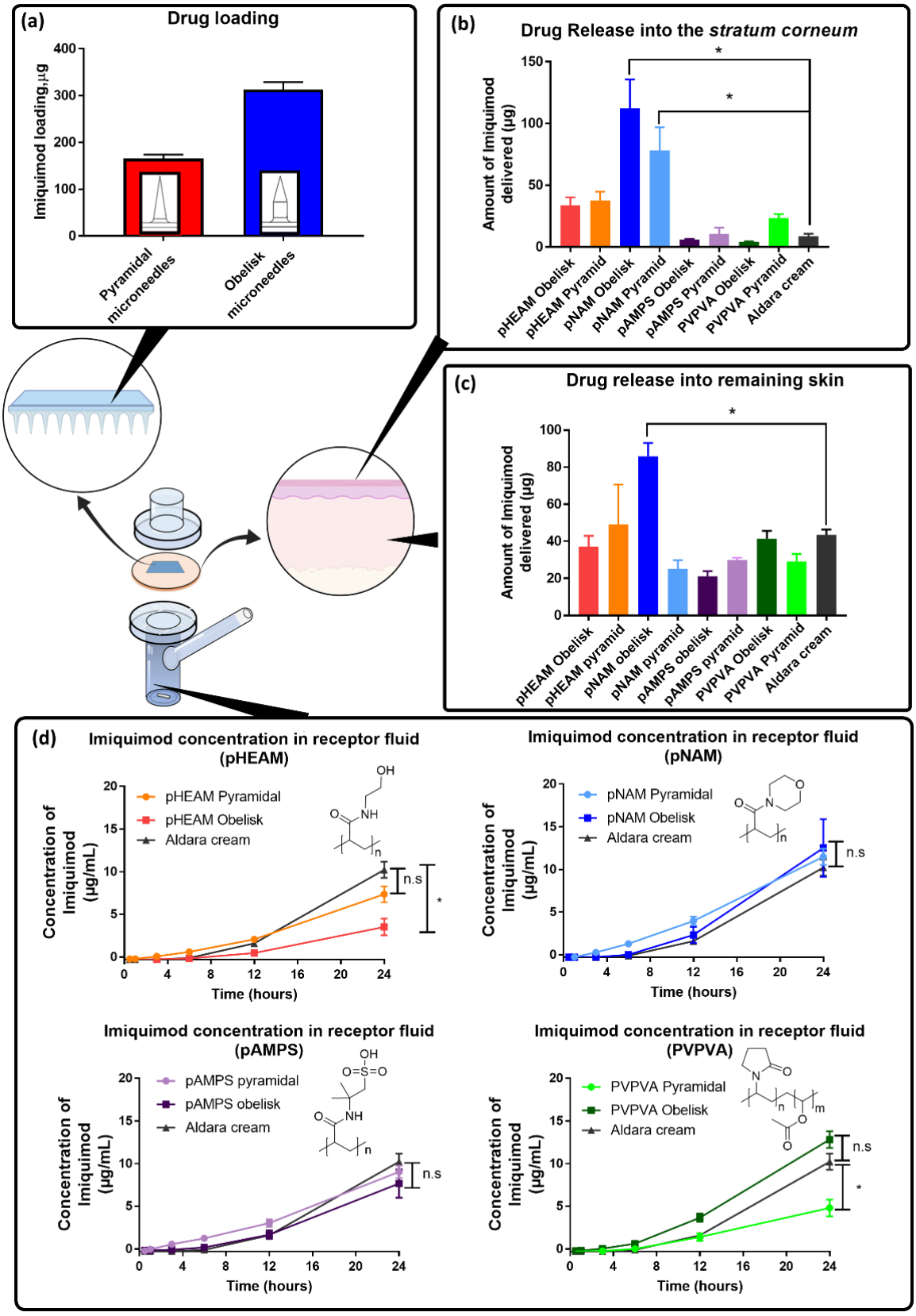

Figure 5-5(a) Drug loading from microneedle patches of different designs-obelisk and pyramidal (mean ± SD, n=8). (b) Amount of drug extracted from stratum corneum obtained from pool tape strips analysis

via HPLC after 24 h permeation study. (c) Amount of drug extracted from remaining skin obtained via HPLC analysis after 24 h permeation study. (d) Drug concentration within receptor fluid as a function of time during permeation study from Aldara™ and imiquimod loaded polymeric microneedles. Data are expressed as mean ± SEM for n = 6. Differences were calculated using one- way ANOVA, followed by Tukey's post hoc test, and deemed significant at $p < 0.05$

From Figure 5-5 **(a)** it is clear that by changing the design of the microneedle from pyramidal to obelisk while casting the same concentration of drug solution, it was possible to increase the drug loading from 150 µg to 300 µg. This is attributed to the volume of the moulds used in fabricating the microneedles. The obelisk microneedle mould has a total of 6 mm^3 mould volume for the needle layer which is twice the mould volume of the pyramidal microneedle mould. Upon skin application imiquimod-loaded polymeric microneedles dissolved in the limited volume of the skin's interstitial fluid to release drug into and across the skin layer. It was apparent that all the formulations evaluated were capable of delivering imiquimod into the *stratum corneum*, remaining skin and into the receptor fluid as shown in Figure 5-5 **(b)-(d)**. The delivery of imiquimod into the *stratum corneum* and remaining skin was statistically similar to that Aldara™ cream for the PVPVA, pHEAM and pAMPS microneedle ($p > 0.05$). By comparing the result from Figure 5-3 **(c)** and Figure 5-5 **(b)-(c)** it is possible to conclude that although PVPVA and pAMPS microneedles resulted in poor insertion efficiency in *ex vivo* skin tissue, the number of microneedles that managed to puncture and dissolved in the skin still resulted similar delivery of imiquimod relative to commercial cream Aldara™ despite the patches having a lower drug loading than the 1000 µg of imiquimod administered from the 20 mg of Aldara™ cream.

On the other hand, it was apparent that both the obelisk and pyramidal designs for imiquimod loaded pNAM microneedle patches resulted in the greatest amount of drug delivered into the *stratum corneum* and while only the obelisk design resulted in the greatest delivery into remaining skin. The differences in the amount of imiquimod delivered into the *stratum corneum* by both types of pNAM microneedles were of statistical significance ($p<0.05$) when compared to Aldara™ cream. In contrast,

both designs for the pHEAM microneedles delivered a statistically similar amount of the drug into the *stratum corneum* and remaining skin when compared to Aldara™ cream, despite displaying similar insertion efficiency to pNAM microneedles. This may be attributed molecular weight of the pHEAM polymer as shown in Table 5-3 which is twice the molecular weight of pNAM, which could result in slower polymer dissolution over 24 hours relative to pNAM, resulting in incomplete imiquimod release from the microneedle patch.

It is also worth noting that the amount of imiquimod administered from the pNAM obelisk microneedle patch was 300 µg. The dose of imiquimod administered from this microneedle patch was much lower than the 1000 µg of imiquimod administered from the 20 mg of Aldara cream (5% w/w) that was applied to the skin area of 3.8 cm^2, in the Franz cell, which is based on a clinical dose for Aldara™ cream for the treatment of BCC [314]. Although the amount imiquimod administered was approximately three folds lower than the clinical dose of Aldara™ cream, the amount of imiquimod that was delivered into both the *stratum corneum* and remaining skin was significantly higher with the pNAM obelisk microneedles relative to Aldara™ cream ($p < 0.05$).

Such enhanced permeation into the *stratum corneum* by both obelisk and pyramidal pNAM microneedles may also be attributed to the behaviour of the polymer upon interacting with the interstitial fluid in the skin. It has been highlighted that the microneedle channels that are formed within the *stratum corneum* during polymeric microneedle application behave as focal points for imiquimod to permeate laterally and to localise in the surrounding corneocytes, thus enhancing delivery to the upper layer of the skin [332]. However, unlike the other polymers used in fabricating microneedles, pNAM has been shown to form a physical hydrogel that swells and doubles in size when the polymer comes into contact with fluid before undergoing dissolution [367]. The swelling of the pNAM polymer upon microneedle application was due to the formation of a physical hydrogel, resulting in enlargement of the microneedle channels. This ultimately results in larger focal points for

imiquimod to radiate laterally towards surrounding corneocytes, thereby enhancing the delivery of imiquimod into the *stratum corneum*.

Such enhanced delivery to the skin surface maybe of great benefit in managing superficial BCC. However, in the management of nodular BCC the microneedle patch must also demonstrate the ability to permeate imiquimod beyond the *stratum corneum* and deeper into the skin [34]. It was apparent that only pNAM obelisk microneedles resulted in the highest delivery of imiquimod into the remaining skin with such difference being statistically significant relative to the commercial control, Aldara™ ($p>0.05$). The observed enhanced delivery of imiquimod into the remaining skin may be attributed to the combinatorial effect of a higher drug loading with obelisk design relative to the pyramidal design coupled with the swelling behaviour of pNAM upon contact with interstitial fluid during microneedle application. The reliance on the swelling behaviour of pNAM alone in enhancing the delivery of imiquimod from the microneedle systems in this case was insufficient for enhancing the delivery of the drug into the remaining skin. This was exemplified by the amount drug delivered with the pNAM pyramidal microneedle, which was not greater than that delivered by Aldara™ cream.

Figure 5-5 **(d)** shows the concentration of imiquimod detected in the receptor fluid over time for different microneedle formulation relative to Aldara™. It can be seen that the concentration of imiquimod in the receptor fluid over time for most microneedle formulations were either statistically similar or lower when compared to Aldara™ over the course of 24 hours. This highlights that over the course of 24 hours, the microneedle patch resulted in either similar or even less (e.g., pHEAM obelisk and PVPVA pyramidal) imiquimod delivery across the skin while delivering a similar quantity of the drug into the remaining skin. However, in the case of pNAM similar imiquimod delivery into the receptor fluid was observed relative to Aldara™ cream, despite the greater intradermal delivery into the skin. It is understood that the amount of drug detected in receptor fluid following Franz cell permeation studies are sometimes used to gauge the likelihood of systemic exposure following formulation administration to the skin [1]. Hence, it could be estimated that the likelihood for systemic

exposure to imiquimod following microneedle treatment is similar when compared to clinical dose of Aldara™ cream application. This suggests that should a patient with nodular BCC receive imiquimod loaded pNAM obelisk microneedle patches, the formulation will provide a simple application strategy to enhance the intradermal delivery of the drug into the skin. However, the likelihood of undesirable side effects associated with imiquimod systemic exposure from these patches will not be any greater than that associated with Aldara™ cream application.

In addition, it is worth discussing the effect of drug partitioning from the delivery systems into *ex vivo* porcine skin as this may affect the overall drug distribution following the permeation study. Indeed, the permeation of drug molecules across the skin is essentially a passive diffusion process that is governed by Fick's law of diffusion. During this process drug molecules partition from a region of high drug concentration (i.e., the delivery system) to a region on lower drug concentration (i.e., the skin tissue and the receptor fluid). Generally, the permeation of compounds across the skin are hindered by the lipophilic *stratum corneum* that acts as the main barrier to drug permeation [368]. However, in this study, the barrier function of the *stratum corneum* have been circumvented through the use of polymeric microneedles thus enabling the delivery systems to be embedded directly within the hydrophilic epidermis and dermis. On top of that, it is known that the pH of the skin changes from pH 4.5 at the *stratum corneum* to pH 7-8 within the viable epidermis and dermis [51]. Due to the presences of amine groups on the drug molecule, imiquimod display low solubility at neutral and basic pH. Therefore, this would suggest that imiquimod would have poor solubility within the epidermis and dermis and thus suffer reduced partitioning from the delivery system to the surrounding skin tissues.

However, the overall process is far more complex as Wagner *et al* have demonstrated that the buffer solution within the receptor compartment of a Franz cell can permeate upwards into the skin [369]. Thus, it can be postulated that the acetate buffer (pH 3.7) from the receptor compartment may have permeated upwards into the skin resulting in overall reduction in the pH of the epidermis and dermis. This reduction in pH within the epidermis and dermis would increase the solubility of

imiquimod and thus the overall partitioning of the drug into these layers of the skin. On top of that, the partitioning of imiquimod into the acidified epidermis and dermis will also compete with the partitioning of the drug into the aqueous receptor fluid which would ultimately affect the overall distribution of the drug in *ex vivo* skin tissue.

It has been shown that the colocalisation of polymers with drug molecules may result in molecular interaction between the two species that mitigates the partitioning of the drug molecules into aqueous media [370]. Based on Figure 5-5, it could be hypothesised that presence of pNAM within skin particularly with the obelisk design relative to other polymeric microneedle systems resulted in strong molecular interactions between the polymer and the ionised imiquimod molecules via ionic hydrogen bonds. This interaction between pNAM and imiquimod reduces the propensity of the drug to partition out of the skin and into the aqueous receptor fluid resulting in enhanced drug retention in the skin. Also, it could not be ruled out that there will be some degree of imiquimod repartitioning back from the receptor fluid into the skin. However, as we have confirmed in our previous work that sink conditions were indeed maintained throughout the permeation study [35]. Therefore, it could be postulated that the effect of repartitioning from the receptor fluid into the skin is minimal due to presence of sink condition.

5.5.6 Drug release study in *ex vivo* human BCC tumour

It was apparent that the quantitative results provided by HPLC analysis permitted comparison of the delivery efficiency of different microneedle formulations relative to the commercial control Aldara™ cream. From the HPLC analysis it was apparent that pNAM obelisk microneedles resulted in higher delivery of imiquimod into both the *stratum corneum* and remaining skin while resulting in similar transdermal delivery into the receptor fluid relative to Aldara™ cream. Nevertheless, HPLC does not provide any details on the dermal distribution of imiquimod and excipient from the delivered formulation. Complementary to the quantitative HPLC data, ToF-SIMS analysis of *ex vivo* human BCC

tissues treated with either Aldara™ cream or pNAM obelisk microneedles was conducted in order to evaluate the distribution of imiquimod within diseased tissues.

Due to the discrepancy in healthy and diseased skin tissues, *ex vivo* human BCC tumours excised from patients attending Moh's micrographic surgery were utilised in the permeation study. Such experimental design was selected as this would provide a better representation and estimation of imiquimod permeation into the tumour relative to healthy human or porcine skin. In addition, as there are a limited number of *ex vivo* BCC tumours, pNAM obelisk microneedles that resulted in the greatest delivery of imiquimod into the porcine skin were chosen for the drug release study into the tumour along with Aldara™ cream, which was chosen as a commercial control.

Figure 5-6 shows ToF-SIMS secondary ion images from BCC tumour cross-sections analysed after a 24-hour permeation study. Owing to the parallel detection capabilities of the ToF-SIMS, secondary ions originating from the BCC tumour tissue, pNAM polymer, substrate (glass slide) and imiquimod were detected and analysed. By monitoring the ion peaks from the ToF-SIMS spectra, visualisation of the localisation and distribution of these secondary ions was achieved. The fragment ion originating from phosphatidylcholine, $C_5H_{15}NPO_4^+$ was used to identify the BCC tumour as this fragment ion has been shown by Munem *et al.* and Nilsson *et al.* to be associated with the cancerous part of the BCC tissue [371,372]. In previous work, it has been shown that the permeation of the imiquimod across the skin could be tracked by monitoring the molecular ion $C_{14}H_{17}N_4^+$ [35,68]. By monitoring the fragment ion peak $C_5H_9NO^+$, this enabled the detection of the localisation of the pNAM polymer within the BCC tumour as shown in Figure 5-6. The peak assignment for pNAM was validated by referring to the fragmentation pattern at *m/z* 99 with the reference spectra of pure pNAM on silicon wafer, as shown in the supplementary data (Figure S5- 5).

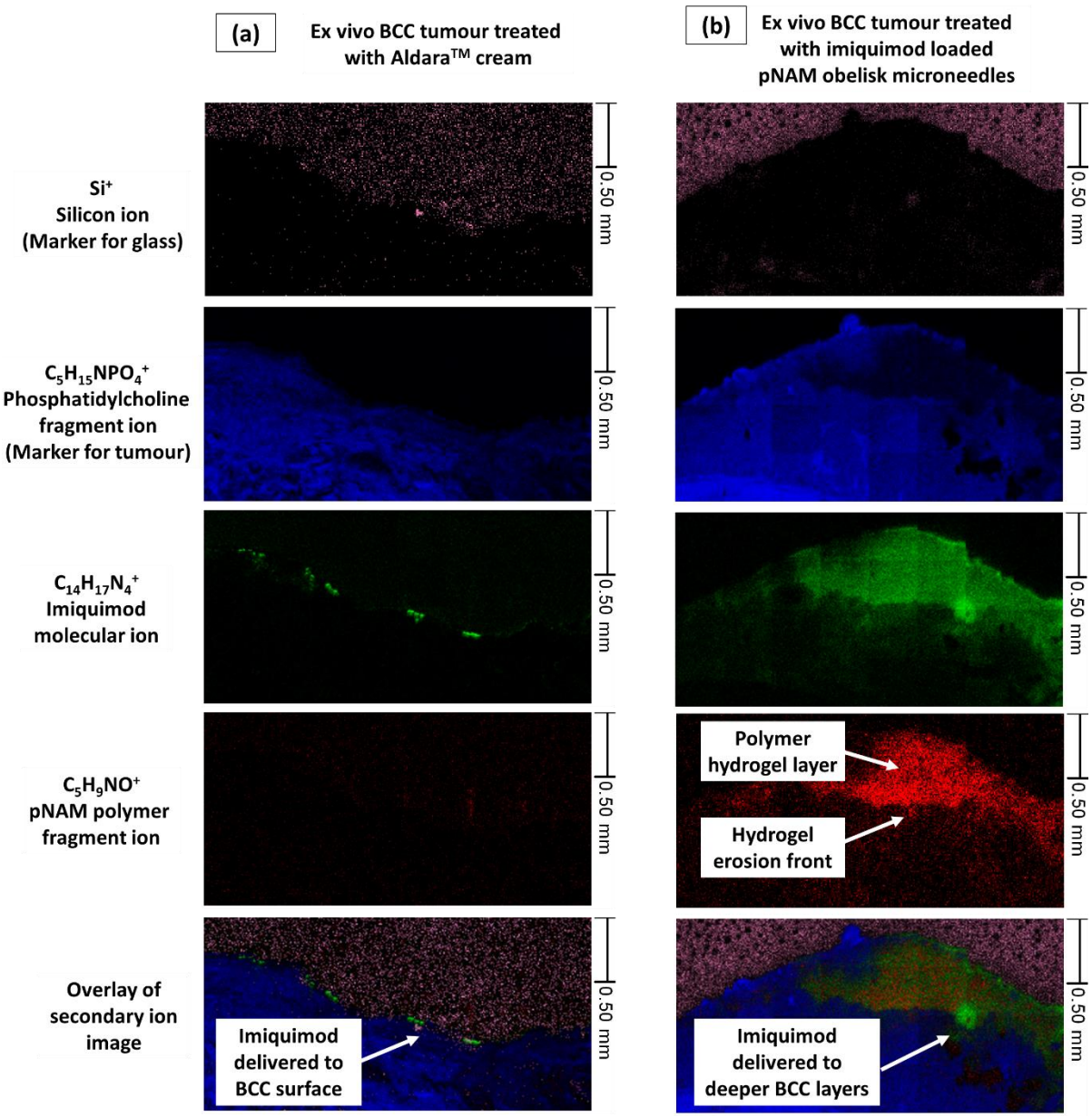

Figure 5-6 ToF-SIMS image of ex vivo human BCC sections from tumour that were treated with (a) Aldara™ cream (5% w/w imiquimod) alone (b) pNAM obelisk microneedles loaded with imiquimod after a 24-hour permeation study. This figure highlights the localisation of dissolved polymer and the release of imiquimod into the tumour when the ex vivo tumour was treated imiquimod loaded microneedles. $C_{14}H_{17}N_4^+$ indicated in green is the molecular ion for imiquimod, $C_5H_{15}NPO_4^+$ indicated in blue is the fragment ion for phosphatidylcholine used to identify the tumour tissue. $C_5H_9NO^+$ indicated in red is the fragment ion pNAM polymer used to polymer within the tumour tissue. Si^+ indicated in pink an inorganic ion of silicon which is used to identify the glass slide (the substrate used to mount the cross-sections). Scale bar: 500 µm.

It is apparent from Figure 5-6 that there is limited availability of imiquimod within deeper BCC layers when the molecule was delivered as a topical cream, Aldara™. However, when imiquimod is delivered as a polymeric microneedle patch, improved delivery of imiquimod into both the upper and deeper layers of the BCC tumour was observed. Such observation is complementary to the HPLC analysis shown Figure 5-5 **(b)-(c)** that highlights greater delivery of imiquimod into the skin surface and remaining skin when the drug is delivered using pNAM obelisk microneedles relative to Aldara™ cream. Typically nodular BCC is much more difficult to treat as the tumour typically manifests from the skin surface and grows downward into the skin, to the depth of 400 µm below the skin surface [34]. The ToF-SIMS analysis of BCC nodular tumour cross-sections from Figure 5-6 suggests that through the application of pNAM obelisk microneedle patch, it was apparent that imiquimod penetrated and permeated into the *ex vivo* BCC tumour the skin to a depth of greater than 600 µm resulting in imiquimod delivery into the deeper layer of the BCC tumour.

In previous work it has been demonstrated for the first time in the microneedle field the capability to simultaneously detect the deposition of both drug and polymer from a dissolving microneedle patch within the skin in a label free manner owing to the parallel detection capability of ToF-SIMS [332]. In the current work, the polymer that is used in fabricating the microneedle patch is pNAM. By monitoring the fragment ion peak at *m/z* 99.04 it was possible to detect the localisation of the polymer within the tumour milieu post application as shown in Figure 5-6. By comparing this finding with the ToF-SIMS analysis of tumour cross-section from samples treated with imiquimod loaded microneedles in Figure 5-6, it was apparent that imiquimod was colocalised in the presence of pNAM polymer within the dermis following skin application. This leaves imiquimod which is embedded in a polymer matrix within the tumour. It was noted that there was more a concentrated layer of pNAM within the upper dermal layer that became progressively dispersed with tumour depth. The more concentrated layer of pNAM within the upper tumour layer was attributed to the formation of pNAM hydrogel within the skin. This is supported by the finding of Gorman *et al.* that showed from their work through the

synthesis of pNAM via photopolymerisation that the polymer behaves as a physical hydrogel, which swells over 120 minutes upon exposure to an aqueous environment [335].

The swelling of the polymer into a physical hydrogel is attributed to the formation of intermolecular interactions between the pNAM polymers as well as the interaction between the polymer and the water molecules as shown in the schematic in Figure 5-7. Upon puncturing the *stratum corneum*, the microneedle is embedded in the water rich dermis. Here the polymeric microneedle begins to absorb water molecules which hydrates the polar hydrophilic acryloylmorpholine group pendant group of pNAM polymers leading to formation of a primary bound water layer. The formation of this primary bound water layer leads to polymer swelling, which exposes the hydrophobic region of the polymer (the backbone), which also interacts with water molecules via Van der Waals forces, which forms the secondary bound water layer leading to further swelling. This ultimately causes additional water molecules to imbibe into the needle structure due to osmosis leading to polymer swelling and dilution. However, the dilution process is opposed by transient physical interactions between the polymer chains leading to an elastic network retraction force [373]. These physical interactions arising from polymer-polymer chain entanglement, hydrogen bonding arising from the nitrogen and oxygen group of the acryloylmorpholine pendant group as well as hydrophobic interactions between the polymer backbones culminates in formation of a physical hydrogels from the pNAM polymers [374].

Evidence that supports the mechanism of swelling of the pNAM polymer was demonstrated by Gorman and co-worker [335]. This was determined by measuring the water absorbance of the polymers over a period of 70 hours. The group discovered that pNAM absorbed water and swells to approximately double its dry weight within two hours upon exposure to excess water. Upon further dilution, the overall weight of the pNAM hydrogel started to decrease which indicate that the hydrogel is slowly undergoing dissolution. Gorman *et al* showed that dissolution curve of the pNAM hydrogel followed a second order exponential decay function with a dissolution rate constant of 0.028 $g^{-1}min^{-1}$ [335]. The second order exponential decay exhibited by the pNAM polymer highlighted

that this class of polymer undergoes chain diffusion and disengagement as the main mechanism for hydrogel erosion as discussed by Chou and Koenig [375]. In addition, evidence for swelling behaviour of pNAM based hydrogel have also been demonstrated by other research group by monitoring the changes in gel weight overtime upon immersion in excess distilled water [376,377].

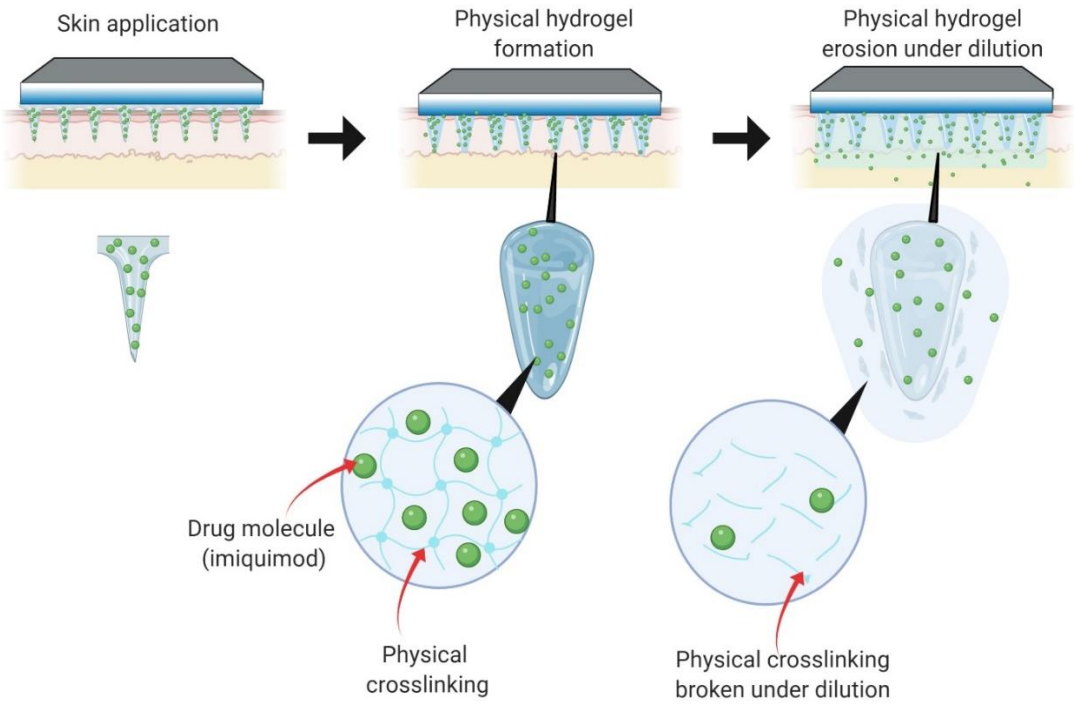

Figure 5-7 Schematic highlighting the mechanism of imiquimod release from pNAM polymeric microneedle. Upon application, the microneedle absorbs interstitial fluid leading to hydrogel formation. However, over time the polymer becomes diluted in the skin leading to hydrogel erosion which causes the release of the drug in the skin. However, the interaction of the drug with the polymer within the skin helps retain the drug intradermally mitigating transdermal release.

However, prolonged exposure to the water rich environment of the dermis weakens these intermolecular interactions between the polymer chains as the individual pNAM polymer begins to form hydrogen bonds with the bulk water molecules within the interstitial fluid. This overall dilution process leads to polymer dissolution via chain disengagement and diffusion which culminates in hydrogel erosion [378,379]. This can be seen in Figure 5-6; the lower layer of the *ex vivo* BCC tumour

treated with imiquimod loaded microneedles displayed lower intensity of $C_5H_9NO^+$ ions which is specific to the pNAM polymer than the upper strata of the tumour highlighting the presence of a hydrogel erosion front. It has been described in the literature that the erosion of polymeric hydrogel matrix is the main mechanism in which hydrophobic drugs are released into an external medium which in this case is the dermal tissue of the BCC tumour [380]. By comparing the signal from the molecular ion for imiquimod, $C_{14}H_{17}N_4^+$ and the signal arising from the fragment ion from pNAM, $C_5H_9NO^+$ we can see some co-localisation of the imiquimod signal with the pNAM hydrogel erosion front. Therefore, in the current work it was demonstrated via ToF-SIMS analysis the existence of a hydrogel forming zone along with hydrogel erosion zone which leads to the release of imiquimod in the BCC tissue by monitoring the ions specific to the pNAM polymer and the drug. The co-localisation of imiquimod in the hydrogel erosion front causes the drug to encounter a region of enhanced viscosity due to the presence of the pNAM polymer within the BCC tissue [72,73]. Such enhanced viscosity, attributed to the presence of polymer chains that have dissolved from the hydrogel layer, retards the permeation of drug molecules across the skin and into the receptor fluid, leading to enhanced localisation within the skin tissue. This may serve as an explanation why the concentration of imiquimod in the receptor fluid as shown in Figure 5-5 **(d)** is statistically similar to that of Aldara™ cream despite the greater intradermal delivery of imiquimod via pNAM obelisk microneedles.

5.5.7 *In vivo* tumour study

It was apparent that imiquimod loaded pNAM obelisk microneedles resulted in enhanced intradermal delivery of the drug into both *ex vivo* porcine skin tissue and *ex vivo* human BCC tumours. Subsequently, the efficacy of the formulation was evaluated in a mouse model for a cutaneous tumour. Prior to the *in vivo* tumour study, a dose tolerability study was conducted by applying drug loaded microneedle patch on healthy mice as shown Figure 5-8 **(a)** that were not challenged with any cutaneous tumour. This was conducted in order to evaluate the tolerability of the imiquimod loaded pNAM microneedle patches and to observe with increasing dose whether the microneedle patch would be tolerated and would not affect the overall health of the mice. It can be seen from

Figure 5-8 **(b)** that the mice suffered a reduction in body weight during the 24-hour microneedle patch application, however such effects were immediately reverse post patch removal. The reduction in body weight was attributed from the observation that the mice found it difficult to consume food and water when their bodies were wrapped with the patch and kinesiology tape. Nevertheless, the ability of the mice to recover to more than their original body weight after being challenged with both 50 µg and 300 µg loaded microneedle patches suggests that the patches were indeed tolerated. This was further corroborated by the observation that the mice did not display any signs of toxicity during the study.

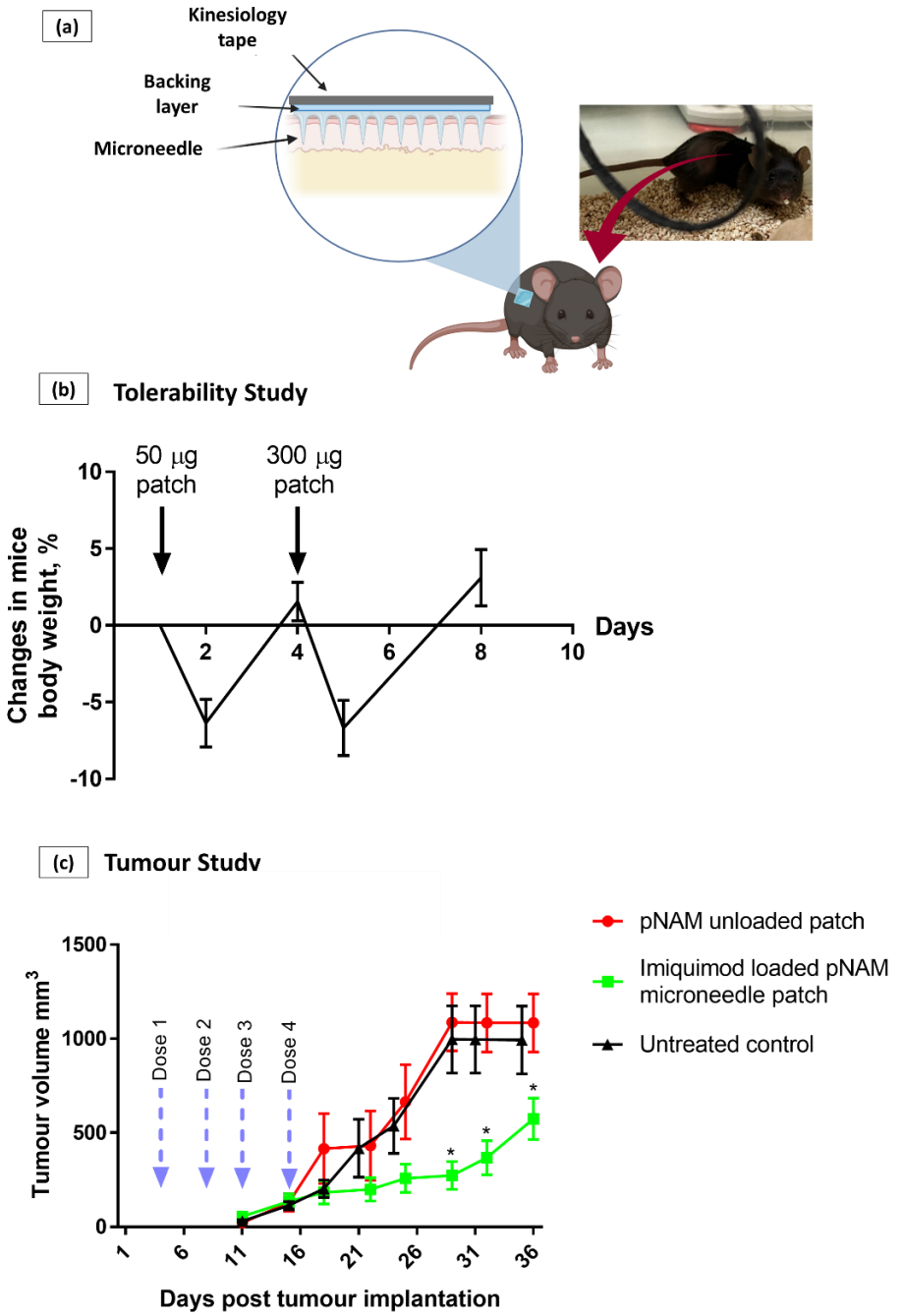

Figure 5-8 (a) schematic highlighting the application on microneedle on a mouse treated with microneedle (b) Changes in mice body weight during dose tolerability study, data are expressed as mean ± SEM, n=3. (c) Changes in tumour volume for respective mice treatment group, data are expressed as mean ± SEM, n=10. Differences were calculated using one- way ANOVA, followed by Tukey's post hoc test, and deemed significant at $p < 0.05$.

Upon conducting the dose tolerability study, the anti-tumour effect of the imiquimod loaded pNAM patches were evaluated *in vivo* using subcutaneous B16F10 melanoma-bearing mice model. This

animal model was chosen as due to the lack of availability of an immunocompetent murine model for BCC. Several groups have attempted to develop a BCC xenograft model in nude mice has been met with very slow tumour uptake and growth [381]. On the other hand, some success have been met when severely immunocompromised mice such as beige-nude or SCID-beige were used [382–384]. However, these immunocompromised models would prove to be unsuitable to screen the efficacy of imiquimod loaded microneedle patch as part of the anti-tumoural activity of imiquimod relies on innate and the adaptive immune responses. Although imiquimod is not approved for melanoma therapy, it was previously shown to display an anti-tumour effect against a melanoma cell line [385,386]. This could be attributed to some mechanistic similarities between the two types of skin tumours through which imiquimod exerts its antitumoural effects. Firstly, imiquimod may induce apoptosis in both type of skin tumours through the activation of CD95 surface death receptors which are present on both BCC and melanoma tumours. Upon binding to the receptor, imiquimod stimulate CD95 receptors to recruit several of proapoptotic factors including caspase-8 to form a death-inducing signalling complex. This complex then initiate a cascade of pro-apoptotic pathways by cleaving various intracellular proteins that culminate in cancer cell apoptosis in both BCC and melanoma cell lines [386,387]. In addition, due to the lipophilic nature of imiquimod, the drug has been proposed to penetrate through the cell membrane and into the cytosol where the drug causes a marked shift of the Bcl-2/Bax-ratio favouring the formation of the pro-apoptotic protein Bax. The Bax protein then translocate to the mitochondria where the protein induces the release of cytochrome *c* into the cytosol leading to the activation of caspase-9. This cascade of reactions then result in the activation of further downstream executioner caspases that culminate in tumour apoptosis in both BCC and melanoma tumours [385,388].

Following tumour implantation, treatments were performed on the melanoma-bearing mice respectively with tumour volume being recorded to compare the antitumoural efficacy between the treatment groups. Mice bearing the melanoma tumour that did not receive any treatment were selected as a negative control. From Figure 5-8 **(c)** it was apparent that there was no statistical difference between untreated control and unloaded pNAM microneedle patch treatment groups

(*p>0.05*). Similar observations have been reported by other researchers who found that the physical application of a microneedle patch alone without the delivery of any anticancer therapeutics did not result in any observable difference to the negative control [66,183]. Collectively, these results suggest that the physical act of applying the patch did not result in any antitumoural effect. From a safety perspective these observations also highlight that the mechanical application of microneedle alone to the tumour is safe and does not exacerbate tumour growth.

In addition, from Figure 5-8 **(c)** it was apparent after four applications of the microneedle patch, no differences in tumour volume were observed, until two weeks after the last dose was applied. However, after two weeks, significant differences in tumour volume were observed between the imiquimod loaded pNAM microneedle patch treatment group and the controls. Coupled with the *in vitro* permeation data, this observation does give strong evidence that the application of imiquimod loaded pNAM microneedles to the tumour site on the mice led to successful release of the drug into the tumour tissue. The reduction in tumour growth in the imiquimod loaded pNAM microneedle is attributed to mode of action of imiquimod which stimulates toll-like receptors 7 (TLR-7) on resident dendritic cells, macrophages and monocytes in the skin leading to cytokine induction which leads to recruitment of plasmacytoid dendritic cells from the blood. In a melanoma mouse model, Drobits *et al.* have shown once these plasmacytoid dendritic cells are recruited to the tumour site, these cells secrete cytolytic molecules which then exert an antitumoural response on the melanoma [389]. The delay in any observable tumour response after the last dose administered may be attributed to the time taken to recruit sufficient number plasmacytoid dendritic cells from the blood to the tumour site.

In term of treatment efficacy, it appears that treatment with imiquimod loaded pNAM microneedles were only capable of slowing down tumour growth but failed to fully eradicate the melanoma. Similar observations have been made by other researchers that utilised a microneedle approach for the delivery of therapeutics into the B16 mouse melanoma tumour model [66,390]. For instance, Pan *et al.*

discovered that the delivery of small interfering RNA that targets the signal transducer and activator of transcription 3 (STAT3), a protein involved in tumour malignancy, using dissolving microneedles were only able to slow down tumour growth instead of complete tumour eradication in B16 mouse melanoma tumour model [184]. Similarly, Ye and co-workers observed that when the immune checkpoint inhibitor, anti-PD1 antibody that is used in the treatment of advanced melanoma was delivered using dissolving microneedles, complete tumour eradication was not achieved but the researchers observed a retardation in tumour growth. Nevertheless, such a delay in tumour growth was far more significant in comparison to mice in the control groups that received no treatment or mice that received treatment via intravenous administration of the anti-PD1 antibody [177]. By comparing the observations from these studies along with results from the current work, this highlights that complete tumour eradication in B16 mouse melanoma tumour model is indeed challenging and is attributed to highly aggressive nature of the tumour which makes complete tumour eradication very challenging [391]. Nevertheless, the retardation in tumour progression does provide an indication that localised intradermal delivery of imiquimod using dissolving polymeric microneedles still provides some level of efficacy in the mice tumour model.

With respect to the type of payload delivered, several groups have utilised and evaluated the effectiveness of different microneedle systems for the delivery of drugs used in BCC treatment. For instance, Jain *et al.* delivered the photosensitizer, 5-aminolevelunic acid, using carboxymethylcellulose coated stainless microneedles into Balb/c mice that were implanted with B-cell lymphoma cells as a skin tumour model. The group discovered that the combination of microneedle-based delivery of the photosensitizer followed with irradiation with red light at 633nm, resulted in significant suppression in tumour growth after 11 days. [175] Although this strategy proved efficacious, the two-step treatment may not be favourable by patients as they will need to attend the dermatology clinic in order to receive the light irradiation step. This additional step would also require the assistance of clinicians in administering the irradiation dose thus adding further cost to the therapy. In contrast, the use of imiquimod loaded pNAM microneedles that only require a one-step application under thumb pressure

would enable patients to self-administer the dose by themselves in the comfort of their home without the need of any healthcare worker. This offers a possibility for a cheaper overall treatment cost relative to the two-step treatment strategy developed by Jain and co-workers.

On the other hand, Naguib *et al.* demonstrated the feasibility of using solid microneedles as a skin pre-treatment via the poke-and-patch strategy to enhance the intradermal delivery of 5-fluorouracil to treat skin tumours. In their *in vivo* work using a mouse model with B16-F10 melanoma tumour, the group showed that topical application of 5-fluorouracil cream on microneedle-perforated skin resulted in significant tumour inhibition relative to the groups that receive no treatment or only 5-FU cream only [66]. When comparing the microneedle systems used by Naguib *et al.* and Jain *et al.*, the use of solid and coated microneedles will pose the issue of dangerous sharp waste disposal after microneedle application, which can be more prominent in poor resource settings. In contrast, this issue is not encountered with the imiquimod loaded pNAM microneedles after application, as the polymeric microneedles will have dissolved after 24 hours, leaving behind the backing layer, thus obviating the issue of sharp injury with needle reinsertion.

5.6 Conclusions

In conclusion, the current work highlights the design, fabrication and evaluation of a series of drug loaded polymeric microneedles of different designs and polymeric chemistries. These microneedle systems were developed as a drug delivery platform for the intradermal delivery of imiquimod for the treatment of nodular BCC. *In vitro* characterisation highlights that these microneedles were capable of breaching the skin down to the depth which nodular BCC typically resides. Permeation studies utilising Franz diffusion cells demonstrated that out of all the formulations developed, imiquimod loaded pNAM obelisk microneedles delivered the highest quantities of imiquimod into the *stratum corneum* and remaining skin relative to the commercial cream Aldara™. This was achieved despite a 3-fold lower drug loading, relative to the current clinical dose of Aldara™ cream used in BCC treatment. This ability of the polymeric microneedle to deliver the drug to the right target site despite

lower drug loading was also demonstrated in a *ex vivo* human BCC tumour. In addition, ToF-SIMS analysis of *ex vivo* human BCC tumour cross-sections highlighted the presence of embedded drug-polymer matrix within tumour, which retains the drug within the tumour while reducing the permeation of the drug across the skin. Lastly, the *in vivo* tumour efficacy study using a mouse model for skin tumours highlighted that the microneedle was capable of delivering the drug into the tumour, resulting in a retardation in tumour growth. In summary, this work suggests that the drug loaded pNAM obelisk polymeric microneedles developed in this work may be of clinical utility for localised intradermal delivery of imiquimod. Such formulations may provide a less invasive intervention to patients who would prefer an alternative treatment to surgery for the treatment of nodular BCC.

5.7 Supplementary Figures

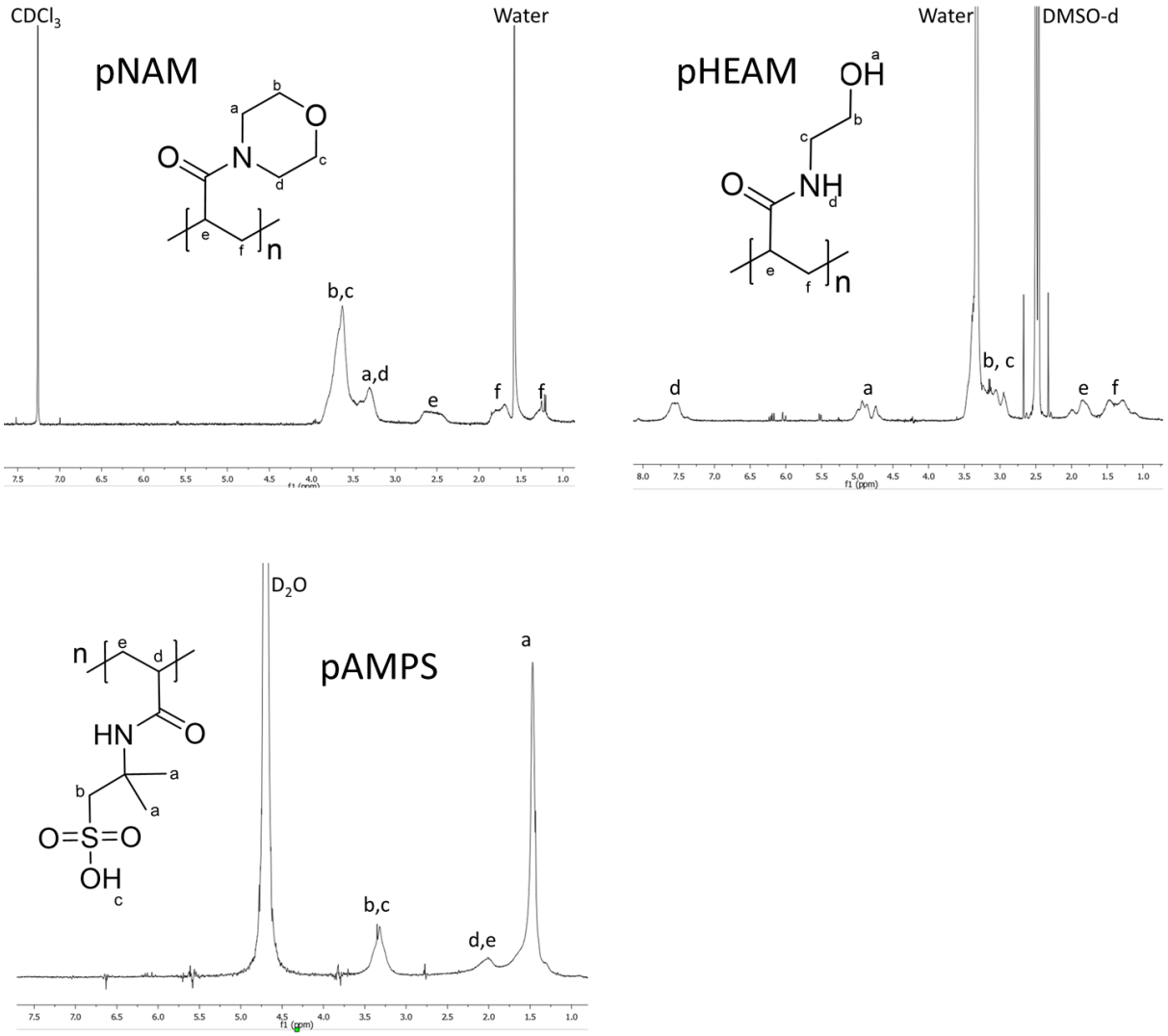

Figure S5- 1 ^{1}H NMR spectra for the respective polymer synthesised-pNAM, pHEAM and pAMPS

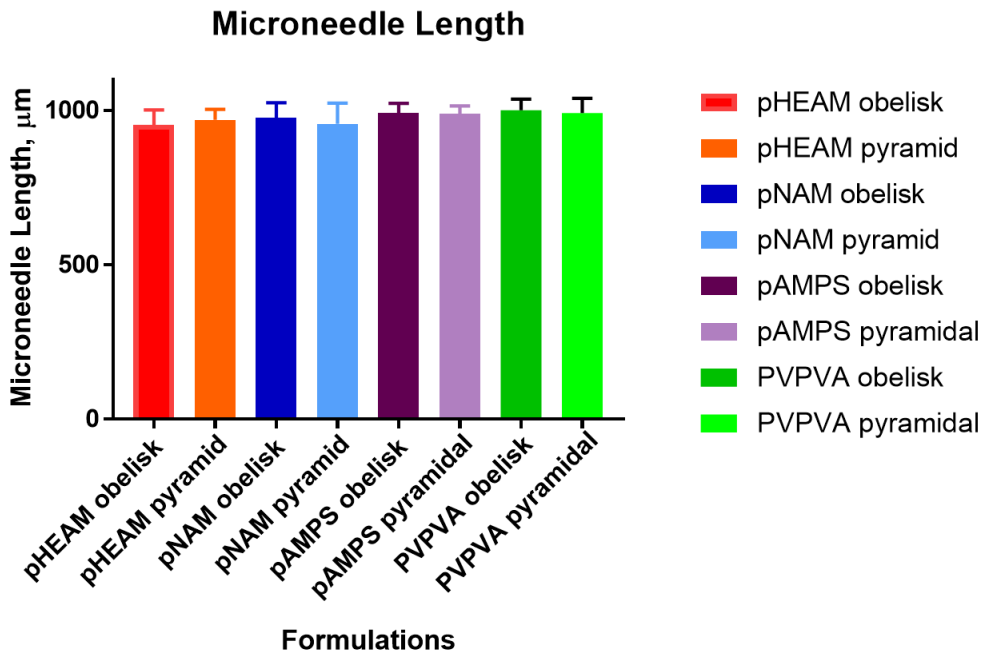

Figure S5- 2 Microneedle length for all microneedle formulation fabricated. Data is expressed as mean ± SD, n=10.

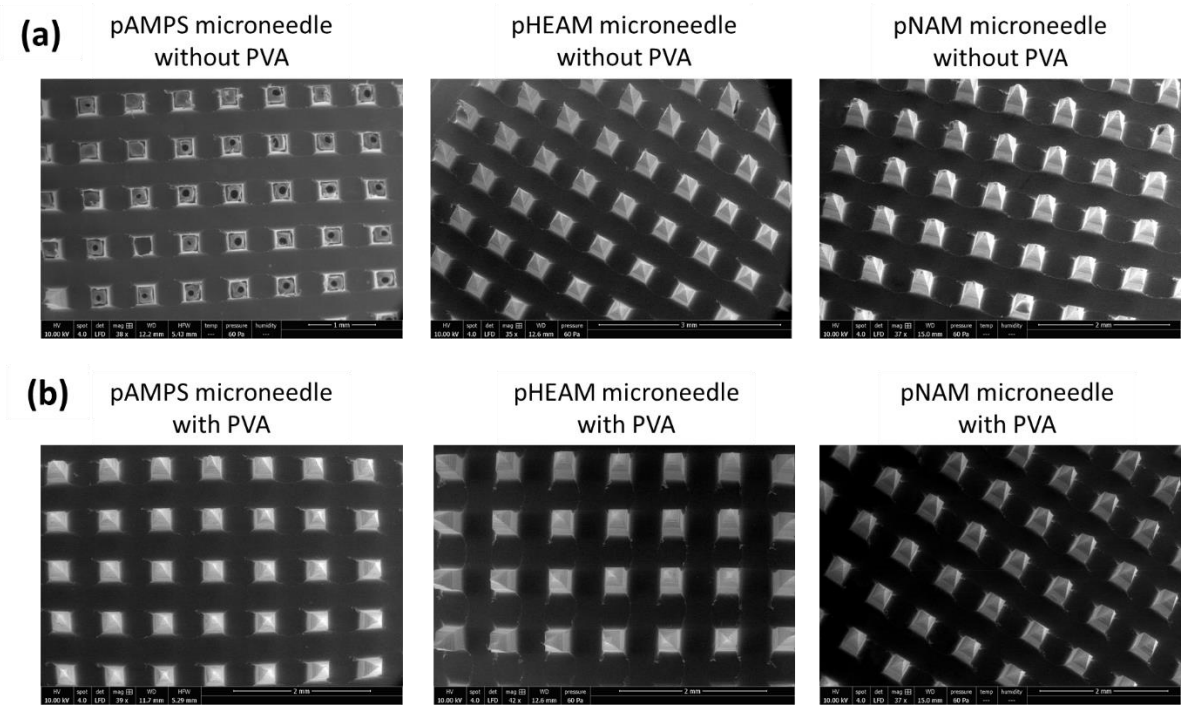

Figure S5- 3 (a) Respective polymeric microneedle fabricated without polyvinyl alcohol (PVA) resulting in microneedles with fractured tips post demoulding. (b) Optimised microneedle formulation via the addition of polyvinyl alcohol (PVA)

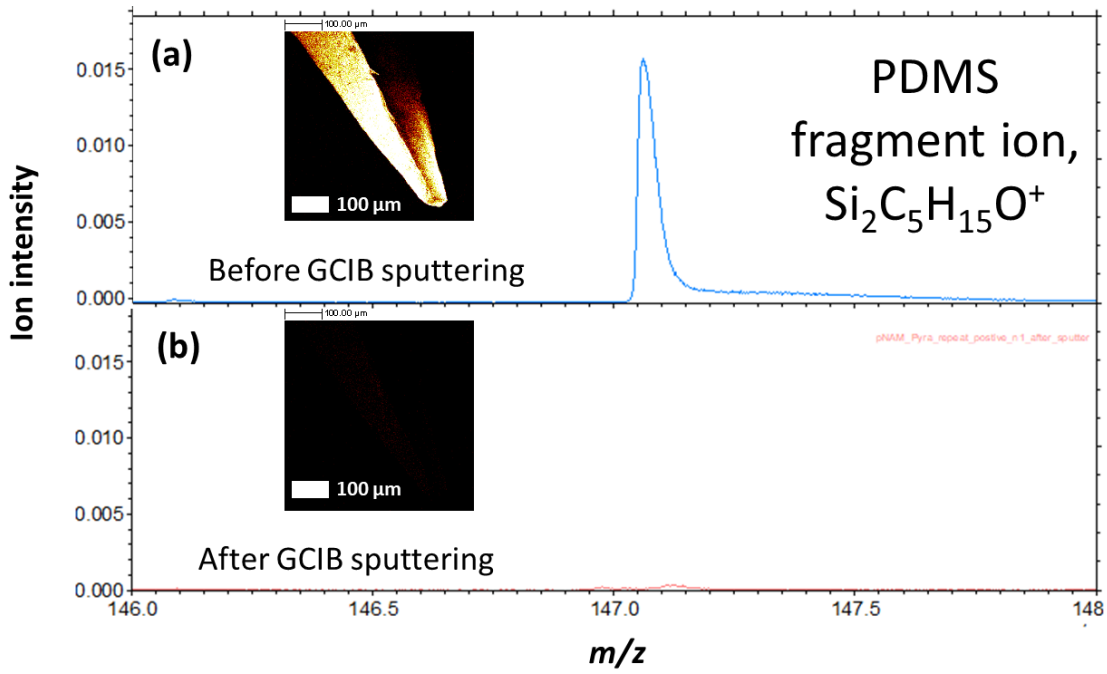

Figure S5- 4 Overlaid ToF-SIMS spectra of (a) pNAM microneedle before sputtering highlighting the presence of $Si_2C_5H_{15}O^+$ as a contaminant on the microneedle(b) pNAM microneedle after sputtering highlighting the absence of $Si_2C_5H_{15}O^+$ thus indicating that PDMS contamination was only localised on the microneedle surface.

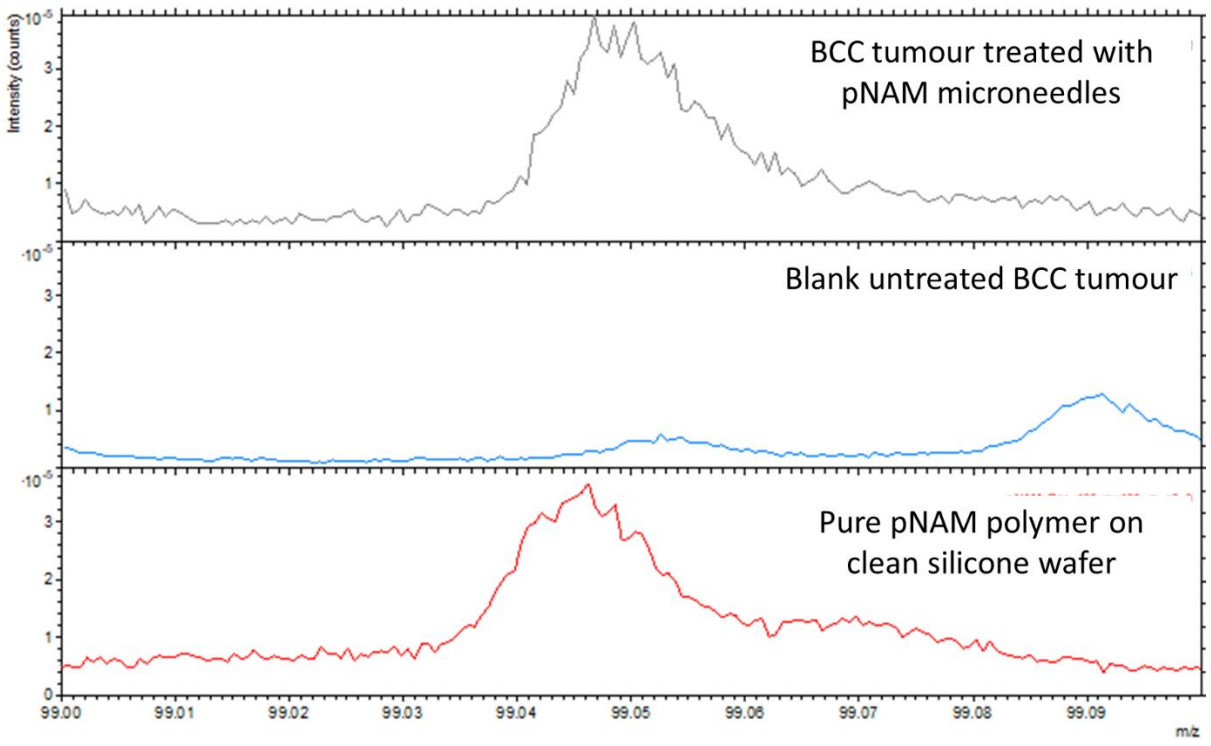

Figure S5- 5 Overlaid ToF-SIMS spectra of (a) BCC tumour treated with pNAM polymeric microneedles (b) blank untreated BCC tumour (c) pure pNAM reference, showing the fragment peak of pNAM ($C_5H_9NO^+$) at m/z = 99 as suitable marker to track the dermal distribution of the polymer within the skin.

Chapter 6 General Conclusions, Future Work and Clinical Translation

6.1 General Conclusion

Despite having a low likelihood to metastasise, BCC may induce substantial destruction to local tissues should the tumour be left untreated. The most effective treatment for BCC is Mohs' micrographic surgery. Although this treatment strategy is effective, the surgical prerequisites are both time-consuming and technical, which are major limitations of this surgical intervention [43,60–62]. In addition, some patients would prefer a less invasive treatment option in which they could self-administer at home. One of these alternative treatments is topical therapy with Aldara™ cream (5% w/w of imiquimod). Despite imiquimod being one of the most efficacious drugs in the management of BCC the drug has a poor permeation profile and thus its use is limited to the management of the superficial variant of the cancer.

The objective of this PhD project was to investigate and develop a drug delivery strategy using microneedles to improve the intradermal delivery of imiquimod for the treatment of nodular BCC. This objective was explored via two different strategies. The first approach involves investigating the use of commercial microneedles in combination with the commercially available Aldara™ cream. On the other hand, the second approach explored the reformulation of imiquimod into a dissolvable microneedle system. These strands of investigations and formulation development have led to a better understanding of how microneedles may be utilised as a drug delivery platform for the management of skin cancers such as nodular BCC.

One of the key findings of this thesis includes the characterisation on the mechanical insertion of microneedles into the skin. It was discovered that biaxial strain indeed influences the penetration of microneedles into the skin. The two commercially microneedle systems investigated, Dermapen® and Dermastamp™ displayed different insertion force profiles with increasing skin strain. For all the strain

levels studied, it was evident that the Dermapen® required less insertion force than the Dermastamp™. In addition, the Dermapen® resulted in smaller variability in insertion efficiency and puncture force while resulting in deeper skin insertion than that of the Dermastamp™. The lower insertion force and deeper penetration conferred by the Dermapen® was attributed to the oscillating feature of the microneedle system which mitigates the effective frictional force encountered by the needle during skin application. Despite the better skin insertion profile displayed by Dermapen® relative to the Dermastamp™, such differences in penetration did not affect the permeation profile of imiquimod across the skin as shown in the *ex vivo* permeation study when a poke-and-patch approach was adopted.

Moving forward, the effectiveness of the oscillating microneedle system, Dermapen, as a device to improve the intradermal delivery of imiquimod was investigated further. It was discovered that the approach in which the microneedles are used in combination with Aldara cream played a pivotal role in the intradermal delivery of imiquimod into the skin. It was evident that in order to successfully deliver imiquimod into the dermis, a patch-and-poke approach is superior to the conventional poke-and-patch strategy. This is based on the ToF-SIMS analysis of porcine skin cross-sections post permeation studies that demonstrated limited dermal permeation when Aldara™ cream was applied to the skin that was pre-treated with the Dermapen. Such limited permeation was similar to that observed when the porcine skin was treated with Aldara™ cream alone. In contrast, when a patch-and-poke strategy was adopted with the Dermapen® in combination with Aldara™ cream, we observed enhanced intradermal delivery of imiquimod into the dermis that persisted for up to 24 hours. In addition, it was also highlighted that the oscillating function of the Dermapen for the patch-and- poke strategy, is a critical factor in providing successful intradermal delivery of imiquimod into the skin. This is because when the patch-and- poke strategy was adopted with the non-oscillating Dermastamp™, we were unable to detect enhanced intradermal delivery of imiquimod into the skin.

The utility of using commercially available solid microneedle system coupled with the use of licensed imiquimod topical cream for treatment of BCC may be of great clinical value for nodular BCC patients who would prefer a less invasive intervention relative to surgery. However, the patch-and-poke administration is a two-step application process, which may decrease patient compliance and the adherence to the treatment. Furthermore, this step still involves topical cream application, which is often unfavourable for some patients due to poor cosmetic sensation upon administration. The propensity for the cream to spread to clothes and adjacent healthy skin is still a problem with the patch-and-poke strategy. Hence, there is an impetus to reformulate imiquimod into a dissolving microneedle system, which would allow for a one-step application. This simple one-step application would be a more preferred treatment option for patients in which they could easily self-administer at home.

Therefore, this drug delivery strategy was explored by designing, fabricating, and evaluating the utility of drug loaded dissolvable polymeric microneedles for the intradermal delivery of imiquimod for the treatment of nodular BCC. PVPVA microneedles loaded with imiquimod were manufactured via a microfabrication and polymer casting technique. Permeation studies highlighted that the imiquimod loaded polymeric microneedles were capable of delivering similar quantities of imiquimod into the skin, despite a 6-fold lower drug loading, relative to the current clinical dose of Aldara™ cream used in BCC treatment. This permeation study showed that dissolvable polymeric microneedles were capable of delivering imiquimod to the right target site despite lower drug loading. This may be of economic benefit as less drug is wasted during administration while also mitigating the likelihood of side effects. In addition, analysis of skin cross sections treated with the microneedle patch highlighted the presence of drug-polymer matrix within the skin. This matrix helped retain the drug in the dermis while reducing the permeation of the drug across the skin. This finding corroborated the mechanistic understanding of how the embedded drug-polymer matrix following polymeric microneedle administration controls the release of drugs within the skin.

Moving forward we explored if using different microneedle designs coupled with the choice of different polymers may improve the delivery of imiquimod into the skin. This was explored in the final chapter of this thesis. Microneedle moulds of different microneedle architectures (obelisk and pyramidal) were produced using micromachining while three different hydrophilic polymers-pNAM, pAMPS and pHEAM were synthesised via free radical polymerisation reaction. The moulds were then used to manufacture different types of dissolving polymeric microneedle patches of different designs and chemistries. The polymeric microneedles were characterised via microscopy, fracture test and *ex vivo* skin insertion studies. ToF-SIMS analysis on microneedles was conducted and showed the homogenous distribution of drug and polymer distribution along the microneedle lengths in a label free fashion. In addition, the chemical sensitivity conferred by ToF-SIMS analysis allowed us to detect and visualise for the first time the presence of polydimethylsiloxane (PDMS) contamination along the polymeric microneedles. Drug release studies into *ex vivo* porcine skin was also conducted in comparison to the commercial cream, Aldara™. It was discovered that microneedles fabricated from pNAM with an obelisk design resulted in significantly greater delivery of imiquimod into the skin relative to Aldara™ cream. This was further corroborated by the successful delivery of imiquimod using pNAM-based obelisk microneedles into human BCC tumours demonstrating the potential of the microneedle-based approach to treat BCC. In addition, the efficacy of the formulation was also evaluated and demonstrated *in vivo* using a rodent model for skin tumours with mice being treated with imiquimod loaded pNAM-based obelisk shaped dissolving microneedles showing a reduction in tumour growth as compared to the control groups.

It was apparent that throughout this work that the application of ToF-SIMS imaging played a pivotal role in elucidating the dermal distribution of active and excipient following microneedle treatment. Conventionally, the most common and widely accepted method of assessing skin permeation typically involves HPLC. Despite the absolute quantitative data conferred by HPLC, this technique does not provide information pertaining to the dermal distribution of the drug and excipients within the skin. In contrast, imaging mass spectrometry techniques, such as ToF-SIMS, were capable of showing the

dermal distribution of active and excipients from the formulation within biological tissues (e.g., porcine skin tissue & human BCC tissue) in a label free fashion. This is evident from the ability to demonstrate the colocalisation of imiquimod and isostearic acid within microneedle channels following the patch-and-poke strategy in Chapter 3. In Chapter 4, this was also demonstrated by the ability to detect the presence a drug-polymer matrix within the skin. The existence of this drug polymer matrix helped provide evidence how dissolving microneedles conferred enhanced intradermal delivery of imiquimod whilst mitigating the movement of the drug across the skin into the receptor fluid. Lastly in Chapter 5, the detection of the presence of imiquimod along with the newly synthesised pNAM within an actual human BCC tumour further demonstrated the analytical power of ToF-SIMS in guiding formulation scientists on the fate and localisation of the active and excipients of the formulation following administration. It is worth emphasising that the ability of ToF-SIMS analysis to image the dermal distribution of drug, excipient within a biological tissue without the need for fluorescent reporter tags obviates the issues of altering the physiochemical properties of the molecule of interest that could lead to inaccurate estimation of the distribution of the molecule within biological tissues.

6.2 Summary of significant results and method development from experimental chapter

In general, a series of method development and optimisation has taken place across the experimental chapters which have led to the development and characterisation of the final polymeric pNAM obelisk microneedle system. In Chapter 2 of this thesis, it has been shown that commercial microneedle systems such as the Dermapen® and the Dermastamp™, are capable of breaching the *stratum corneum* which led to the generation of microneedle channels within the skin. In order to evaluate and quantify these insertion profiles between the two systems, various insertion studies were developed and utilised. Firstly, this chapter highlights the development of a novel biaxial stretch rig that was used to investigate the effect of skin strain on microneedle insertion into the skin. The development of such device highlighted that the Dermapen® required less force for microneedle insertion into the skin for all skin strains investigate while displaying superior insertion reproducibility

relative to the Dermastamp™. This chapter also highted the utilisation of the *in vitro* Parafilm M® insertion study as a simple and inexpensive method to evaluate and estimate the microneedle penetration prior to *ex vivo* porcine skin insertion. In addition, this chapter also featured the development and utilisation of the dye binding study as a method to estimate microneedle insertion depth into *ex vivo* skin. Through the use of these insertion tests, it was shown that the Dermapen® possessed superior insertion profile relative to the Dermastamp™ in puncturing the skin down to a depth of ≈ 600 µm which nodular BCC typically resides. The insertion tests utilised in this chapter were later employed as to estimate and quantify microneedle insertions later chapters. Overall, Chapter 2 of this thesis identified that the Dermapen® was indeed the superior commercial microneedle system relative to the Dermastamp™.

In Chapter 3 of this thesis, the utility of Dermapen® in enhancing the delivery of imiquimod into the skin was explored further. It was shown that post-treatment of the skin with the Dermapen® after Aldara™ application, known as "patch-and-poke", was superior to the conventional "poke-and-patch" strategy in enhancing the intradermal delivery of imiquimod into the skin. However, such improvement in intradermal delivery of imiquimod was not apparent when the "patch-and-poke" strategy utilised a non-oscillating microneedle applicator, the Dermastamp™. Enhancement in intradermal delivery of imiquimod via the "patch-and-poke" approach was visualised through ToF-SIMS analysis of skin cross-sections that were cryosection through partial OCT embedding. The application of ToF-SIMS analysis within this chapter expanded upon the method developed by Al-Mayahy *et al*. [68] by exploring the capability of this analytical method to track the co-localisation of both active (imiquimod) and excipient (isosteric acid) within skin tissues. The result obtained within this chapter demonstrated for the first time the ability to track both active and excipients from a microneedle treatment in a label free fashion. The methodology developed within this chapter was later used to analyse the colocalisation of drug and other excipients such as polymers within the skin as demonstrated in Chapter 4 and Chapter 5.

It has been highlighted in Chapter 4 that there is an impetus to reformulate imiquimod into a dissolving microneedle system due the limitation associated with the "patch-and-poke" strategy. Therefore, Chapter 4 of this thesis highlighted the development and optimisation of the methodology to produce dissolving microneedles via the use of micromachining and micromoulding. A dissolving polymeric microneedle system was fabricated through the use of a commercially available polymer, PVPVA that has never been used in microneedle production before. The microneedle system developed was capable of delivering similar quantities of imiquimod intradermally, despite a 6-fold lower drug loading, relative to the current clinical dose of Aldara™ cream used in BCC treatment. This chapter also highlighted the importance of incorporating plasticiser such as PEG 400 during microneedle production as this mitigate the likelihood of microneedle fracturing during the demoulding stage. The knowledge of incorporating of plasticisers such as PEG 400 into polymeric microneedle formulations was later applied to the development of other polymeric microneedle systems in Chapter 5. The parallel detection capability of ToF-SIMS demonstrated in Chapter 3 was further explored and utilised in Chapter 4 by tracking the colocalisation of both drug and polymer within the skin tissue. This was the first study within the microneedle field that demonstrated the capability to simultaneously detect the deposition of both drug and polymer from a dissolving microneedle patch in a label free fashion.

The advances and method optimisations developed in the earlier chapters were then applied to Chapter 5. In this final experimental chapter, a series of novel polymers that has never been used in microneedle fabrication were synthesised. These polymers are similar to PVPVA used in Chapter 4 because they are also hydrophilic. This enabled the polymers to be dissolved into aqueous solutions which are then used to formulate dissolving microneedles via the same micromachining and micromoulding process developed in Chapter 4. Based on the knowledge gained from Chapter 4, each of the microneedle formulation developed in Chapter 5 incorporated plasticisers such as PEG 400 and PVA to help mitigate the propensity of needle fracture during microneedle demoulding. This enabled the production of intact and sharp microneedles on a clean and smooth base. The Parafilm M® and dye binding study that was developed and optimised in Chapter 2 were applied to characterised the

series of polymeric microneedle developed in this chapter. These insertion tests showed that the pNAM obelisk microneedles displayed the best insertion depth and efficiency out of all the polymeric microneedles developed. In addition, the pNAM obelisk microneedle was capable of delivering imiquimod into *ex vivo* human BCC tumours while also demonstrating efficacy *in vivo* using a rodent model for skin tumours. The capability of the ToF-SIMS analytical method developed Chapter 3 was further demonstrated in Chapter 5 through the detection of the presence of imiquimod along with the newly synthesised pNAM within an actual human BCC tumour. Indeed, there is a series of method development and optimisation throughout the earlier chapters within this thesis. These methods are later applied to the final series of experiments in Chapter 5. Such methodologies enabled the development and characterisation of a series of imiquimod loaded polymeric microneedles. Out of all the polymeric microneedles developed within this body of work, it was identified that the pNAM obelisk microneedles was capable of achieving the highest intradermal delivery of imiquimod into the skin. The pNAM obelisk microneedles developed may be of therapeutic value for the treatment of nodular BCC in patients who would prefer an alternative treatment to surgery.

6.3 Future Work

The results presented within this thesis explored the utility of microneedles as a drug delivery platform to enhance imiquimod delivery into the skin for the treatment of nodular BCC. The successful permeation enhancement of imiquimod into the skin through the use of solid microneedles via the patch-and-poke approach along with the reformulation of imiquimod into dissolvable microneedles demonstrated the clinical potential that microneedles could have in managing dermatological conditions such as skin cancers. Such treatment can easily be self-administered by patients thus mitigating the clinical burden imposed by the disease on the healthcare system. Moving forward, there are some recommendations that can be carried out to further improve our mechanistic understanding on the insertion profile, drug release behaviour and efficacy from the microneedle systems developed. In addition, these future works could also help refine the microneedle systems developed in order to further improve the efficacy for the management of nodular BCC.

In Chapter 2 in this thesis, skin insertion studies using *ex vivo* porcine skin was utilised to investigate the effect of biaxial strain (stretching) on the insertion of commercial cosmetic microneedles system into the skin. This experimental set-up proved to be a valuable tool in distinguishing the insertion profile (insertion efficiency and force needed for insertion) from two different commercial microneedle systems. It would be of great heuristic value to use such experimental set-up to elucidate the effect of biaxial strain on the insertion profile of polymeric microneedle patches fabricated from different polymers with different geometries. Such information will help us understand if the insertion profile of microneedle patches is dependent on polymer chemistry and needle design. The different skin strain generated may mimic the effect of biological variability of the skin arising from anatomical locations and aging.

In Chapter 3 of this thesis, we demonstrated via ToF-SIMS label free imaging that using the patch-and-poke approach with the Dermapen® in combination Aldara™ resulted in co-localised delivery of both imiquimod and isostearic acid. As it has been discussed in Chapter 3, although isostearic acid has been traditionally used as a surfactant in most topical and cosmetic products, the fatty acid surfactant has been shown by Walter *et al.* to display pharmacological properties independent of the immune-mediated response induced by imiquimod [286]. In addition, it has also been highlighted by Walter *et al.* that the presence of isosteric acid is pertinent to the overall efficacy of Aldara™ cream. However, in Chapter 4 and Chapter 5 we have reformulated imiquimod into dissolvable microneedles in the absence of isostearic acid. Due to the poor water solubility of isostearic acid, the fatty acid was not incorporated into the aqueous drug and polymer blend during the fabrication of dissolvable polymeric microneedle [392].

Therefore, it is suggested that a potential research avenue that warrants further investigation is to identify a way of reformulating both imiquimod and isosteric acid into a single dissolvable microneedle system. One strategy that could be used is to first reformulate both imiquimod and isostearic acid into solid lipid nanoparticle which is then incorporated into dissolving microneedle systems. This solid lipid

nanoparticle-based dissolving microneedles strategy have been explored by Permana *et al.* and has been shown to be successful in delivering the antifilariasis drugs doxycycline, diethylcarbamazine and albendazole intradermally [393]. The co-delivery of both imiquimod and isostearic using solid lipid nanoparticles may prove to be more efficacious that the delivery of imiquimod alone using dissolving microneedles.

In addition, it has been reported that the incorporation of drug molecules and biologics into microneedle systems such as dissolving, coated and hydrogel forming microneedles enhances the stability of therapeutics. This is attributed to the interaction of the therapeutics with the polymer matrix that results in reduced molecular mobility of the incorporated molecules. The restricted molecular mobility results in reduced kinetics of possible chemical and physical degradation pathways, leading to improved stability. The interaction of the drug molecules with polymers through hydrogen bonding also results in the formation of a stabilisation shell around the incorporated therapeutic, which mitigates dehydration induced changes during storage. Nevertheless, long-term stability studies of the microneedle formulations developed in the current work will need to be done in order to establish the stability of the formulations long-term. When conducting these stability studies, it is suggested that both the stability of the incorporated therapeutic along with the mechanical properties of the overall microneedle patches during long term storage would need to be evaluated. This is because the hygroscopic nature of hydrophilic polymers used in this work could have adverse effects on the needle structure and subsequently, the ability of the microneedle array to successfully penetrate the skin. Further studies into these effects could help establish the viability of the microneedle patches after prolonged storage.

These stability studies should also be complemented with research looking into appropriate primary packaging for microneedles. As dissolving and hydrogel forming microneedle are deemed “self-disabling” once the formulations are exposed to liquid or humid environment, it is necessary that the packaging in which these microneedles are stored confer protection against such environmental

factors. Work that looks into these primary packaging would be imperative and would help the transition of microneedle technology from a laboratory setting to patients.

In Chapter 5 of this thesis, the efficacy of imiquimod loaded microneedle patches was evaluated in B16 melanoma model in HHDII/HLA- DP4 mice. Although imiquimod has been shown to be efficacious in slowing down tumour growth in the mouse model for melanoma, it is acknowledged that the use of this animal model may not be an accurate animal model to predict the efficacy of the formulation developed for BCC [389]. One of the challenges in developing formulation for BCC is the lack of good and accurate pre-clinical animal models for BCC. Tumour xenograft models are the standard used in assessing the efficacy of new treatments at the pre-clinical stage. However, it has been shown that successful and reproducible human BCC xenograft implantations in mice model have been attempted but have been met with little success. These animal models yielded low tumour uptake and growth making these models unsuitable to evaluate formulation efficacy [381]. Some level of success have been achieved when these xerographs are implanted in severely immunocompromised murine models such as beige-nude, SCID-beige mice or NOD/SCID mice [382–384]. However, these immunocompromised models may not be suited to screen the efficacy of imiquimod loaded microneedle patch as part of the anti-tumoural activity of imiquimod relies on the innate and the adaptive immune responses. Therefore, future work in establishing an immunocompetent mouse model for BCC would pertinent in order to evaluate the efficacy of these imiquimod loaded microneedle patches for BCC treatment. The ideal BCC animal model ought to be orthotopic, have short tumour latency, display similar tumour profile to humans, predictable growth rate as well as capable of producing identical tumour replicates for formulation screening and evaluation.

It has been highlighted that one of the mechanisms for imiquimod induced antitumour response is via the innate and the adaptive immune responses. Another research avenue worth exploring is to carry out imaging mass spectrometry analysis on tumours from mice that have not been treated with imiquimod microneedles and those who have received treatment with imiquimod microneedles. By

doing so we can observe the change in the metabolic and immune profile of the local tumour milieu following the administration of the imiquimod loaded microneedles. However, as most of the immune response mediated my imiquimod leads to the production of proteins and peptides such as interleukins, TNF-α, interferon-α and granulocyte colony-stimulating factor, it is postulated that ToF-SIMS imaging may not have the sensitivity and mass-resolving power needed to detect such proteins. However, with the recent development and introduction of the Hybrid-SIMS also known as the 3D OrbiSIMS, such analysis would be achievable. The Hybrid-SIMS is equipped with an Orbitrap™ mass analyser that confers the instrument with a mass-resolving power of >240,000 at *m/z* 200 and mass accuracy <1 p.p.m. Such resolving power would permit the detection and analysis of ions with enhanced sensitivity in comparison to the ToF-SIMS analysis conducted in the present work. In addition, Passarelli *et al.* has shown that the Hybrid-SIMS may also be used to image the drug distribution down to single cell analysis [394]. Such approach could be extended to single cell analysis of both tumour cells and immune cells within the tumour milieu following the treatment with imiquimod loaded dissolving microneedles. This would permit us to establish the changes in both metabolic and immune profile within the tumours prior and post-treatment. Nevertheless, such analysis would need rigorous optimisation and validation before such analysis and tumour profiling could be achieved.

The results within this thesis have shown that microneedles indeed provide a viable approach to enhance the delivery of imiquimod for the treatment of skin tumours such as BCC. When developed further as suggested by these future works, this drug delivery platform could prove to be of great clinical value in the management of BCC, which could lessen the burden of skin cancers on dermatologist workload while providing a simple and effective treatment in which patients could self-administer the medicine at home. In summary, this future work would aid the development and clinical translation of these dissolving microneedle systems. However, before such a transition into clinical settings could occur, some translation challenges would need to be considered and addressed. Such translational hurdles are discussed in the last section of this chapter.

6.4 Clinical Translation and future perspectives

At the time of writing this thesis there are no commercially available dissolvable microneedle systems for clinical application on the market. The microneedle product, which is closest to FDA approval is a formulation of zolmitriptan, that is delivered transdermally via drug-coated microneedle arrays. The microneedle system known Qtrypta™, owned by Zosano Pharma is anticipated to be approved for clinical use by 2021 for acute migraine attacks as the proprietary formulation successfully demonstrated efficacy, safety and tolerability in phase 2 and 3 clinical trials. Nevertheless, the lack microneedle products on the market at the moment for clinical use highlights that there are indeed several translation hurdles that are currently hindering the progression of microneedle systems from bench to bedside.

One of the factors that needs to be acknowledged and considered is the need to incorporate a feedback system into the microneedle products developed. This would provide end-user the confidence and certainty that the microneedle patches have been successfully inserted into the skin. Through engagement with potential end-users, Donnelly and co-workers have identified that this is one of the major hurdles in translating microneedle systems into clinical practice [395]. Several attempts to incorporate a simple feedback mechanism into microneedle systems have been explored by several researchers. Norman *et al.* reported the use of a simple, low-cost snap-based device that provides audible feedback upon microneedle application. The group discovered that there was a significantly higher end-user preference for microneedle systems that incorporated the audible snap-based feedback system relative to microneedle systems that did not have this function [396]. Furthering this, Vicente-pérez *et al.* explored the use of a low-cost pressure-indicating sensor film (PISF), Pressurex-micro® Green attached to the backing layer of microneedle patches. This acts as a feedback system to indicate successful microneedle insertion. The film undergoes a colour change when a pressure of greater than 18.6 Ncm^{-2} has been applied to the skin, which is sufficient for successful microneedle insertion [309]. Therefore, if the microneedle systems developed in this project were to be translated into clinical practice for the treatment of nodular or even superficial BCC, the incorporation of a simple

feedback system (e.g. snap-based device or even colour changing backing layer) would provide reassurance to the patient that they have administered the anticancer medicine accurately.

Sterility will be another factor to consider in the translation of dissolvable microneedle products into clinical practice. From a commercial standpoint, the choice of the sterilisation method will be critical as this will ultimately impact the cost of the final product. McCrudden *et al.* was the first to explore the method of sterilisation of microneedle patches. They discovered that using terminal sterilisation techniques such as steam autoclaving and dry sterilisation resulted in substantial irreversible damage to dissolving and hydrogel-forming microneedle systems [313]. This is attributed to the hygroscopic nature of the hydrophilic polymers used in fabricating these polymeric microneedle systems. Furthering this, Swathi *et al.* explored the effect of gamma irradiation on dissolving microneedles. Four different dissolving microneedles systems fabricated from sodium carboxymethyl cellulose (CMC), polyvinylpyrrolidone (PVP) K30, PVP K90 and sodium hyaluronate (HU) were explored. Upon exposure to gamma irradiation, it was discovered that CMC and PVP K30 microneedles were affected by this mode of sterilisation resulting in poor mechanical properties and needle architecture. However, the appearance, properties and release profile of PVP K90 and HU were unaffected by the dose of gamma irradiation used [397]. In comparison, the current work utilised hydrophilic polymers to fabricate dissolvable microneedle systems. It is anticipated that these microneedle systems would be susceptible to irreversible damage should steam autoclaving or dry sterilisation are utilised as a method of terminal sterilisation since the polymers used in the current work are also hydrophilic. It is proposed that the PVPVA microneedles and pNAM microneedles fabricated might be more suited to be sterilised via gamma irradiation. However, this should be accompanied by further testing to evaluate if the appearance and release profile of these systems have been altered post-sterilisation. Should this method of sterilisation also be deemed unsuitable, then it is likely that aseptic manufacture would be the way to produce these microneedles.

Another factor to consider is the possible scale-up of the manufacturing process of these dissolvable microneedles. With regards to the production method used in this study, which involved centrifugation and polymer blend casting, such methodology would be most suited for lab-based research and is not suitable for the manufacture of patches at a commercial scale. This is because laboratory-based procedures are typically difficult to scale-up, with issues revolving around cost-efficiency of mass manufacture as well as turnaround time.

Therefore, a method to produce large quantities of dissolvable microneedle patches ought to be investigated. Such production would be imperative particularly when large number of microneedle patches are needed during phase 2 and 3 clinical trials and ultimately for commercial manufacture when the products have gained regulatory approval. The use of aqueous drug-polymer blend casting method used in this work could be potentially be translated into the scalable roller system manufacturing method developed by Lutton *et al.* [299]. The use of the roller system would provide a potential scale-up manufacturing method at a commercial scale, enabling the transition from laboratory to industry manufacture and subsequent clinical practice.

Another major hurdle to consider would be the need to establish standardised quality control tests to evaluate the properties and performance of microneedle-based medical products at the final stage of mass production. Indeed, there are strict guidelines and pharmacopoeial standards that a medicine would need to meet prior to release for human use. However, such guidelines and standards are yet to be established for microneedle-based formulations. It is anticipated that such standards and tests will emerged once microneedle-based medicine are commercialised as such tests are typically derived from products that have been approved by regulatory bodies as part of a manufacturer's submitted dossier. The development of such guidelines and standardised tests would also aid researchers within the field on the choice of experiments that ought to be done when developing new microneedle systems. Despite the uncertainties with regards to standardised quality control tests, considerable strides have been made in this direction. For instance, the FDA has recently published draft guidance

on “microneedling” for cosmetic applications [398]. It is predicted that this draft guidance would act as a foundation to develop guidelines for microneedle-based product for medical applications in the future. This is further corroborated by establishment of PATH Center of Excellence for Microarray Patch Technology, a non-profit, international health organisation working on progressing microneedle technology for effective and safe clinical use. Recently, PATH has released information detailing their four-year initiative in propelling the development of microneedle-based drug delivery system for clinical use [399]. As an emerging pharmaceutical technology, microneedles display considerable advantages such as being patient friendly, easy to apply and remove, minimally invasive and painless. The versatility and diversity in microneedle designs allow the device to be tailored to nature of the disease intended to be treated. Such advantages may have a significant clinical impact in the foreseeable future. However, before commercialisation and transition into clinical practice can take place, the translational challenges identified above ought to be acknowledged and addressed.

Chapter 7 References

1. *Topical and Transdermal Drug Delivery*. (John Wiley & Sons, Inc., 2011). doi:10.1002/9781118140505

2. van Smeden, J. *et al.* The important role of stratum corneum lipids for the cutaneous barrier function. *Biochim. Biophys. Acta* **1841**, 295–313 (2014).

3. Menon, G. K., Cleary, G. W. & Lane, M. E. The structure and function of the stratum corneum. *Int. J. Pharm.* **435**, 3–9 (2012).

4. Donnelly, R. F., Singh, T. R. R., Morrow, D. I. J. & Woolfson, A. D. *Microneedle-Mediated Transdermal and Intradermal Drug Delivery*. (John Wiley & Sons, Ltd, 2012). doi:10.1002/9781119959687

5. Baroni, A. *et al.* Structure and function of the epidermis related to barrier properties. *Clin. Dermatol.* **30**, 257–262 (2012).

6. Mukhtar, H. *Pharmacology of the Skin*. (CRC Press, 1992).

7. Barry, B. W. *Dermatological Formulations - Percutaneous Absorption*. (Marcel Dekker, 1983).

8. Kobayashi, T. *et al.* Homeostatic Control of Sebaceous Glands by Innate Lymphoid Cells Regulates Commensal Bacteria Equilibrium. *Cell* **176**, 982-997.e16 (2019).

9. Hu, Y., Converse, C., Lyons, M. C. & Hsu, W. H. Neural control of sweat secretion: a review. *Br. J. Dermatol.* **178**, 1246–1256 (2018).

10. Paus, R. & Cotsarelis, G. the Biology of Hair Follicles. *N. Engl. J. Med.* **341**, 491–497 (2014).

11. Meidan, V. M. Methods for quantifying intrafollicular drug delivery: A critical appraisal. *Expert Opin. Drug Deliv.* **7**, 1095–1108 (2010).

12. Aulton, M. E. *Aulton's Pharmaceutics The Design And Manufacture of Medicines*. (Churchill

Livingstone, 2011).

13. Tfayli, A., Piot, O., Pitre, F. & Manfait, M. Follow-up of drug permeation through excised human skin with confocal Raman microspectroscopy. *Eur. Biophys. J.* **36**, 1049–1058 (2007).

14. Thomas, B. J. & Finnin, B. C. The transdermal revolution. *Drug Discov. Today* **9**, 697–703 (2004).

15. Rothman, S. The principles of percutaneous absorption. *Transl. Res.* **28**, 1305–1321 (1943).

16. Mark R Prausnitz, R. L. Transdermal drug delivery. *Nat. Biotechnol.* **26**, 1261–1268 (2007).

17. Hadgraft, J. Skin deep. *Eur. J. Pharm. Biopharm.* **58**, 291–299 (2004).

18. Finnin, B. C. & Morgan, T. M. Transdermal penetration enhancers: Applications, limitations, and potential. *J. Pharm. Sci.* **88**, 955–958 (1999).

19. Chandrashekar, N. S. & Rani, R. H. Physicochemical and Pharmacokinetic Parameters in Drug Selection and Loading for Transdermal Drug Delivery. *Indian J. Pharm. Sci.* **70**, 94–96 (2008).

20. Wiedersberg, S. & Guy, R. H. Transdermal drug delivery: 30 + years of war and still fighting! *J. Control. Release* **190**, 150–156 (2014).

21. Lane, M. E. Skin penetration enhancers. *Int. J. Pharm.* **447**, 12–21 (2013).

22. Trommer, H. & Neubert, R. H. . Overcoming the Stratum Corneum: The Modulation of Skin Penetration. *Ski. Pharmacol Physiol* **19**, 106–121 (2006).

23. Scheuplein, R. J. Mechanism of Percutaneous Absorption. *J. Invest. Dermatol.* **48**, 79–88 (1966).

24. Patzelt, A. & Lademann, J. Expert Opinion on Drug Delivery Recent advances in follicular drug delivery of nanoparticles. *Expert Opin. Drug Deliv.* **00**, 1–12 (2020).

25. Ciaźyńska, M., Narbutt, J., Woźniacka, A. & Lesiak, A. Trends in basal cell carcinoma incidence rates: A 16-yearretrospective study of a population in central Poland. *Postep. Dermatologii i Alergol.* **35**, 47–52 (2018).

26. Armstrong, B. K. & Kricker, A. The epidemiology of UV induced skin cancer. *J. Photochem. Photobiol. B Biol.* **63**, 8–18 (2001).

27. Wu, S., Han, J., Li, W. Q., Li, T. & Qureshi, A. A. Basal-cell carcinoma incidence and associated risk factors in U.S. women and men. *Am. J. Epidemiol.* **178**, 890–897 (2013).

28. Cameron, M. C. *et al.* Basal cell carcinoma: Epidemiology; pathophysiology; clinical and histological subtypes; and disease associations. *J. Am. Acad. Dermatol.* **80**, 303–317 (2019).

29. Diffey, B. L. & Langtry, J. A. A. Skin cancer incidence and the ageing population. *Br. J. Dermatol.* **153**, 679–680 (2005).

30. Suppa, M. *et al.* Dermoscopic variability of basal cell carcinoma according to clinical type and anatomic location. *J. Eur. Acad. Dermatology Venereol.* **29**, 1732–1741 (2015).

31. Kuijpers, D. I. M., Thissen, M. R. T. M. & Neumann, M. H. A. Basal cell carcinoma: treatment options and prognosis, a scientific approach to a common malignancy. *Am. J. Clin. Dermatol.* **3**, 247–259 (2002).

32. Crowson, A. N. Basal cell carcinoma : biology , morphology and clinical implications. *Mod. Pathol.* **19**, (2006).

33. Colver, G. B. *Skin Cancer A Practical Guide to Management*. (Taylor & Francis, 2002).

34. Williams, H. C. *et al.* Surgery Versus 5% Imiquimod for Nodular and Superficial Basal Cell Carcinoma: 5-Year Results of the SINS Randomized Controlled Trial. *J. Invest. Dermatol.* **137**, 614–619 (2017).

35. Sabri, A. *et al.* Intradermal delivery of an immunomodulator for basal cell carcinoma; expanding the mechanistic insight in solid microneedle enhanced delivery of hydrophobic molecules. *Mol. Pharm.* (2020). doi:10.1021/acs.molpharmaceut.0c00347

36. Goldenberg, G., Golitz, L. . & Fitzpatrick, J. Histopathology of Skin Cancer. in *Managing Skin*

Cancer (eds. Stockfleth, E., Rosen, T. & Schumaak, S.) 17–35 (Springer-Verlag Berlin Heidelberg, 2010). doi:10.1007/978-3-540-79347-2

37. Mackiewicz-Wysocka, M., Bowszyc-Dmochowska, M., Strzelecka-Węklar, D., Dańczak-Pazdrowska, A. & Adamski, Z. Reviews Basal cell carcinoma – diagnosis. *Współczesna Onkol.* **4**, 337–342 (2013).

38. Mehta, K. S. *et al.* Metastatic Basal Cell Carcinoma: A Biological Continuum of Basal Cell Carcinoma? *Case Rep. Dermatol. Med.* **2012**, 1–4 (2012).

39. Wu, X., Elkin, E. E. & Marghoob, A. A. Burden of basal cell carcinoma in USA. *Futur. Oncol.* **11**, 2967–74 (2015).

40. Loo, E. Van *et al.* Surgical excision versus Mohs ' micrographic surgery for basal cell carcinoma of the face : A randomised clinical trial with 10 year follow-up q. *Eur. J. Cancer* **50**, 3011–3020 (2014).

41. Mohs, F. Chemosurgery: a microscopically controlled method of cancer excision. *Arch. Surg.* **42**, 279–95 (1941).

42. Macfarlane, L., Waters, A., Evans, A., Affleck, A. & Fleming, C. Seven years ' experience of Mohs micrographic surgery in a UK centre , and development of a UK minimum dataset and audit standards. *Clin. Exp. Dermatol.* **38**, 262–269 (2013).

43. Coyle, M. J. & Takwale, A. Nonsurgical Management of Non-Melanoma Skin Cancer. in *Maxillofacial Surgery* 761–764 (Elsevier Inc., 2017). doi:10.1016/B978-0-7020-6056-4.00055-1

44. Morton, C. A., Birnie, A. J. & Eedy, D. J. British Association of Dermatologists' guidelines for the management of squamous cell carcinoma in situ (Bowen's disease) 2014. *Br. J. Dermatol.* **170**, 245–260 (2014).

45. Dolmans, D. E. J. G. J., Fukumura, D. & Jain, R. K. Photodynamic therapy for cancer. *Nat. Rev.*

Cancer **3**, 380–387 (2003).

46. Harris, F. & Pierpoint, L. PhotodynamicTherapy Based on 5-Aminolevulinic Acid and Its Use as an Antimicrobial Agent. *Med. Res. Rev.* **29**, 1292–1327 (2012).

47. Donnelly, R. F., Morrow, D. I. J., McCarron, P. A., Garland, M. J. & Woolfson, A. D. Influence of solution viscosity and injection protocol on distribution patterns of jet injectors: Application to photodynamic tumour targeting. *J. Photochem. Photobiol. B Biol.* **89**, 98–109 (2007).

48. Longley, D. B., Harkin, D. P. & Johnston, P. G. 5-Fluorouracil: mechanisms of action and clinical strategies. *Nat. Rev. Cancer* **3**, 330–338 (2003).

49. Sharma, M., Sharma, G., Singh, B. & Katare, O. Stability Kinetics of Imiquimod: Development and Validation of an Analytical Method. *J Chromatogr Sci* **57**, 583–591 (2019).

50. Chollet, J. L. *et al.* Development of a topically active imiquimod formulation. *Pharm. Dev. Technol.* **4**, 35–43 (1999).

51. Wagner, H., Kostka, K. H., Lehr, C. M. & Schaefer, U. F. pH profiles in human skin: Influence of two in vitro test systems for drug delivery testing. *Eur. J. Pharm. Biopharm.* **55**, 57–65 (2003).

52. Paula, D. De, Martins, C. A. & Bentley, M. V. L. B. Development and validation of HPLC method for imiquimod determination in skin penetration studies. *Biomed. Chromatogr.* **22**, 1416–1423 (2008).

53. Donnelly, R. F., McCarron, P. A., Zawislak, A. A. & David Woolfson, A. Design and physicochemical characterisation of a bioadhesive patch for dose-controlled topical delivery of imiquimod. *Int. J. Pharm.* **307**, 318–325 (2006).

54. Venturini, C. G. *et al.* Co-encapsulation of imiquimod and copaiba oil in novel nanostructured systems: Promising formulations against skin carcinoma. *Eur. J. Pharm. Sci.* **79**, 36–43 (2015).

55. Sharma, M., Sharma, G., Singh, B. & Katare, O. P. Systematically Optimized Imiquimod-Loaded

Novel Hybrid Vesicles by Employing Design of Experiment (DoE) Approach with Improved Biocompatibility, Stability, and Dermatokinetic Profile. *AAPS PharmSciTech* **20**, (2019).

56. Schön, M. P. & Schön, M. The small-molecule immune response modifier imiquimod – its mode of action and clinical use in the treatment of skin cancer. *Expert Opin. Ther. Targets* **10**, 69–76 (2006).

57. Anne Skelton, L. The effective treatment of basal cell carcinoma. *Br. J. Nurs.* **18**, 346–350 (2009).

58. Lacarrubba, F., Nasca, M. R. & Micali, G. Advances in the use of topical imiquimod to treat dermatologic disorders. *Ther. Clin. Risk Manag.* **4**, 87–97 (2008).

59. Jansen, M. H. E. *et al.* Five-Year Results of a Randomized Controlled Trial Comparing Effectiveness of Photodynamic Therapy , Topical Imiquimod , and Topical 5-Fluorouracil in Patients with Superficial Basal Cell Carcinoma. *J. Invest. Dermatol.* **138**, 527–533 (2017).

60. Göppner, D. & Leverkus, M. Basal cell carcinoma: from the molecular understanding of the pathogenesis to targeted therapy of progressive disease. *J. Skin Cancer* **2011**, 650258 (2011).

61. Nijssen, A. *et al.* Discriminating basal cell carcinoma from its surrounding tissue by raman spectroscopy. *J. Invest. Dermatol.* **119**, 64–69 (2002).

62. Wiltfang, J., Naujokat, H. & Farrier, J. N. *Cutaneous Lesions of the Periorbital and Lid Region*. *Maxillofacial Surgery* (Elsevier, 2017). doi:10.1016/B978-0-7020-6056-4.00053-8

63. Goldenberg, G. & Hamid, O. Nonsurgical treatment options for basal cell carcinoma - focus on advanced disease. *J. Drugs Dermatol.* **12**, 1369–78 (2013).

64. Lien, M. H. & Sondak, V. K. Nonsurgical treatment options for Basal cell carcinoma. *J. Skin Cancer* **2011**, 571734 (2011).

65. Calzavara-pinton, P. G., Venturini, M. & Sala, R. Photodynamic therapy : update 2006 Part 1 :

Photochemistry and photobiology. *J. Eur. Acad. Dermatology Venereol.* **21**, 293–302 (2007).

66. Naguib, Y. W., Kumar, A. & Cui, Z. The effect of microneedles on the skin permeability and antitumor activity of topical 5-fluorouracil. *Acta Pharm. Sin. B* **4**, 94–99 (2014).

67. Ma, M. *et al.* Development of nanovesicular systems for dermal imiquimod delivery: physicochemical characterization and in vitro/in vivo evaluation. *J. Mater. Sci. Mater. Med.* **26**, (2015).

68. Al-Mayahy, M. H. *et al.* Insight into imiquimod skin permeation and increased delivery using microneedle pre-treatment. *Eur. J. Pharm. Biopharm.* **139**, 33–43 (2019).

69. Devaux, S. *et al.* Adherence to topical treatment in psoriasis: A systematic literature review. *J. Eur. Acad. Dermatology Venereol.* **26**, 61–67 (2012).

70. Lee, W. R. *et al.* Laser-assisted topical drug delivery by using a low-fluence fractional laser: Imiquimod and macromolecules. *J. Control. Release* **153**, 240–248 (2011).

71. Hanna, E., Abadi, R. & Abbas, O. Imiquimod in dermatology: an overview. *Int. J. Dermatol.* **55**, 831–844 (2016).

72. Chu, L. Y. & Prausnitz, M. R. Separable arrowhead microneedles. *J. Control. Release* **149**, 242–249 (2011).

73. Ribeiro, L. N. M. *et al.* Advances in Hybrid Polymer-Based Materials for Sustained Drug Release. **2017**, (2017).

74. Larrañeta, E., Lutton, R. E. M., Woolfson, A. D. & Donnelly, R. F. Microneedle arrays as transdermal and intradermal drug delivery systems: Materials science, manufacture and commercial development. *Mater. Sci. Eng. R Reports* **104**, 1–32 (2016).

75. Donnelly, R. F. *et al.* Microneedle Arrays Allow Lower Microbial Penetration Than Hypodermic Needles In Vitro. **26**, 2513–2522 (2009).

76. Schauber, J. & Gallo, R. L. Antimicrobial peptides and the skin immune defense system. *J. Allergy Clin. Immunol.* **122**, 261–266 (2008).

77. Harder, J., Bartels, J., Christophers, E. & Schröder, J.-M. A peptide antibiotic from human skin. *Nature* **387**, 861–861 (1997).

78. Liu, L. *et al.* Structure and mapping of the human beta-defensin HBD-2 gene and its expression at sites of inflammation. *Gene* **222**, 237–44 (1998).

79. Park, J., Allen, M. G. & Prausnitz, M. R. Biodegradable polymer microneedles : Fabrication , mechanics and transdermal drug delivery. **104**, 51–66 (2005).

80. Davies, P. N., Worthington, H. E. C., Podczeck, F. & Newton, J. M. The determination of the mechanical strength of tablets of different shapes. *Eur. J. Pharm. Biopharm.* **67**, 268–276 (2007).

81. Cohen, B. E. & Elbuluk, N. Microneedling in skin of color: A review of uses and efficacy. *J. Am. Acad. Dermatol.* **74**, 348–355 (2016).

82. Ma, G. & Wu, C. Microneedle , bio-microneedle and bio-inspired microneedle : A review. *J. Control. Release* **251**, 11–23 (2017).

83. Martin S. Gerstel, V. A. P. United States Paten. *Patentimages.Storage.Googleapis. …* 1–4 (1972).

84. Kim, Y. C., Park, J. H. & Prausnitz, M. R. Microneedles for drug and vaccine delivery. *Adv. Drug Deliv. Rev.* **64**, 1547–1568 (2012).

85. Hashmi, S. *et al.* Genetic transformation of nematodes using arrays of micromechanical piercing structures. *Biotechniques* **19**, 766–770 (1995).

86. Henry, S., Mcallister, D. V, Allen, M. G. & Prausnitz, M. R. Microfabricated Microneedles : A Novel Approach to Transdermal Drug Delivery. *J. Pharm. Sci. Vol.* **87**, 8–11 (1998).

87. Prausnitz, M. R. Microneedles for transdermal drug delivery. *Adv. Drug Deliv. Rev.* **56**, 581–587

(2004).

88. Atmar, R. L., Patel, S. M. & Keitel, W. A. Intanza ® : a new intradermal vaccine for seasonal influenza. *Expert Rev. Vaccines* **9**, 1399–1409 (2010).

89. Icardi, G., Orsi, A., Ceravolo, A. & Ansaldi, F. Current evidence on intradermal influenza vaccines administered by Soluvia™ licensed micro injection system. *Hum. Vaccin. Immunother.* **8**, 67–75 (2012).

90. Ansaldi, F., Durando, P. & Icardi, G. Intradermal influenza vaccine and new devices: a promising chance for vaccine improvement. *Expert Opin. Biol. Ther.* **11**, 415–427 (2011).

91. Sullivan, S. J., Jacobson, R. & Poland, G. A. Advances in the vaccination of the elderly against influenza: role of a high-dose vaccine. *Expert Rev. Vaccines* **9**, 1127–1133 (2010).

92. Bragazzi, N. L., Orsi, A., Ansaldi, F., Gasparini, R. & Icardi, G. Fluzone® intra-dermal (Intanza®/Istivac® Intra-dermal): An updated overview. (2016). doi:10.1080/21645515.2016.1187343

93. Sticchi, L., Alberti, M., Alicino, C. & Crovari, P. The intradermal vaccination: past experiences and current perspectives. *J. Prev. Med. Hyg.* **51**, 7–14 (2010).

94. Banks, S. L. *et al.* Flux across of microneedle-treated skin is increased by increasing charge of naltrexone and naltrexol in vitro. *Pharm. Res.* **25**, 1677–1685 (2008).

95. Bal, S. *et al.* In vivo visualization of microneedle conduits in human skin using laser scanning microscopy. *Laser Phys. Lett.* **7**, 242–246 (2010).

96. Gupta, J., Gill, H. S., Andrews, S. N. & Prausnitz, M. R. Kinetics of skin resealing after insertion of microneedles in human subjects. *J. Control. Release* **154**, 148–155 (2011).

97. Kalluri, H. & Banga, A. K. Formation and closure of microchannels in skin following microporation. *Pharm. Res.* **28**, 82–94 (2011).

98. Brogden, N. K. *et al.* Diclofenac delays micropore closure following microneedle treatment in human subjects. *J. Control. release* **163**, 220–9 (2012).

99. Ghosh, P., Brogden, N. K. & Stinchcomb, A. L. Fluvastatin as a micropore lifetime enhancer for sustained delivery across microneedle-treated skin. *J. Pharm. Sci.* **103**, 652–660 (2014).

100. Wermeling, D. P. *et al.* Microneedles permit transdermal delivery of a skin-impermeant medication to humans. *Proc. Natl. Acad. Sci.* **105**, 2058–2063 (2008).

101. Gill, H. S. & Prausnitz, M. R. Coated microneedles for transdermal delivery. *J. Control. Release* **117**, 227–237 (2007).

102. Davis, S. P., Landis, B. J., Adams, Z. H., Allen, M. G. & Prausnitz, M. R. Insertion of microneedles into skin : measurement and prediction of insertion force and needle fracture force. *J. Biomech.* **37**, 1155–1163 (2004).

103. Garland, M. J. *et al.* Microneedle arrays as medical devices for enhanced transdermal drug delivery. *Expert Rev. Med. Devices* **8**, 459–482 (2011).

104. Wang, P. M., Cornwell, M., Hill, J. & Prausnitz, M. R. Precise Microinjection into Skin Using Hollow Microneedles. *J. Invest. Dermatol.* **126**, 1080–1087 (2006).

105. Martanto, W., Moore, J. S., Couse, T. & Prausnitz, M. R. Mechanism of fluid infusion during microneedle insertion and retraction. *J. Control. Release* **112**, 357–361 (2006).

106. Gupta, J., Park, S. S., Bondy, B., Felner, E. I. & Prausnitz, M. R. Infusion pressure and pain during microneedle injection into skin of human subjects. *Biomaterials* **32**, 6823–6831 (2011).

107. Lee, J. W., Park, J. H. & Prausnitz, M. R. Dissolving microneedles for transdermal drug delivery. *Biomaterials* **29**, 2113–2124 (2008).

108. Bediz, B. *et al.* Dissolvable microneedle arrays for intradermal delivery of biologics: Fabrication and application. *Pharm. Res.* **31**, 117–135 (2014).

109. Demuth, P. C., Garcia-Beltran, W. F., Ai-Ling, M. L., Hammond, P. T. & Irvine, D. J. Composite dissolving microneedles for coordinated control of antigen and adjuvant delivery kinetics in transcutaneous vaccination. *Adv. Funct. Mater.* **23**, 161–172 (2013).

110. Sullivan, S. P., Murthy, N. & Prausnitz, M. R. Minimally invasive protein delivery with rapidly dissolving polymer microneedles. *Adv. Mater.* **20**, 933–938 (2008).

111. Miyano, T. *et al.* Sugar micro needles as transdermic drug delivery system. *Biomed. Microdevices* **7**, 185–188 (2005).

112. Loizidou, E. Z. *et al.* European Journal of Pharmaceutics and Biopharmaceutics Structural characterisation and transdermal delivery studies on sugar microneedles : Experimental and finite element modelling analyses. *Eur. J. Pharm. Biopharm.* **89**, 224–231 (2015).

113. Chen, W. *et al.* Improved polyvinylpyrrolidone microneedle arrays with non-stoichiometric cyclodextrin. *J. Mater. Chem. B* **2**, (2014).

114. Liu, S. *et al.* Transdermal delivery of relatively high molecular weight drugs using novel self-dissolving microneedle arrays fabricated from hyaluronic acid and their characteristics and safety after application to the skin. *Eur. J. Pharm. Biopharm.* **86**, 267–276 (2014).

115. Donnelly, R. F. *et al.* Hydrogel-forming microneedle arrays for enhanced transdermal drug delivery. *Adv. Funct. Mater.* **22**, 4879–4890 (2012).

116. Donnelly, R. F. *et al.* Hydrogel-forming microneedle arrays exhibit antimicrobial properties: Potential for enhanced patient safety. *Int. J. Pharm.* **451**, 76–91 (2013).

117. Donnelly, R. F. *et al.* Hydrogel-forming microneedles prepared from 'super swelling' polymers combined with lyophilised wafers for transdermal drug delivery. *PLoS One* **9**, (2014).

118. Gill, H. S., Denson, D. D., Burris, B. A. & Prausnitz, M. R. Effect of Microneedle Design on Pain in Human Volunteers. *Clin J Pain* **24**, 585–594 (2008).

119. Chen, M. C., Huang, S. F., Lai, K. Y. & Ling, M. H. Fully embeddable chitosan microneedles as a sustained release depot for intradermal vaccination. *Biomaterials* **34**, 3077–3086 (2013).

120. Kolli, C. S. & Banga, A. K. Characterization of solid maltose microneedles and their use for transdermal delivery. *Pharm. Res.* **25**, 104–113 (2008).

121. Chua, B., Desai, S. P., Tierney, M. J., Tamada, J. A. & Jina, A. N. Effect of microneedles shape on skin penetration and minimally invasive continuous glucose monitoring in vivo. *Sensors Actuators, A Phys.* **203**, 373–381 (2013).

122. Aoyagi, S., Izumi, H. & Fukuda, M. Biodegradable polymer needle with various tip angles and consideration on insertion mechanism of mosquito's proboscis. *Sensors Actuators A Phys.* **143**, 20–28 (2008).

123. Li, C. G., Lee, C. Y., Lee, K. & Jung, H. An optimized hollow microneedle for minimally invasive blood extraction. *Biomed Device* **15**, 17–25 (2012).

124. Zhao, X., Li, X., Zhang, P., Du, J. & Wang, Y. Tip-loaded fast-dissolving microneedle patches for photodynamic therapy of subcutaneous tumor. *J. Control. Release* **286**, 201–209 (2018).

125. Liu, S. *et al.* Improvement of Transdermal Delivery of Exendin-4 Using Novel Tip-Loaded Microneedle Arrays Fabricated from Hyaluronic Acid. *Mol. Pharm.* **13**, 272–279 (2016).

126. Donnelly, R. F. *et al.* Microneedle-mediated intradermal nanoparticle delivery: Potential for enhanced local administration of hydrophobic pre-formed photosensitisers. *Photodiagnosis Photodyn. Ther.* **7**, 222–231 (2010).

127. Van Der Maaden, K. *et al.* Layer-by-Layer Assembly of Inactivated Poliovirus and N-Trimethyl Chitosan on pH-Sensitive Microneedles for Dermal Vaccination. *Langmuir* **31**, 8654–8660 (2015).

128. Nguyen, H. & Banga, A. Enhanced skin delivery of vismodegib by microneedle treatment. *Drug*

Deliv. Transl. Res. **5**, 407–23 (2018).

129. Yu, W. *et al.* Polymer microneedles fabricated from alginate and hyaluronate for transdermal delivery of insulin. *Mater. Sci. Eng. C* **80**, 187–196 (2017).

130. Lee, J. Y., Park, S. H., Seo, I. H., Lee, K. J. & Ryu, W. H. Rapid and repeatable fabrication of high A/R silk fibroin microneedles using thermally-drawn micromolds. *Eur. J. Pharm. Biopharm.* **94**, 11–19 (2015).

131. Larrañeta, E. *et al.* Microwave-assisted preparation of hydrogel-forming microneedle arrays for transdermal drug delivery applications. *Macromol. Mater. Eng.* **300**, 586–595 (2015).

132. Zhang, Y., Jiang, G., Yu, W., Liu, D. & Xu, B. Microneedles fabricated from alginate and maltose for transdermal delivery of insulin on diabetic rats. *Mater. Sci. Eng. C* **85**, 18–26 (2018).

133. A.M., R., D.L., B., Bouwstra, J. A., F.P.T, B. & C.W.J, O. Monitoring the penetration process of single microneedles with varying tip diameters. *J. Mech. Behav. Biomed. Mater.* **40**, 397–405 (2014).

134. Du, G., Zhang, Z., He, P., Zhang, Z. & Sun, X. Journal of the Mechanical Behavior of Biomedical Materials Determination of the mechanical properties of polymeric microneedles by micromanipulation. *J. Mech. Behav. Biomed. Mater.* **117**, 104384 (2021).

135. Gittard, S. D. *et al.* The effects of geometry on skin penetration and failure of polymer microneedles. *J. Adhes. Sci. Technol.* **27**, 227–243 (2013).

136. Khanna, P., Luongo, K., Strom, J. A. & Bhansali, S. Axial and shear fracture strength evaluation of silicon microneedles. *Microsyst. Technol.* **16**, 973–978 (2010).

137. Donnelly, R. F. *et al.* Design , Optimization and Characterisation of Polymeric Microneedle Arrays Prepared by a Novel Laser-Based Micromoulding Technique. 41–57 (2011). doi:10.1007/s11095-010-0169-8

138. Lutton, R. E. M. *et al.* Microneedle characterisation: the need for universal acceptance criteria and GMP specifications when moving towards commercialisation. *Drug Deliv. Transl. Res.* **5**, 313–331 (2015).

139. Lee, H. S., Ryu, H. R., Roh, J. Y. & Park, J. H. Bleomycin-Coated Microneedles for Treatment of Warts. *Pharm. Res.* **34**, 101–112 (2017).

140. Kochhar, J. S. *et al.* Effect of microneedle geometry and supporting substrate on microneedle array penetration into skin. *J. Pharm. Sci.* **102**, 4100–4108 (2013).

141. Verbaan, F. J. *et al.* Improved piercing of microneedle arrays in dermatomed human skin by an impact insertion method. *J. Control. Release* **128**, 80–88 (2008).

142. Jeong, H. R., Kim, J. Y., Kim, S. N. & Park, J. H. Local dermal delivery of cyclosporin A, a hydrophobic and high molecular weight drug, using dissolving microneedles. *Eur. J. Pharm. Biopharm.* **127**, 237–243 (2018).

143. Yu, W. *et al.* Fabrication of biodegradable composite microneedles based on calcium sulfate and gelatin for transdermal delivery of insulin. *Mater. Sci. Eng. C* **71**, 725–734 (2017).

144. Ling, M. H. & Chen, M. C. Dissolving polymer microneedle patches for rapid and efficient transdermal delivery of insulin to diabetic rats. *Acta Biomater.* **9**, 8952–8961 (2013).

145. Kim, M. Y., Jung, B. & Park, J. H. Hydrogel swelling as a trigger to release biodegradable polymer microneedles in skin. *Biomaterials* **33**, 668–678 (2012).

146. Loizidou, E. Z., Inoue, N. T., Ashton-Barnett, J., Barrow, D. A. & Allender, C. J. Evaluation of geometrical effects of microneedles on skin penetration by CT scan and finite element analysis. *Eur. J. Pharm. Biopharm.* **107**, 1–6 (2016).

147. Lee, K., Lee, C. Y. & Jung, H. Dissolving microneedles for transdermal drug administration prepared by stepwise controlled drawing of maltose. *Biomaterials* **32**, 3134–3140 (2011).

148. Zhu, D. D., Wang, Q. L., Liu, X. B. & Guo, X. D. Rapidly separating microneedles for transdermal drug delivery. *Acta Biomater.* **41**, 312–319 (2016).

149. Donnelly, R. F. *et al.* Optical coherence tomography is a valuable tool in the study of the effects of microneedle geometry on skin penetration characteristics and in-skin dissolution. *J. Control. Release* **147**, 333–341 (2010).

150. Godin, B. & Touitou, E. Transdermal skin delivery: Predictions for humans from in vivo, ex vivo and animal models. *Adv. Drug Deliv. Rev.* **59**, 1152–1161 (2007).

151. Vora, L. K. *et al.* Novel bilayer dissolving microneedle arrays with concentrated PLGA nano-microparticles for targeted intradermal delivery: Proof of concept. *J. Control. Release* **265**, 93–101 (2017).

152. Moss, G. P., Gullick, D. R. & Wilkinson, S. C. Predictive methods in percutaneous absorption. *Predict. Methods Percutaneous Absorpt.* 1–199 (2015). doi:10.1007/978-3-662-47371-9

153. Franz, T. J. Percutaneous absorption. On the relevance of in vitro data. *J. Invest. Dermatol.* **64**, 190–195 (1975).

154. Benson, H. A. E., Watkinson, A. C. & Wiley InterScience (Online service). *Transdermal and topical drug delivery : principles and practice*. (Wiley, 2012).

155. Bronaugh, R. L. & Stewart, R. F. Methods for in vitro percutaneous absorption studies IV: The flow-through diffusion cell. *J. Pharm. Sci.* **74**, 64–67 (1985).

156. Cao, Y., Tao, Y., Zhou, Y. & Gui, S. Development of sinomenine hydrochloride-loaded polyvinylalcohol/maltose microneedle for transdermal delivery. *J. Drug Deliv. Sci. Technol.* **35**, 1–7 (2016).

157. Verbaan, F. J. *et al.* Assembled microneedle arrays enhance the transport of compounds varying over a large range of molecular weight across human dermatomed skin. *J. Control.*

Release **117**, 238–245 (2007).

158. Ng, K. W. *et al.* Development of an ex vivo human skin model for intradermal vaccination: Tissue viability and Langerhans cell behaviour. *Vaccine* **27**, 5948–5955 (2009).

159. Bronaugh, R., Stewart, R. & Simon, M. Methods for In Vitro Percutaneous Absorption Studies VII: Use of Excised Human Skin. *J. Pharm. Sci.* **75**, 1094–1097 (1986).

160. Gudjonsson, J. E., Johnston, A., Dyson, M., Valdimarsson, H. & Elder, J. T. Mouse Models of Psoriasis. *J. Invest. Dermatol.* 1292–1308 (2007). doi:10.1038/sj.jid.5700807

161. Moss, G. P., Gullick, D. R. & Wilkinson, S. C. Methods for the Measurement of Percutaneous Absorption. in *Predictive Methods in Percutaneous Absorption* 25–42 (Springer Berlin Heidelberg, 2015). doi:10.1007/978-3-662-47371-9_2

162. Jacobi, U. *et al.* Porcine ear skin : an in vitro model for human skin. *Ski. Res. Technol.* **13**, 19–24 (2007).

163. Ranamukhaarachchi, S. A., Lehnert, S., Ranamukhaarachchi, S. L. & Sprenger, L. A micromechanical comparison of human and porcine skin before and after preservation by freezing for medical device development. *Nat. Publ. Gr.* **6**, 1–9 (2016).

164. Netzlaff, F. *et al.* Comparison of bovine udder skin with human and porcine skin in percutaneous permeation experiments. *ATLA Altern. to Lab. Anim.* **34**, 499–513 (2006).

165. Dick, I. P. & Scott, R. C. Pig Ear Skin as an In-vitro Model for Human Skin Permeability. *J. Pharm. Pharmacol.* **44**, 640–645 (1992).

166. Sintov, A. C. & Greenberg, I. Comparative percutaneous permeation study using caffeine-loaded microemulsion showing low reliability of the frozen/thawed skin models. *Int. J. Pharm.* **471**, 516–524 (2014).

167. Barbero, A. M. & Frasch, H. F. Effect of Frozen Human Epidermis Storage Duration and

Cryoprotectant on Barrier Function Using Two Model Compounds. *Skin Pharmacol. Physiol.* **29**, 31–40 (2016).

168. Sanchez, W. Y., Prow, T. W., Sanchez, W. H., Grice, J. E. & Roberts, M. S. Analysis of the metabolic deterioration of ex vivo skin from ischemic necrosis through the imaging of intracellular NAD(P)H by multiphoton tomography and fluorescence lifetime imaging microscopy. *J. Biomed. Opt.* **15**, 046008 (2010).

169. Donnelly, R. F. *et al.* Microneedle-mediated intradermal delivery of 5-aminolevulinic acid: Potential for enhanced topical photodynamic therapy. *J. Control. Release* **129**, 154–162 (2008).

170. Mikolajewska, P. *et al.* Microneedle pre-treatment of human skin improves 5-aminolevulininc acid (ALA)- and 5-aminolevulinic acid methyl ester (MAL)-induced PpIX production for topical photodynamic therapy without increase in pain or erythema. *Pharm. Res.* **27**, 2213–2220 (2010).

171. Donnelly, R. F. *et al.* Microneedle arrays permit enhanced intradermal delivery of a preformed photosensitizer. *Photochem. Photobiol.* **85**, 195–204 (2009).

172. Zhang, J. *et al.* Use of Drawing Lithography-Fabricated Polyglycolic Acid Microneedles for Transdermal Delivery of Itraconazole to a Human Basal Cell Carcinoma Model Regenerated on Mice. *Jom* **68**, 1128–1133 (2016).

173. Donnelly, R. F. *et al.* Hydrogel-forming and dissolving microneedles for enhanced delivery of photosensitizers and precursors. *Photochem. Photobiol.* **90**, 641–647 (2014).

174. Kolde, G., Rowe, E. & Meffert, H. Effective photodynamic therapy of actinic keratoses and Bowen's disease using microneedle perforation. *Br. J. Dermatol.* **168**, 450–452 (2013).

175. Jain, A. K., Lee, C. H. & Gill, H. S. 5-Aminolevulinic acid coated microneedles for photodynamic therapy of skin tumors. *J. Control. Release* **239**, 72–81 (2016).

176. Wang, C., Ye, Y., Hochu, G. M., Sadeghifar, H. & Gu, Z. Enhanced Cancer Immunotherapy by Microneedle Patch-Assisted Delivery of Anti-PD1 Antibody. *Nano Lett.* **16**, 2334–2340 (2016).

177. Ye, Y. *et al.* Synergistic Transcutaneous Immunotherapy Enhances Antitumor Immune Responses through Delivery of Checkpoint Inhibitors. *ACS Nano* **10**, 8956–8963 (2016).

178. Bhowmik, T. *et al.* A novel microparticulate vaccine for melanoma cancer using transdermal delivery. *J. Microencapsul.* **28**, 294–300 (2011).

179. Hu, Y. *et al.* Microneedle-assisted dendritic cell-targeted nanoparticles for transcutaneous DNA immunization. *Polym. Chem.* **6**, 373–379 (2015).

180. Zeng, Q., Gammon, J. M., Tostanoski, L. H., Chiu, Y. C. & Jewell, C. M. In Vivo Expansion of Melanoma-Specific T Cells Using Microneedle Arrays Coated with Immune-Polyelectrolyte Multilayers. *ACS Biomater. Sci. Eng.* **3**, 195–205 (2017).

181. Wang, X. *et al.* Treating cutaneous squamous cell carcinoma using 5-aminolevulinic acid polylactic-co-glycolic acid nanoparticle-mediated photodynamic therapy in a mouse model. *Int. J. Nanomedicine* **10**, 347 (2015).

182. Chen, M. C., Lin, Z. W. & Ling, M. H. Near-infrared light-activatable microneedle system for treating superficial tumors by combination of chemotherapy and photothermal therapy. *ACS Nano* **10**, 93–101 (2016).

183. Dong, L. *et al.* Au Nanocage-Strengthened Dissolving Microneedles for Chemo-Photothermal Combined Therapy of Superficial Skin Tumors. *ACS Appl. Mater. Interfaces* **10**, 9247–9256 (2018).

184. Pan, J. *et al.* Intradermal delivery of STAT3 siRNA to treat melanoma via dissolving microneedles. *Sci. Rep.* **8**, 1–11 (2018).

185. Hamdan, I. M. N. *et al.* Intradermal Delivery of a Near-infrared Photosensitizer Using Dissolving

Microneedle Arrays. *J. Pharm. Sci.* **107**, 1–12 (2018).

186. Ruan, W., Zhai, Y., Yu, K., Wu, C. & Xu, Y. Coated microneedles mediated intradermal delivery of octaarginine / BRAF siRNA nanocomplexes for anti-melanoma treatment. *Int. J. Pharm.* **553**, 298–309 (2018).

187. Hao, Y. *et al.* Near-Infrared Responsive PEGylated Gold Nanorod and Doxorubicin Loaded Dissolvable Hyaluronic Acid Microneedles for Human Epidermoid Cancer Therapy. *Adv. Ther.* **1800008**, 1–14 (2018).

188. Tham, H. P. *et al.* Microneedle-Assisted Topical Delivery of Photodynamically Active Mesoporous Formulation for Combination Therapy of Deep-Seated Melanoma. *ACS Nano* **12**, 11936–11948 (2018).

189. Pei, P., Yang, F., Liu, J., Hu, H. & Du, X. Composite-dissolving microneedle patches for chemotherapy and photothermal therapy in superficial tumor treatment. *Biomater. Sci.* **6**, 1414–1423 (2018).

190. Hao, Y. *et al.* Near-infrared responsive 5-fluorouracil and indocyanine green loaded MPEG-PCL nanoparticle integrated with dissolvable microneedle for skin cancer therapy. *Bioact. Mater.* **5**, 542–552 (2020).

191. Uddin, M. J. *et al.* 3D printed microneedles for anticancer therapy of skin tumours. *Mater. Sci. Eng. C* **107**, 110248 (2020).

192. Song, G. *et al.* Separable Microneedles for Synergistic Chemo-Photothermal Therapy against Superficial Skin Tumors. *ACS Biomater. Sci. Eng.* **6**, 4116–4125 (2020).

193. Abdelghany, S. *et al.* Nanosuspension-based dissolving microneedle arrays for intradermal delivery of curcumin. *Pharmaceutics* **11**, (2019).

194. Kim, H. *et al.* Biodegradable Microneedle Patch Delivering Antigenic Peptide–Hyaluronate

Conjugate for Cancer Immunotherapy. *ACS Biomater. Sci. Eng.* **5**, 5150–5158 (2019).

195. Chen, Y. *et al.* Multifunctional Graphene-Oxide-Reinforced Dissolvable Polymeric Microneedles for Transdermal Drug Delivery. *ACS Appl. Mater. Interfaces* **12**, 352–360 (2020).

196. Wang, C., Ye, Y. & Gu, Z. Local delivery of checkpoints antibodies. *Hum. Vaccines Immunother.* **13**, 245–248 (2017).

197. Starr, N. J. *et al.* Enhanced vitamin C skin permeation from supramolecular hydrogels , illustrated using in situ ToF-SIMS 3D chemical profiling. *Int. J. Pharm.* **563**, 21–29 (2019).

198. Vasquez, K. O., Casavant, C. & Peterson, J. D. Quantitative Whole Body Biodistribution of Fluorescent- Labeled Agents by Non-Invasive Tomographic Imaging. *PLoS One* **6**, (2011).

199. Zhang, G., Moore, D. J., Sloan, K. B., Flach, C. R. & Mendelsohn, R. Imaging the Prodrug-to-Drug Transformation of a 5-Fluorouracil Derivative in Skin by Confocal Raman Microscopy. *J. Invest. Dermatol.* **127**, 1205–1209 (2007).

200. Saar, B. G., Contreras-Rojas, L. R., Xie, X. S. & Guy, R. H. Imaging drug delivery to skin with stimulated raman scattering microscopy. *Mol. Pharm.* **8**, 969–975 (2011).

201. Votteler, M. *et al.* Raman spectroscopy for the non-contact and non-destructive monitoring of collagen damage within tissues. *J. Biophotonics* **5**, 47–56 (2012).

202. Förster, M., Bolzinger, M. A., Montagnac, G. & Briançon, S. Confocal raman microspectroscopy of the skin. *Eur. J. Dermatology* **21**, 851–863 (2011).

203. Touboul, D., Brunelle, A. & Laprévote, O. Improvement of Biological Time-of-Flight- Secondary Ion Mass Spectrometry Imaging with a Bismuth Cluster Ion Source. *J Am Soc Mass Spectrom* **16**, 1608–1618 (2005).

204. Vandikas, M., Hellström, E., Malmberg, P. & Osmancevic, A. Imaging of vitamin D in psoriatic skin using time-of- flight secondary ion mass spectrometry (ToF-SIMS): A pilot case study. *J.*

Steroid Biochem. Mol. Biol. **189**, 154–160 (2019).

205. Saleem, M. & Galla, H. J. Surface view of the lateral organization of lipids and proteins in lung surfactant model systems-A ToF-SIMS approach. *Biochim. Biophys. Acta - Biomembr.* **1798**, 730–740 (2010).

206. Briggs, D. (David) & Seah, M. P. *Practical surface analysis*. (Wiley, 1990).

207. Berman, E. S. F. *et al.* Chemometric and statistical analyses of ToF-SIMS spectra of increasingly complex biological samples. *Surf. Interface Anal.* **41**, 97–104 (2009).

208. Sodhi, R. N. S. Time-of-flight secondary ion mass spectrometry (TOF-SIMS):— versatility in chemical and imaging surface analysis. *Analyst* **129**, 483–487 (2004).

209. Watrous, J. D. & Dorrestein, P. C. Imaging mass spectrometry in microbiology. *Nat. Rev. Microbiol.* **9**, 683–694 (2011).

210. Vickerman, J. C. *ToF-SIMS — An Overview*. (2016).

211. Rabbani, S., Barber, A. M., Fletcher, J. S., Lockyer, N. P. & Vickerman, J. C. TOF-SIMS with argon gas cluster ion beams: A comparison with C 60+. *Anal. Chem.* **83**, 3793–3800 (2011).

212. Wagner, M. S. Molecular depth profiling of multilayer polymer films using time-of-flight secondary ion mass spectrometry. *Anal. Chem.* **77**, 911–922 (2005).

213. Mahoney, C. M., Kushmerick, J. G. & Steffens, K. L. Investigation of damage mechanisms in PMMA during ToF-SIMS depth profiling with 5 and 8 keV SF5 + primary ions. *J. Phys. Chem. C* **114**, 14510–14519 (2010).

214. Gillen, G. & Roberson, S. Preliminary evaluation of an SF5+ polyatomic primary ion beam for analysis of organic thin films by secondary ion mass spectrometry. *Rapid Commun. Mass Spectrom.* **12**, 1303–12 (1998).

215. Muramoto, S. *et al.* ToF-SIMS analysis of adsorbed proteins: Principal component analysis of

the primary ion species effect on the protein fragmentation patterns. *J. Phys. Chem. C* **115**, 24247–24255 (2011).

216. Oshima, S., Kashihara, I., Moritani, K., Inui, N. & Mochiji, K. Soft-sputtering of insulin films in argon-cluster secondary ion mass spectrometry. *Rapid Commun. Mass Spectrom.* **25**, 1070–1074 (2011).

217. Denbigh, J. L. & Lockyer, N. P. ToF-SIMS as a tool for profiling lipids in cancer and other diseases. *Mater. Sci. Technol.* **31**, 137–147 (2015).

218. Park, J.-W. *et al.* Differentiation between human normal colon mucosa and colon cancer tissue using ToF-SIMS imaging technique and principal component analysis. *Appl. Surf. Sci.* **255**, 1119–1122 (2008).

219. Kulp, K. S. *et al.* Chemical and biological differentiation of three human breast cancer cell types using time-of-flight secondary ion mass spectrometry. *Anal. Chem.* **78**, 3651–3658 (2006).

220. Baker, M. J. *et al.* ToF-SIMS PC-DFA analysis of prostate cancer cell lines. *Appl. Surf. Sci.* **255**, 1084–1087 (2008).

221. Gazi, E. *et al.* Imaging ToF-SIMS and synchrotron-based FT-IR microspectroscopic studies of prostate cancer cell lines. *Appl. Surf. Sci.* **231**–**232**, 452–456 (2004).

222. Starr, N. J. *et al.* Age-Related Changes to Human Stratum Corneum Lipids Detected Using Time-of-Flight Secondary Ion Mass Spectrometry Following in Vivo Sampling. *Anal. Chem.* **88**, 4400–4408 (2016).

223. Judd, A. M., Scurr, D. J., Heylings, J. R., Wan, K. & Gary, P. Distribution and Visualisation of Chlorhexidine Within the Skin Using ToF-SIMS : A Potential Platform for the Design of More Efficacious Skin Antiseptic Formulations. *Pharm Res* **30**, 1896–1905 (2013).

224. Sjövall, P. *et al.* Imaging of distribution of topically applied drug molecules in mouse skin by

combination of time-of-flight secondary ion mass spectrometry and scanning electron microscopy. *Anal. Chem.* **86**, 3443–3452 (2014).

225. Kubo, A. *et al.* The stratum corneum comprises three layers with distinct metal-ion barrier properties. *Sci. Rep.* **3**, 1731 (2013).

226. Okamoto, M., Tanji, N., Katayama, Y. & Okada, J. TOF-SIMS investigation of the distribution of a cosmetic ingredient in the epidermis of the skin. *Appl. Surf. Sci.* **252**, 6805–6808 (2006).

227. Holmes, A. M., Scurr, D. J., Heylings, J. R., Wan, K. & Moss, G. P. Dendrimer pre-treatment enhances the skin permeation of chlorhexidine digluconate: Characterisation by in vitro percutaneous absorption studies and Time-of-Flight Secondary Ion Mass Spectrometry. *Eur. J. Pharm. Sci.* **104**, 90–101 (2017).

228. Kezutyte, T., Desbenoit, N., Brunelle, A. & Briedis, V. Studying the penetration of fatty acids into human skin by ex vivo TOF-SIMS imaging. *Biointerphases* **8**, 3 (2013).

229. Čižinauskas, V., Elie, N., Brunelle, A. & Briedis, V. Fatty acids penetration into human skin *ex vivo* : A TOF-SIMS analysis approach. *Biointerphases* **12**, 011003 (2017).

230. Čižinauskas, V., Elie, N., Brunelle, A. & Briedis, V. Skin Penetration Enhancement by Natural Oils for Dihydroquercetin Delivery. *Molecules* **22**, 1536 (2017).

231. Sjövall, P. *et al.* Imaging the distribution of skin lipids and topically applied compounds in human skin using mass spectrometry. *Sci. Rep.* **8**, 1–14 (2018).

232. Kawashima, T., Aoki, T., Taniike, Y. & Aoyagi, S. Examination of beauty ingredient distribution in the human skin by time-of-flight secondary ion mass spectrometry. *Biointerphases* **15**, 031013 (2020).

233. Matter, M. T. *et al.* Multiscale Analysis of Metal Oxide Nanoparticles in Tissue: Insights into Biodistribution and Biotransformation. *Adv. Sci.* **7**, 1–11 (2020).

234. Gilmore, I. S. & Seah, M. P. Electron flood gun damage in the analysis of polymers and organics in time-of-flight SIMS. *Appl. Surf. Sci.* **187**, 89–100 (2002).

235. Kezutyte, T., Desbenoit, N., Brunelle, A. & Briedis, V. Studying the penetration of fatty acids into human skin by ex vivo TOF-SIMS imaging. *Biointerphases* **8**, 3 (2013).

236. Candi, E., Schmidt, R. & Melino, G. The cornified envelope: A model of cell death in the skin. *Nat. Rev. Mol. Cell Biol.* **6**, 328–340 (2005).

237. Sabri, A. *et al.* Expanding the applications of microneedles in dermatology. *Eur. J. Pharm. Biopharm.* **140**, 121–140 (2019).

238. Kaushik, S. *et al.* Lack of Pain Associated with Microfabricated Microneedles. 2000–2002 (2001).

239. Hurtado, M. M., Peppelman, M., Zeng, X., van Erp, P. E. J. & Van Der Heide, E. Tribological behaviour of skin equivalents and ex-vivo human skin against the material components of artificial turf in sliding contact. *Tribol. Int.* **102**, 103–113 (2016).

240. Edwards, C., Heggie, R. & Marks, R. A study of differences in surface roughness between sun-exposed and unexposed skin with age. *Photodermatol. Photoimmunol. Photomed.* **19**, 169–174 (2003).

241. Nagano, K. *et al.* Skin microstructure deformation with displacement map convolution. *ACM Trans. Graph.* **34**, (2015).

242. WA, W. A. Biaxial tension test of human skin in vivo. *Biomed Mater Eng* **4**, 473–86 (1994).

243. Keyes, J. *et al.* Design and Demonstration of a Microbiaxial Optomechanical Device for Multiscale Characterization of Soft Biological Tissues with Two-Photon Microscopy. *Microsc Microanal* **17**, 167–75 (2011).

244. Lanir, Y. & Fung, Y. Two-dimentional Mechanical Properties of Rabbit Skin - II Experimental

Results. *J. Biomech.* **7**, 171–182 (1973).

245. Flynn, C. & Rubin, M. B. An anisotropic discrete fibre model based on a generalised strain invariant with application to soft biological tissues. *Int. J. Eng. Sci.* **60**, 66–76 (2012).

246. Benech-Kieffer, F. *et al.* Percutaneous Absorption of Sunscreens in vitro: Interspecies Comparison, Skin Models and Reproducibility Aspects. *Skin Pharmacol. Physiol.* **13**, 324–335 (2000).

247. Badran, M. M., Kuntsche, J. & Fahr, A. Skin penetration enhancement by a microneedle device (Dermaroller) in vitro: Dependency on needle size and applied formulation. *Eur. J. Pharm. Sci.* **36**, 511–523 (2009).

248. Larrañeta, E. *et al.* A proposed model membrane and test method for microneedle insertion studies. *Int. J. Pharm.* **472**, 65–73 (2014).

249. Bhatnagar, S., Dave, K. & Venuganti, V. V. K. Microneedles in the clinic. *J. Control. Release* **260**, 164–182 (2017).

250. Maiti, R. *et al.* In vivo measurement of skin surface strain and sub-surface layer deformation induced by natural tissue stretching. *journa l Mech. Behav. Biomed. Mater.* **62**, 556–569 (2016).

251. Maiti, R. *et al.* In vivo measurement of skin surface strain and sub-surface layer deformation induced by natural tissue stretching. *J. Mech. Behav. Biomed. Mater.* **62**, 556–569 (2016).

252. Hutton, A. R. J. *et al.* Transdermal delivery of vitamin K using dissolving microneedles for the prevention of vitamin K de fi ciency bleeding. *Int. J. Pharm.* **541**, 56–63 (2018).

253. Andrews, S. N., Jeong, E. & Prausnitz, M. R. Transdermal delivery of molecules is limited by full epidermis, not just stratum corneum. *Pharm. Res.* **30**, 1099–1109 (2013).

254. Mccrudden, M. T. C. *et al.* Microneedle applications in improving skin appearance. *Exp. Dermatol.* **24**, 561–566 (2015).

255. Izumi, H. *et al.* Combined harpoonlike jagged microneedles imitating Mosquito's proboscis and its insertion experiment with vibration. *Electr. Eng. Japan* **3**, 425–431 (2008).

256. Yokoyama, Y. & Okabe, S. Reduction of kinetic friction by harmonic vibration in an arbitrary direction. *Bull. JSME-Japan Soc. Mech. Eng.* **14**, 139–146 (1971).

257. Olatunji, O., Das, D. B., Garland, M. J., Belaid, L. & Donnelly, R. F. Influence of Array Interspacing on the Force Required for Successful Microneedle Skin Penetration: Theoretical and Practical Approaches. *J. Pharm. Sci.* **102**, 1209–1221 (2013).

258. Xiang, X. *et al.* Quantitative Assessment of Healthy Skin Elasticity: Reliability and Feasibility of Shear Wave Elastography. *Ultrasound Med. Biol.* **43**, 445–452 (2017).

259. Valentini, L., Bittolo Bon, S., Lopez-Manchado, M. A., Mussolin, L. & Pugno, N. Development of conductive paraffin/graphene films laminated on fluoroelastomers with high strain recovery and anti-corrosive properties. *Compos. Sci. Technol.* **149**, 254–261 (2017).

260. Branski, L. K. *et al.* A porcine model of full-thickness burn, excision and skin autografting. *Burns* **34**, 1119–1127 (2008).

261. Aziz, J. *et al.* Molecular Mechanisms of Stress-Responsive Changes in Collagen and Elastin Networks in Skin. *Ski. Pharmacol Physiol* **629**, 190–203 (2016).

262. Kim, Y. C., Park, J.-H. & Prausnitz, M. R. Microneedles for drug and vaccine delivery. *Adv. Drug Deliv. Rev.* **64**, 1547–1568 (2012).

263. Prieto-Granada, C. & Rodriguez-Waitkus, P. Basal cell carcinoma: Epidemiology, clinical and histologic features, and basic science overview. *Curr. Probl. Cancer* **39**, 198–205 (2015).

264. Franchimont, C., Pierard, G. E. & Cauwenberge, D. V. A. N. Episodic progression and regression of basal cell carcinomas. *Br. J. Dermatol.* **106**, 305–310 (1982).

265. Tinelli, M., Ozolins, M., Bath-hextall, F. & Williams, H. C. What determines patient preferences

for treating low risk basal cell carcinoma when comparing surgery vs imiquimod ? A discrete choice experiment survey from the SINS trial. *BMC Dernatology* **12**, 1–11 (2012).

266. Nakagawa, N., Matsumoto, M. & Sakai, S. In vivo measurement of the water content in the dermis by confocal Raman spectroscopy. *Ski. Res. Technol.* **1**, 137–141 (2010).

267. Yang, Y. *et al.* Effect of Size, Surface Charge, and Hydrophobicity of Poly(amidoamine) Dendrimers on Their Skin Penetration. *Biomacromol* **13**, 2154−2162 (2012).

268. Judd, A. M., Scurr, D. J., Heylings, J. R., Wan, K.-W. & Moss, G. P. Distribution and Visualisation of Chlorhexidine Within the Skin Using ToF-SIMS: A Potential Platform for the Design of More Efficacious Skin Antiseptic Formulations. *Pharm. Res.* **30**, 1896–1905 (2013).

269. Mccaffrey, J., Donnelly, R. F. & Mccarthy, H. O. Microneedles : an innovative platform for gene delivery. *Drug Deliv. Transl. Res.* **5**, 424–437 (2015).

270. Gujjar, M., Arbiser, J., Coulon, R. & Banga, A. K. Localized delivery of a lipophilic proteasome inhibitor into human skin for treatment of psoriasis. *J. Drug Target.* **2330**, 1–5 (2015).

271. Davies, D. J., Ward, R. J. & Heylings, J. R. Multi-species assessment of electrical resistance as a skin integrity marker for in vitro percutaneous absorption studies. *Toxicol. Vitr.* **18**, 351–358 (2004).

272. Chen, Q. & Thouas, G. A. Metallic implant biomaterials. *Mater. Sci. Eng. R Reports* **87**, 1–57 (2015).

273. Niinomi, M. Recent research and development in metallic materials for biomedical, dental and healthcare products applications. *Metall. Mater. Trans. A* **33A**, 477–486 (2002).

274. Ahmed Saeed AL-Japairai, K. *et al.* Current trends in polymer microneedle for transdermal drug delivery. *Int. J. Pharm.* **587**, 119673 (2020).

275. Stein, P. *et al.* Efficacy of Imiquimod-Based Transcutaneous Immunization Using a Nano-

Dispersed Emulsion Gel Formulation. *PLoS One* **9**, e102664 (2014).

276. Maibach, H. I. Dermal Absorption Models in Toxicology and Pharmacology. *Clin. Toxicol.* **45**, 736–736 (2007).

277. Banga, A. K. Microporation applications for enhancing drug delivery. *Expert Opin. Drug Deliv.* **6**, 343–354 (2009).

278. Ng, S.-F., Rouse, J. J., Sanderson, F. D., Meidan, V. & Eccleston, G. M. Validation of a Static Franz Diffusion Cell System for In Vitro Permeation Studies. *AAPS PharmSciTech* **11**, 1432–1441 (2010).

279. Tranoulis, A., Laios, A., Mitsopoulos, V., Lutchman-Singh, K. & Thomakos, N. Efficacy of 5% imiquimod for the treatment of Vaginal intraepithelial neoplasia—A systematic review of the literature and a meta-analysis. *Eur. J. Obstet. Gynecol. Reprod. Biol.* **218**, 129–136 (2017).

280. Johnsen, G. K., Martinsen, Ø. G. & Grimnes, S. Estimation of In Vivo Water Content of the Stratum Corneum from Electrical Measurements. *Open Biomed. Eng. J.* **3**, 8–12 (2009).

281. Porta Siegel, T. *et al.* Mass Spectrometry Imaging and Integration with Other Imaging Modalities for Greater Molecular Understanding of Biological Tissues. *Mol. Imaging Biol.* **20**, 888–901 (2018).

282. Elias, P. M. Stratum Corneum Defensive Functions : An Integrated View. *J. Invest. Dermatol.* **125**, 183–200 (2005).

283. Milewski, M. & Stinchcomb, A. L. Vehicle Composition Influence on the Microneedle-Enhanced Transdermal Flux of Naltrexone Hydrochloride. *Pharm Res* **28**, 124–134 (2011).

284. Buhse, L. *et al.* Topical drug classification. *Int. J. Pharm.* **295**, 101–112 (2005).

285. Aungst, B. J. Structure/Effects Studies of Fatty Acid Isomers as Skin Penetration Enhancers and Skin Irritants. *Pharmaceutical Research* **6**, 244–247 (1989).

286. Walter, A. *et al.* Aldara activates TLR7-independent immune defence. *Nat. Commun.* **4**, 1560 (2013).

287. Offeman, R. D., Franqui-espiet, D., Cline, J. L., Robertson, G. H. & Orts, W. J. Extraction of ethanol with higher carboxylic acid solvents and their toxicity to yeast. *Sep. Purif. Technol.* **72**, 180–185 (2010).

288. Zduńska, K., Kołodziejczak, A. & Rotsztejn, H. Is skin microneedling a good alternative method of various skin defects removal. *Dermatol. Ther.* **31**, 1–8 (2018).

289. Singh, T. R. R., Dunne, N. J., Cunningham, E. & Donnelly, R. F. Review of patents on microneedle applicators. *Recent Pat. Drug Deliv. Formul.* **5**, 11–23 (2011).

290. Lin, W. *et al.* Well-defined star polymers for co-delivery of plasmid DNA and imiquimod to dendritic cells. *Acta Biomater.* **48**, 378–389 (2017).

291. Egawa, M., Arimoto, H., Hirao, T., Takahashi, M. & Ozaki, Y. Regional difference of water content in human skin studied by diffuse-reflectance near-infrared spectroscopy: Consideration of measurement depth. *Appl. Spectrosc.* **60**, 24–28 (2006).

292. Sauder, D. N. Immunomodulatory and pharmacologic properties of imiquimod. *J. Am. Acad. Dermatol.* **43**, S6–S11 (2000).

293. Prausnitz, M. R. Microneedles for transdermal drug delivery. *Adv. Drug Deliv. Rev.* **56**, 581–587 (2004).

294. Kolter, K. & Flick, D. Structure and dry binding activity of different polymers, including Kollidon® VA 64. *Drug Dev. Ind. Pharm.* **26**, 1159–1165 (2000).

295. Patel, D., Kumar, P. & Thakkar, H. P. Journal of Drug Delivery Science and Technology Lopinavir metered-dose transdermal spray through microporated skin : Permeation enhancement to achieve therapeutic needs. *J. Drug Deliv. Sci. Technol.* **29**, 173–180 (2015).

296. Teodorescu, M. & Bercea, M. Polymer-Plastics Technology and Engineering Poly (vinylpyrrolidone) – A Versatile Polymer for Biomedical and Beyond Medical Applications Poly (vinylpyrrolidone) – A Versatile Polymer for Biomedical and Beyond Medical Applications. *Polym. Plast. Technol. Eng.* **54**, 923–943 (2015).

297. Taresco, V. *et al.* Rapid Nanogram Scale Screening Method of Microarrays to Evaluate Drug-Polymer Blends Using High-Throughput Printing Technology. *Mol. Pharm.* **14**, 2079–2087 (2017).

298. García-López, E., Siller, H. R. & Rodríguez, C. A. Study of the fabrication of AISI 316L microneedle arrays. *Procedia Manuf.* **26**, 117–124 (2018).

299. Lutton, R. E. M. *et al.* A novel scalable manufacturing process for the production of hydrogel-forming microneedle arrays. *Int. J. Pharm.* **494**, 417–429 (2015).

300. Mahomed, A., Hukins, D. W. L. & Kukureka, S. N. Swelling of medical grade silicones in liquids and calculation of their cross-link densities. *Med. Eng. Phys.* **32**, 298–303 (2010).

301. Ronnander, P., Simon, L., Spilgies, H., Koch, A. & Scherr, S. Dissolving polyvinylpyrrolidone-based microneedle systems for in-vitro delivery of sumatriptan succinate. *Eur. J. Pharm. Sci.* **114**, 84–92 (2018).

302. Dillon, C., Hughes, H., Reilly, N. J. O. & Mcloughlin, P. Formulation and characterisation of dissolving microneedles for the transdermal delivery of therapeutic peptides. *Int. J. Pharm.* **526**, 125–136 (2017).

303. Quinn, H. L., Bonham, L., Hughes, C. M. & Donnelly, R. F. Design of a Dissolving Microneedle Platform for Transdermal Delivery of a Fixed-Dose Combination of Cardiovascular Drugs. *J. Pharm. Sci.* **104**, 3490–3500 (2015).

304. Moore, A. 7 Final Report on the Safety Assessment of Polyvinylpyrrolidone/Vinyl Acetate Copolymer. *Int. J. Toxicol.* **2**, 141–159 (1983).

305. Sun, W. *et al.* Polyvinylpyrrolidone microneedles enable delivery of intact proteins for diagnostic and therapeutic applications. *Acta Biomater.* **9**, 7767–7774 (2013).

306. Xue, P., Zhang, X., Chuah, Y. J., Wu, Y. & Kang, Y. Flexible PEGDA-based microneedle patches with detachable PVP-CD arrowheads for transdermal drug delivery. *RSC Adv.* **5**, 75204–75209 (2015).

307. McGrath, M. G. *et al.* Production of dissolvable microneedles using an atomised spray process: Effect of microneedle composition on skin penetration. *Eur. J. Pharm. Biopharm.* **86**, 200–211 (2014).

308. Park, Y. *et al.* Fabrication of Degradable Carboxymethyl Cellulose (CMC) Microneedle with Laser Writing and Replica Molding Process for Enhancement of Transdermal Drug Delivery. **118**, 110–118 (2016).

309. Vicente-pérez, E. M. *et al.* The Use of a Pressure-Indicating Sensor Film to Provide Feedback upon Hydrogel-Forming Microneedle Array Self-Application In Vivo. *Pharm. Res.* **33**, 3072–3080 (2016).

310. Albanna, M. & Holmes IV, J. *Skin Tissue Engineering and Regenerative Medicine*. (Academic Press, 2016).

311. Carr, A. V., Feller, E., Zakka, F. R., Griffith, R. C. & Schechter, S. A Case Report of Basal Cell Carcinoma in a Non-Sun-Exposed Area: A Rare Presentation Mimicking Recurrent Perianal Abscess. *Case Rep. Surg.* **2018**, 1–5 (2018).

312. Shamblin, S. L. & Zografi, G. The effects of absorbed water on the properties of amorphous mixtures containing sucrose. *Pharmaceutical Research* **16**, 1119–1124 (1999).

313. Mccrudden, M. T. C. *et al.* Considerations in the sterile manufacture of polymeric microneedle arrays. *Drug Deliv. Transl. Res.* **5**, 3–14 (2014).

314. FDA. Food and Drug Administration approval for imiquimod - Aldara cream 5%. (1997).

315. Rossi, A. *et al.* Minoxidil Use in Dermatology, Side Effects and Recent Patents. *Recent Pat. Inflamm. Allergy Drug Discov.* **6**, 130–136 (2012).

316. Rehman, K. *et al.* Probing the effects of fish oil on the delivery and inflammation-inducing potential of imiquimod. *Int. J. Pharm.* **490**, 131–141 (2015).

317. Buchmann, S. Main Cosmetic Vehicles. in *Handbook of Cosmetic Science and Technology* (eds. Barel, A., Paye, M. & Maibach, H.) 99–124 (Taylor & Francis, 2005).

318. González-vázquez, P. *et al.* Transdermal delivery of gentamicin using dissolving microneedle arrays for potential treatment of neonatal sepsis. *J. Control. Release* 0–1 (2017). doi:10.1016/j.jconrel.2017.07.032

319. Jung, J. E., Rah, D. K. & Kim, Y. O. Effects of preoperative biopsies on recurrence in head and neck skin cancer. *Arch. Plast. Surg.* **39**, 518–521 (2012).

320. Kamyab-Hesari, K. *et al.* Diagnostic accuracy of punch biopsy in subtyping basal cell carcinoma. *J. Eur. Acad. Dermatology Venereol.* **28**, 250–253 (2014).

321. Saurer, E. M., Flessner, R. M., Sullivan, S. P., Prausnitz, M. R. & Lynn, D. M. Layer-by-layer assembly of DNA- and protein-containing films on microneedles for drug delivery to the skin. *Biomacromolecules* **11**, 3136–3143 (2010).

322. Kagan, L. *et al.* The role of the lymphatic system in subcutaneous absorption of macromolecules in the rat model. *Eur. J. Pharm. Biopharm.* **67**, 759–765 (2007).

323. Yamaoka, T., Tabata, T. & Ikada, Y. Comparison of Body Distribution of Poly (viny1 alcohol) with Other Water-soluble Polymers after Intravenous Administration. 479–486 (1995).

324. Hespe, W., Meier, A. M. & Blankwater, Y. J. Excretion and distribution studies in rats with two forms of 14carbon-labelled polyvinylpyrrolidone with a relatively low mean molecular weight

after intravenous administration - PubMed. *Arzneimittelforschung* 1158–1162 (1977). Available at: https://pubmed.ncbi.nlm.nih.gov/578432/. (Accessed: 25th July 2020)

325. Jacobi, U., Tassopoulos, T., Surber, C. & Lademann, J. Cutaneous distribution and localization of dyes affected by vehicles all with different lipophilicity. *Arch. Dermatol. Res.* **297**, 303–310 (2006).

326. Lademann, J. *et al.* Influence of nonhomogeneous distribution of topically applied UV filters on sun protection factors. *J. Biomed. Opt.* **9**, 1358 (2004).

327. Chapman, S. J., Walsh, A., Jackson, S. M. & Friedmann, P. S. Lipids, proteins and corneocyte adhesion. *Arch. Dermatol. Res.* **283**, 167–73 (1991).

328. Dacosta Byfield, S., Chen, D., Yim, Y. M. & Reyes, C. Age distribution of patients with advanced non-melanoma skin cancer in the United States. *Arch. Dermatol. Res.* **305**, 845–850 (2013).

329. Jensen, A. *et al.* Mortality in Danish patients with nonmelanoma skin cancer, 1978-2001. *Br. J. Dermatol.* **159**, 419–425 (2008).

330. Stern, R. S. Cost effectiveness of Mohs micrographic surgery. *J. Invest. Dermatol.* **133**, 1129–1131 (2013).

331. Paredes, A. J. *et al.* Microarray Patches : Poking a Hole in the Challenges Faced When Delivering Poorly Soluble Drugs. *Adv. Funct. Mater.* **2005792**, 1–27 (2020).

332. Sabri, A. H. *et al.* Intradermal delivery of imiquimod using polymeric microneedles for basal cell carcinoma. *Int. J. Pharm.* **589**, 119808 (2020).

333. Ahmad, S. *et al.* Preparation and Evaluation of Skin Wound Healing Chitosan-Based Hydrogel Membranes. *AAPS PharmSciTech* **19**, 3199–3209 (2018).

334. Bal, A., Özkahraman, B. & Özbaş, Z. Preparation and characterization of pH responsive poly(methacrylic acid-acrylamide-N-hydroxyethyl acrylamide) hydrogels for drug delivery

systems. *J. Appl. Polym. Sci.* **133**, (2016).

335. Gorman, M., Chim, Y. H., Hart, A., Riehle, M. O. & Urquhart, A. J. Poly (N -acryloylmorpholine): A simple hydrogel system for temporal and spatial control over cell adhesion. *J. Biomed. Mater. Res. - Part A* 1809–1815 (2013). doi:10.1002/jbm.a.34853

336. Fink, J. K. *Compatibilization*. *Reactive Polymers Fundamentals and Applications* (William Andrew, 2013). doi:10.1016/b978-1-4557-3149-7.00016-4

337. Grishin, D. F. & Grishin, I. D. Controlled radical polymerization: Prospects for application for industrial synthesis of polymers (Review). *Russ. J. Appl. Chem.* **84**, 2021–2028 (2011).

338. Oytun, F., Kahveci, M. U. & Yagci, Y. Sugar overcomes oxygen inhibition in photoinitiated free radical polymerization. *J. Polym. Sci. Part A Polym. Chem.* **51**, 1685–1689 (2013).

339. Whitfield, R., Parkatzidis, K., Rolland, M., Truong, N. P. & Anastasaki, A. Tuning Dispersity by Photoinduced Atom Transfer Radical Polymerisation: Monomodal Distributions with ppm Copper Concentration. *Angew. Chemie - Int. Ed.* **58**, 13323–13328 (2019).

340. Moad, G. *Radical Polymerization*. *Polymer Science: A Comprehensive Reference, 10 Volume Set* **3**, (Elsevier B.V., 2012).

341. Georges, M. K., Veregin, R. P. N., Hamer, G. K. & Kazmaier, P. M. Breathing new life into the free radical polymerization process. *Macromol. Symp.* **103**, 89–103 (1994).

342. Gooch, J. W. *Encyclopedic Dictionary of Polymers*. *Encyclopedic Dictionary of Polymers* (Springer New York, 2011). doi:10.1007/978-1-4419-6247-8

343. Cioffi, M., Hoffmann, A. C. & Janssen, L. P. B. M. Rheokinetics and the influence of shear rate on the trommsdorff (Gel) effect during free radical polymerization. *Polym. Eng. Sci.* **41**, 595–602 (2001).

344. Zhan, P. *et al.* Methyl methacrylate-styrene copolymers prepared by utilizing the Trommsdorff

effect in an inverted two-stage extruder. *Mater. Res. Express* **7**, (2020).

345. Ainseba-Chirani, N., Dembahri, Z., Tokarski, C., Rolando, C. & Benmouna, M. Newly designed polyacrylamide/dextran gels for electrophoresis protein separation: Synthesis and characterization. *Polym. Int.* **60**, 1024–1029 (2011).

346. Abdel-Razik, E. A. Homogeneous graft copolymerization of acrylamide onto ethylcellulose. *Polymer (Guildf).* **31**, 1739–1744 (1990).

347. Montserrat, S. & Colomer, P. The effect of the molecular weight on the glass transition temperature in amorphous poly(ethylene terephthalate). *Polym. Bull.* **12**, 173–180 (1984).

348. Asgreen, C., Knopp, M. M., Skytte, J. & Löbmann, K. Influence of the polymer glass transition temperature and molecular weight on drug amorphization kinetics using ball milling. *Pharmaceutics* **12**, (2020).

349. Tadlaoui, K., Pietrasanta, Y., Michel, A. & Verney, V. Influence of molecular weight on the glass transition temperature and the melt rheological behaviour of methyl methacrylate telomers. *Polymer (Guildf).* **32**, 2234–2237 (1991).

350. Fox, T. G. & Flory, P. J. Second-order transition temperatures and related properties of polystyrene. I. Influence of molecular weight. *J. Appl. Phys.* **21**, 581–591 (1950).

351. Shibata, M., Kimura, Y. & Yaginuma, D. Thermal properties of novel supramolecular polymer networks based on poly(4-vinylpyridine) and disulfonic acids. *Polymer (Guildf).* **45**, 7571–7577 (2004).

352. Wu, S., Yang, X., Zou, M., Hou, Z. & Yan, J. A New Method Without Organic Solvent to Targeted Nanodrug for Enhanced Anticancer Efficacy. *Nanoscale Res. Lett.* **12**, (2017).

353. Permana, A. D. *et al.* Dissolving microneedle-mediated dermal delivery of itraconazole nanocrystals for improved treatment of cutaneous candidiasis. *Eur. J. Pharm. Biopharm.* **154**,

50–61 (2020).

354. Levine, H. & Slade, L. *Water as a plasticizer: physico-chemical aspects of low-moisture polymeric systems*. *Water Science Reviews 3* (2010). doi:10.1017/cbo9780511552083.002

355. Martin, J. R., Johnson, J. F. & Cooper, R. Mechanical Properties of Polymers : The Influence of Molecular Weight and Molecular Weight Distribution. *J. Macromol. Sci. Part C* 57–199 (2006). doi:10.1080/15321797208068169

356. Lamm, M. E. *et al.* Tuning Mechanical Properties of Biobased Polymers by Supramolecular Chain Entanglement. *Macromolecules* **52**, 8967–8975 (2019).

357. Lee, I.-C., He, J.-S., Tsai, M.-T. & Lin, K.-C. Fabrication of a novel partially dissolving polymer microneedle patch for transdermal drug delivery. *J. Mater. Chem. B* **3**, 276–285 (2015).

358. Khan, S., Boateng, J. S., Mitchell, J. & Trivedi, V. Formulation, Characterisation and Stabilisation of Buccal Films for Paediatric Drug Delivery of Omeprazole. *AAPS PharmSciTech* **16**, 800–810 (2015).

359. Van Der Maaden, K., Sekerdag, E., Jiskoot, W. & Bouwstra, J. Impact-insertion applicator improves reliability of skin penetration by solid microneedle arrays. *AAPS J.* **16**, 681–684 (2014).

360. Nguyen, H. X. *et al.* Poly (vinyl alcohol) microneedles: Fabrication, characterization, and application for transdermal drug delivery of doxorubicin. *Eur. J. Pharm. Biopharm.* **129**, 88–103 (2018).

361. Kellner, M., Radovanovic, P., Matovic, J. & Liska, R. Novel cross-linkers for asymmetric poly-AMPS-based proton exchange membranes for fuel cells. *Des. Monomers Polym.* **17**, 372–379 (2014).

362. Yu, J. *et al.* Microneedle-array patches loaded with hypoxia-sensitive vesicles provide fast

glucose-responsive insulin delivery. *Proc. Natl. Acad. Sci. U. S. A.* **112**, 8260–8265 (2015).

363. Jacob, D., Joan Taylor, M., Tomlins, P. & Sahota, T. S. Synthesis and Identification of FITC-Insulin Conjugates Produced Using Human Insulin and Insulin Analogues for Biomedical Applications. *J. Fluoresc.* **26**, 617–629 (2016).

364. Gross, J. H. Analysis of silicones released from household items and baby articles by direct analysis in real time-mass spectrometry. *J. Am. Soc. Mass Spectrom.* **26**, 511–521 (2015).

365. Carter, S.-S. D. *et al.* PDMS leaching and its implications for on-chip studies focusing on bone regeneration applications. *Organs-on-a-Chip* **2**, 100004 (2020).

366. Kim, S. H., Moon, J. H., Kim, J. H., Jeong, S. M. & Lee, S. H. Flexible, stretchable and implantable PDMS encapsulated cable for implantable medical device. *Biomed. Eng. Lett.* **1**, 199–203 (2011).

367. Gorman, M., Chim, Y. H., Hart, A., Riehle, M. O. & Urquhart, A. J. Poly (N -acryloylmorpholine): A simple hydrogel system for temporal and spatial control over cell adhesion. 1809–1815 (2013). doi:10.1002/jbm.a.34853

368. Bartosova, L. & Bajgar, J. Transdermal Drug Delivery In Vitro Using Diffusion Cells. *Curr. Med. Chem.* **19**, 4671–4677 (2012).

369. Wagner, H., Kostka, K. H., Lehr, C. M. & Schaefer, U. F. Drug distribution in human skin using two different in vitro test systems: Comparison with in vivo data. *Pharm. Res.* **17**, 1475–1481 (2000).

370. Miyajima, M., Koshika, A., Okada, J. & Ikeda, M. Effect of polymer/basic drug interactions on the two-stage diffusion-controlled release from a poly(L-lactic acid) matrix. *J. Control. Release* **61**, 295–304 (1999).

371. Nilsson, K. D. *et al.* TOF-SIMS imaging reveals tumor heterogeneity and inflammatory response

markers in the microenvironment of basal cell carcinoma TOF-SIMS. *Biointerphases* **041012**, (2020).

372. Munem, M. *et al.* Chemical imaging of aggressive basal cell carcinoma using time-of-flight secondary ion mass spectrometry. *Biointerphases* **13**, 03B402 (2018).

373. Hoffman, A. S. Hydrogels for biomedical applications. *Adv. Drug Deliv. Rev.* **54**, 3–12 (2002).

374. Lu, H. *et al.* Recent advances of on-demand dissolution of hydrogel dressings. *Burn. Trauma* 1–13 (2018). doi:10.1186/s41038-018-0138-8

375. Miller-Chou, B. A. & Koenig, J. L. A review of polymer dissolution. *Prog. Polym. Sci.* **28**, 1223–1270 (2003).

376. J, Z., Y, L. & A, W. Study on Superabsorbent Composite XXV. Synthesis, Characterization, and Swelling Behaviors of Poly(acrylic acid-co-N-acryloylmorpholine)/Attapulgite Superabsorbent Composites. *Polym. Polym. Compos.* **16**, 101–113 (2008).

377. Fares, M. M. & Al-Shboul, A. M. Stimuli pH-responsive (N-vinyl imidazole-co-acryloylmorpholine) Hydrogels; Mesoporous and Nanoporous Scaffolds. *J. Biomed. Mater. Res. - Part A* **100 A**, 863–871 (2012).

378. Nam, K., Watanabe, J. & Ishihara, K. The characteristics of spontaneously forming physically cross-linked hydrogels composed of two water-soluble phospholipid polymers for oral drug delivery carrier I : hydrogel dissolution and insulin release under neutral pH condition. *Eur. J. Pharm. Sci.* **23**, 261–270 (2004).

379. Meis, C. M. *et al.* Self-Assembled, Dilution-Responsive Hydrogels for Enhanced Thermal Stability of Insulin Biopharmaceuticals. (2020). doi:10.1021/acsbiomaterials.0c01306

380. McKenzie, M. *et al.* Hydrogel-based drug delivery systems for poorly water-soluble drugs. *Molecules* **20**, 20397–20408 (2015).

381. Grimwood, R. E. *et al.* Transplantation of human basal cell carcinomas to athymic mice. *Cancer* **56**, 519–523 (1985).

382. Grimwood , Ronald Tharp, M. D. Growth of Human Basal Cell Carcinomas Transplanted to C57/Balb/C bgJ/bgJ- nu/nu (Beige-Nude) Mice. *J Dermatol Surg Oncol* **17**, 661–666 (1991).

383. Carlson, J. A., Combates, N. J., Stenn, K. S. & Prouty, S. M. Anaplastic neoplasms arising from basal cell carcinoma xenotransplants into SCID-beige mice. *J. Cutan. Pathol.* **29**, 268–278 (2002).

384. Wang, G. Y. *et al.* Establishment of murine basal cell carcinoma allografts: A potential model for preclinical drug testing and for molecular analysis. *J. Invest. Dermatol.* **131**, 2298–2305 (2011).

385. El-Khattouti, A. *et al.* Imiquimod-induced apoptosis of melanoma cells is mediated by ER stress-dependent Noxa induction and enhanced by NF-κB inhibition. *J. Cell. Mol. Med.* **20**, 266–286 (2016).

386. Schön, M. P. *et al.* Death receptor-independent apoptosis in malignant melanoma induced by the small-molecule immune response modifier imiquimod. *J. Invest. Dermatol.* **122**, 1266–1276 (2004).

387. Berman, B., Sullivan, T., De Araujo, T. & Nadji, M. Expression of Fas-receptor on basal cell carcinomas after treatment with imiquimod 5% cream or vehicle. *Br. J. Dermatology, Suppl.* **149**, 59–61 (2003).

388. Vidal, D., Matias-Guiu, X. & Alomar, A. Open study of the efficacy and mechanism of action of topical imiquimod in basal cell carcinoma. *Exp. Dermatol.* **29**, 518–525 (2004).

389. Drobits, B. *et al.* Imiquimod clears tumors in mice independent of adaptive immunity by converting pDCs into tumor-killing effector cells. *J. Clin. Invest.* **122**, (2012).

390. Huang, S. *et al.* Dextran methacrylate hydrogel microneedles loaded with doxorubicin and trametinib for continuous transdermal administration of melanoma. *Carbohydr. Polym.* **246**, 116650 (2020).

391. Overwijk, W. W. & Restifo, N. P. B16 as a Mouse Model for Human Melanoma. *Curr. Protoc. Immunol.* **39**, 1–29 (2000).

392. Andersen, F. A. Final report on the safety assessment of trichloroethane. *Int. J. Toxicol.* **27**, 107–138 (2008).

393. Permana, A. D. *et al.* Solid lipid nanoparticle-based dissolving microneedles: A promising intradermal lymph targeting drug delivery system with potential for enhanced treatment of lymphatic filariasis. *J. Control. Release* **316**, 34–52 (2019).

394. Passarelli, M. K. *et al.* The 3D OrbiSIMS—label-free metabolic imaging with subcellular lateral resolution and high mass-resolving power. *Nat. Methods* **14**, (2017).

395. Donnelly, R. F. *et al.* Hydrogel-forming microneedle arrays can be effectively inserted in skin by self-application: A pilot study centred on pharmacist intervention and a patient information leaflet. *Pharm. Res.* **31**, 1989–1999 (2014).

396. Norman, J. J. *et al.* Microneedle patches: Usability and acceptability for self-vaccination against influenza. *Vaccine* **32**, 1856–1862 (2014).

397. Swathi, H. P. *et al.* Effect of gamma sterilization on the properties of microneedle array transdermal patch system. *Drug Dev. Ind. Pharm.* **46**, 606–620 (2020).

398. FDA. Regulatory Considerations for Microneedling Devices FDA-2017-D-4792. 1–12 (2017).

399. The PATH Center of Excellence for Microarray Patch Technology | PATH. Available at: https://www.path.org/resources/path-center-excellence-microarray-patch-technology/. (Accessed: 27th October 2020)

Chapter 8 Appendix I – Human BCC Tissue Study Ethical Approval

NHS SCOTLAND
Research Ethics Service

East of Scotland Research Ethics Service *(EoSRES)*

Please note: This is the favourable opinion of the REC only and does not allow you to start your study at NHS sites in England until you receive HRA Approval

TAyside medical Science Centre
Residency Block Level 3
George Pirie Way
Ninewells Hospital and Medical School
Dundee DD1 9SY

Dr John Mckenna
Consultant Dermatologist
University Hospitals Leicester
Leicester Royal Infirmary
University Hospitals Leicester Dermatology Departmer
Infirmary Square, Leicester,
LE1 5WW

Date: 06 November 2019
Your Ref:
Our Ref: DL/19/ES/0108
Enquiries to: Mrs Diane Leonard
Direct Line: 01382 383871
Email: eosres.tayside@nhs.net

Dear Dr Mckenna

Study title: **Drug penetration through skin & basal cell carcinoma (BCC): Analysis by Time of flight-Secondary Ion Mass Spectroscopy (TOF-SIMS), 3D Hybrid-Secondary Ion Mass Spectrometry (Hybrid SIMS) and Confocal Raman Microscopy**
REC reference: **19/ES/0108**
Protocol number: **1.0**
IRAS project ID: **130880**

Thank you for your letter of 05 November 2019, responding to the Proportionate Review Sub-Committee's request for changes to the documentation for the above study.

The revised documentation has been reviewed and approved on behalf of the PR sub-committee.

Confirmation of ethical opinion

On behalf of the Committee, I am pleased to confirm a favourable ethical opinion for the above research on the basis described in the application form, protocol and supporting documentation as revised.

Conditions of the favourable opinion

The REC favourable opinion is subject to the following conditions being met prior to the start of the study.

Confirmation of Capacity and Capability (in England, Northern Ireland and Wales) or NHS management permission (in Scotland) should be sought from all NHS organisations involved in the study in accordance with NHS research governance arrangements. Each NHS organisation must confirm through the signing of agreements and/or other documents that it has given permission for the research to proceed (except where explicitly specified otherwise).

disability confident EMPLOYER

1

Guidance on applying for HRA and HCRW Approval (England and Wales)/ NHS permission for research is available in the Integrated Research Application System.

For non-NHS sites, site management permission should be obtained in accordance with the procedures of the relevant host organisation.

Sponsors are not required to notify the Committee of management permissions from host organisations.

Registration of Clinical Trials

It is a condition of the REC favourable opinion that **all clinical trials are registered** on a publicly accessible database. For this purpose, 'clinical trials' are defined as the first four project categories in IRAS project filter question 2. Registration is a legal requirement for clinical trials of investigational medicinal products (CTIMPs), except for phase I trials in healthy volunteers (these must still register as a condition of the REC favourable opinion).

Registration should take place as early as possible and within six weeks of recruiting the first research participant at the latest. Failure to register is a breach of these approval conditions, unless a deferral has been agreed by or on behalf of the Research Ethics Committee (see here for more information on requesting a deferral: https://www.hra.nhs.uk/planning-and-improving-research/research-planning/research-registration-research-project-identifiers/

As set out in the UK Policy Framework, research sponsors are responsible for making information about research publicly available before it starts e.g. by registering the research project on a publicly accessible register. Further guidance on registration is available at: https://www.hra.nhs.uk/planning-and-improving-research/research-planning/transparency-responsibilities/

You should notify the REC of the registration details. We routinely audit applications for compliance with these conditions.

It is the responsibility of the sponsor to ensure that all the conditions are complied with before the start of the study or its initiation at a particular site (as applicable).

After ethical review: Reporting requirements

The attached document "After ethical review – guidance for researchers" gives detailed guidance on reporting requirements for studies with a favourable opinion, including:

- Notifying substantial amendments
- Adding new sites and investigators
- Notification of serious breaches of the protocol
- Progress and safety reports
- Notifying the end of the study, including early termination of the study
- Final report

The latest guidance on these topics can be found at https://www.hra.nhs.uk/approvals-amendments/managing-your-approval/.

Ethical review of research sites

The favourable opinion applies to all NHS/HSC sites taking part in the study, subject to management permission being obtained from the NHS/HSC R&D office prior to the start of the study (see "Conditions of the favourable opinion" above).

Approved documents

The documents reviewed and approved by the Committee are:

Document	Version	Date
IRAS Application Form [IRAS_Form_15082019]		15 August 2019
IRAS Checklist XML [Checklist_08102019]		08 October 2019
IRAS Checklist XML [Checklist_05112019]		05 November 2019
Letter from funder [Funding Letter from CDT]		01 October 2018
Other [Peer Review Form]		25 October 2018
Other [Supervisor 1 CV Dr John McKenna]		
Other [Supervisor 2 CV Dr Maria Marlow]		
Other [Supervisor 3 CV Dr David Scurr]		
Other [Supervisor 4 CV Dr Volha Shpadaruk]		
Other [Supervisor 5 CV Dr Joel Segal]	1.0	19 August 2019
Other [Protocol (highlighted changes)]	2.0	18 September 2019
Other [Response to Provisional Opinion]		18 September 2019
Other [Response to Ethic Request for Further Information]	1.0	07 October 2019
Other [Response to Ethic Request for Further Clarification]	1.0	05 November 2019
Other [130880 Qualitative-protocol-development-tool v3.0_4_November 2019_tracked changes]	3.0	04 November 2019
Participant consent form [Clean copy]	2.0	18 September 2019
Participant consent form [Tracked changes]	2.0	18 September 2019
Participant information sheet (PIS) [Clean copy]	2.0	18 September 2019
Participant information sheet (PIS) [Highlighted changes]	2.0	18 September 2019
Research protocol or project proposal [130880 Qualitative-protocol-development-tool v1.0 22nd May 2019]	3.0	04 November 2019
Summary CV for Chief Investigator (CI) [Chief Investigator (Dr John McKenna) CV 11.4.18 v1]		11 April 2018
Summary CV for student [Akmal Sabri CV]		

Statement of compliance

The Committee is constituted in accordance with the Governance Arrangements for Research Ethics Committees and complies fully with the Standard Operating Procedures for Research Ethics Committees in the UK.

User Feedback

The Health Research Authority is continually striving to provide a high quality service to all applicants and sponsors. You are invited to give your view of the service you have received and the application procedure. If you wish to make your views known please use the feedback form available on the HRA website: http://www.hra.nhs.uk/about-the-hra/governance/quality-assurance/

HRA Learning

We are pleased to welcome researchers and research staff to our HRA Learning Events and online learning opportunities– see details at: https://www.hra.nhs.uk/planning-and-improving-research/learning/

19/ES/0108	**Please quote this number on all correspondence**

Yours sincerely

D Leonard

for Mrs Natalie McInally
Vice-Chair

Email: eosres.tayside@nhs.net

Enclosures: "After ethical review – guidance for researchers"

Copy to: Mrs Carolyn Maloney

Ymchwil Iechyd a Gofal Cymru
Health and Care Research Wales

NHS
Health Research Authority

Mr Akmal Bin Sabri
Boots Science Building
University Park
Nottingham
NG7 2RD

Email: hra.approval@nhs.net
HCRW.approvals@wales.nhs.uk

22 November 2019

Dear Mr Akmal Bin Sabri

HRA and Health and Care Research Wales (HCRW) Approval Letter

Study title:	**Drug penetration through skin & basal cell carcinoma (BCC): Analysis by Time of flight-Secondary Ion Mass Spectroscopy (TOF-SIMS), 3D Hybrid-Secondary Ion Mass Spectrometry (Hybrid SIMS) and Confocal Raman Microscopy**
IRAS project ID:	**130880**
REC reference:	**19/ES/0108**
Sponsor	**University Hospital Leicester**

I am pleased to confirm that HRA and Health and Care Research Wales (HCRW) Approval has been given for the above referenced study, on the basis described in the application form, protocol, supporting documentation and any clarifications received. You should not expect to receive anything further relating to this application.

Please now work with participating NHS organisations to confirm capacity and capability, in line with the instructions provided in the "Information to support study set up" section towards the end of this letter.

How should I work with participating NHS/HSC organisations in Northern Ireland and Scotland?
HRA and HCRW Approval does not apply to NHS/HSC organisations within Northern Ireland and Scotland.

If you indicated in your IRAS form that you do have participating organisations in either of these devolved administrations, the final document set and the study wide governance report (including this letter) have been sent to the coordinating centre of each participating nation. The relevant national coordinating function/s will contact you as appropriate.

Please see IRAS Help for information on working with NHS/HSC organisations in Northern Ireland and Scotland.

How should I work with participating non-NHS organisations?
HRA and HCRW Approval does not apply to non-NHS organisations. You should work with your non-NHS organisations to obtain local agreement in accordance with their procedures.

What are my notification responsibilities during the study?

The standard conditions document "*After Ethical Review – guidance for sponsors and investigators*", issued with your REC favourable opinion, gives detailed guidance on reporting expectations for studies, including:

- Registration of research
- Notifying amendments
- Notifying the end of the study

The HRA website also provides guidance on these topics and is updated in the light of changes in reporting expectations or procedures.

Who should I contact for further information?
Please do not hesitate to contact me for assistance with this application. My contact details are below.

Your IRAS project ID is **130880**. Please quote this on all correspondence.

Yours Sincerely
Beverley Mashegede

Email: hra.approval@nhs.net

Copy to: Mrs Carolyn Maloney, Sponsor Contact

List of Documents

The final document set assessed and approved by HRA and HCRW Approval is listed below.

Document	*Version*	*Date*
IRAS Application Form [IRAS_Form_15082019]		15 August 2019
IRAS Checklist XML [Checklist_05112019]		05 November 2019
Letter from funder [Funding Letter from CDT]		01 October 2018
Other [Peer Review Form]		25 October 2018
Other [Supervisor 1 CV Dr John McKenna]		
Other [Supervisor 2 CV Dr Maria Marlow]		
Other [Supervisor 3 CV Dr David Scurr]		
Other [Supervisor 4 CV Dr Volha Shpadaruk]		
Other [Supervisor 5 CV Dr Joel Segal]	1.0	19 August 2019
Other [Response to Provisional Opinion]		18 September 2019
Other [Response to Ethic Request for Further Information]		07 October 2019
Other [Response to Ethic Request for Further Clarification]		05 November 2019
Participant consent form [Clean copy]	2.0	18 September 2019
Participant information sheet (PIS) [Clean copy]	2.0	18 September 2019
Research protocol or project proposal [130880 Qualitative-protocol-development-tool v1.0 22nd May 2019]	3.0	04 November 2019
Summary CV for Chief Investigator (CI) [Chief Investigator (Dr John McKenna) CV 11.4.18 v1]		11 April 2018
Summary CV for student [Akmal Sabri CV]		

IRAS project ID	130880

Information to support study set up

The below provides all parties with information to support the arranging and confirming of capacity and capability with participating NHS organisations in England and Wales. This is intended to be an accurate reflection of the study at the time of issue of this letter.

Types of participating NHS organisation	Expectations related to confirmation of capacity and capability	Agreement to be used	Funding arrangements	Oversight expectations	HR Good Practice Resource Pack expectations
Single centre study.	This is a single site study sponsored by the participating NHS organisation. You should work with your sponsor R&D office to make arrangements to set up the study. The sponsor R&D office will confirm to you when the study can start following issue of HRA and HCRW Approval.	This is a non-commercial single site study taking place in the NHS where that single NHS organisation is also the study sponsor. Therefore, no study agreements are required.	Funded by EPSRC-Engineering & Physical Sciences Research Council. Funding letter submitted.	A PI is expected at the participating organisation.	All study activities will be undertaken by local staff employed by the NHS organisation. Therefore, no honorary research contracts or letters of access are expected for this study.

Other information to aid study set-up and delivery

This details any other information that may be helpful to sponsors and participating NHS organisations in England and Wales in study set-up.
The applicant has indicated that they do not intend to apply for inclusion on the NIHR CRN Portfolio.